University of South Carolina
Scholar Commons

Theses and Dissertations

12-15-2014

Synthesis of AU and AG Catalysts with Controlled Sizes of Metal Particles

Eleni A. Kyriakidou
University of South Carolina - Columbia

Follow this and additional works at: http://scholarcommons.sc.edu/etd

Recommended Citation

Kyriakidou, E. A.(2014). *Synthesis of AU and AG Catalysts with Controlled Sizes of Metal Particles.* (Doctoral dissertation). Retrieved from http://scholarcommons.sc.edu/etd/2925

This Open Access Dissertation is brought to you for free and open access by Scholar Commons. It has been accepted for inclusion in Theses and Dissertations by an authorized administrator of Scholar Commons. For more information, please contact SCHOLARC@mailbox.sc.edu.

SYNTHESIS OF AU AND AG CATALYSTS WITH CONTROLLED SIZES OF METAL PARTICLES

by

Eleni A. Kyriakidou

Bachelor of Science
Aristotelian University of Thessaloniki, 2007

Master of Science
Aristotelian University of Thessaloniki, 2007

Submitted in Partial Fulfillment of the Requirements

For the Degree of Doctor of Philosophy in

Chemical Engineering

College of Engineering and Computing

University of South Carolina

2014

Accepted by:

Michael D. Amiridis, Major Professor

John R. Regalbuto, Committee Member

Harry J. Ploehn, Committee Member

Yeomin Yoon, Committee Member

Lacy Ford, Vice Provost and Dean of Graduate Studies

© Copyright by Eleni A. Kyriakidou, 2014
All Rights Reserved.

DEDICATION

To my parents, Aggelos and Athanasia, who gave me roots and wings.

ACKNOWLEDGEMENTS

My greatest gratitude goes to my advisor, Professor Michael D. Amiridis for guiding, inspiring and encouraging me throughout my graduate studies. His technical advice was essential to the completion of this dissertation and has taught me innumerable lessons and insights on the workings of academic research in general. Many thanks also go to the member of my committee, Dr. John R. Regalbuto, and Dr. Oleg S. Alexeev. I appreciate all their contributions of time and ideas to make my Ph.D. experience productive and stimulating. I would also like to acknowledge my Ph.D. examining committee, Dr. Harry J. Ploehn, and Dr. Yeomin Yoon for your insight and suggestions, which are precious to me.

The friendship of Dr. Vityuk and Christina Papadimitriou is much appreciated and has led to many interesting and good-spirited discussions relating to this research. I am also grateful to my colleagues Dr. Nazarpoor and Konstantin Khivantsev for helping considerably with realizing the dendrimer synthetic route optimizations. My thanks go to John Meynard Tengco and Shuo Cao for helping with various aspects of the Strong Electrostatic Adsorption technique.

Last, but not least, I would like to thank my fiancé Eric for his understanding and love during the past few years. My parents, Aggelos and Athanasia, receive my deepest gratitude and love for their dedication and the many years of support during my undergraduate studies that provided the foundation for this work.

ABSTRACT

The performance of supported metal catalysts largely depends on the structure and composition of the metal particles and the nature of the support. In order to achieve better control over these parameters, synthetic route based on the use of templating agents has been proposed. Among the different templating agents, poly(amidoamine) (PAMAM) dendrimers have attracted a lot of recent attention as nanoparticle stabilizers. In this thesis, Au/G4OH nanocomposites were synthesized in aqueous solutions and used as precursors for the preparation of SiO_2-supported Au nanoparticles. Elemental analysis, UV-Vis, and STEM measurements were used to estimate the extent of the Au-dendrimer interactions and to illustrate how the solution pH affect the number of Au atoms complexed with each dendrimer molecule, as well as the final size of the SiO_2-supported gold particles. At pH=7, Au_5/G4OH nanocomposites with sizes of Au particles below 2 nm can be formed and used as precursors for the preparation of solid materials. We show that such nanocomposites can be deposited intact on the surface of SiO_2 and yield highly dispersed and nearly uniform Au nanoparticles with dimensions on the order of 1.6 nm.

One of the simplest, least expensive methods of catalyst preparation is the wet impregnation, where an oxide support is contacted for a certain time with a liquid solution containing the metal precursor. In certain circumstances when the impregnation conditions are controlled it is possible to end up with uniform and highly dispersed metal particles. One of these examples is the "Strong Electrostatic Adsorption" (SEA). In this thesis, the extension of SEA is made to an important noble metal, silver. Evaluation of

the uptake of Ag diammine ($Ag(NH_3)_2^+$) over supports with low and mid-point of zero charge (PZC) (Nb_2O_5, SiO_2, Al_2O_3 and ZrO_2) was performed and this knowledge was used to prepare highly dispersed monometallic Ag nanoparticles. Temperature-programmed reduction (TPR) was used to determine the reduction temperature of the final Ag/SiO_2 (low-PZC) and Ag/Al_2O_3 (mid-PZC) catalytic materials. Finally, STEM and XRD measurements were also used to image and determine the size of the resulting supported metal nanoparticles, respectively.

TABLE OF CONTENTS

LIST OF TABLES

LIST OF FIGURES

CHAPTER 1

CATALYSIS BY METAL COLLOIDS-POLY(AMIDOAMINE) (PAMAM) DENDRIMERS AS STABILIZERS OF METAL NANOPARTICLES

1.1 Metal Colloids

Electrostatic and steric factors are used most frequently to explain the stability of colloidal suspensions.[1,2] The classical theory of Derjaguin, Landau, Verwey, and Overbeek (DLVO) explains the kinetic stability of colloids by positing an energy barrier which metal anions/cations and surfactant molecules must overcome in order to form complexes.[3] This barrier is formed due to superposition of repulsive (Coulomb interaction) electric double layer and attractive van der Waals potentials (Fig. 1.1).[3-5] Shiraishi et al. reported that at high pH negatively charged carboxylate groups of a 3-mercaptopropionic acid caused the formation of an electric double layer that stabilizes metal particles in the dispersed state. However, when these groups are substantially protonated at low pH and their charge is neutralized, van der Waals attractions dominate and drive the aggregation of metal particles.[6]

In steric stabilization, metal nanoparticles are separated from each other by larger molecules of surfactants, acting as protective shields. Coordination of metals to such molecules prevents their agglomeration.[8,9] Finally, an electrosteric stabilization has the advantage of providing an electrical double layer of repulsive forces as well as the steric

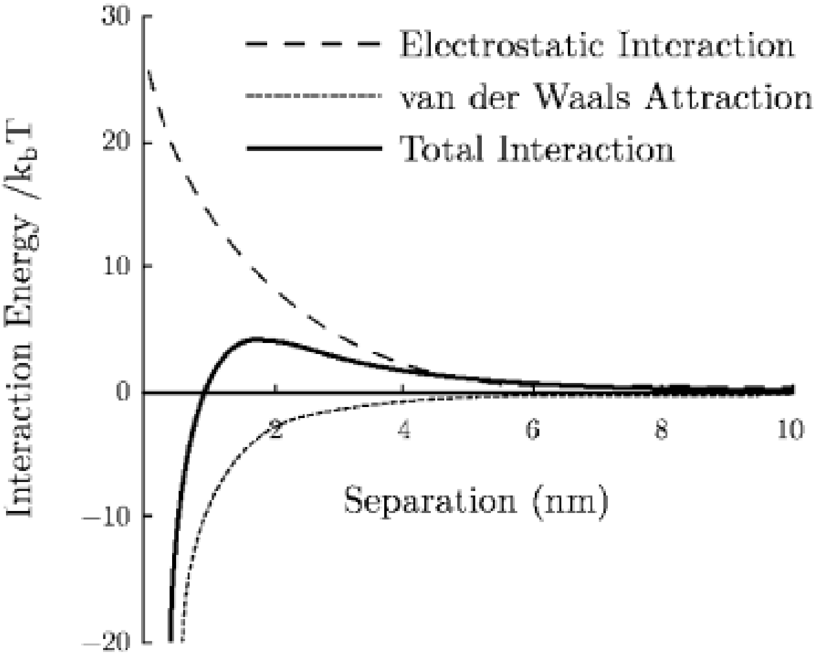

Figure 1.1 Two potentials considered by the classical DLVO theory and their resulting superposition. The separation distance refers to the surface-to-surface distance. In this example, it can be seen that a small energy barrier must be overcome to form an aggregate.[3]

barrier. An example of this kind of stabilization occurs in the case of the late suspension coated with block copolymers of poly(ethylene oxide) of low molecular weight in the presence of salts.[10]

Poly(vinyl pyrrolidone) (PVP) is a polymer commonly used for nanoparticle stabilization and catalysis, because it fulfills both steric and ligand requirements.[1,11,12] Many PVP-stabilized monometallic (e.g., Ir [12], Pt [13,14], Ag [15], Ru [16,17], Rh [18], Au [19]) and bimetallic (e.g., PdAg [20], AgRh [21,22], PtRu [16], CuPd [23], RhPt [24], AgPt [25] and AuAg [26]) nanoparticles have been synthesized. Among them, PVP-stabilized Pd nanoparticles with sizes in the 1.1-2.5 nm range prepared by refluxing solutions of palladium(II) chloride and PVP showed small catalytic activity for hydrogenation of 1,3-cyclo-octadiene.[27] On the other hand, PVP-stabilized PdAu nanoparticles with sizes on the order of 3 nm were found to be more active in this reaction.[28] Finally, PVP-stabilized Ni(0) nanoparticles with dimensions of approximately 3.6 nm were found to be much more active for the production of H_2 from $NaBH_4$ than bulk nickel.[29]

Many other polymers such as di and tri-block copolymers [30,31], star polymers (SPs) [32], poly(ethylene glycol) [33], poly(vinyl alcohol) (PVA) [34], poly(styrene) (PS) [35], poly(methyl hydrosilane) (PMHS) [12], poly(pyrroles) [36], poly(*o*-methoxy aniline) (POMA) [37], poly(ethylene imine) (PEI) [38], sulfonated cardo poly(arylene ether sulfone) (SPES) [39], chitosan [40] and Nafion [41] have also been used as efficient steric stabilizers for metal nanoparticles in solution.

1.2 Properties of PAMAM dendrimers

PAMAM dendrimers were extensively used as efficient steric stabilizes during the last decade.[42-44] Dendrimers are highly branched 3D globular macromolecules with a specific molecular weight and sizes in the 1–100 nm range.[1,45,46] In contrast to traditional polymers, dendrimers have unique structures possessing three basic architectural components: a core, an interior of shells (generations) consisting of repeating branch-cell units, and terminal functional groups (the outer shell or periphery).[47-49] Poly(propylene imine) (PPI) was the first dendrimer that was synthesized, followed by many new classes of dendrimers such as PAMAM and Fréchet-type polyether dendrimers.[50-52] Among these dendrimers, PAMAM dendrimers (Fig. 1.2) constitute the dendrimer family that is most extensively characterized and commercially available.[49]

PAMAM dendrimers consist of repeating tertiary amine and amide branching units, which are displayed in geometrically progressive numbers as a function of generation.[53] The most characteristic chemical property of amines is their ability to act as nucleophiles because they possess a lone pair of electrons on the nitrogen atom. They also act as bases by accepting protons from a variety of acids in aqueous solutions.[54] The high density PAMAM dendritic molecules, consisting of nitrogen ligands in concert with the possibility of attaching various functional groups such as amines, carboxyl, etc. to their periphery make them particularly attractive as high-capacity chelating agents for transition metal cations.[45,55,56] Since dendrimer dimensions and end groups can be varied, they are typically named by their generation (e. g., G1, G2, etc.) and exterior functionality (e.g., $-NH_2$, -OH).[57] Unfortunately, the complex multistep synthesis of dendrimers results in expensive products with limited use for large-scale industrial applications.[42]

When the dendrimer generation is four or higher, the conformational flexibility of the PAMAM molecule is sterically limited and the dendrimer structure assumes a densely packed globular shape.[58,59] Generation 4 or higher PAMAM dendrimers are the most commonly used for preparations of metal/dendrimer nanocomposites. G4-NH_2 and

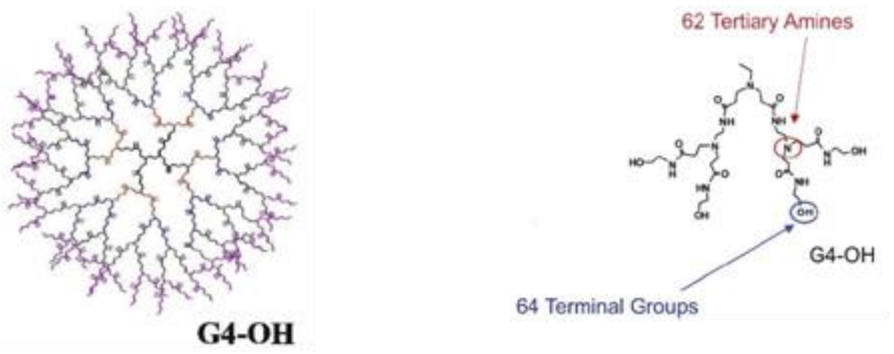

Figure 1.2 Poly(amidoamine) (PAMAM) dendrimers.[60,62]

G4-OH dendrimers are approximately 4.5nm in diameter and contain 62 interior tertiary amine groups and 64 peripheral functional groups.[60] The terminal groups in G4-OH dendrimers are less reactive than those in G4-NH_2 and the former type of dendrimers allows to avoid the competitive binding of metal ion(s) to the dendrimer periphery and the formation of intradendrimer nanoparticles.[60,61]

CHAPTER 2

SYNTHESIS OF MONOMETALLIC DENDRIMER-ENCAPSULATED NANOPARTICLES IN SOLUTION

2.1 Complexation of metal cations with dendrimers

Since metal cation/dendrimer complexation is an acid-base reaction, it is important to understand how the choice of ligands influences complexation rates of individual metal cations. The choice of donor atoms for each specific metal cation can be determined based on the Hard and Soft Acid and Base (HSAB) principle of Pearson.[63] The HSAB principle can be used in order to select an effective ligand (i.e., Lewis base) for a given metal ion (i.e, Lewis acid). Table 2.1 shows the binding constants of metal cations to selected unidendate ligands. The OH^- ligand is representative of ligands with negatively charged “hard” O donors such as carboxylate, phenolate, hydroxymate, etc.[64] Conversely, NH_3 is representative of ligands with “hard” saturated N donors (e.g. aliphatic amines), whereas imidazole is representative of “borderline” hard/soft ligands with unsaturated N donors.[64] Consistent with the HSAB principle, Table 2.1 shows that soft metal ions such Ag(I), Pd(II), Au(I) and Ag(I) tend to form more stable complexes with ligands containing S donors. In contrast, hard metal ions such Fe(III) and UO_2^{2+} tend to prefer hard ligands with O donors; whereas borderline hard/soft metal ions such

Table 2.1 Binding constants for selected metal cations with hydroxide, ammonia, imidazole, and mercaptoethanol complexes in aqueous solution.[64]

Metal Ion	**log K_1 (OH^-)**	**log K_1 (NH_3)**	**log K_1 (Imidazole)**	**log K_1 ($HOCH_2CH_2S^-$)**
Cu^{2+}	6.3	4.04	4.96	8.1
Ag^{+}	2.0	3.3	3.43	11.34
Au^{+}	2.7	5.6	5.64	18.77
Hg^{2+}	10.6	8.8	8.68	27.21
Mn^{2+}	3.4	1.0	1.04	1.62
Fe^{3+}	11.81	3.8	3.82	8.59
Co^{2+}	3.9	2.1	2.23	3.06
Ni^{2+}	4.1	2.7	2.43	6.65
UO_2^{2+}	8.2	2.0	1.90	3.42
Pd^{2+}	13.0	9.6	10.14	24.42
Zn^{2+}	5.0	2.21	2.66	3.19

as Cu(II), Co(II), Ni(II), Zn(II) and Mn(II) can bind with soft/hard ligands containing N, O and S donors depending on their specific affinity toward the ligands.[64,65] Based on this table the Gx-NH_2 PAMAM dendrimers will selectively bind Cu(II) over the first-row transition metal ions such as Co(II), Ni(II), and U(VI).[87] However, in contrast to these expectations, Ottaviani et al. showed an efficient and selective binding of U(VI) to the G6-NH_2 dendrimer. Specifically, electron paramagnetic resonance (EPR) studies of Cu(II) and U(VI) in aqueous solutions of the G6-NH_2 PAMAM dendrimer showed that uranyl ions compex stronger with the amine groups of the PAMAM dendrimer compared to the copper cations.[66] This example suggests that besides ligands preferences, other parameters such as the solution pH, for example, could influence the complexation process and should be taken into consideration.

The synthesis of dendrimer-encapsulated metal nanoparticles (DENs) was first demonstrated by Crooks et al. and Tomalia et al. in 1998. It was suggested that metal cations partition into the dendrimer interior because of a strong ionic or covalent interaction with interior amines.[67,68] Later studies showed that byproducts of this reaction can be removed from the solution by dialysis.[69] It was suggested that the formation of metal nanoparticles takes place upon reduction of metal cations mixed with dendrimers. When the metal particles thus formed are effectively trapped within the interior of the dendrimer, a subsequent deposition on the support surface can lead to a catalyst with small (~1 nm) metal nanoparticles.[44,60] Monometallic Pt, Ag, Au, Cu, Pd, Rh, Ir, and Ru nanoparticles have been prepared in solution using this approach.[70-72] The formation of bimetallic systems via this preparation route was also reported.[60,73,74] Unfortunately, recent results indicate that the metal/dendrimer complexation process is not simple and straightforward as it was initially anticipated.[75,76] For instance, the interaction of some metal cations with dendrimers depends on the solution pH, while the reduction of the metal/dendrimer solution may not necessarily lead to the formation of metal nanoparticles.[58,76,77] Finally, the encapsulation of metal cations that have weak affinity to amines, such as silver for example, in the dendrimer interior is pretty challenging.[44,78,79]

2.2 Evidence of Complexation of Pd and Pt with dendrimers

Since optical properties of metal nanoparticles are dominated by the collective oscillation of surface electrons, resulting from their interaction with electromagnetic radiation, UV-vis spectroscopy was used frequently to characterize metal nanoparticles in solution.[80-82] When a metallic nanoparticle is irradiated by light, the oscillating electric field causes the surface electrons to oscillate coherently and induces the formation of a dipole in the nanoparticle.[62,83] The collective oscillation of the surface electrons is called the surface plasmon resonance (SPR) of the particle.[84] The wavelength of the plasmon resonance bands depends on a number of factors, among which the interaction of the metal nanoparticles with their surroundings is important.

There are many literature examples in which UV-vis spectroscopy is used as a sufficient technique that provides information for the complexation of metal cations with functional groups in the dendrimer interior. Fig. 2.1(a) shows an example of such data. UV-vis spectra characterizing K_2PdCl_4 in solution display a band at 207 nm and a shoulder at 235 nm both of which correspond to the $PdCl_3(H_2O)^-$ species. When the G4-OH dendrimer was added to this solution, a strong ligand-to-metal charge transfer (LMCT) band appeared at 224 nm, suggesting the formation of $(Pd^{2+})_{40}$/G4-OH due to covalent bonding between Pd^{2+} cations and the interior tertiary amines of the dendrimer.

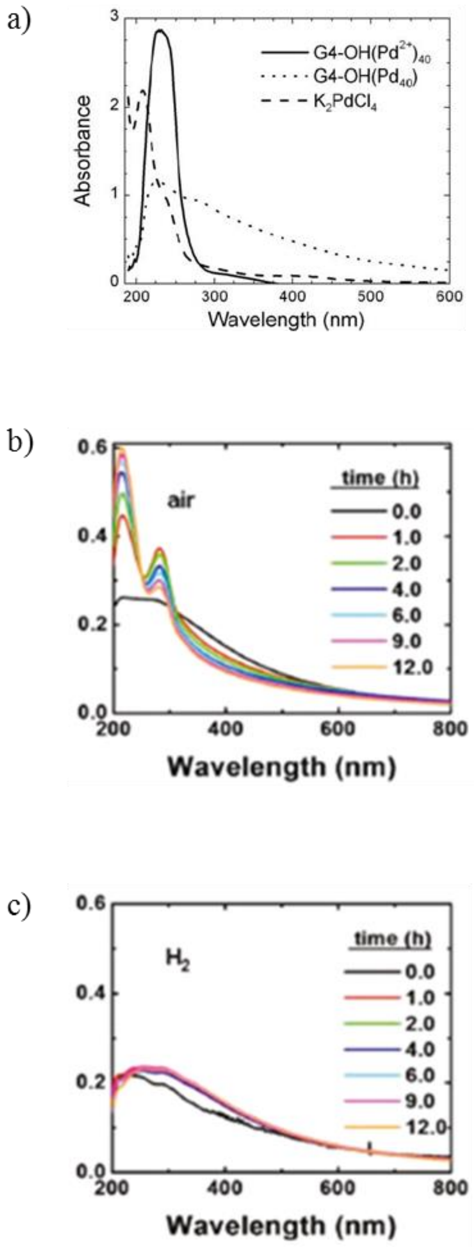

Figure 2.1 UV-vis spectra of aqueous solutions containing: K_2PdCl_4, G4-OH(Pd^{2+})$_{40}$, and G4-OH(Pd_{40}) (a) [60] and Time-resolved UV-vis absorbance spectra of G6-OH(Pd_{147}) DEN solutions. The aqueous DEN solutions were purged with air (b) and H_2 (c).[75]

[60,85,86] When an excess of $NaBH_4$ was added to $(Pd^{2+})_{40}$/G4-OH, the solution color turned from pale yellow to dark brown and the LMCT bands in the UV-vis absorption spectra disappeared. Based on these two observations, it was concluded that zerovalent Pd DENs were formed.[60] This suggestion was further tested with X-ray photoelectron spectroscopy (XPS) and spectra collected for (Pd_{147})/G6-OH treated with $NaBH_4$ indeed showed Pd 3d5/2 and 3d3/2 features at 335.7 and 341.0 eV, respectively, confirming the presence of zerovalent Pd.[75]

Exposure to air of the reduced metal/dendrimer solution may lead to reoxidation of the DENs. In the case of (Pd_{147})/G6-OH, peaks at 218 and 280 nm emerged in UV-vis spectra after 1 h of exposure to O_2, indicating that partial oxidation of Pd and subsequent recomplexation of Pd^{2+} to the interior tertiary amines of the G6-OH dendrimers took place under these conditions (Fig. 2.1(b)). In contrast, in the presence of a reducing medium (H_2-saturated water) the oxidation of (Pd_{147})/G6-OH is eliminated, since these LMCT bands are absent in all the UV-vis spectra (Fig. 2.1(c)).[75]

Unfortunately, the various preparation steps of DENs are more complex than it was initially suggested by Crooks et al. and Tomalia et al..[67,68] Furthermore, both the complexation and the reduction processes taking place in solution are subjects for further investigations.[76] For instance, EXAFS data collected for G4-OH$(Pt^{2+})_{60}$ indicate that the $PtCl_4^{2-}$ complex loses only one chloride ligand upon complexation with the dendrimer.[87] Furthermore, NMR data obtained for $PtCl_4^{2-}$/G2-OH treated with $NaBH_4$ suggest that the majority of Pt is present in solution in a cationic form and some of these species are bound to tertiary and amide nitrogens.[69] No significant changes in the UV-vis spectrum were observed when the $(Ir^{3+})_{40}$/G4-OH solution was reduced with $NaBH_4$ and H_2. In this case, both reduction treatments were further examined using XANES and the data obtained provide no indications that iridium was reduced using these reducing agents.[77]

2.3 Complexation kinetics

Data available in literature suggest that cations of most metals do not complex with dendrimers instantly and UV-vis spectroscopy is used most often to examine the complexation kinetics. For instance, Somorjai et al. showed that the complexation process for $RhCl_3$ with the G4-OH dendrimer is completed only after 18 h, as evidenced by a lack of changes in UV-vis bands at 200, 226, and 300 nm (Fig. 2.2(a)).[88] However, which of these bands is responsible for the specific Rh-G4OH interactions remains largely unknown since no specific assignment were provided in this report. Similarly, UV-vis data reported for $RuCl_3$ and G4OH by Amiridis et al. suggest that approximately 3 days are required to finish the complexation process.[89] In addition, the time-dependent UV-vis spectra of $IrCl_3 \cdot 3H_2O$ and G4-OH PAMAM dendrimer solution mixture shows gradual changes occurring over seven days (Fig. 2.2(b)).[77]

It is evident that in some specific cases, metal precursors can undergo hydrolysis and this process could be time dependent as well. If this is a case, UV-vis spectrum will reflect changes caused by hydrolysis and complexation. Therefore, it is preferable to use aged precursor solutions (prehydrolyzed) in the complexation process in order to measure the complexation kinetic more accurately. Crooks et al. examined changes in the UV-vis spectra during hydrolysis of $PtCl_4^{2-}$ over time and showed that bands at 215 and 230 nm characterizing these species decline in intensity for approximately 15 h and remain nearly constant thereafter (Fig. 2.3(a)). This fact allowed to suggest that the reaction between

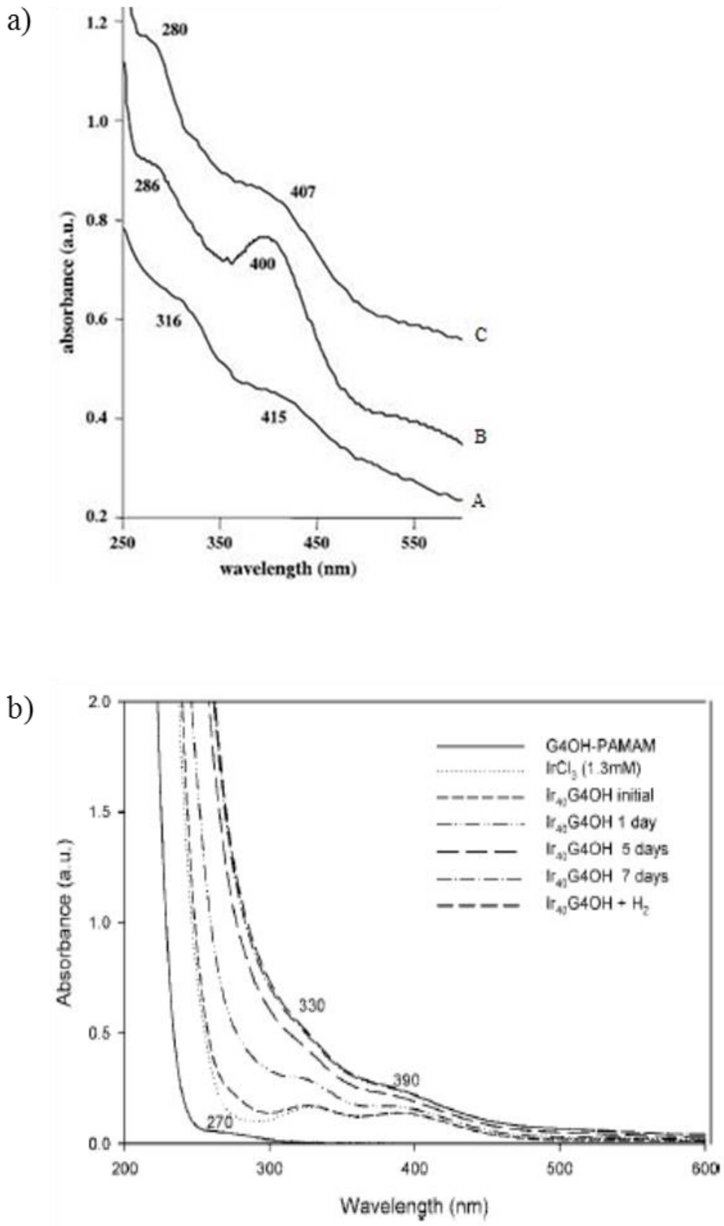

Figure 2.2 UV-vis spectra of aqueous solutions containing (A) $RuCl_3$, (B) $RuCl_3$ and G4-OH-PAMAM dendrimer solution immediately after initial mixing, (C) same solution as (B) maintained under inert atmosphere 3 days after initial mixing (a) and time-dependent UV-vis spectra for $Ir_{40}G4OH$ (b).[77,89]

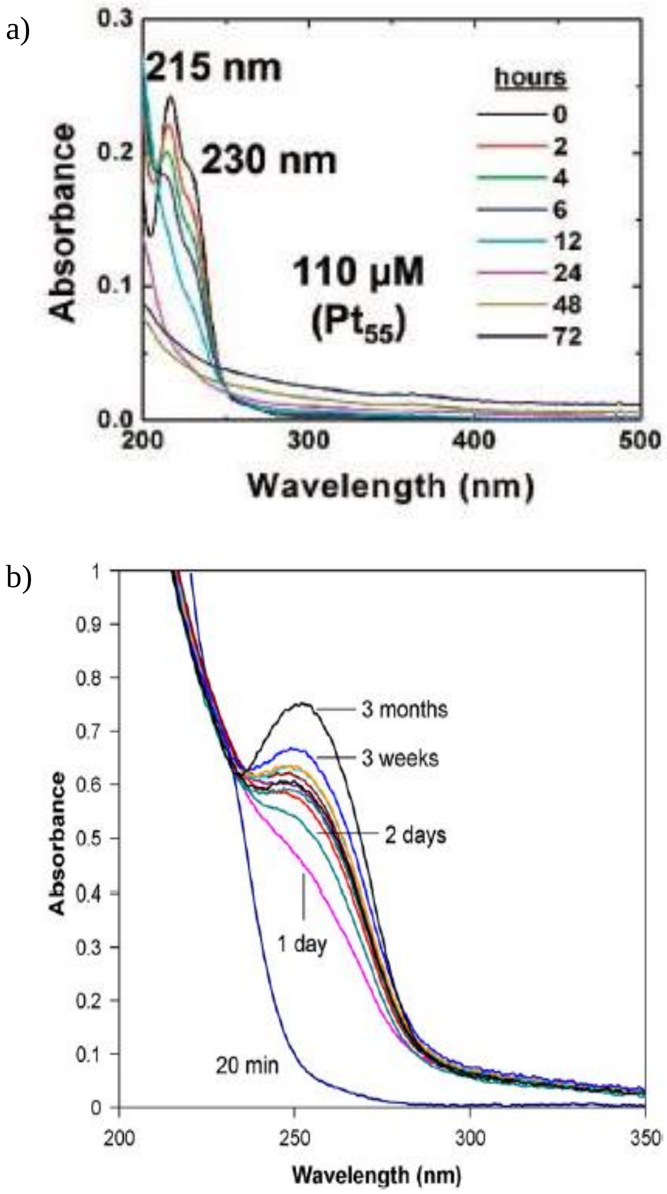

Figure 2.3 Time dependent UV-vis for: hydrolysis of K_2PtCl_4, prior mixing with dendrimer solution (a), increasing values of complexation time of Pt_{40}G4OH (b).[90,91]

Pt^{2+} and G4-OH dendrimer is a two-step process in which $PtCl_4^{2-}$ first undergoes and then the hydrolysis product reacts with interior tertiary amines of the dendrimer to form covalent bonds.[90] The signature of the ligand exchange reactions of $PtCl_4^{2-}$ and its aquated products with PAMAM is a ligand-to-metal charge transfer (LMCT) absorption peak at 250 nm.[85,87,91] Ploehn et al. examined the complexation reaction of K_2PtCl_4 with the G4OH dendrimer using the precursor solution that was aged for at least 1 day and observed that the height of the LMCT band at 250 nm increased sharply during first 3days but did not approach a steady state even after a 3 months period (Fig. 2.3(b)).[91]

2.4 Complexation of copper with dendrimers

First reports on dendrimer-encapsulated metal ions were focused on Cu^{2+} because changes in UV-vis spectra illustrating the complexation process can be interpreted fairly easy in this case.[44,67] More specifically, in the absence of G4-OH dendrimer, Cu^{2+} exists in solution primarily as $[Cu(H_2O)_6]^{2+}$, which results in a broad weak absorption band centered at 810 nm, corresponding to d-d transitions for the Cu^{2+} (Fig. 2.4(a)). In the presence of G4-OH PAMAM dendrimers, a strong band at 300 nm appears, while the absorption band centered at 810 nm shifts to 605 nm, indicating the LMCT transition.[44,67] The absorbance at 605 nm increases along with an increase in the Cu^{2+}/G4-OH mol ratio.

From these data it was found that each G4-OH molecule can strongly complex up to 16 Cu^{2+} cations (Fig. 2.4(b)).[44,67] The reduction of copper/dendrimer composites with $NaBH_4$ leads to an immediate change in color of the solution from blue to golden brown.[92] TEM micrographs reveal the presence of Cu particles with a diameter < 1.8 nm, which is much smaller than the 4.5 nm diameter of G4-OH, suggesting Cu particles are residing in the dendrimer interior.[67] In contrast, Cu particles formed after the reduction of

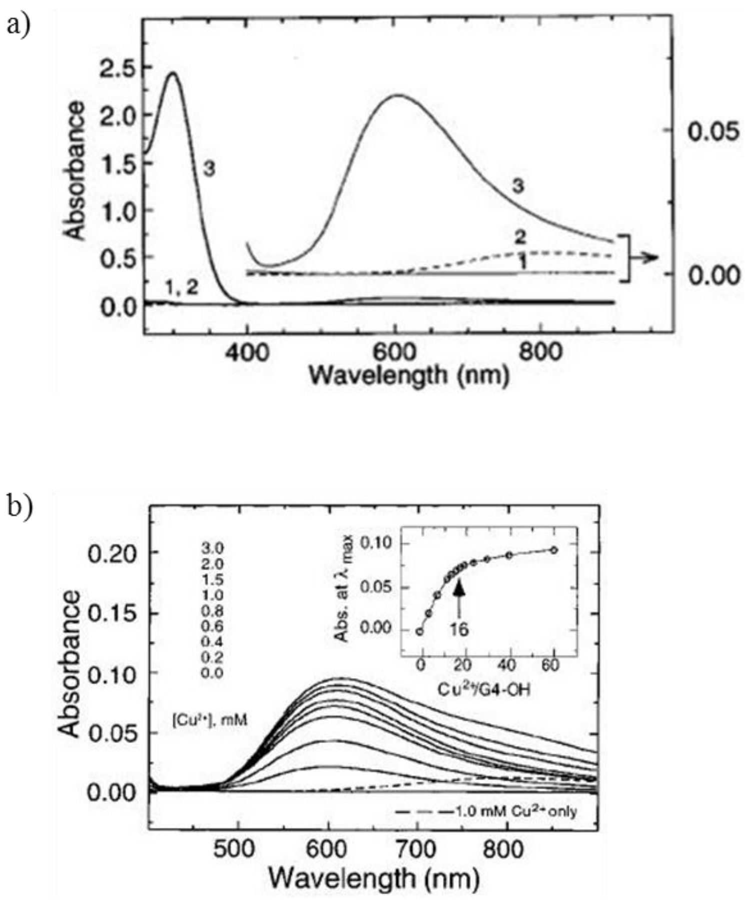

Figure 2.4 Absorption spectra of $CuSO_4$: in the presence (solid line, curve 3) and in the absence (dashed line, curve 2) of G4-OH. Curve 1 is the absorption spectrum of G4-OH vs water [67,99] (a) and as a function of the Cu^{2+}/G4-OH ratio. The inset is a spectrophotometric titration plot showing absorbance at λ_{max} as a function of number of Cu^{2+} ions per G4-OH [44] (b).

$Cu(II)/G4-NH_2$ PAMAM dendrimer solution, were approximately 4.8 nm in diameter, suggesting that Cu adsorbed by amine terminal groups aggregates into large particles outside the dendrimer structure.[93]

The ability of Cu to complex with various functional groups of the dendrimer is a subject of a great debate in literature. For example, FTIR spectra showed that after addition of Cu(II) to a $G3-NH_2$ aqueous solution, the Amide II band at 1543 cm^{-1} weakened while the C=O stretching mode (Amide I) at 1648 cm^{-1} shifted to 1637 cm^{-1}, suggesting that Cu coordinates to nitrogen or oxygen atoms of amide groups.[93] In contrast, DFT calculations suggest that oxygen atoms in amides have a higher affinity to protons than nitrogen atoms, suggesting that Cu^{2+} cations would rather bind to oxygen than to nitrogen in amides.[94-96] Furthermore, computational calculations reported for complexes of Cu^{2+} with the $G0-NH_2$ and G0-OH dendrimers showed that Cu^{2+} cations prefer forming tetracoordinated complexes in which two tertiary amine groups and the oxygen sites of the two amide groups are involved.[96,97] In addition, the formation of bidentate complexes with the two amide sites alone is quite possible.[96,97] Finally, EXAFS data suggest that Cu^{2+} cations can form octahedral complexes involving only the tertiary amine groups of $Gx-NH_2$ PAMAM at pH 7.0, suggesting that the solution pH can alter the coordination of Cu^{2+} cations to the amine/amide functional groups (Fig. 2.5).[98]

2.5 pH effect on dendrimer protonation

Considerable efforts have been dedicated to understanding the properties of PAMAM dendrimers in acidic solutions. Dendrimers as weak polyelectrolytes that are

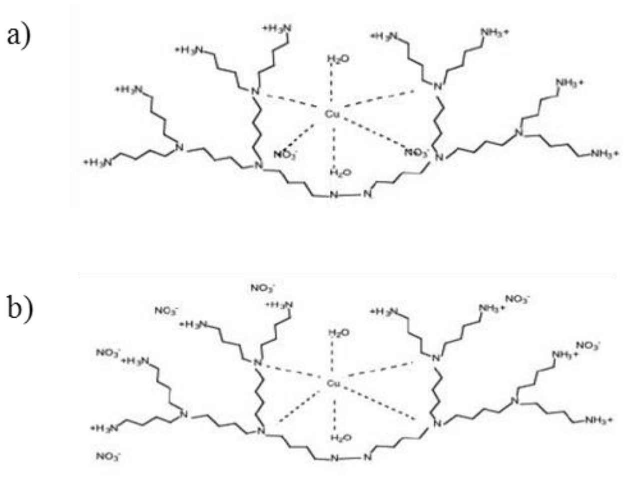

Figure 2.5 Postulated mechanisms of Cu^{2+} uptake by Gx-NH_2 PAMAAM dendrimers in aqueous solutions containing NO_3^- counter ions at room temperature and neutral pH ($6.0 < pH < 9.0$).[100,101]

only partially ionized so that their charge varies with the solution pH.[102-104] For instance, the acid-base equilibrium in the dendrimer solution follows:

$$NR_xH_{3-x} + H^+ \leftrightarrow NR_xH_{4-x}^+$$

where x = 1, 2, or 3 for primary, secondary, or tertiary amines, respectively.[105,106]

The primary and tertiary amine groups of the dendrimer are characterized by different pK_a values. Primary amines are more basic than the tertiary ones and, therefore, are characterized by higher pK_a values.[107] Protonation mechanisms proposed for Gx-NH_2 PAMAM dendrimers suggest that at pH ~ 7.0 not only primary but some tertiary amines are also become protonated (Fig. 2.6).[108,109] Although theoretically derived protonation models were used in these reports for the analysis of experimental titration data, they were not validated by independent experimental measurements and/or calculations. On the other hand, Diallo et al. determined pK_a values for tertiary and primary amine groups from inflection points of titration curves obtained for solutions of different dendrimers. For example, pK_a values characterizing the tertiary amine groups in G3-NH_2, G4-NH_2, and G5-NH_2 PAMAM dendrimers were found to be 6.52, 6.85 and 7.16, respectively, consistent with earlier literature reports.[109] In contrast, pK_a values for terminal NH_2 groups in same dendrimers were found to be 9.90, 10.29, 10.77, respectively, and these values are for 1–1.5 units larger than those reported previously.[100,108,109]

Several attempts were made to understand the dependence of dendrimer structure on the degree of protonation.[110,111] The mean-square radius of gyration (R_G^2) provides a quantitative characterization of the dendrimer size. Significant molecular swelling, reflected by a significant increase in the radius of gyration R_G, has been repeatedly

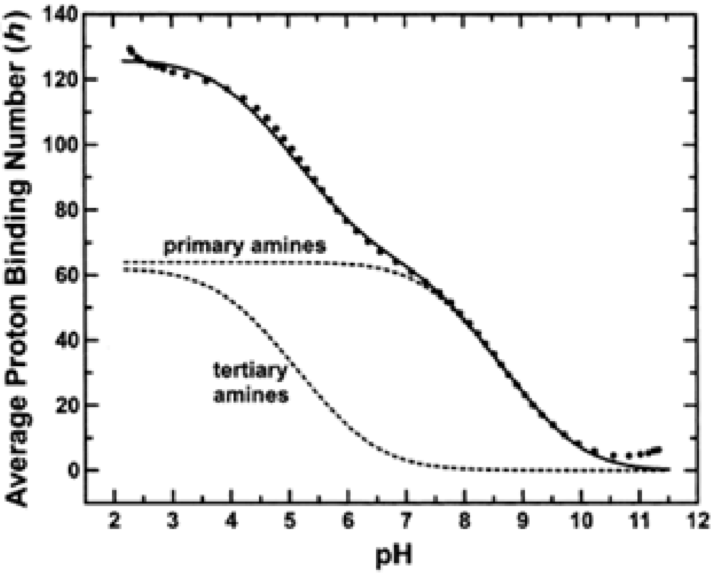

Figure 2.6 Proton binding curve for the G4-NH_2 dendrimer plotted as the average proton binding per dendrimer number vs pH. The circles represent experimental data, the solid line is the best theoretical fit to the experimental data, and the dashed lines are shell-level binding curves for the outermost shell of 64 primary amine sites; all the inner shells contain a total of 62 tertiary amine sites.[109]

predicted by computational investigations, regardless of the difference in the detailed simulation algorithm.[112,113] However, such swelling behavior was not observed experimentally since no obvious changes in R_G have been reported.[114,115] For example, when a neutral generation 4 (G4) dendrimer is progressively charged to its fully protonated state, an increase in R_G smaller than 4% has been revealed through the quantitative small angle scattering (SANS) data analysis.[110] Despite the similarity in size, there are dramatic changes in the conformations. For example, the conformation at basic pH has a "dense core" with maximum density at the dendrimer core and uniform void spacings, whereas ion pairing (strong intramolecular hydrogen bonding within the dendrimer-water-counter ion systems) at acidic pH leads to a "dense shell" with maximum density at the dendrimer periphery but non-uniform void spacings.[71,111,115] The fact that the dendrimer is protonated and has maximum density at the core for basic pH, suggests that under basic conditions it would be easier for a metal cation to penetrate through the dendrimer shell and enter its interior.

2.6 pH effect on complexation

Several literature examples demonstrate how the protonation of dendrimers can have an effect on the metal/dendrimer coordination. For instance, EPR data suggest that at low pH values, Cu^{2+} cations compete with protons for binding sites of amine terminated PAMAM dendrimers. Progressive penetration of Cu^{2+} ions into the dendrimer structure occurs with an increase in pH.[116,117] Furthermore, the size of the metal nanoparticles formed strongly depends on the solution pH.[94] Fig. 2.7 displays HRTEM images of Cu/G0-NH_2 at various pH values. At pH = 3, the average diameter of Cu

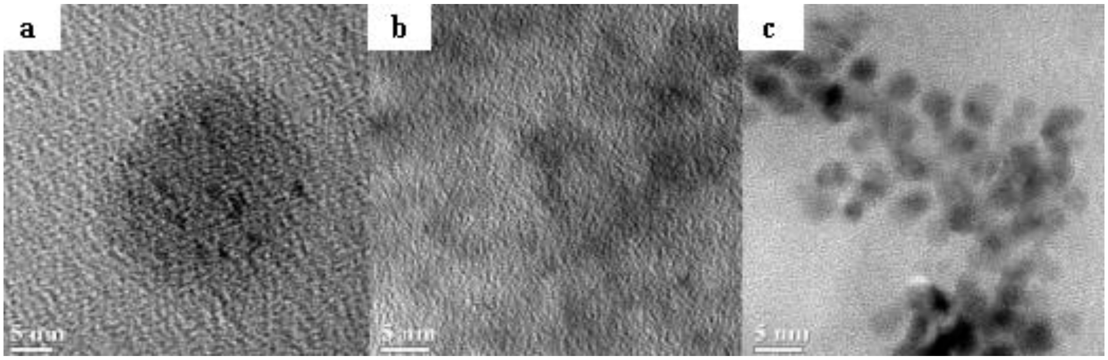

Figure 2.7 HRTEM images of Cu/G0-NH_2 nanoparticles formed upon UV irradiation at pH = 3.0 (a), pH = 7.8 (b), and pH = 11.0 (c).[94]

nanoparticles formed is ~1 nm and the nanoparticles are clearly isolated from each other. As the solution becomes more basic, the average size of the Cu nanoparticles increases. At pH = 11, the nanoparticles have an average diameter of ~3 nm, larger than the size of the G0-NH_2 dendrimer itself.[94] On the other hand, an average size of Pt/G6-OH nanoparticles does not depend on the solution pH. For instance, the average diameter of G6-OH(Pt_{147}) at pH 10 is 1.7 ± 0.4 nm, while at pH 7, the size of the DENs is essentially the same: 1.8 ± 0.4 nm.[118]

The pH-induced conformational changes combined with protonation/ deprotonation data suggest that encapsulation/release of metal cations by the dendrimer in solution can be controlled by pH.[42,119] For example, it was shown that when the pH of $Cu(NO_3)_2$/G4-OH solution was increased from 5.0 to 7.0, an almost 50% increase in the absorbance at 300 nm was observed. These data suggest that the solution pH regulates the number of Cu^{2+}/dendrimer contacts and, therefore, the number of Cu^{2+} cations complexed with tertiary amines of the dendrimer (Fig. 2.8).[101] However, the following decrease in the absorbance observed at pH 9 can be attributed to the low degree of $Cu(NO_3)_2$ ionization in this pH range.[102,120]

Many literature examples demonstrate that dendrimers are capable of complexing metal cations even under acidic conditions, when their primary and tertiary amines are completely protonated. Although it is not clear how the complexation is taking place, a possible explanation can be that depending on the nature of the metal cations added to the dendrimer solution at low pH values, the initially protonated tertiary amines can be partially deprotonated. For example, Balogh et al. carried out potentiometric titrations of PAMAM-NH_2 dendrimers and their Ag^+ complexes at two different Ag/dendrimer molar

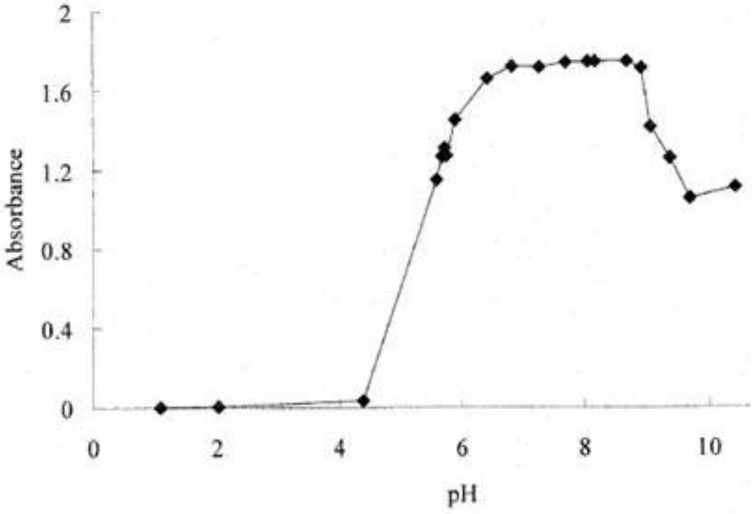

Figure 2.8 UV-vis absorbance for different pH values at 300 nm for Cu^{2+}/G4-OH.[101]

ratios (Ag^+/dendrimer = 30:1 and Ag^+/dendrimer = 45:1).[121] These authors showed that the complexation of Ag^+ to the PAMAM-NH_2 dendrimer induces deprotonation of the nitrogen binding sites, which is reflected in the different shape of the curves related to titration of the dendrimer in the absence (circles) and presence (squares and triangles) of silver ions (Fig. 2.9). Comparison of both titration curves reveals that binding of Ag^+ ions to PAMAM-NH_2 occurs in the pH range of 2.8-7.

The effectiveness of the complexation process can be expressed by the extent of binding (EOB) [i.e., number of moles of bound metal per mole of dendrimer], the fractional binding (FB) [i.e., % of metal bound to the dendrimers], and the retention (r) of metal cations, which are given by:

$$EOB = \frac{M_b}{C_d}; \qquad FB = 100 \cdot \left(\frac{M_b}{M_0}\right); \qquad M_b = M_0 - M_a; \qquad r = 100 - FB$$

where M_b (mol/L) is the concentration of metal after dialysis (strongly bound to the dendrimer), M_0 (mol/L) is the concentration of metal before dialysis, M_a (mol/L) is the metal concentration inside the dialyzed solution, and C_d (mole/L) is the concentration of dendrimer in solution.[100,122,123]

Literature data available for Pt/G4OH nanocomposites show that the actual number of Pt atoms strongly bound to G4-OH is less than the nominal $(Pt^{2+})_n$/G4-OH ratio. Moreover, for $n < 30$, 5-10% of Pt remains weakly bound or unbound with G4OH, while at higher $(Pt^{2+})_n$/G4-OH ratios ($n > 30$), the solution contains a significant fraction of weakly bound or unbound $PtCl_4^{2-}$ (Fig. 2.10(a)).[91] Furthermore, Diallo et al. showed that both EOB and FB of Cu^{2+} in aqueous solutions of Gx-NH_2 PAMAM dendrimers go through a maximum as the metal ion loading increases.[100,122] Maximum EOB values for the G_x-NH_2 dendrimer (where x = 3 – 8) were observed at pH of 5.9 - 6.1. However, no

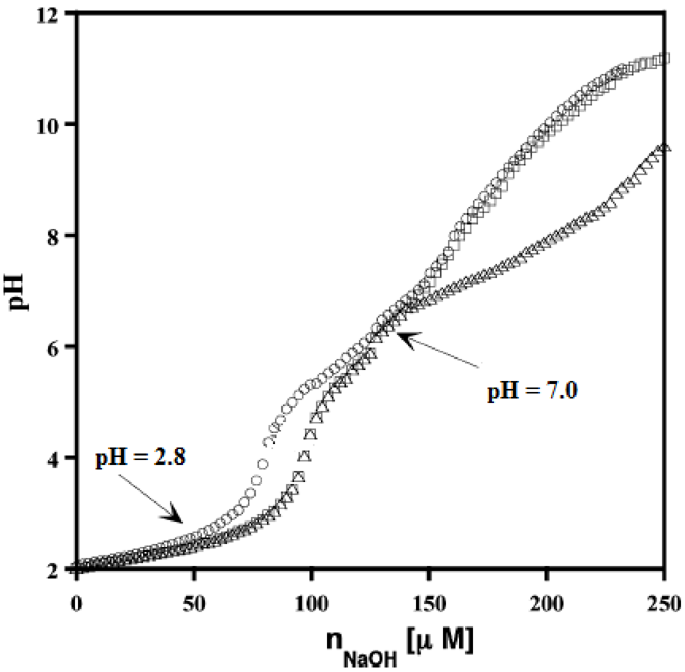

Figure 2.9 Potentiometric titration curves of PAMAM-NH_2 (circles), Ag^+/PAMAM-NH_2 = 30:1 (squares), and Ag^+/PAMAM-NH_2 = 45:1 systems (triangles).[121]

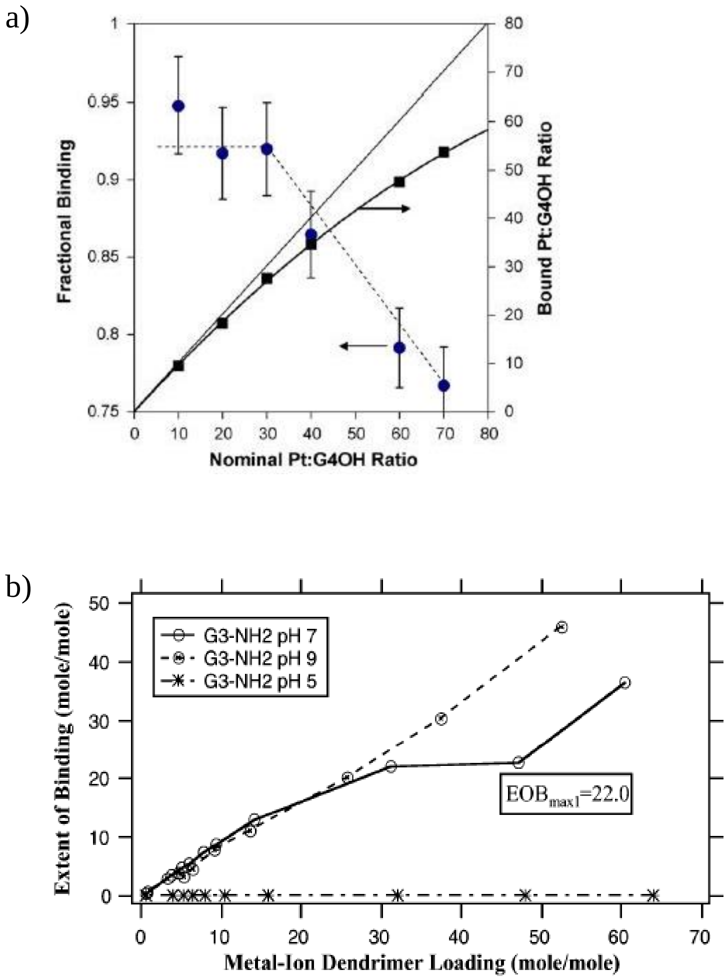

Figure 2.10 Fractional binding of Pt in $(Pt^{2+})_n$/G4-OH solutions (circles, left axis) as a function of nominal Pt:G4-OH ratio (n), as calculated from AA results. The actual number of bound Pt atoms per G4-OH molecule is also plotted (squares, right axis). The solid diagonal shows the expected trend if all Pt atoms from the precursor were bound [91] (a), Extent of binding and fractional binding of Cu^{2+} cations in aqueous solutions of PAMAM dendrimers as a function of metal ion-dendrimer with pH adjustments at room temperature [45,100] (b).

binding of Cu^{2+} cations was observed at lower pH values as the nitrogen binding sites of the dendrimer become protonated. These results clearly illustrate the effect of metal ion-dendrimer loading on EOB. As this loading increases, the number of Cu^{2+} cations available for binding increase. However, the number of nitrogen binding sites decrease as they become protonated. The net result of these two opposing effects is that the EOB, of Cu^{2+} cations, goes to a maximum in aqueous solutions of PAMAM dendrimers as copper-dendrimer loading increases.[122]

Increasing the metal-ion/dendrimer solution pH is possible to lead to an increase of the EOB of the metal cations, which can be attributed to the low extent of protonation of the dendrimer amine groups. For instance, by adjusting the pH of the Cu^{2+}/PAMAM dendrimer solution to 9.0 (Fig. 2.10(b)), the EOB of Cu^{2+} increases linearly with increasing metal ion-dendrimer ratio and 100% of the Cu^{2+} cations are bound to the dendrimer. A more complex metal cation uptake behavior is observed at pH = 7.0. In this case, the EOB of Cu^{2+} in aqueous solutions of the Gx-NH_2 PAMAM dendrimers goes through a series of two distinct binding steps as metal ion-dendrimer loading increases.[45,100] Moreover, the EOB of Ag(I), Fe(III) with G4-NH_2 PAMAM dendrimers for different metal ion-dendrimer loading is maximum for pH 11 and 7, respectively (Fig. 2.11).[65] The same trend is followed by the Co(II)/G4-NH_2 and Ni(II)/G4.5(COONa) solutions, since their EOB is maximized at pH 11 and 9, respectively.[65]

However, there are some metals capable of interacting strongly with dendrimers even under acidic conditions. For example, Schuster et al. observed, for acidic pH, significant binding of Hg(II) to water-soluble benzyolthiourea modified PAMAM (BTUPAMAM) dendrimers (Fig. 2.12(a)).[123] Moreover, Diallo et al. showed that at pH 3

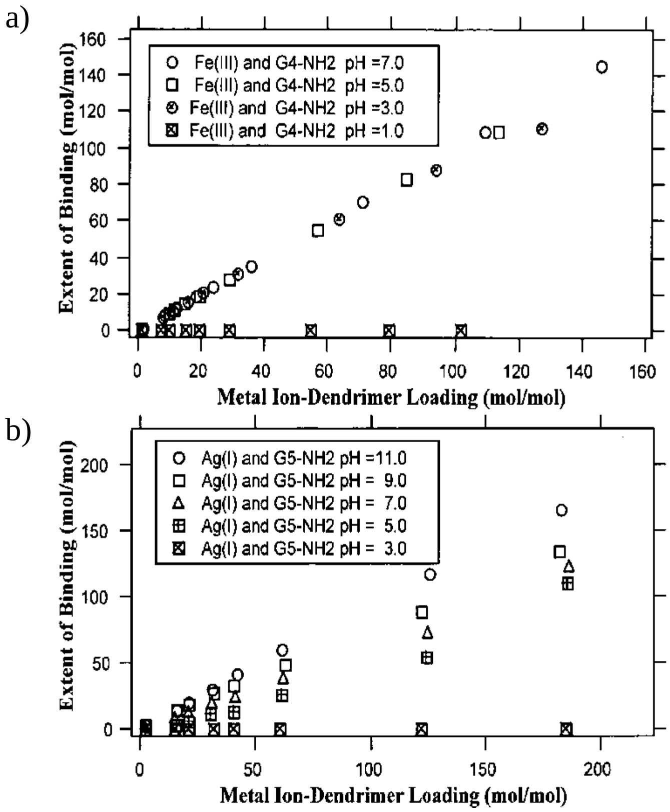

Figure 2.11 Extent of binding of Ag(I) (a) and Fe(III) (b) in aqueous solutions of PAMAM-NH_2 dendrimer at room temperature as a function of solution pH and metal ion dendrimer loading.[45,55,65]

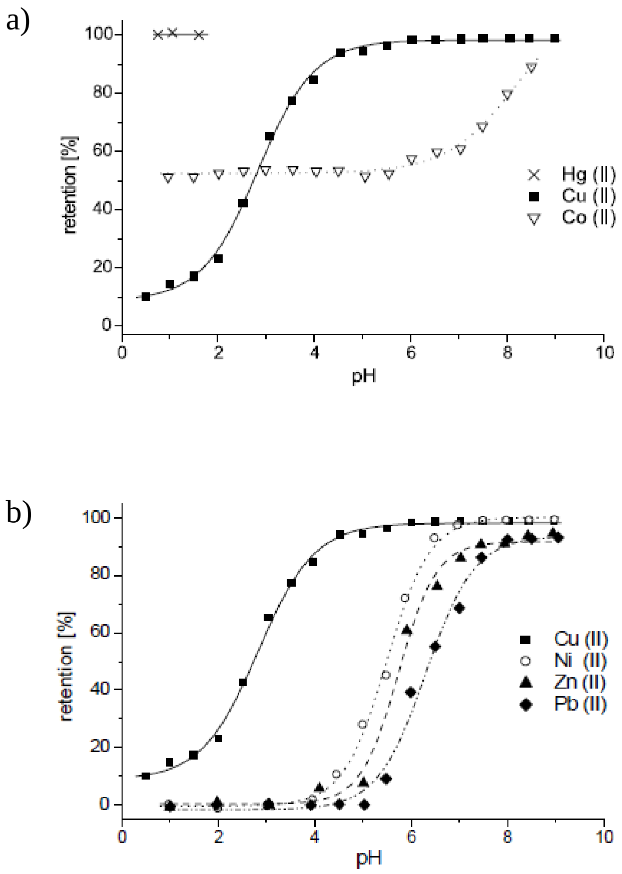

Figure 2.12 Retention profiles of Hg(II), Cu(II), Co(II) (a) and Cu(II), Ni(II), Zn(II) and Pb(II) (b) as a function of pH (polymer: benzoylthiourea modified PAMAM dendrimer).[123]

U(VI) strongly bound to the G4-NH_2 PAMAM dendrimer (with FB ~ 76-87%) even though its tertiary and primary amine groups are fully protonated. This strongly suggests that the complexation of Hg(II) and U(VI) by BTUPAMAM and G4-NH_2 PAMAM dendrimers, respectively, under acidic conditions involves the deprotonation step which is followed by coordination of metal cations.[55,123] The FB of U(VI) to the G4-NH_2 PAMAM dendrimer at pH 3.0 is slightly lower than at pH 7.0, which is attributed to a slight decrease in the number of available coordination sites due to the expansion of the fully protonated PAMAM dendrimer in aqueous solution at pH 3.0. This hypothesis is consistent with studies of the conformation of a G4-NH_2 PAMAM dendrimer in aqueous solutions, showing a 4% increase of the dendrimer radius of gyration (R_G) in aqueous solutions at pH ~ 4.5.[45,55]

While mercury and uranyl are strongly bound to the PAMAM dendrimers and can be retained quantitatively even in a strongly acidic media, the complexation of Co(II), Cu(II), Hg(II), Ni(II), Pb(II) and Zn(II) metal cations depends on the pH of the solution. Based on the retention curves shown in Fig. 2.12(b) Cu(II) can be completely retained at pH $\geq$ 4. In contrast to Cu(II) and Hg(II), nickel, lead, and zinc are not bound below pH 4 but are almost completely retained at pH > 7. Moreover, a distinct retention profile was observed for cobalt. At least 50% of Co(II) is bound to the dendritic complexing agent over the entire pH range. In solutions with pH > 7, the amount of metal cations retained by the membrane is increased up to 90%.[123]

Despite the fact that Ag(I), Fe(II), Co(II), Ni(II), Hg(II), and U(VI) can be retained inside the dendrimer solution in the specific pH range, there is no information available in the literature specifying what functional groups of the dendrimer interact with these metal cations.

2.7 Formation of metal nanoparticles in solution

Several experimental facts are believed to show the formation of metal nanoparticles in solution. For instance, a color change of the G4-OH-Pt(II) complex solution after reduction with $NaBH_4$ to dark yellow considered to be an indication of the formation of Pt^0 nanoparticles (~1.5 nm).[69,85,87] XPS of the DENs deposited onto Au, showed that prior the solution reduction the $Pt(4f_{7/2})$ and $Pt(4f_{5/2})$ peaks are present at 72.8 and 75.7 eV, respectively, but after reduction they shift to 71.3 and 74.4 eV, respectively, which is consistent with the change in oxidation state from +2 to 0.[87] In contrast, XANES and EXAFS data collected for G4OH-$(Pt^{2+})_{40}$ and G4OH-$(Pt^{4+})_{40}$ aqueous solutions treated with $NaBH_4$, showed that when $NaBH_4$ was used as the reducing agent, the local environment of Pt in the final solution was nearly identical to that in the starting solution before exposure to the reducing agent.[124] Treatment with H_2 of G4OH-$(Pt^{4+})_{40}$ showed a relatively small Pt-Pt contribution with a coordination number of 1.3, which is increased to 2.6 after 48 h reduction in H_2.[124] On the other hand, Crooks et al. used EXAFS on reduced with H_2 G6-OH(Pt_{100}) and G6-OH(Pt_{200}) solutions of wet DENs for 20 h, showed no changes in the Pt-Pt CN, indicating that no further reduction occurs for these DENs in the presence of an aqueous solution saturated with H_2.[90] The reduction of wet and dry samples of G6-OH$(Pt^{2+})_n$ DENs with $NaBH_4$ showed that only 14% of the total number of encapsulated Pt^{2+} ions are reduced during the preparation of G6-OH(Pt_{55}) DENs.[90]

Furthermore, XPS data of dendrimer encapsulated Rh_{30} nanoparticles (reduction with $NaBH_4$) showed that only 56% Rh was metallic. The remaining portion of Rh was oxidized due to air exposure during the preparation of the sample for XPS measurements and/or incomplete reduction of $RhCl_3$ during the synthesis.[88] This is consistent with Rh *K*-edge XANES data (Fig. 2.13), indicating that the white line area decreased only slightly after the treatment with $NaBH_4$ and suggesting that the clusters formed in the Rh/G4-OH solution incorporate Rh in a cationic form.[88]

There some indications in literature that reduction of Cu^{2+}/G3-NH_2 solution can lead to the formation of Cu nanoparticles. For example, the Cu^{2+}/G3-NH_2 solution color changed immediately upon reduction from pink or blue to golden brown and the broad absorption band centered at 535 nm was replaced by a monotonically increasing spectrum of nearly exponential slope towards shorter wavelengths.[93] Similarly, a golden brown solution was formed upon reduction of DAB-Am_n-$Cu(II)_x$ (where n = 4 – 64 and x = n/2) with $NaBH_4$. UV-vis spectra further suggest that the reduction process goes to a completion in this case because the characteristic d – d band of Cu(II) species typically observed at 630 nm disappeared from the spectrum.[125] Moreover, similarities between EXAFS spectra of the reduced DAB-Am_n-$Cu(II)_x$ complexes and that of the copper foil demonstrate the existence of metallic Cu(0) domains in the reduced DAB-Am_n-$Cu(0)_{cluster}$ (Fig. 2.14).[125] Unfortunately, this study does not reveal any information concerning the oxidation state of Cu(II) in solution. Based on these observations it can be noted that there is no detailed information regarding the reduction of copper cations in the presence of PAMAM dendrimers or other nanoparticle stabilizer in solution.

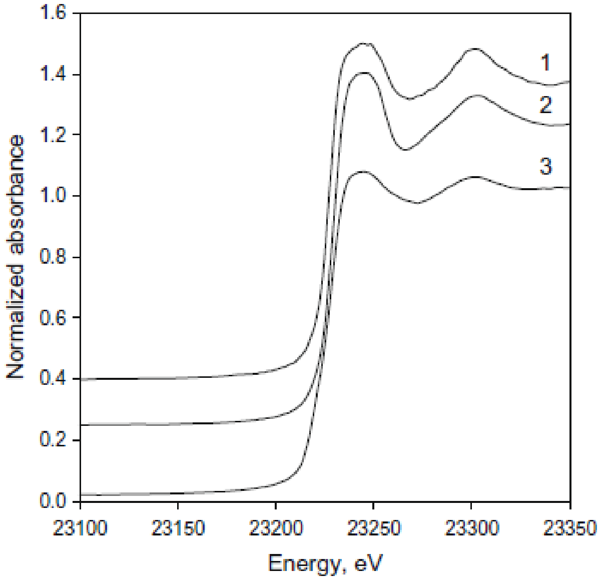

Figure 2.13 XANES spectra of (1) $RhCl_3$ in aqueous solution, (2) $(Rh^{3+})_{20}$/G4-OH in aqueous solution, and (3) $(Rh^{3+})_{20}$/G4-OH treated with $NaBH_4$ in aqueous solution.[70]

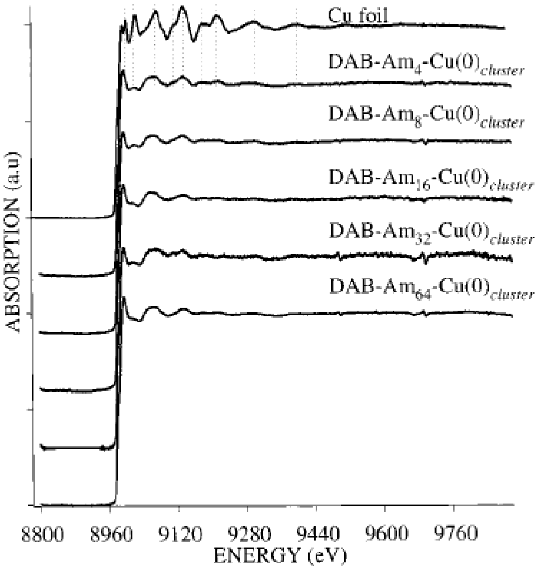

Figure 2.14 EXAFS spectra of the reduced DAB-Am$_n$-Cu(II)$_x$ (n = 4 to 64, x = n/2) complexes and Cu foil.[125]

2.8 Ag Monometallic Dendrimer Stabilized Nanoparticles

Colloidal silver has attracted considerable attention because of potential applications in areas such as photography, biological labeling, photonics, nanoelectronics, optical filter, surface-enhanced Raman scattering (SERS) detections, and catalysis.[80,126] More than 700 tons of silver are used annually in the world for the oxidation of methanol to formaldehyde and ethylene to ethylene oxide because both of these products are essential to the plastic industry.[80,127,128] Since the catalytic activity of metal nanoparticles depends greatly on their dimensions, it is essential to develop a preparation method that yields silver nanoparticles with well-controlled sizes and shapes.

2.8.1 Chemical Reduction Methods

The most common method of producing silver nanoparticles (Ag NPs) is the chemical reduction method, which involves the use of a soluble silver salt, a stabilizer, such as polymers, and a reducing agent, such as $NaBH_4$, citrate, glucose, hydrazine, or ascorbic acid.[38,129,130] The reducing ability of the reducing agent determines the kinetics of the formation of these nanoparticles. For instance, strong reductants (e.g., borohydride, hydrazine) can lead to small, somewhat monodisperse particles, while the nanoparticles obtained by reduction with weaker reducing agents (e.g., citrate, irradiation) tend to be more polydispersed in size.[131-133] Martínez-Castañón et al. using a template less chemical reduction method, synthesized micro-sized silver particles with a wide particle distribution (1.5μm – 15μm) and with polyhedron and dendritic morphologies, by simply changing the amount of ascorbic acid added to the reaction.[129]

Aqueous solutions of sodium borohydrite and silver nitrate are used most often to form silver nanoparticles in solution. Hydrogen gas is produced by the reduction of silver ions (Eq. 1) as well as the slow reduction of water by sodium borohydrite at room temperature (Eq. 2).[134,135]

$$Ag^{+} + BH_4^{-} + 3H_2O \rightarrow Ag + H_3BO_3 + \frac{7}{2}H_{2(g)} \qquad \text{(Eq. 1)}$$

$$BH_4^{-} + 3H_2O \rightarrow H_2BO_3^{-} + 4H_{2(g)} \qquad \text{(Eq. 2)}$$

To avoid the oxidation of borohydrite at room temperature (Eq. 2), sodium borohydrite solution must be freshly prepared. Purging the solution with an inert gas, such as nitrogen, is the commonly used method of minimizing oxygen in the solution.[134]

Unfortunately, the size and shape of Ag NPs that are synthesized by the chemical reduction method is not always reproducible. Moreover, the reducing agents that are used for the synthesis of silver nanoparticles are often associated with environmental toxicity or biological hazards.[133] Therefore, it desirable to develop green synthetic routes for silver nanoparticles using extracts of bio-organisms as capping and/or reducing agents (e.g, polysaccharides, polyphenols, tollens agent, irradiation, biological reduction, and polyoxometalate). However, understanding the mechanism by which these biomolecules could be involved in the synthesis is lacking.[80,136]

2.8.2 Polymers as silver nanoparticle stabilizers

An attractive alternative is to generate metal nanoparticles by utilizing reagents which can act both as reducing and stabilizing agents. Shumaker-Parry et al. examined the synthesis of AgNPs using poly(allylamine) (PAAm) as a stabilizing and reducing agent, so that additional reducing agents can be avoided from the system. TEM analysis confirmed the formation of nanoparticles with an average diameter 4.4 ± 0.9 nm.[137] Recent studies have shown that polyethylene glycol (PEG) can act both as the stabilizer and the reducing agent for silver nanoparticles through the oxidation of hydroxyl groups of PEG to aldehyde groups ($CH_2CH_2OH \rightarrow CH_2CHO$). However, this method leads to relative large silver nanoparticles with sizes in the 4 – 20 nm range.[138] It was also suggested that PVP promotes the nucleation of metallic silver because silver ions can be reduced by the lone pair of electrons which is present on both nitrogen and oxygen atoms in the PVP molecule.[139-141] Meanwhile, the particles prepared by this method are usually irregular in shape (e.g. spheres, dendrites, nanoprisms) and their size would be larger than 20 nm.[126,142,143]

2.8.2.1 Dendrimers as silver nanoparticle stabilizers

Recently, dendrimer templating synthesis of silver nanoparticles has been developed because of dendrimer's unique structures, properties and their ability to complex a great variety of ions in their interior.[144] Unfortunately, the size of the silver nanoparticles obtained via this route was larger than 10 nm, much larger than the dendrimer itself, indicating that silver nanoparticles are not formed inside the dendrimers.[145] For example, Kakkar et al. suggested that the terminal hydroxyl groups of the 3,5-dihydroxybenzyl alcohol (DHBA)-based dendrimers can reduce the silver cations, leading to the formation of > 15 nm silver nanoparticles in solution.[146] Furthermore, Sun et al. reported the formation of ~ 10 nm silver nanoparticles by direct heating of $AgNO_3$/G3-PPI aqueous solution in a microwave oven.[147] Finally, silver nanoparticles with 26 nm diameter were synthesized by a heat treatment of a third-generation poly(propyleneimine) dendrimer $AgNO_3$/G3-PPI without using an additional reducing agents.[148]

2.8.2.1.1 PAMAM Dendrimers as silver nanoparticle stabilizers

The morphology of silver nanoparticles in solution depends on the stabilizer that is used (Fig. 2.15).[126] For instance, the morphology of PVP protected silver reduced with H_2 was found to be dendritic (Fig. 2.15(a)), while discrete Ag nanoparticles were obtained when G1.5 PAMAM was added as a co-protective agent in the Ag/PVP solution (Fig. 2.15(b)). When only G1.5 PAMAM dendrimer was used as a protective agent (Fig. 2.15(c)), the mean diameter of silver nanoparticles was determined to be 7.85 nm, much larger than the diameter of the G1.5 PAMAM dendrimer.[126] Moreover, when a small silver/dendrimer ratio is used, small Ag nanoparticles can be formed is solution. This observation was regarded as an indication for the formation of Ag nanoparticles in the dendrimer interior. A characteristic example is the formation of small silver nanoparticles (0.48 – 2.3 nm), when Ag/G5-OH solution was reduced using ultraviolet irradiation. The Ag nanoparticles formed were evidently much smaller than the diameter of the G5-OH dendrimer (4.5nm).[149] Furthermore, relatively small Ag nanoparticles (3.96 nm) have been synthesized using a 1,8-naphthalimide-labelled PAMAM dendrimer (PAMAM-N), which is a non-commercially available derivative of PAMAM dendrimers.[150] Unfortunately, there are no experimental data confirming the formation of Ag/dendrimer complexes in solution.

While dendrimers cannot complex silver nanoparticles, they are capable of stabilizing silver colloids.[151] For example, Prasad et al. reported the preparation 20 nm silver nanoparticles by amine terminated PAMAM dendrimers in the absence of reducing agents.[152] Furthermore, Esumi et al. reported the preparation of 5.6 – 7.5 nm silver/dendrimer nanocomposites in aqueous solutions containing G3-5 PAMAM-NH_2

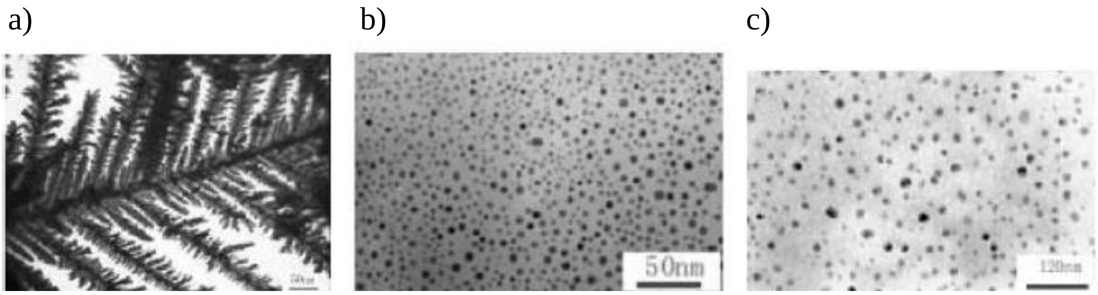

Figure 2.15 The TEM micrographs of Ag nanoparticles when the molar ratios of PVP, G1.5 PAMAM dendrimer and $AgNO_3$ was 2:0:1 (a), 1:1:1 (b) and 0:1:2 (c), respectively.[126]

dendrimers. In the latter example, the solution was reduced with $NaBH_4$ and the result suggest that the use of a reducing agent may lead to the formation of smaller Ag nanoparticles.[153]

In order to avoid a possible complexation of silver cations with the terminal functional groups of the dendrimer, Malý et al. selected PAMAM-OH dendrimers as a model system, since their motivation was to form nanoparticles inside the polymeric shell. Silver dendrimer nanocomposites were synthesized by mixing (G5-7)-OH PAMAM dendrimers with $AgNO_3$ followed by reduction with $NaBH_4$. The UV-vis spectra of the PAMAM-OH G7 dendrimer after the addition of several different concentrations of Ag^+ showed that a novel peak emerged at $\lambda_{max} \approx 410$ nm, indicating the formation of silver nanoparticles.[71] TEM images of Ag-dendrimer nanocomposites (DNCs) showed individually resolved and homogeneously distributed Ag nanoparticles which differ in the average diameter (3.12 – 7.58 nm) depending on the Ag^+/dendrimer ratio and the generation of dendrimer used.[71] Finally, silver nanoparticles (~15 nm) larger than the diameter of the dendrimer (~2.5 nm) were formed, when $Ag/G1.0(OH)_{16}$ nanocomposites were treated with $NaBH_4$ or hydrazine in solution.[154]

Another indication that Ag cannot complex with dendrimers is the fact that Ag nanoparticles aggregate to larger particles, especially when the silver concentration in the solution is increased.[78,155] The formation of Ag NPs is typically confirmed by UV-vis or TEM data.[156] For example, Imae et al. synthesized $Ag/G4\text{-}NH_2$ nanocomposites with average Ag particle sizes in the 6.2 – 12.2 nm range, depending on the silver/dendrimer ratio used. The wide nanoparticle distribution combined with the fact that the particle size obtained was larger than the diameter of $G4\text{-}NH_2$ indicate that the silver nanoparticles were not formed within the dendrimer interior.[61] Furthermore, Fig. 2.16 shows that the intensity of UV-vis spectra at 433 nm was increased for 8 h, indicating the formation and growth of Ag nanoparticles in solution. XPS measurements showed that Ag was fully reduced inside the solution.[74] Furthermore, when the molar ratio of Ag/dendrimer was decreased from 30 to 10, the average particle diameters were increased from 1.4 to 7.1 nm.[74]

2.8.2.1.2 Intradendrimer Displacement Reactions

Although it is not possible to prepare Ag particles inside Gn-OH dendrimers by direct loading of metal cations into the dendrimer interior, stable Ag DENs can be prepared by a metal displacement reaction, which is a more challenging synthetic procedure (Fig. 2.17).[44,60,78] In this approach, DENs prepared from a particular metal, such as Cu, can be exchanged with another metal, such as Ag, Au, Pt, Pd as long as the latter is a stronger oxidizing agent than the former (Table 2.2).[60,78] The standard reduction potential E_o^r is measured under standard conditions (i.e., 25^0C, 1 atm pressure, solutes at a concentration of 1 M) and is defined relative to a standard hydrogen electrode with a potential of zero volts.[157,158]

$$2H^+ \text{ (1 M)} + 2e^- \rightarrow H_2 \text{ (g, 1 atm)} \qquad \text{(Eq. 3)}$$

Redox reactions can be divided into a reduction half-reaction and an oxidation half-reaction. If the redox potential is positive, the reaction proceeds spontaneously as written, while if the potential is negative, then the reverse reaction is spontaneous. For instance, the redox potential for the $Cu(s) + 2Ag^+_{(aq)} \rightarrow Cu^{2+}_{(aq)} + 2Ag(s)$ reaction is equal to $E_o^r = 0.80 - 0.34 = 0.46$ V, indicating that the reaction proceeds spontaneously as written.[157]

Table 2.2 Standard Reduction Potentials at 25 °C.

	Reduction Half – React	E_o^r (V)	
Weaker	$Au^{3+} + 3e^- \rightarrow Au$	1.50	Stronger
reducing agent	$Pt^{2+} + 2e^- \rightarrow Pt$	1.12	oxidizing agent
↓	$Pd^{2+} + 2e^- \rightarrow Pd$	0.95	↑
	$Ag^+_{(aq)} + e^- \rightarrow Ag_{(s)}$	0.80	
	$Fe^{3+}_{(aq)} + e^- \rightarrow Fe^{2+}_{(aq)}$	0.77	
	$Cu^{2+}_{(aq)} + 2e^- \rightarrow Cu_{(s)}$	0.34	
	$2H^+_{(aq)} + 2e^- \rightarrow H_{2(g)}$	0	
Stronger	$Ni^{2+}_{(aq)} + 2e^- \rightarrow Ni_{(s)}$	-0.25	Weaker
reducing agent	$Zn^{2+}_{(aq)} + 2e^- \rightarrow Zn_{(s)}$	-0.76	oxidizing agent

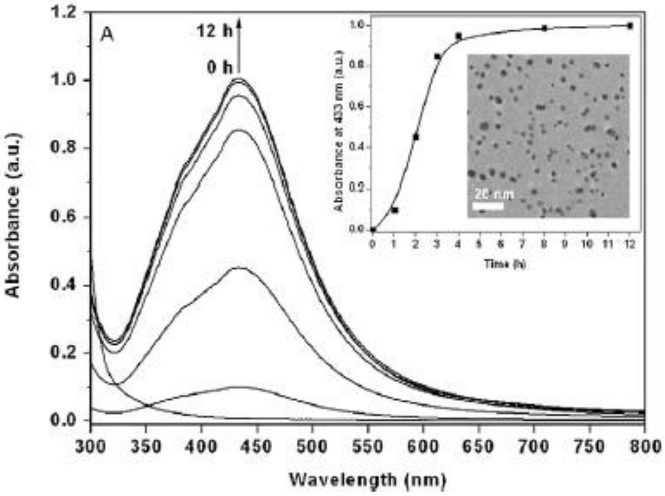

Figure 2.16 UV-vis absorption spectra of $AgNO_3$/ HPAMAM-$N(CH_3)_2$ mixture (N/Ag = 15) at the different reaction time. Inserts: relationship between reaction time and the corresponding intensity of the plasmon peaks; TEM images of corresponding nanoparticles after one month.[74]

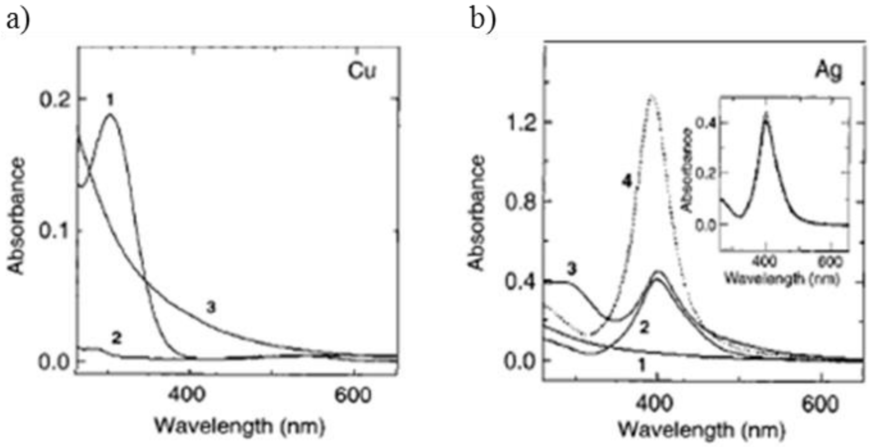

Figure 2.17 (a) Absorption spectra of aqueous $Cu(NO_3)_2$ in the presence of G6-OH before (pH 7.7, spectrum 1; pH 3.0, spectrum 2) and after (pH 7.5, spectrum 3) reduction with excess of BH_4^-. (b) Absorption spectra after addition of $AgNO_3$ to G6-OH(Cu_{55}) (spectrum 2, pH 3.0; spectrum 3, pH 7.5). Spectrum 4 was obtained 1 h after reduction with BH_4^- of Ag^+/G6-OH. The inset in (b) shows spectra obtained at different time after the displacement reaction (solid line, 10 min; dashed, 18 h).[78]

By using the intradendrimer exchange method, stable and small (~2 nm) Au nanoparticles can be prepared by the Cu exchange reaction:

$$2Au^{3+} + 3Cu^{0} \leftrightarrow 2Au^{0} + 3Cu^{2+}$$

An initially blue solution of Cu^{2+}/G5-OH turns brown after addition of $NaBH_4$, indicating the formation of Cu clusters.[159] This process must be carried out under N_2 in order to avoid the oxidation of copper inside the solution.[160] Furthermore, intradendrimer displacement reactions have been carried out for the Pt-Au system. When $HAuCl_4$ is added to an aqueous solution of (Cu_{55})/G6-OH at pH 3, a new broad absorption feature which corresponds to the plasmon resonance absorption of Au appears at ~520 nm. When the pH of this solution is increased to 7.5, a new band centered at 290 nm appears. This feature arises from the Cu^{2+}/dendrimer LMCT transition and therefore confirms the presence of both Au and Cu^{2+} within the dendrimer.[78] XPS data also confirm intradendrimer replacement of Cu by Pt: the Cu(2p) peaks originally present disappear, and new Pt(4f) peaks at 71.5 and 75.2 eV appear. HRTEM indicated that the average diameters for the Au and Pt nanoparticles are 2.3 ± 0.3 and 1.4 ± 0.2 nm, respectively.[78]

Silver DENs have also been synthesized using and intradendrimer displacement reactions. The procedure initially involves the formation of $(Cu^{2+})_{55}$/G6-OH under inert atmosphere, followed by adjustment of the solution pH to 7.5, in order to maximize the amount of copper cations complexed with the dendrimer (Fig. 2.17(a)). When Ag^{+} is added to (Cu_{55})/G6-OH solution (pH 3.0), a new absorption band centered at 400 nm appears (Fig. 2.17(b)), which corresponds to the plasmon resonance of Ag nanoparticles. When the pH of the solution is adjusted to 7.5, the Ag plasmon peak does not change much but a new peak at 300 nm appears, indicating that at pH 7.5 Cu^{2+} resides within the dendrimer. Thus, both the metallic Ag nanoparticles and the Cu^{2+} ions generated by the displacement reaction are present within dendrimers simultaneously. Ag is considered to be a stronger oxidizing agent compared to Cu (Table 2.2), that makes Ag^+ cations capable of oxidizing Cu^0 nanoparticles to Cu^{2+} while at the same time Ag^+ cations are reduced to Ag^0. This displacement method can be used to prepare other types of noble metal particles, such as Au, Pt, and Pd, because the standard potentials (E^0) of the corresponding half reactions are more positive than those for the $Cu^{2+}/Cu(s)$ system. Finally, Ag nanoparticles synthesized by primary displacement of dendrimer-encapsulated Cu nanoparticles can themselves be displaced to yield Au, Pt, or Pd nanoparticles by secondary displacement reactions.[78]

High-resolution transmission electron microscopy (HRTEM) indicates that Ag particles in the resulting (Ag_{110})/G6-OH DENs have an average diameter of 1.7 ± 0.4 nm, which is bigger than the calculated value of 1.5 nm.[78,161] This inconsistency between the observed and calculated values may be due to agglomeration of Ag particles on the Cu TEM grid. XPS data collected for these samples indicate that after exposure of (Cu_{55})/G6-OH to Ag^+ at pH 3.0, Cu(2p) peaks are absent but two new Ag peaks appear at 367.9 eV ($3d_{5/2}$) and 373.9 eV ($3d_{3/2}$). Taken together, these results confirm that the displacement of Cu by Ag is nearly complete.[78]

CHAPTER 3

SYNTHESIS OF BIMETALLIC DENDRIMER-DERIVED NANOCOMPOSITES IN SOLUTION

Nanoparticles composed of two different metals are of greater interest than monometallic ones because their catalytic properties could be completely different from those of monometallic counterparts.[43,162] For example, Fig. 3.1 shows that the bimetallic $Pt_{16}Au_{16}/SiO_2$ catalyst is more active in CO oxidation than corresponding monometallic catalysts.[163] In spite of the commercial importance of bimetallic catalysts, their active sites or phases often are not well defined and understood.[57] In general, monodisperse stable bimetallic DENs can be synthesized by co-complexation, sequential loading, and partial displacement techniques.[44,57,62]

3.1 Co-complexation Method

In the co-complexation synthesis, both metal precursors are introduced into the PAMAM dendrimer solution simultaneously. After the completion step is completed, the solution is typically treated with a reducing agent to form reduced metal nanoparticles ($M_A^0M_B^0$). Co-complexation has been used to prepare a variety of bimetallic DENs (Figure 3.2), including PdPt [164-166], PdRh [166,167], PdAu [168-170], PtAu [169], AuAg [171,172], PdCu [173,174], FePt [175], NiSn [176], AuNi [177,178], PtRu [180], AgCu [180]. In preparations of G4NH$_2$-(PdPt) and G4NH$_2$-(PdRh) DENs, the primary amine groups of

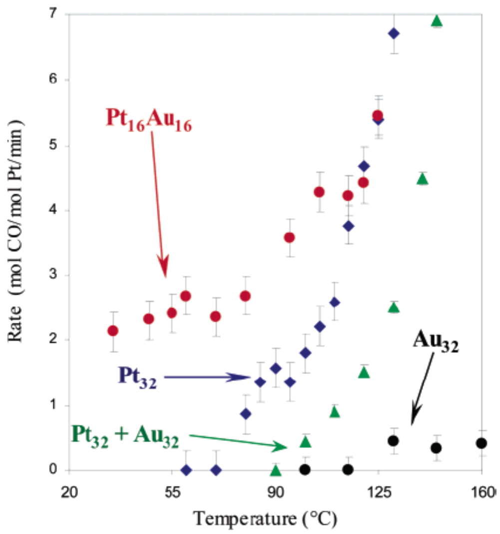

Figure 3.1 CO oxidation catalysis by silica supported Pt_{32}, Au_{32}, $Pt_{16}Au_{16}$, and Pt_{32}+Au_{32} NPs. Rate is reported as moles CO converted per total moles Pt per minute; Au_{32}, the rate is in moles CO converted per total mole Au per minute.[163]

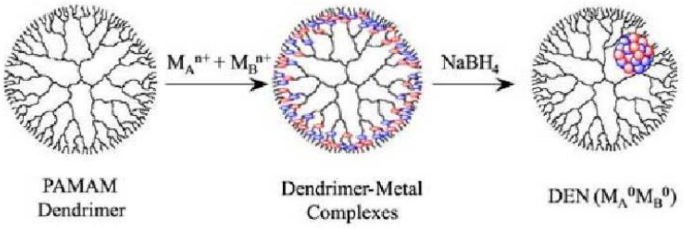

Figure 3.2 Co-complexation synthesis.[62]

dendrimer were protonated by adjusting the solution pH to 3 prior the addition of the metal precursors.[167,181,182] When the complexation step was completed (76 and 24 h for G4NH$_2$-(PdPt) and G4NH$_2$-(PdRh), respectively), solutions were treated with NaBH$_4$. PdPt DENs thus formed were found to be nearly uniform with spherical shape of metal particles having an average diameter of 2.5 nm, which is smaller than the diameter of the G4-OH dendrimer (4.5 nm).[166] Furthermore, Pt-Ru/SiO$_2$ catalysts prepared by the co-complexation method was found to be much more active for the liquid-phase hydrogenation of 3,4-epoxy-1-butene (EpB) than a conventional catalyst with a similar composition.[179]

The UV-vis spectroscopy has been used in preparations of bimetallic systems to monitor the complexation process. For example, the characteristic SPR bands at 214 and 208 nm for monometallic PtCl$_4^{2-}$ and PdCl$_4^{2-}$, respectively, disappeared after the addition of G4OH and a new band emerged at 230 nm, indicating that both metal cations are complexed with the internal functional groups of the dendrimer.[165,181] After reduction of the complexed bimetallic solution with NaBH$_4$, the band at 230 nm completely disappeared and a new broad absorption band appears over a wide range of wavelength regardless of the Pt/Pd ratio used.[181] The spectra of the resulting nanoparticles were found to be different not only from those of the monometallic Pt or Pd nanoparticles but also from those characterizing their physical mixtures, which can be attributed to the change in the dielectric function caused by mixing atoms of two different metals.[183] Furthermore, the energy dispersive spectroscopy (EDS) analysis of two individual nanoparticles indicated that the atom %'s of Pd and Pt were in a good agreement with the mol %'s of PdCl$_4^{2-}$ and PtCl$_4^{2-}$ used in the original synthesis mixture. The single-particle EDS measurements suggested that bimetallic nanoparticles (rather than physical mixtures of monometallic nanoparticles) are present within the dendrimer.[164] Finally, Crooks et al. proved the formation of bimetallic $G4NH_2(Pd_{27.5}Au_{27.5})$ nanoparticles using EDS as well, showing an average composition of 48 ± 3% Pd and 52 ± 3% Au, which is in agreement with the molar percentages of $PdCl_4^{2-}$ and $AuCl_4^-$ used in the original mixture (50% each).[8]

Unfortunately, UV-vis spectroscopy cannot always provide accurate information concerning the formation and structure of bimetallic nanoparticles. Alloying or the formation of core-shell type particles is expected to cause a shift of the surface plasmon resonance band. In the case of Au-Pt/G5.5COOH prepared by co-complexation, the shift for the gold plasmon band was not observed, although XPS data indicated that bimetallic particles are formed.[169] Specifically, small shoulders due to oxidized gold (84.5 and 89 eV) were observed and these shoulders declined in intensity after the addition of platinum while bands corresponding to the oxidized Pt species appeared in spectra. This observation showed that Au atoms withdrew some electrons from platinum atoms, suggesting that gold and platinum are not separated but coexist in one metal particle. However the structure of bimetallic particles such as core-shell, random uniform alloy, reverse core-shell, and mosaic structure, etc., cannot be determined from these results.[169]

When metal precursors are introduced simultaneously to the dendrimer, they compete with each other for binding sites. It is feasible that the most reactive complex will occupy the majority of available sites. It is possible to control this process by adding the less reactive complex first. This method was employed for preparations of PtCu DENs. In this case, $PtCl_4^-$ was allowed to interact with G5OH for 2 days before $Cu(NO_3)_2$ was added since Cu^{2+} binds to this dendrimer in a matter of minutes. The pH of the Pt^{2+} solution was adjusted to 7 before the addition of the second metal.[184] The same procedure was followed for the preparation of PdCu DENs.[174] The DEN precursor solutions exhibit strong absorptions bands at ~230 and 290 nm and an isosbestic point at 261 nm. These peaks arise from ligand-to-metal charge-transfer (LMCT) bands associated with the dendrimer/metal-ion complexes.[174] The reduction of the metal-cation/dendrimer precursor complex with BH_4^- yields DENs with diameters of metal particles in the range of 1.2 – 1.3 nm. The coordination environments of these two metals were measured by EXAFS and the formation of an alloy structure was confirmed.[174]

3.2 Sequential Loading

This method involves the initial complexation and reduction of a "seed" metal (M_A), followed by the complexation and subsequent reduction of the second metal (M_B) to produce the M_AM_B bimetallic system (Fig. 3.3). In general, the sequential loading of metals is desirable for the preparation of bimetallic DENs with core/shell structures.[57,62] Several bimetallic DENs have been prepared via this route, including AuAg [171,172], [Au](Pd) [185-187], [Pd](Au) [185,186], [Au](Ag) [172] and [AuAg](Au).[172] The prominent band at 221 nm is present in UV-vis spectra of G6-OH$(Pd^{2+})_n$ (n = 29, 60, 73, 87, and 118) prior to addition of Au^{3+} which can be assigned to a ligand-to-metal charge transfer (LMCT) between interior amines of the dendrimer and Pd^{2+} cations. It was not possible to obtain reliable UV-vis spectra of the dendrimer composite with both $PdCl_4^{2-}$ and $AuCl_4^-$, because hydroxyl groups on the surface of the dendrimer reduce the Au complex. UV-vis spectra of the DENs obtained after the complexation and reduction with BH_4^-, showed that in all cases, the absorbance increases as the wavelength decreases, which is consistent with the presence of nanoscale particles. Additionally, the LMCT band at 221 nm is absent, indicating essentially complete reduction of the Pd complex.[170] EXAFS

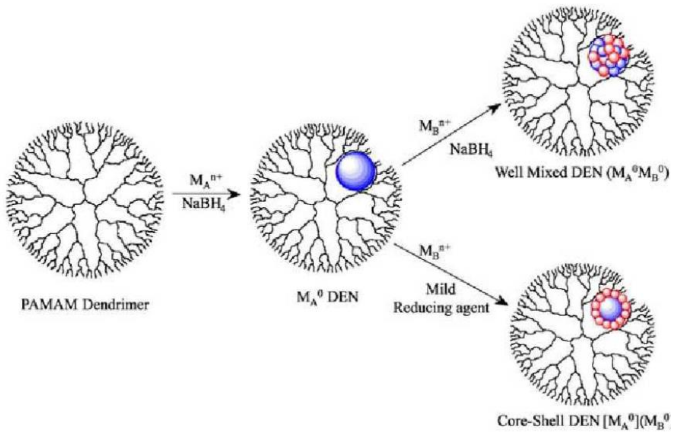

Figure 3.3 Sequential loading method.[62]

data collected for PdAu DENs suggest that more Pd atoms reside on the surface of metal particles than it would be anticipated for a random alloy. This means that the PdAu DENs are quasi-random alloys with a Au-rich core and a Pd-rich shell.[170] TEM images showed sizes of metal particles of 1.4 ± 0.3 nm for G6-OH($Pd_{118}Au_{29}$), 1.5 ± 0.2 nm for G6-OH($Pd_{73}Au_{73}$), and 1.5 ± 0.3 nm for all of the other PdAu DENs.[170] Since peripheral hydroxyl groups in this dendrimer have the sufficient reducing power to convert $AuCl_4^-$ to zerovalent Au, a quaternized PAMAM dendrimer (G6-Q_{116}) can be used for the preparation of Pd/Au bimetallic dendrimer encapsulated nanoparticles. A HRTEM micrograph of G6-Q_{116}($Pd_{75}Au_{75}$) showed that particles have an average size of 1.8 ± 0.4 nm.[186]

The UV-vis spectra of G6-OH[Pd_{55}](Au_{255}) with G6-OH(Au_{310}) and the co-complexation product G6-OH($Pd_{55}Au_{255}$) are compared in Fig. 3.4. The plasmon shoulder of the G6-OH[Pd_{55}](Au_{255}) solution is red shifted by ~10 nm as compared to that characterizing the G6-OH(Au_{310}) solution. This small shift is due to a difference in the composition and structure of these two DECs. The more important result in Fig. 3.4, however, is the absence of a plasmon shoulder arising from the co-complexation product G6-OH($Pd_{55}Au_{255}$). This result clearly indicates that there are major differences between the two types of DECs, and it is believed these differences provide strong evidence for geometrically well-defined core/shell structures arising from the sequential-loading method while alloy-like structures result from the co-complexation method.[186]

The preparation of bimetallic DENs is more challenging than the preparation of the monometallic ones, because the complexation time and the pH conditions, under which the metal/dendrimer complexation is favored, can be different between the two metals. To successfully encapsulate both metal cations within the dendrimer interior,

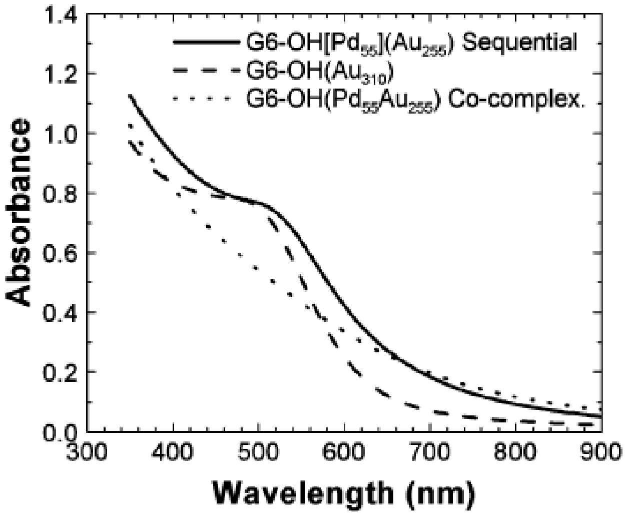

Figure 3.4 UV-vis spectra of solutions of G6-OH[Pd_{55}](Au_{255}), prepared by the sequential-loading method, and G6-OH(Au_{310}) and G6-OH($Pd_{55}Au_{255}$) prepared by the co-complexation method.[186]

their complexation time and the solution pH should be taken into consideration. For example, Ploehn et al., reported the synthesis of $(Pt^{2+})_{20}(Ru^{3+})_{20}$/G4-OH bimetallic DENs by adding K_2PtCl_4 to the G4-OH aqueous solution. The pH of the $(Pt^{2+})_{20}$/G4-OH solution decreased from 6.5 to 2.7, after 3 days of complexation. After 7 days of complexation and before the addition of the second metal, the solution pH was adjusted to 7.0 because tertiary amines are protonated at pH < 5 (pK_a ~ 6.5), preventing ligand exchange reactions between metal cations and G4-OH. The addition of $RuCl_3$ to the aqueous solution of $(Pt^{2+})_{20}$/G4-OH yields $(Pt^{2+})_{20}(Ru^{3+})_{20}$/G4-OH.

UV-vis spectra of $(Pt^{2+})_{20}(Ru^{3+})_{20}$/G4-OH solutions which were obtained with and without pH adjustments prior to the addition of $RuCl_3$ are shown in Fig. 3.5. When no pH adjustments were used (Fig. 3.5, curve 2), a distinct peak around 311 nm emerged in the spectrum of $(Pt^{2+})_{20}(Ru^{3+})_{20}$/G4-OH, which is similar to that typically observed for $RuCl_3$ in pure water. This implies that Ru^{3+} has preferentially complexed with water rather than G4-OH at low solution pH probably because of the protonation of amine and amide groups of the PAMAM dendrimer. The absence of the 311 nm peak in the case of the pH-adjusted $(Pt^{2+})_{20}(Ru^{3+})_{20}$/G4-OH solution (Fig. 3.5, curve 1) indicates that Ru^{3+} has complexed with $(Pt^{2+})_{20}$/G4-OH to form $(Pt^{2+})_{20}(Ru^{3+})_{20}$/G4-OH.[188]

3.3 Partial Displacement

Preparations of bimetallic nanoparticles by conducting partial displacement reactions are desirable when the metal precursor has a potential to react with reduced atoms of the other metal (Fig. 3.6). It was suggested that when less than a stoichiometric amount of Ag^+, Au^{3+}, Pd^{2+}, or Pt^{2+} is added to a G6-OH(Cu_n) solution, or if less than a stoichiometric amount of Au^{3+}, Pd^{3+}, or Pt^{2+} is added to a G6-OH(Ag_{2n}) solution, bimetallic AgCu, AuCu, AuAg, PdCu, PdAg, PtCu, and PtAg particles should be formed.

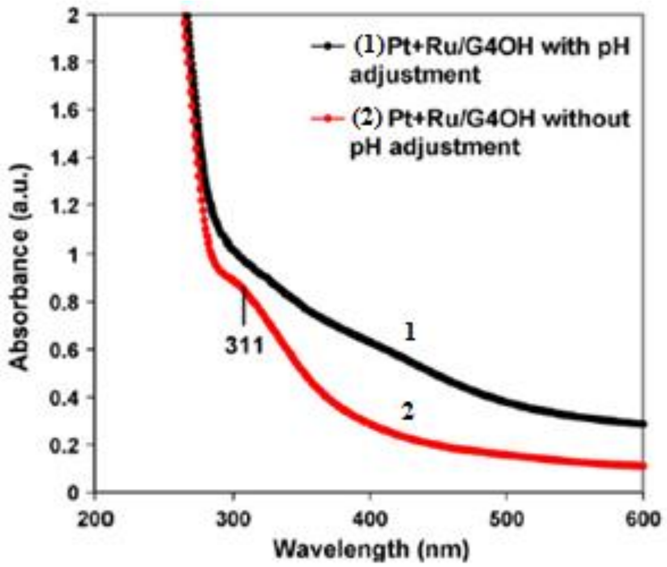

Figure 3.5 UV-visible absorption spectra of: $(Pt^{2+})_{20}(Ru^{3+})_{20}$/G4-OH complex solutions with (1), without (2) adjusting the pH of $(Pt^{2+})_{20}$/G4-OH solution to 7.0 before the addition of $RuCl_3$.[188]

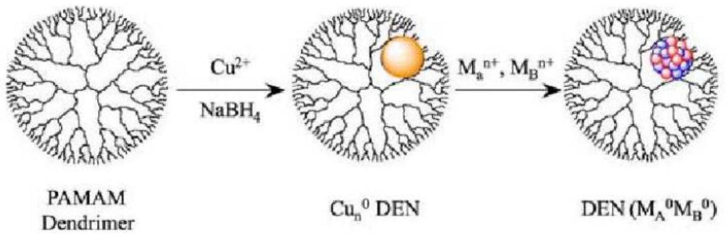

Figure 3.6 Partial Displacement Synthesis.[62]

[44,57,78] Unfortunately, only the preparation of PdAu has been reported in literature. This preparation involves the synthesis of G5-OH$(Cu)_{40}$ DENs followed by reduction with $NaBH_4$. The solution pH was adjusted to 3 to hydrolyze excess $NaBH_4$ and then returned to pH 7. Appropriate volumes of K_2PtCl_4 and $HAuCl_4$ were degassed separately, mixed, and immediately added to the G5-OH$(Cu)_{40}$ solution. The Cu^0 DENs then act as the reducing agent for both Pt and Au, yielding bimetallic G5-OH(PtAu) nanoparticles. The formation of metal particles with wide particle size distributions is the general disadvantage of this preparation method.[57,189]

3.4 Preparation of Ag-Bimetallic nanoparticles in solution

AuAg alloy structures were synthesized by the co-complexation method in which both metals were loaded into the dendrimer and simultaneously reduced with $NaBH_4$. The sequential loading method was used to synthesize core/shell materials having either Ag or Au shells. In all cases, the resulting bimetallic nanoparticles were < 3 nm in diameter.[172] The UV-vis spectra of the bimetallic AuAg/G6-OH system, which was synthesized via the simultaneous addition of $HAuCl_4$ and $AgNO_3$ to the dendrimer solution, suggest that AuAg alloys exhibit a single peak. This peak shifts from that of pure Au (~530 nm) to that of pure Ag (~400 nm) as the Ag/Au molar ratio in the nanoparticles is increased (Fig. 3.7(a)).[172] Esumi et al. observed the same trend in the UV-vis spectra of the AuAg/G5-COOH system prepared by co-complexation.[171] However, as Ag is deposited onto the Au seed, two plasmon bands appear. For example, in the spectrum of G6-OH$[Au_{55}](Ag_{95})$ there is a narrow band corresponding to the Ag shell at 410 nm and a broader plasmon band at 510 nm arising from the Au core (Fig. 3.7(b)).[172] For the largest core/shell structure, G6-OH$[Au_{55}](Ag_{450})$, the absorption spectrum is similar to that of pure Ag since only a single peak is present. TEM images

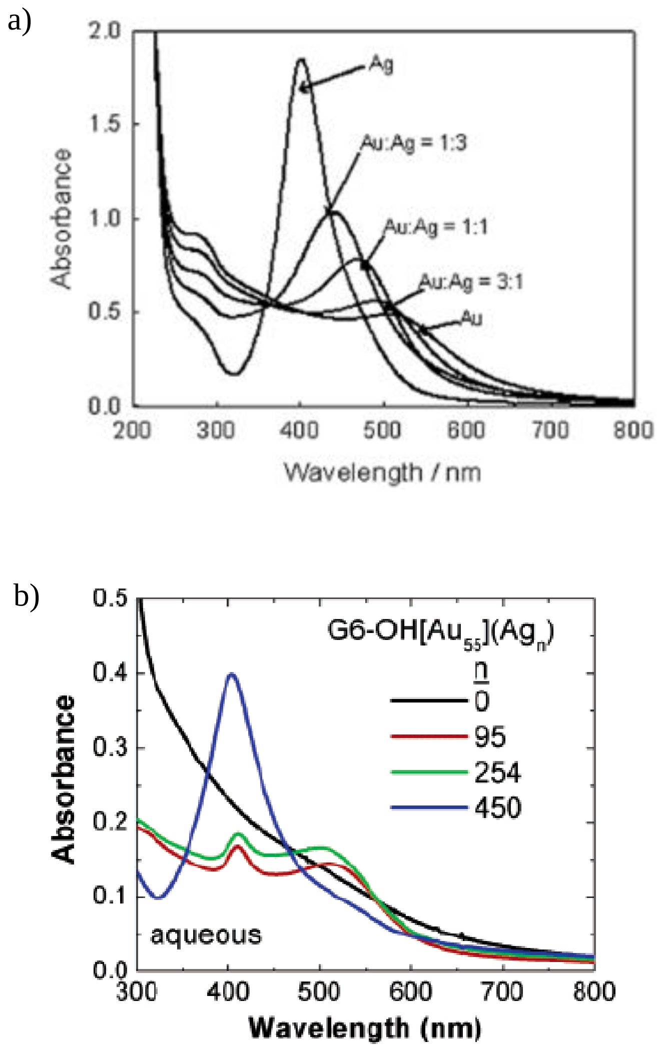

Figure 3.7 UV-vis spectra of: AuAg/G5-COOH with [metal ion]:[terminal group] = 1:10 (a) and G6-OH(Au_{55}) seeds and the G6-OH[Au_{55}](Ag_n) (n = 95, 254, 450) series of core/shell bimetallic nanoparticles.[171,172]

show that for G6-OH[Au_{55}](Ag_n), when n = 0, 95, 254, and 450, the size of metal particles is 1.4 ± 0.2, 1.6 ± 0.3, 1.9 ± 0.3, and 2.4 ± 0.3 nm, respectively.[172]

Luo et al. reported the synthesis of G5.0-NH_2-templated Ag-Cu nanoparticles by co-complexation followed by reduction with $NaBH_4$ or $N_2H_4 \cdot H_2O$.[180] The diameter of Ag-Cu bimetallic nanoparticles was found to be 5.6 ± 0.4nm, a little larger than that of the G5.0-NH_2 PAMAM dendrimer (5.4nm). This comparison suggests that the dendrimer acted as an outer template for the formation of metal clusters.[174] Under the same experimental conditions but with $NaBH_4$ as the reducing agent, rod-shaped Ag-Cu bimetallic nanoclusters were obtained (Fig. 3.8). The average diameter and length of these rod-shaped nanoclusters were 7.1nm and 0.5μm, respectively.[180] Such different shapes of the metal cluster were likely caused by the differences in the reduction rate of metal ions with $NaBH_4$ and $N_2H_4 \cdot H_2O$.[180]

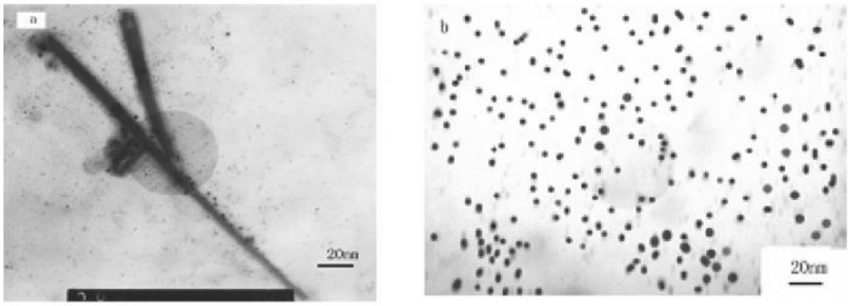

Figure 3.8 TEM of Ag-Cu bimetallic nanoclusters prepared by the reduction with $NaBH_4$ (a) and $N_2H_4 \cdot H_2O$ (b) in the presence of G5.0-NH_2 PAMAM dendrimers with Ag/Cu ratio of 1.5:1.5.[180]

CHAPTER 4

DEPOSITION AND ACTIVATION OF DENDRIMER-DERIVED METAL NANOPARTICLES

4.1 Deposition of metal-dendrimer nanocomposites onto solid supports

While complexation and reduction steps involved in preparations of DENs are complex, most methods which can be used for deposition of DENs onto surfaces of porous support are rather straightforward. Techniques, such as the deposition of empty dendrimers onto supports followed by the complexation of metal precursors to form dendrimer-metal complexes have been reported in literature.[190] Wetness impregnation methods can be used to deposit DENs onto a variety of porous oxide supports, although this often requires concentrating DENs solutions to the point when the dendrimer agglomeration may become problematic.[8,44] In wet impregnation, the support is added to a metal/dendrimer solution and the metal precursor is either adsorbed spontaneously on the support or precipitated after changes in the solution pH are made. To overcome large volumes of an aqueous waste that are involved in the wet impregnation method, the incipient wetness impregnation can be used. In this preparation, a solution of the active precursor is added to the dry support powder until all pores of the support are filled with liquid.[66] At neutral or basic pH the dendrimer surface groups as well as the oxide surfaces are negatively changed, making it unlikely that dendrimer-support interactions drive the adsorption.[191] For instance, bimetallic DENs prepared from hydroxyl-terminated PAMAM dendrimers can be deposited by "slow adsorption" techniques, in which DENs are stirred with an oxide support at appropriate pH.[162,163]

Wet impregnation requires evaporation of the solvent, resulting to an increase in the metal/dendrimer nanoparticles concentration in solution, while low dendrimer concentrations can be maintained during a sol-gel synthesis, minimizing the possibility of particle agglomeration in solution.[168,192,193] Crooks et al. reported the synthesis of Au and Pd DENs using the wet impregnation and sol-gel chemistry. When these techniques were used to prepare Au and Pd DENs on the titania support, an average size of DENs formed was in the 1.7 -2 nm range. However, when these samples were calcined at 500°C to remove the dendrimer component, an average size of metal particles was increased to 7.2 nm in the case of the sample prepared by wet impregnation while in the case of the sole-gel synthesis only a slight increase in the nanoparticle size to 2. 7 nm was observed.[193] Finally, it has been reported that sonication can be used for immobilization of Pd, PdAu, Rh, and Pt DENs onto the SBA-15 mesoporous silica support.[88,194] In this case, however, it is not clear if metal nanoparticles were formed after the sonication step or sonication simply assisted in the deposition of metal-dendrimer nanocomposites, which already contained metal particles.

4.2 Activation of Dendrimer-Derived Catalyst and Dendrimer Thermal Removal

After the deposition of the dendrimer-encapsulated nanoparticles on the support, the dendrimer component must be removed in order to render metal particles and make them accessible to reactants.[195-197] Several studies have shown that the PAMAM dendrimer backbone is relatively unstable and undergoes decomposition at temperatures as low as 75^oC.[193,198,199] The specific activation conditions required for each individual catalyst would likely depend on the metal, the support, the metal loading, the dendrimer loading, and metal/dendrimer ratios, suggesting that it may be necessary to optimize activation conditions for each individual catalyst. Using treatment temperatures at or near 300 ^oC, supported Pt [196,198,199], Pt-Au [163], Pt-Cu [184], and Ru [89,200] nanoparticles have been prepared. Zaera et al. showed that oxygen treatments are in general more effective than hydrogen treatments for exposing the surface of metal particles to reactants.[201] Furthermore, Amiridis et al. reported that the treatment of Rh_{20}-G4OH/ZrO_2 with an O_2/He mixture at 425 ^oC for 1 h followed by H_2 at 300 ^oC for 1 h removes the dendrimer component and reduces Rh to the metallic state, as evidenced by Rh *K*-edge XANES data.[70] Moreover, Williams et al. suggested that the dendrimer thermal decomposition under oxygen and hydrogen was more complete than in He in the case of Ir/γ-Al_2O_3.[77] It was also shown that supported G5-OH($Pt_{16}Au_{16}$) can be "activated" by heating under oxidizing (O_2) and/or reducing (H_2) atmospheres.[163]

However, when severe treatment conditions are used, there is a risk of metal sintering.[200,202,203,] For instance, while thermogravimetric analysis (TGA) data indicate that the organic matter can be completely removed from Pd and Au DENs immobilized onto TiO_2 at 500^oC, there is a 40% and 80 % increase in the size of Au and Pd particles, respectively.[193] Furthermore, EXAFS data showed that treatments of G4OH-$(Pt^{4+})_{40}$/γ-Al_2O_3 in a 10% O_2/He mixture at 400^oC for 2 h followed by reduction in H_2 at 300 ^oC led to an increase in the Pt-Pt first-shell coordination number from 5.6 to 11.2.[124]

4.3 Activation of Dendrimer-Derived Catalyst and Dendrimer Removal (Plasma)

The sintering of the metal nanoparticles during the dendrimer removal step is a major challenge which remains to be solved for the successful application of this synthetic route. Alternative dendrimer removal techniques have to be taken into account to minimize or decrease the sintering of metal nanoparticles. The plasma treatment could be just one out of many possibilities. The basic principle of the plasma process is the use high-energy particles from a weakly ionized plasma source to bombard the surface.[204-206] One of the advantages of plasma is that it can be operated at relatively low temperatures without damaging the substrate.[205,207,208] The bulk properties of materials typically remain unchanged during the process of plasma treatment. The plasma treatment is frequently used to clean and modify the surfaces of materials, including polymers, platinum, graphite, glassy carbon, carbon black, and glass.[209-211] For instance, it has been reported in literature that the thickness of polymer films deposited on aluminum substrates decreased when exposed to a highly dissociated oxygen plasma.[212] Furthermore, XPS analysis of ZrO_2 powders impregnated with $Ni(NO_3)_2$ showed that $Ni(NO_3)_2$ decomposed into oxides under Ar plasma treatment (Fig. 4.1). More specifically, a N_{1s} peak at 406.8 eV from NO_3^- appeared before the Ar plasma treatment but disappeared after that. After the Ar plasma treatment, the Ni_{2p} peak of $Ni(NO_3)_2$ at 856.6 eV, shifted to 855.2 eV due to the formation of NiO and $Ni(OH)_2$ species.[213]

The time consumption for the process depends on the type of plasma used.[214] It has been reported that for short time periods (< 4 min), Ar^+ plasma essentially eliminates any detectable background organic contaminations from Ag nanorod substrates and did not change substantially their morphology. However, upon longer exposure times (> 10 min) to the Ar^+ plasma, distinct morphological changes on the aligned Ag nanorod arrays

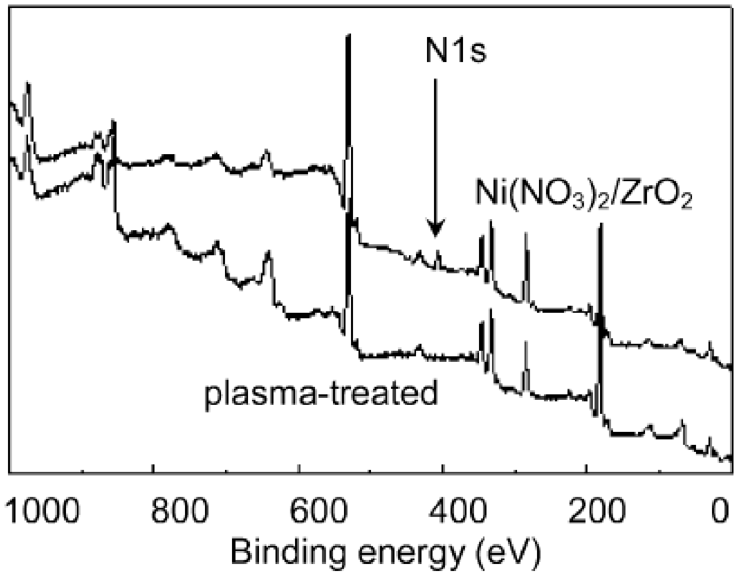

Figure 4.1 XPS spectra of untreated/plasma-treated $Ni(NO_3)_2/ZrO_2$ (5 wt % NiO).[213]

were observed.[215] Baker et al. found that RF (radio frequency) discharge in argon-oxygen mixtures was more effective at removing organic contamination from copper and aluminum than the nonreactive plasma.[216] Unfortunately, when oxygen plasma treatment applied to gold surfaces containing monolayers of hexadecanethiolate, generated a heavily contaminated surface with highly oxidized sulfur species, while hydrogen plasma was able to remove self-assembled monolayers.[217] Moreover, oxygen plasma, can cause silver surfaces to oxidize and thus argon plasma is required to remove the silver oxide.[218]

In order to prevent damages to the surface by plasma ions, a careful consideration of the plasma source energy range is required. For instance, alumina losses all its surface area when passed through plasmas that are too ‘hot’.[219] Moreover, Ar gas plasma process applied for the removal of antitarnish layers on the Ag and Cu surfaces for short process time (RF = 100 W for 10 s) did not cause a significant change in either the Ag or Cu surface in terms of the surface morphology, while the treatment with high power and long treatment time (RF = 600 W for 30 s) made the surfaces slightly smoother. The plasma cleaning process with RF = 600 W for 30 s was able to remove the antirarnish layers from both the Ag and Cu surfaces. However, in this case cross-contamination between the Ag and Cu surfaces was detected.[220]

CHAPTER 5

PREPARATION AND QUANTITATIVE ANALYSIS OF PAMAM-STABILIZED METAL NANOCOMPOSITES IN AQUEOUS SOLUTION: EFFECT OF DIALYSIS AND PH ADJUSTMENT

5.1 Introduction

Catalysis is a surface phenomenon which involves only metal atoms exposed on the surface of metal particles. Tiny metal particles are shown to exhibit properties which are significantly different from those of bulk metals. Gold particles provide the best example to illustrate this point. For example, while large gold particles are completely inert for many reactions, gold particles with sizes below 3 nm are very active for CO oxidation.[221-223] In general, metal particles with sizes in the nanometer range have higher dispersion and hence provide larger amount of active sites on which the reaction can occur.[224] The concentration of low coordinated sites, such as steps and kinks, is relative abundant in nanomaterials and these sites usually provide low activation barriers for the adsorption of reactants.[66,225,226]

Conventional catalyst preparation techniques involve impregnation of metal salts (wet impregnation, incipient wetness) followed by thermal treatments and often result in wide size distributions of metal particles.[227] When used for preparations of bimetallic systems, these traditional techniques yield catalysts containing both monometallic and bimetallic particles with varying compositions. The use of well-defined organometallic cluster complexes as precursors helps to overcome these problems.[228] Molecular cluster complexes typically have well-defined structures that can be retained throughout catalyst preparation steps.[229] Unfortunately, limited number of such compounds is commercially available. Furthermore, the advantage of their structural uniformity can be lost after the activation step on which different treatments at elevated temperatures are used to remove ligands.[57] The synthesis of colloidal metal nanoparticles has made it possible to synthesize monodisperse and nearly uniform metal nanoparticles with dimensions in the 1-10 nm range.[230-232] These colloidal nanoparticles can be used as heterogeneous catalysts in the same way as molecular clusters.[1,202,203] Their preparation process involves the reduction of metal salts in the presence of stabilizers and the following immobilization of the colloidal solution onto the surface of a porous oxide support.[233-235]

Among such stabilizers, Poly(amidoamine) (PAMAM) dendrimers have recently attracted a lot of attention because these macromolecules offer a variety of functional groups and have interior voids which can be used to trap and protect metal nanoparticles in solution until they are delivered to a support.[8,70,233] These features offer an opportunity to control the architecture and the size of metal nanoparticles in solution and maximize the uniformity of active metal sites in supported catalytic materials. While the synthesis of metal-dendrimer nanocomposites incorporating noble metals has been reported in literature, a limited number of reports describing the preparation of such nanocomposites from base metals is available.[91] Furthermore, little is known about the complexation of the base metal cations with PAMAM dendrimers, the strength of metal-dendrimer interactions, and how these interactions can be effected by preparation conditions.[75]

Despite the advantages of using dendrimers as nanoparticle stabilizers, the uptake of metal cations M^{n+}, where M^{n+} = Cu(II), Fe(III), Au(III), Ni(II), Co(II), Mn(II), Zn(II) and Ag(I), by dendrimers with non-complexing terminal groups, such as PAMAM-OH, is still not well understood. From a more fundamental point of view, little is known of the effects of dendrimer tertiary amine/amide and terminal groups' chemistry on the metal cation binding capacity and selectivity of PAMAM dendrimers in aqueous solutions.[236] Moreover, it has been reported in literature that although it is not possible to prepare Ag particles inside PAMAM-OH dendrimer by direct reduction of interior cations, stable dendrimer-encapsulated Ag particles can be prepared by a metal displacement reaction.[78,236] In this approach, dendrimer encapsulated nanoparticles (DENs) prepared from a particular metal such as Cu, can be exchanged with Ag as long as the latter metal is more noble than the former. Thus, key unanswered questions are whether the attainment of the Cu^0-Ag^+ displacement reaction depends on the solution pH and the successful reduction of Cu^{2+} cations inside the dendrimer solution.

This research project is dedicated to a systematic investigation of the evidence of metal cation/dendrimer complexation, the determination of the complexation time, as well as the effects of metal cation acidity, the solution pH and metal cation/dendrimer loading on the extent of binding (EOB) and fractional binding (FB) of metal cations M^{n+} to EDA core, fourth generation hydroxyl terminated PAMAM dendrimers (G4OH). Furthermore, we will focus on the Cu^0-Ag^+ intradendrimer displacement reactions followed by variations of the solution pH at different stages of the preparation procedure, with an overall goal to gain a better understanding of the intradendrimer displacement reaction preparation technique. The following specific objectives are proposed for this project:

1. *Determination of the complexation time of the M^{n+}/G4OH system and effect of the metal cation concentration on the M^{n+}/G4OH complexation time.* The complexation step involves interactions between the metal cations and the tertiary amine and amide groups of the dendrimer, which will be monitored in the present work by using UV-vis spectroscopy. Data available in literature suggest that cations of most metals do not complex with dendrimers instantly and UV-vis spectroscopy is used most often to examine the complexation kinetics.[88] Therefore, the UV-vis absorbance of the band that is responsible for the specific M^{n+}/G4OH interaction will be recorded over time in order to establish the optimal time for the completion of the M^{n+}/G4OH complexation reaction. Finally, the effect of M^{n+}/G4OH concentration on the complexation time will be addressed by changing the metal-to-dendrimer ratios, followed by characterization by UV-vis spectroscopy.
2. *Investigation of the strength/weakness of the metal cation - G4OH interaction*. To achieve this goal, M^{n+}/G4OH solutions with different molar ratios will be prepared, complexed at the appropriate amount of time and their solution pH will be recorded. The M^{n+}/G4OH solutions will be subsequently dialyzed using benzoylated cellulose tubing to remove the uncomplexed metal cations. The percentage of the metal cations retained inside the dialysis sack over the initial amount of M^{n+} used (Fractional Binding - FB), as well as the experimentally obtained M^{n+}/G4OH molar ratio (Extent of Binding – EOB) will be evaluated as a function of dialysis time. Both FB and EOB will give us an indication of the strength of M^{n+}/G4OH interaction. The concentration of M^{n+} cations retained

inside the dialyzed solution will be measured using Atomic Absorption Spectroscopy (AAS).

3. *Significance of interior functional groups of the G4OH dendrimer in the complexation process.* In order to address this goal the EOB of G4OH-$(M^{n+})_{30}$ will be compared with the corresponding EOB of G4NH_2-$(M^{n+})_{30}$ solutions after 1 day of dialysis. Comparing the EOB of metal cations with dendrimers containing complexing and non-complexing terminal groups, such as G4NH_2 and G4OH, respectively, will give us an indicating for the degree of participation of the interior functional groups of the dendrimer in the complexation process.
4. *Determination of the stage throughout the DENs preparation procedure that dialysis should be applied.* It has been reported in literature that dialysis can be applied prior or after treatment with $NaBH_4$ of the M^{n+}/G4OH complexed solutions.[88,189] In order to determine when it is most appropriate to perform the dialysis step, G4OH-$(M^{n+})_{30}$ solutions will be prepared for Ag^+, Co^{2+}, Ni^{2+}, Cu^{2+}, and Mn^{2+} and dialyzed before the performance of the reduction step. The obtained FB will be compared with the FB of the reduced solution, undergoing dialysis for the same period of time. This data will allow us to understand whether the dialysis procedure should be applied prior or after treatment with $NaBH_4$ of the M^{n+}/G4OH solutions.
5. *Analysis of the effect of pH on the ability of G4OH dendrimers to complex with metal cations in aqueous solution.* In order to investigate the effect of concentration of metal cations on the binding ability of G4OH dendrimer, the pH of Cu^{2+}/G4OH and Fe^{3+}/G4OH solutions will be fixed to 6.1 and 7.0, respectively, for varying metal/dendrimer molar ratios. The resulting solutions

will be dialyzed and the EOB/FB of Cu^{2+}, Fe^{3+}/G4OH with and without pH adjustments will be compared. It is expected, that increase in the solution pH will increase the amount of available binding sites in the interior of the dendrimer (deprotonation), leading to subsequent increase of the metal cation uptake by G4OH dendrimers.

6. *Fundamental understanding of the Cu^0-Ag^+ intradendrimer displacement reactions.* In order to achieve this goal Cu^{2+}/G4OH solutions with different molar ratios will be prepared, followed by appropriate pH adjustments and treatment with $NaBH_4$, in order to obtain (ideally) reduced G4OH-(Cu^0) nanocomposites. After the completion of the reduction step, Ag^+ cations will be added in the G4OH-(Cu^0) solution. Assuming that the intradendrimer displacement reactions are taking place, Ag, being nobler than Cu, will be capable of displacing it. The resulting solutions will be dialyzed and the concentration of Ag and Cu will be recorded (AAS) as a function of dialysis time. Finally, the influence of the initially used Cu^{2+}/G4OH molar ratio as well as the amount of Ag^+ added in the solution on the experimentally obtained Ag^+/G4OH molar ratio, will be examined systematically.

5.2 Experimental

5.2.1 Reagents and materials

Hydroxyl- and amine-terminated poly(amidoamine) (PAMAM) dendrimers (generation 4, denoted as G4OH and $G4NH_2$, 10 wt% in methanol), were purchased from Dendritech and Aldrich, respectively. Prior to use, the methanol solvent was removed under the flow of UHP N_2 (National Welders) at room temperature and 0.42 mM G4OH and 0.18mM $G4NH_2$ stock solutions were prepared in DI water. $AgNO_3$ (99+%),

$Co(NO_3)_2 \cdot 6H_2O$ (98%), $Ni(NO_3)_2 \cdot 6H_2O$ (99.999%), $Mn(NO_3)_2 \cdot 4H_2O$ (≥ 97%), and $NaBH_4$ (99%) were purchased from Aldrich, $Zn(NO_3)_2 \cdot 6H_2O$ (98+%) and $Fe(NO_3)_3 \cdot 9H_2O$ (98+%) from Strem Chemicals, and $HAuCl_4 \cdot 3H_2O$ (≥ 49%), $Cu(NO_3)_2 \cdot 3H_2O$ (98-102%) from Alfa Aesar and used as received. Furthermore, NaOH (1 N) and HCl (≥ 36.5-38%) were purchased from Reagents, Inc. and BDH Aristar, respectively, and HNO_3 (69-70%), $CaCl_2 \cdot 2H_2O$ (≥ 99%) from EMD Chemicals. A "benzoylated" tubing (Aldrich D7884), which is capable of retaining solutes with molecular weights greater than 2000 Da, was used for purification of samples by dialysis. Prior to use, the dialysis tubing was soaked for several hours in deionized (DI) water. All water was deionized to a resistivity of ≥ 17.5 MΩ-cm using a Nanopure system (Barnstead).

5.2.2 UV-vis spectroscopy

UV-vis absorption measurements were carried out at room temperature using a Shimadzu UV 2010 spectrophotometer and quartz cells with the 10 mm path length. An identical cell filled with deionized water was used as the background.

5.2.3 Atomic Absorption Spectroscopy (AAS)

AAS was used (PerkinElmer AAnalyst 400) to quantify concentrations of Ag, Cu, Fe, Au, Co, Ni, Zn, and Mn in liquid samples. Calibration standards were made from 1.0g/L metal stock solutions purchased from EMD Chemicals (Ni), J. T. Baker (Ag, Cu, Zn), VWR (Mn), Ricca Chemicals (Fe), LabGuard® (Co) and Aldrich (Au). The calibration standards were verified by the use of an independent check standard (J. T. Baker) diluted with 2% (v/v) HNO_3 for all the elements except Ag and Au for which independent check standards were purchased from Ultra Scientific and EMD Chemicals, respectively, and diluted with 5% (v/v) HNO_3. Since silver and gold are light sensitive, their solutions were stored in amber glass volumetric flasks. The samples and the standard solutions of Ag and Au were diluted with 5% HNO_3 and 5% HCl, respectively, to keep the element in solution. 0.2% $CaCl_2$ was added to Mn and Fe samples and standards in order to overcome the depression due to silicon. Finally, Cu, Ni, Zn samples were diluted with deionized water. Samples were diluted to concentrations that fall in the analytical range up to 5, 1.6, 3, 5, 1, 4, 0.75, 0.6 mg/L, for Ag, Cu, Fe, Au, Co, Ni, Zn and Mn, respectively.

5.2.4 Sample Preparation

Our sample preparation procedures generally follow those published previously.[69,85,87] We mixed the stock G4OH solution with an appropriate amount of 3.74 mM $Cu(NO_3)_2$, 2.91 mM $CuCl_2$, 3.5 mM $Ni(NO_3)_2$, 3.4 mM $Co(NO_3)_2$, 2.5 mM $Fe(NO_3)_3$, 8.1 mM $Mn(NO_3)_2$, 6.8 mM $Zn(NO_3)_2$, 1.4 mM $HAuCl_4$ or 58.9 mM $AgNO_3$ to produce solutions containing fixed amounts of metal cations$^{.}$ (i.e., $1.6 \cdot 10^{-2}$ mmol Cu^{2+} (from $Cu(NO_3)_2$), $1.2 \cdot 10^{-2}$ mmol Cu^{2+} (from $CuCl_2$), $1.5 \cdot 10^{-2}$ mmol Ni^{2+}, $1.5 \cdot 10^{-2}$ mmol Co^{2+}, $7 \cdot 10^{-3}$ mmol Fe^{3+}, $3.06 \cdot 10^{-2}$ mmol Mn^{2+}, $2.7 \cdot 10^{-2}$ mmol Zn^{2+}, $7 \cdot 10^{-3}$ mmol Au^{3+} and 3.14 mmol Ag^{+}) and having Metal/G4OH ratios between 0.5 and 80. Solutions of Au, Ag and Co were thoroughly stirred and stored in darkness. Moreover, G4OH-$(Au^{3+})_n$ solution was stirred for 1 h without taking into consideration the fact that $HAuCl_4$ can be auto-reduced by the dendrimer.[160,186,237] The pH of these solutions was measured and the metal/dendrimer complexation was monitored by UV– vis measurements. The amount of G4OH, used for the preparation of the metal/dendrimer solutions, depends on the desired metal/dendrimer ratio. Specifically, in order to prepare Fe^{3+}/G4OH solution with molar ratios 0.5, 2, 5, 10, 20, 30, 60 and 80, the concentration of G4OH in the final Fe^{3+}/G4OH solution was 0.39, 0.31, 0.23, 0.16, 0.1, 0.07, 0.04 and 0.03 mM, respectively. The concentration of G4OH used for the preparation of solutions with different metal cations can be found in Table 5.1.

In some experiments, G4OH-$(M^{n+})_x$ solutions were dialyzed using benzoylated cellulose tubing to remove uncomplexed metal cations or impurities. It was shown previously that the benzoylated tubing retains G4OH and G4OH-$(M^{n+})_x$ through exhaustive dialysis experiments.[238] In our standard dialysis protocol, 15 mL of sample was placed in a soaked and pre-washed dialysis tubing. The water bath (~2 L DI water) was continuously stirred and changed at least 10 times over 24 h. The precursor concentrations (mM) and volumes (mL) used for the dialysis and pH adjustments experiments are shown in Table 5.2. For instance, the Fe^{3+}/G4-OH dialyzed solutions were 0.46 mM in Fe^{3+}, prepared using 2.8 mL from the 2.5 mM $Fe(NO_3)_3$ precursor stock solution (Table 5.2).

5.3 Results and discussion

5.3.1 Quantitative analysis of Cu-PAMAM ligand exchange reaction: Time, pH and concentration effects

The structure of copper(II)-dendrimer complexes have been studied extensively both experimentally and computationally.[56,67,68] Turro et al. showed using electron paramagnetic resonance (EPR) spectroscopy that the structure of Cu(II) complexes with NH_2-terminated dendrimers depends on the Cu(II) concentration and the solution pH.[116,117] Gentle et al. and Diallo et al. suggested that copper(II) ions are capable of complexing with primary and tertiary amines, as well as with amides of NH_2-terminated G4 dendrimers on the basis of EXAFS data.[95,100] Although, there is plenty of literature available regarding the complexation of Cu(II) with amine terminated PAMAM dendrimers, limited information is provided for the complexation of Cu(II) with hydroxyl

Table 5.1 Concentration of G4OH (mM*10) used for preparations of M^{m+}/G4OH solutions with various ratios (pH and UV-vis measurements (1st row), dialysis and pH adjustment experiments (2nd row)).

Molar ratio **Metal Cation**	**0.5**	**2**	**5**	**10**	**13**	**16**	**20**	**30**	**40**	**60**	**80**
Fe^{3+}	3.9	3.1	2.3	1.6			1.0	0.7		0.4	0.3
		2.3					0.23	0.15		0.08	0.06
Au^{3+}		2.6	1.7	1.1				0.4		0.2	
		0.45	0.18	0.09				0.03		0.015	
$Cu^{2+}(Cu(NO_3)_2)$	4.0	3.4	2.7	2.0	1.7	1.5	1.3	0.68		1.0	
	4.0	1.0	0.4	0.2	0.15	0.12	0.1	0.07			
$Cu^{2+}(CuCl_2)$	9.5	2.4		0.47	0.36	0.30	0.24	0.16		0.008	
Zn^{2+}		3.7	3.2					1.5		0.9	
		1.8	0.7					0.1		0.06	
Ag^{+}	4.19		4.06					3.5		2.9	
	4.19		0.419					0.07		0.035	
Mn^{2+}		3.8	3.3					1.6		1.0	
		0.5	0.2					0.033		0.017	
Co^{2+}	4.0	3.4	2.6	1.3			1.2	0.9	0.7	0.5	
			0.2					0.04		0.02	
Ni^{2+}		3.4	2.6	1.9			1.2	0.9	0.7	0.5	
		1.7	0.68					0.11		0.06	

Table 5.2 Precursor concentrations (mM) and volumes (mL) used for the dialysis and pH adjustments experiments.

Metal Cation	**Fe^{3+}**	**Au^{3+}**	**Cu^{2+} ($Cu(NO_3)_2$**	**Cu^{2+} ($CuCl_2$)**	**Zn^{2+}**	**Ag^{+}**	**Ni^{2+}**	**Mn^{2+}**	**Co^{2+}**
Concentration of metal cation (mM)	0.46	0.09	0.2	0.2	0.36	0.21	0.34	0.1	0.34
Stock precursor solution (mL)	2.8	0.95	0.8	1	0.79	0.05	1.46	0.19	1.7

terminated commercially available PAMAM dendrimers.

5.3.1.1 Evidence of G4OH-(Cu^{2+})$_n$ complexation

In aqueous solutions Cu^{2+} exists primarily as $[Cu(H_2O)_6]^{2+}$, which gives rise to a broad, weak absorption band centered at 800 nm (Fig. 5.1). PAMAM dendrimers do not have prominent absorbance in the 200 – 800 nm region because of the aliphatic nature of their molecular backbone.[239] The addition of ligands to Cu^{2+} leads to the formation of complexes by the successive displacement of water molecules. These Cu^{2+} complexes typically have d-d transitions in a tetragonally distorted octahedral or square-planar ligand fields.[44,56,67] In the presence of G4OH, λ_{max} for d-d transitions shifts to 605 nm (Fig. 5.1). In addition, a strong band assigned to a ligand-to-metal-charge-transfer (LMCT) emerges at 300 nm.[44,55,67] Same experiments carried out by Crooks et al. with the $CuSO_4$ precursor confirmed our observations.[67] Literature data suggest that bands characterizing Cu^{2+}-G4OH complexes (i.e., at 300 nm and 605 nm) decline in intensity with decreasing pH, indicating that the complexation process in this case is pH dependent. More specifically, when the solution pH was adjusted to 3.0, these two bands essentially disappeared and a broad weak band from $[Cu(H_2O)_6]^{2+}$ species appeared at approximately 800 nm.[56]

5.3.1.2 Complexation kinetics – Determination of complexation time and effect of Cu^{2+} concentration on complexation time (UV-vis spectroscopy)

To determine which parameters have an effect on the Cu^{2+}-G4OH complexation, samples of G4OH-(Cu^{2+})$_n$ (where n = 0.5, 2, 5, 10, 13, 16, 20 and 60) were prepared. In all these preparations, the amount of Cu^{2+} used was fixed to $1.6\cdot10^{-2}$ mmol but the amount of G4OH was varied depending on the required Cu/G4OH molar ratio. All samples were stirred for the extended period of time. Aliquots (2.6 ml) of each solution

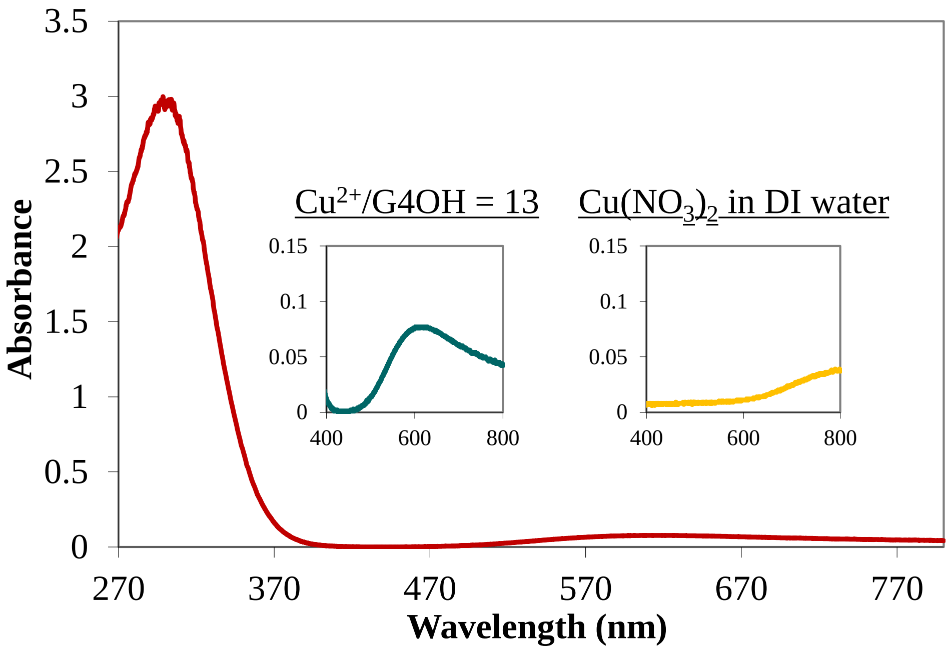

Figure 5.1 UV-vis spectra of G4OH-$(Cu^{2+})_{13}$ solution after 30min of complexation. Aliquots of the solution (2.22 mM Cu^{2+}) were diluted by a factor of 16 immediately prior to UV-vis measurements.

were taken at different periods of time, diluted by a factor of 16, and examined by UV-vis. The results shown in (Fig. 5.2(a)) indicate that the absorbance of these samples at 605 nm after 5 days of complexation was exactly the same as the one obtained after 30 min of complexation. This result suggests that the complexation of Cu^{2+} with G4OH was completed roughly after approximately 30 min. The data shown in Figs. 5.2 a and b further suggest that the maximum Cu^{2+}/G4OH ratio that can be obtained at pH 5.8 is equal to 13.[106] Similar experiments with the same dendrimer and $CuSO_4$ conducted by Crooks et al. suggest that the maximum Cu^{2+}/G4OH ratio is approximately 16.[67] Spectroscopic results available in literature for amine-terminated PAMAM dendrimers (G4-NH_2) suggest that each dendrimer can absorb at most 36 Cu^{2+} cations most of which are bound to terminal amine groups.[67]

5.3.1.3 The effect of dialysis on Fractional Binding (FB) and Extent of Binding (EOB)

Fig. 5.3(a) shows that FB of Cu(II) in aqueous solutions of G4-OH PAMAM dendrimers increases until G4OH-$(Cu^{2+})_{10}$ is reached and then gradually declines. The FB values characterizing G4OH-$(Cu^{2+})_n$ solutions for n = 13, 16, 20 and 30 after 24 h of dialysis are 50.6, 49.8, 40.1, and 22.2 %, respectively, indicating that the FB of Cu decreases for $n \geq 10$. For n = 10 and pH = 6.1, the data show that only ~ 16% of Cu is dialyzed from the Cu^{2+}/G4OH solution, which is an indication that 16% of Cu is weakly bound or unbound with the G4OH dendrimer. For n > 10, the solution pH drops below 6.1 and the data show a significant decrease in FB of Cu. This result can be explained by protonation of tertiary amines in the dendrimer interior (pKa = 6.3 – 6.7).[108,149]

To gain insights into the relationship between EOB, Cu(II)-dendrimer loading, and dendrimer protonation, the pH of each equilibrated copper-dendrimer aqueous solution was also measured. Fig. 5.3(b) shows the effect of metal ion-dendrimer loading

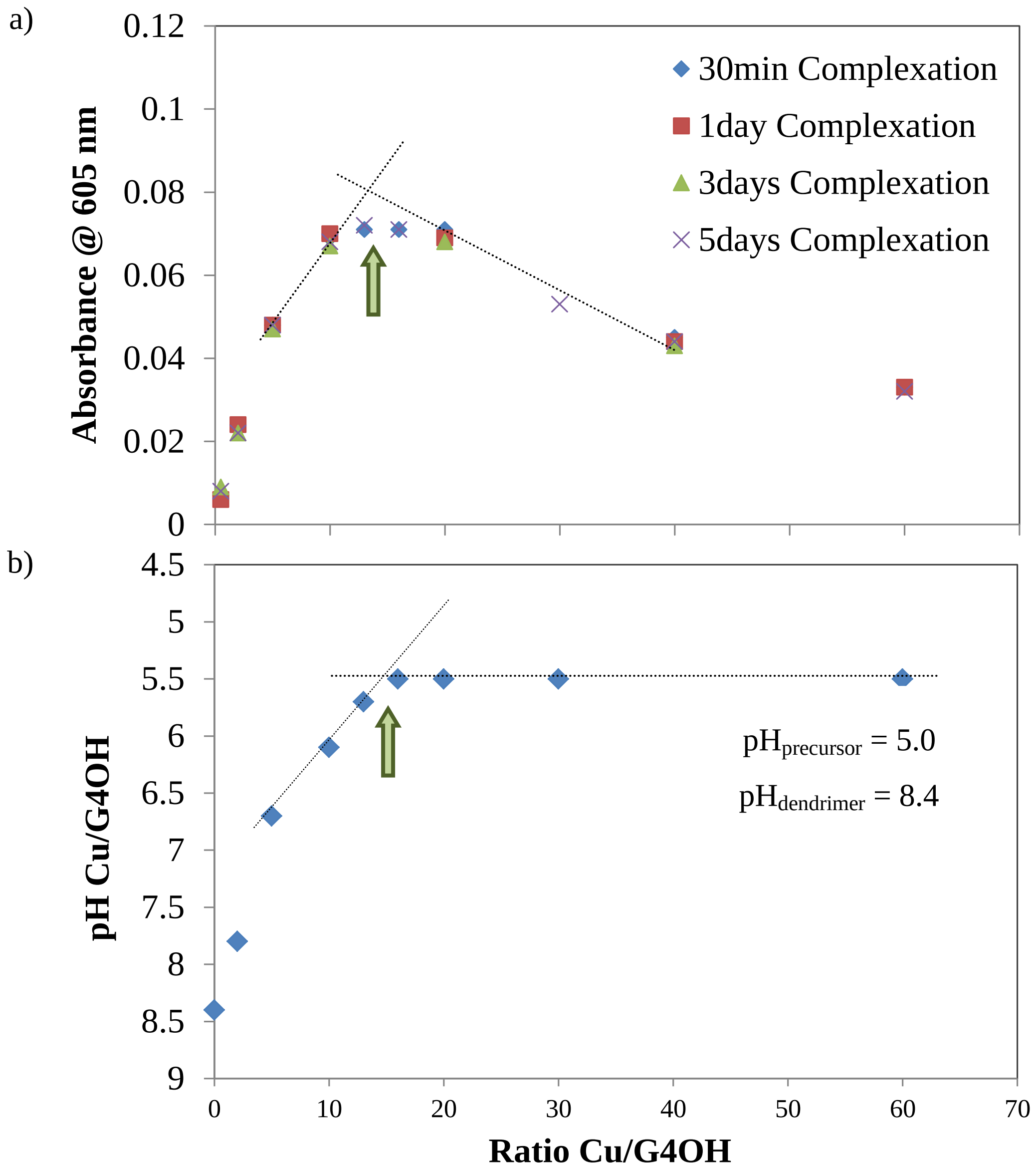

Figure 5.2 a) Absorbance of G4OH-$(Cu^{2+})_x$ complex at 605 nm (n = 0.5, 2, 5, 10, 13, 16, 20 and 60) as a function of the complexation time and Cu^{2+}/G4-OH theoretical ratio. b) The solution pH as a function of the theoretical Cu^{2+}/G4-OH ratio.

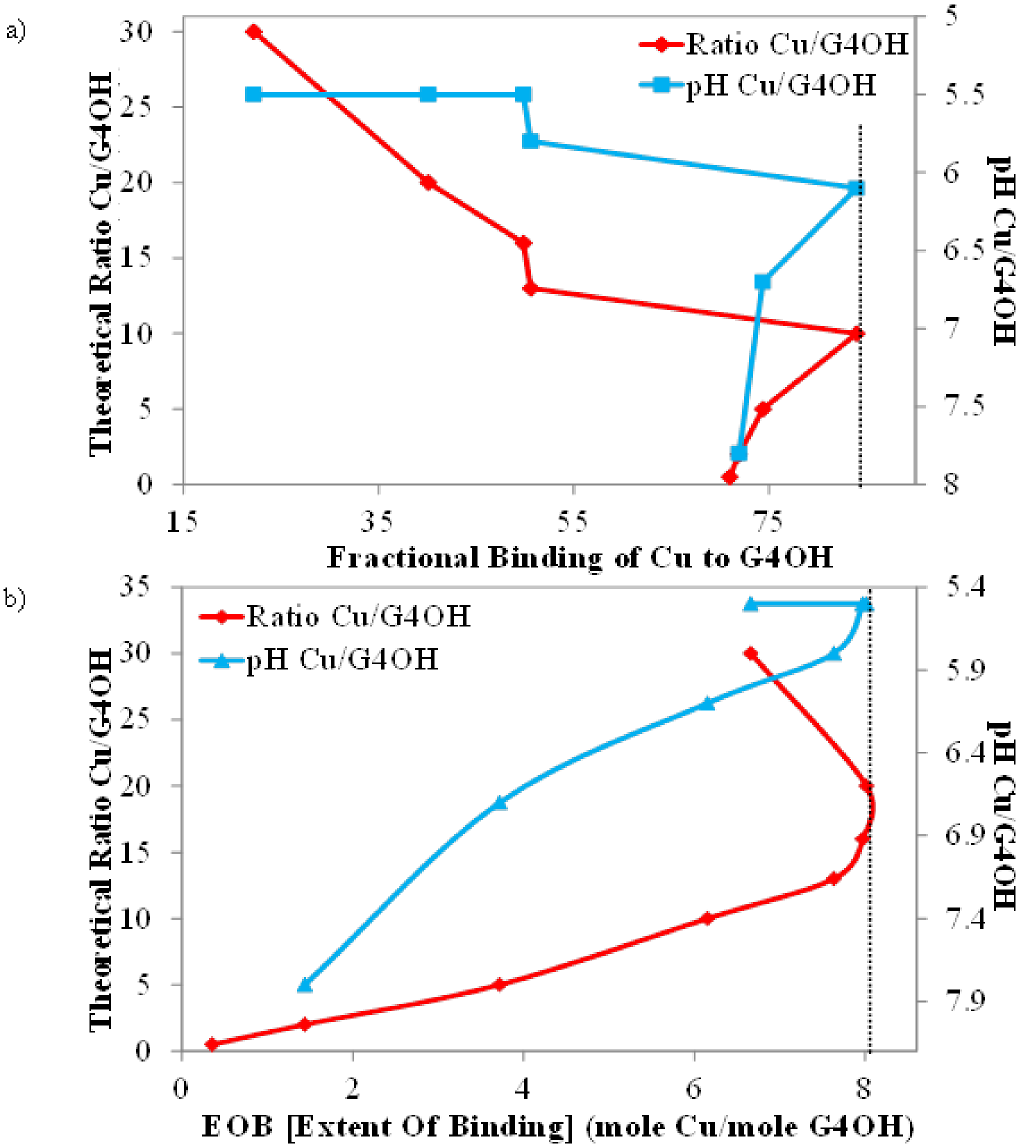

Figure 5.3 Theoretical Cu to G4-OH ratio and the solution pH as a function of the Fractional Binding (a) and Extent of Binding (b) after 24h dialysis. The red and blue curves correspond to the Cu/G4OH ratio and the solution pH, respectively.

on EOB. As this loading increases, the number of Cu(II) cations available for binding increase. However, the number of nitrogen binding sites decrease as they become protonated. The net result of these two opposing effects is that the EOB of Cu(II) cations goes to a maximum in aqueous solutions of G4OH dendrimers as copper-dendrimer loading increases.[122] The maximum EOB is 8 and is observed for G4OH-$(Cu^{2+})_{13}$ and at pH ~ 5.8.

5.3.1.4 Comparison of the EOB of G4OH-$(Cu^{2+})_n$ composites for $Cu(NO_3)_2$ and $CuCl_2$

In order to investigate the effect of the copper precursor on the complexation process, G4OH-$(Cu^{2+})_n$ (where n = 2, 10, 13, 16, 20, 30 and 60) solutions were prepared using a stock solution containing 2.91 mM $CuCl_2$. These solutions were dialyzed for 24 h and their EOB was compared with the corresponding EOB for Cu^{2+}/G4OH solutions prepared from $Cu(NO_3)_2$. Fig. 5.4 illustrates that theoretical and experimental EOB values are consistent with each other only for Cu to dendrimer ratios up to 5. However, at higher ratios, theoretical and experimental values differ substantially. For example, for the calculated metal/dendrimer ratio of 13, the experimental EOB values were found to be 8 and 4.6 for $Cu(NO_3)_2$ and $CuCl_2$, respectively, indicating that the uptake of Cu^{2+} by the dendrimer is higher in the former case.

Experiments with $CuCl_2$ and the G4-NH_2 PAMAM dendrimer described in literature showed that for G4NH_2-$(Cu^{2+})_{18}$ the EOB was 13, which is ~ 28% lower than the initial loading but still is much higher than the 38.5 and 64.6% decrease in EOB observed for G4OH-$(Cu^{2+})_{13}$ using $Cu(NO_3)_2$ and $CuCl_2$, respectively. The enhanced complexation of Cu^{2+} to G4NH_2 dendrimers is attributed to the complexation of copper cations to the primary amines of the dendrimer.[122]

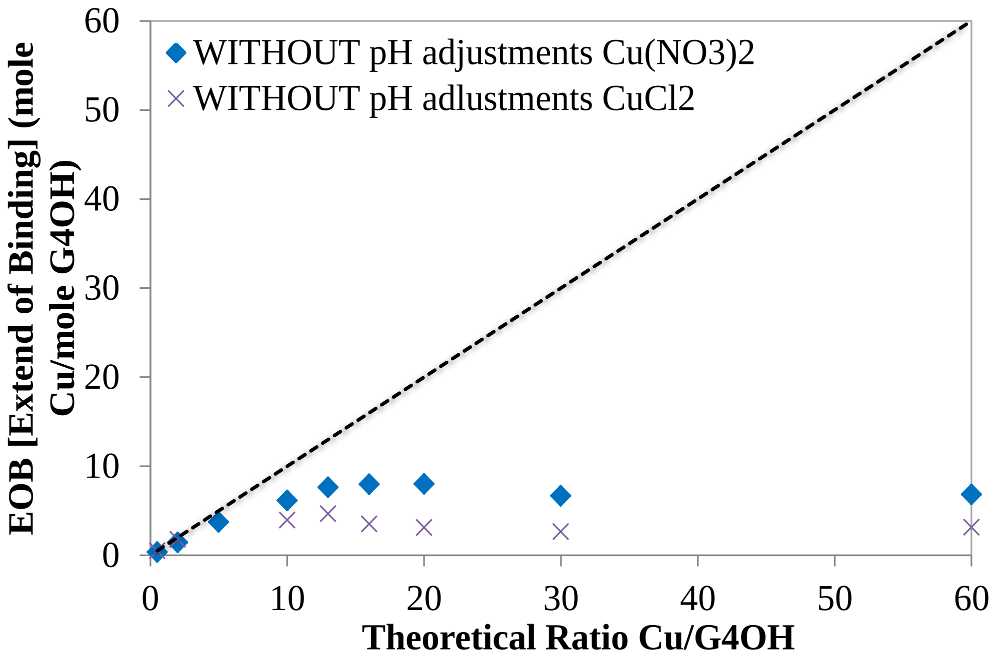

Figure 5.4 Extent of Binding [EOB] of $Cu(NO_3)_2$ and $CuCl_2$ to G4-OH PAMAM dendrimers after 24 h dialysis without pH adjustments.

5.3.1.5 Effect of pH adjustments on the EOB of G4OH-$(Cu^{2+})_n$ composites

Diallo et al.[122] and Crooks et al.[99] have reported measurements of the EOB of Cu(II) in aqueous solution of EDA core PAMAM amine terminated dendrimers. However, the pH of the Cu(II)-dendrimer solutions was not controlled in both of these reports. In a later report, Diallo et al. suggested that approximately 95-100% of Cu(II) can be retained by the dendrimer when a significant fraction of amine groups is unprotonated at pH 7.0 and pH 9.0.[100] Unfortunately, there is no such data available for G4OH dendrimer.

Fig. 5.5 illustrates the effect of metal ion-dendrimer loading and the solution pH on the EOB of Cu(II) in aqueous solutions of G4OH dendrimers. In these experiments, the Cu(II)-dendrimer molar ratio was varied from 13 to 60 but the solution pH was adjusted to 6.1 in all experiments, since at this pH the maximum FB of Cu^{2+} to G4OH was observed. At pH 6.1, the EOB of Cu(II) increases almost linearly with increasing the metal ion-dendrimer loading. When the pH of the G4OH-$(Cu^{2+})_{30}$ and G4OH-$(Cu^{2+})_{60}$ solutions was adjusted to 6.1, the EOB values were increased for 43 and 72%, respectively, as compared to those in experiments without pH adjustments. However, while pH adjustments improve EOB values, the difference between calculated and experimental EOB values remains substantial.

5.3.2 Quantitative analysis of Fe-PAMAM ligand exchange reactions: Time, pH and concentration effects

The mechanistic details and kinetics of the Fe^{3+}/G4OH complexation have not received sufficient attention in literature, and so we do not fully understand how the PAMAM dendrimer influences the architecture of the final Fe-PAMAM composite.

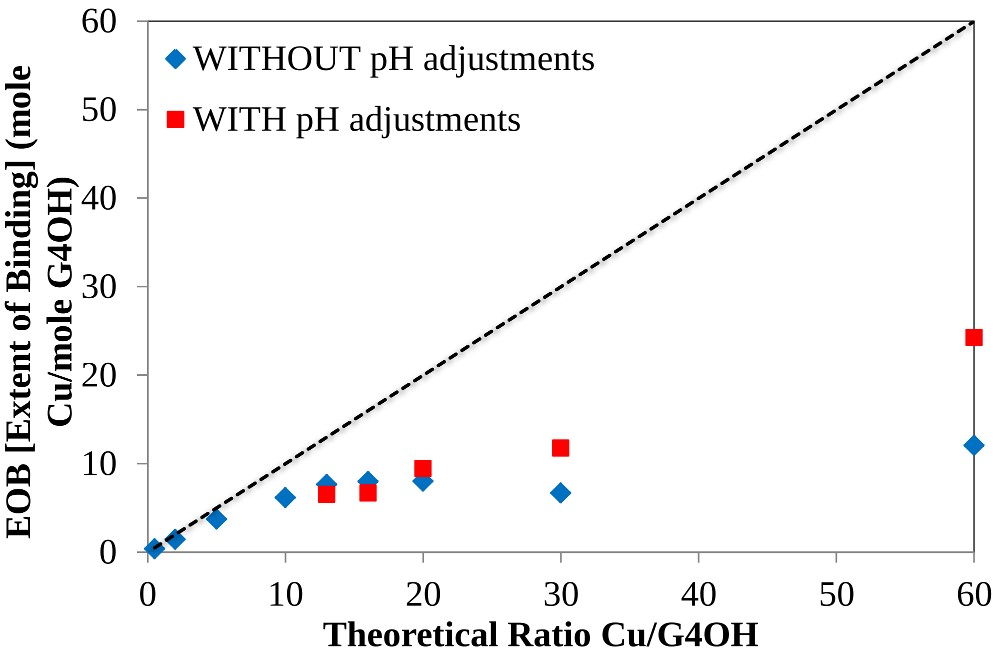

Figure 5.5 EOB of Cu to G4OH PAMAM dendrimers after 24 h dialysis with and without pH adjustments (pH ~ 6.1). The pH was adjusted using 0.1 N NaOH.

Recently, Crooks et al. reported the synthesis of subnanometer (0.9 ± 0.2 nm) G6-$C_{12}(Fe_{55})$ DENs using $FeCl_3$ and G6-C_{12} PAMAM dendrimer modified on its periphery with 256 dodecyl groups.[240] Furthermore, Baker Jr et al. synthesized FeS nanoparticles using generation 4 PAMAM dendrimers terminated with amino (G4-NH_2), hydroxyl (G4-NClyOH), and carboxyl (G4-SAH) groups.[241] Unfortunately, there is no literature available for the complexation of $Fe(NO_3)_3$ with hydroxyl terminated PAMAM dendrimers. The following work investigates the kinetics of the complexation step and the effect of pH on the Fe^{3+}/G4OH complexation process.

5.3.2.1 pH effect on the stability of G4OH-$(Fe^{3+})_n$ nanocomposites

One of the most conspicuous features of the ferric ion in aqueous solutions is the tendency to hydrolyze and/or form complexes.[242] Iron(III) has an affinity for ligands that incorporate oxygen, such as the -OH terminal groups of the dendrimer, or the O donor in the amide dendrimer functional groups. This can be attributed to the relatively high binding constants ($\log K_1 = 11.81$) of Fe^{3+} for O donors. The affinity of iron(III) for amine ligands is very low ($\log K_1 = 3.8$).[64,65] No simple ammine complexes of Fe exist in aqueous solutions as the addition of aqueous ammonia precipitates Fe in a form of hydroxide. Chelating amines, such as EDTA, do form definite complexes with Fe among which, the 7-coordinated $[Fe(EDTA)H_2O]^-$ ion could be mentioned.[243,244] Depending on the solution pH, different hydrolysis products can be formed, which can subsequently interact with various ligands to form Fe(III) complexes in solution.[242]

In order to determine the effect of pH on the stability of G4OH-$(Fe^{3+})_n$ solutions, eight G4OH-$(Fe^{3+})_n$ solutions with molar ratios n = 0.2, 2, 5, 10, 20, 30, 60 and 80 were prepared. The solution pH was measured and plotted as a function of molar ratio (Fig. 5.6). For n = 30, 60, and 80, the solution pH was found to be ~ 2.8 and these solutions

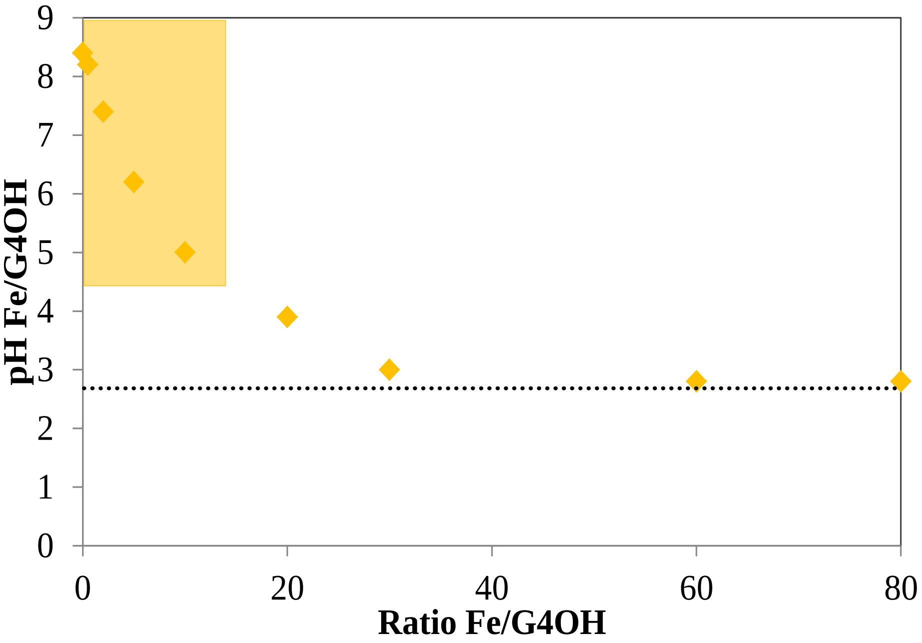

Figure 5.6 pH of G4OH-(Fe^{3+})$_n$ solutions (n = 0.5, 2, 5, 10, 20, 30, 60 and 80) as a function of the theoretical G4OH-(Fe^{3+})$_n$ ratio. The pH was recorded after 10 min of complexation for molar ratios $n < 20$, and after 2 days of complexation for $n \geq 20$.

were stable for more than a month. In this pH range (slightly higher than 2.0), it is expected that $[Fe(H_2O)_5(OH)]^{2+}$ is formed, which is then converted to the hydroxo-bridged dinuclear species $[(H_2O)_4Fe(\mu\text{-}OH)_2Fe(H_2O)_4]^{4+}$. The pH of the G4OH-$(Fe^{3+})_{20}$ solution is ~ 3.8 and the solution was stable for a shorter period of time (3 days). The increase in the G4OH-$(Fe^{3+})_n$ solution pH for $n < 20$ leads to the formation of unstable solutions in which a red-brown precipitate appears within 15 min of complexation. This behavior can be attributed to the formation of additional polynuclear species, colloidal gels, and finally a precipitate of red-brown hydrated ferric oxide.[242,245]

5.3.2.2 Evidence of G4OH-$(Fe^{3+})_n$ complexation

Fig. 5.7 shows the absorption spectra of Fe^{3+} coordinated to different ligands. More specifically, in the absence of the G4OH dendrimer (dashed line), Fe^{3+} exists primarily as $[Fe(H_2O)_5(OH)]^{2+}$ since the pH of the $Fe(NO_3)_3$ precursor is 2.5. The UV-vis spectrum of these species is characterized by in a weak asymmetric absorption band centered at 300 nm with a shoulder at 350 nm which can be attributed to a monomeric hydrolyzed surface iron species.[245] Two weaker bands observed at 675 and 750 nm (inset) are characteristic of $[Fe(H_2O)_6]^{3+}$ species. When dendrimer is added to the Fe^{3+} solution, the weak bands at 675 and 750 nm are obscured by the low energy tails into the visible of LMCT absorptions.[245] All the absorption bands emerged in Fig. 5.7, correspond to charge-transfer absorptions, since high spin octahedral iron(III) compounds are d^5, they have a $^6A_1$ ground state and all their excited states have a different spin multiplicity. Consequently, d-d transitions are spin and parity forbidden.[246]

Upon addition of the G4OH dendrimer to the $Fe(NO_3)_3$ solution to form G4OH-$(Fe^{3+})_{30}$ composites, the 300 nm band shifts to 271 nm after 30 min of complexation. Furthermore, the intensity of the absorption bands at 300 and 350 nm declines as

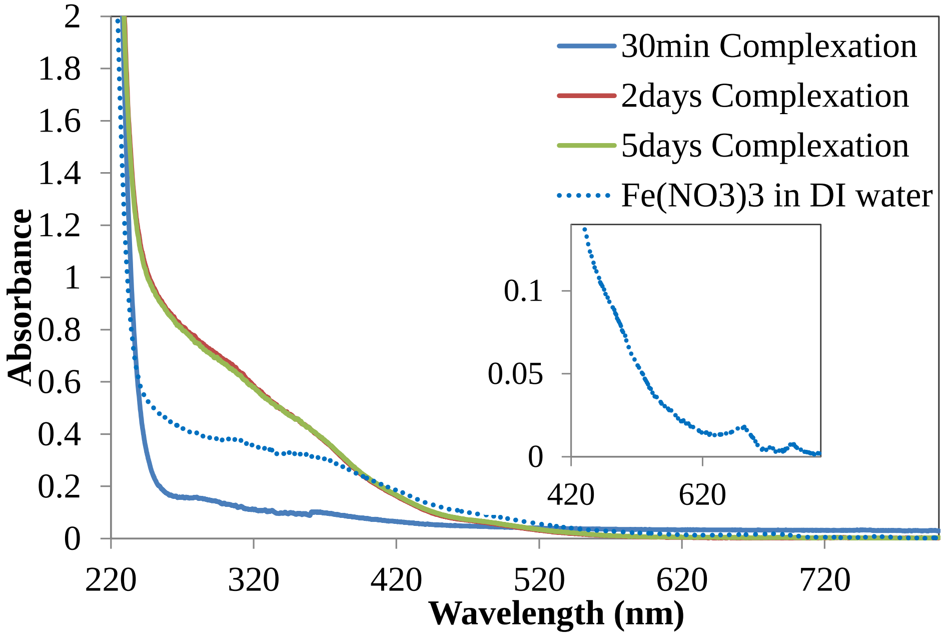

Figure 5.7 UV-vis spectra of G4OH-(Fe^{3+})$_{30}$ after 2 days of complexation. The solution contained $7.0 \cdot 10^{-3}$ mmol of $Fe(NO_3)_3$ from the $Fe(NO_3)_3$ stock solution. The concentration of G4-OH used was 0.069 mM (555 µL from a 0.42mM G4OH stock solution). The inset plot shows the UV-vis spectrum of the solution containing the same concentration of Fe^{3+} as in G4OH-(Fe^{3+})$_{30}$ (0.34 mM) but instead of G4OH was used DI water. Aliquots of the solutions were diluted by a factor of 7.7 immediately prior to the UV-vis measurement.

compared to the solution containing the same concentration of only $Fe(NO_3)_3$ (dashed line). At longer complexation times, both peaks increase in intensity and the band at 271 nm shifts back to 300 nm, while the position of the 350 nm band remains unchanged during the complexation process. The red shift of the band at 300 nm indicates the reduction in the symmetry of the coordination sphere of Fe(III) cations which concomitantly increases their extinction coefficients.[245] Similar observations reported for Ru indicate that the increase in the absorption intensity is associated with the formation of dendrimer-cation complexes.[89] These changes in the absorption spectra suggest that the complexation process for G4OH-$(Fe^{3+})_{30}$ is completed after approximately 2 days.

5.3.2.3 Complexation kinetics-Determination of complexation time (UV-vis spectroscopy)

The complexation rate presumably depends on the Fe/G4OH ratio and on the PAMAM solution concentration. To illustrate this point, two more samples G4OH-$(Fe^{3+})_{60}$ and G4OH-$(Fe^{3+})_{80}$ were synthesized. Both of these samples contain the same amount of Fe^{3+} moles ($7 \cdot 10^{-3}$ mmol) as the G4OH-$(Fe^{3+})_{30}$ sample reported previously. However, the Fe^{3+} concentration was different in these three preparations because different volumes of solutions were used, depending on the required amount of G4OH. For instance, the Fe^{3+} concentration in G4OH-$(Fe^{3+})_{30}$, G4OH-$(Fe^{3+})_{60}$, and G4OH-$(Fe^{3+})_{80}$ solutions was 1.14, 1.57, 1.73 mM, respectively. Each solution was diluted by a factor 7.7 and UV-vis spectra were measured. Fig. 5.8 illustrates the UV-vis absorption at 300 nm for G4OH-$(Fe^{3+})_n$ solutions with molar ratios n = 30, 60, and 80.

In the case of the G4OH-$(Fe^{3+})_{30}$ sample, the absorbance at 300 nm was 40% higher after 2 days of complexation than that observed after 30 min of complexation. However, no significant changes were observed in spectra when complexation time was further increased from 2 to 5days. On the other hand, the absorption at 300 nm remains

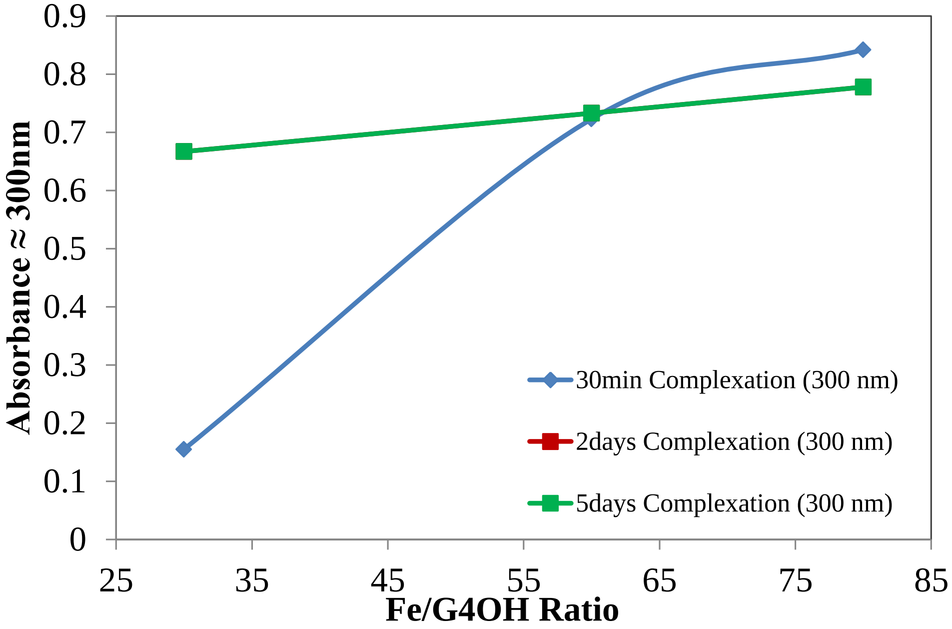

Figure 5.8 UV-vis absorbance at 300 nm characterizing G4OH-$(Fe^{3+})_x$ solutions (where x = 30, 60 and 80) as a function of complexation time and the Fe^{3+}/G4OH theoretical ratio. Aliquots of the solutions were diluted by a factor of 7.7 immediately prior to the UV-vis measurement. All solutions contained the same amount of Fe^{3+} (7.0 moles of $Fe(NO_3)_3$ from the $Fe(NO_3)_3$ stock solution). The concentration of G4OH dendrimer in the final solution was 0.069, 0.038 and 0.029 mM for Fe^{3+}/G4-OH molar ratios 30, 60 and 80, respectively.

unchanged with time in the case of G4OH-$(Fe^{3+})_{60}$ and G4OH-$(Fe^{3+})_{80}$ samples, indicating that for n ≥ 60 the complexation process is completed within first 30 min. The LMCT absorption band at 300 nm increases quadratically with the number of bound Fe atoms per G4OH for 30 min complexation, while for 2 or 5 days of complexation it increases linearly with the number of bound Fe atoms per G4OH. This suggests that the average structure of the light-absorbing Fe-O (or N) centers does not vary much after 2 days of complexation.[91]

5.3.2.4 Effect of dialysis on FB and EOB

Fig. 5.9(a) shows the fractional binding for G4OH-$(Fe^{3+})_n$ after 20 h of dialysis as a function of the theoretical Fe/G4OH ratio (n) and the solution pH. For n = 30, the data show that ~ 10% of the added Fe can be dialyzed from the Fe^{3+}/G4OH solution, suggesting that 10% of Fe is weakly bound or unbound with the G4OH dendrimer. For n < 30, the solution pH becomes greater than 3, and ferric oxide precipitates within 15 min of complexation (marked with the orange rectangular). For n > 30, the data show a significant decrease in the Fe fractional binding. The fractional binding for n = 60 and 80 is 78 and 53%, respectively, indicating that the G4OH dendrimer does not bind all of the Fe. To quantify this, we estimated the EOB, which is actually the number of Fe atoms actually bound per one G4OH molecule (Fig. 5.9(b)).

For n = 30 and the solution pH = 3, about 26 Fe atoms are irreversibly bound to each G4OH molecule (Fig. 5.9(b)). For n = 60 and the solution pH = 2.8, the number of irreversibly bound Fe atoms increases to approximately 47 per G4OH. These data are described by a parabola with maximum (or minimum) at n = 60. The main conclusion from Fig. 5.9 is that the actual number of Fe atoms that are irreversibly bound to G4OH

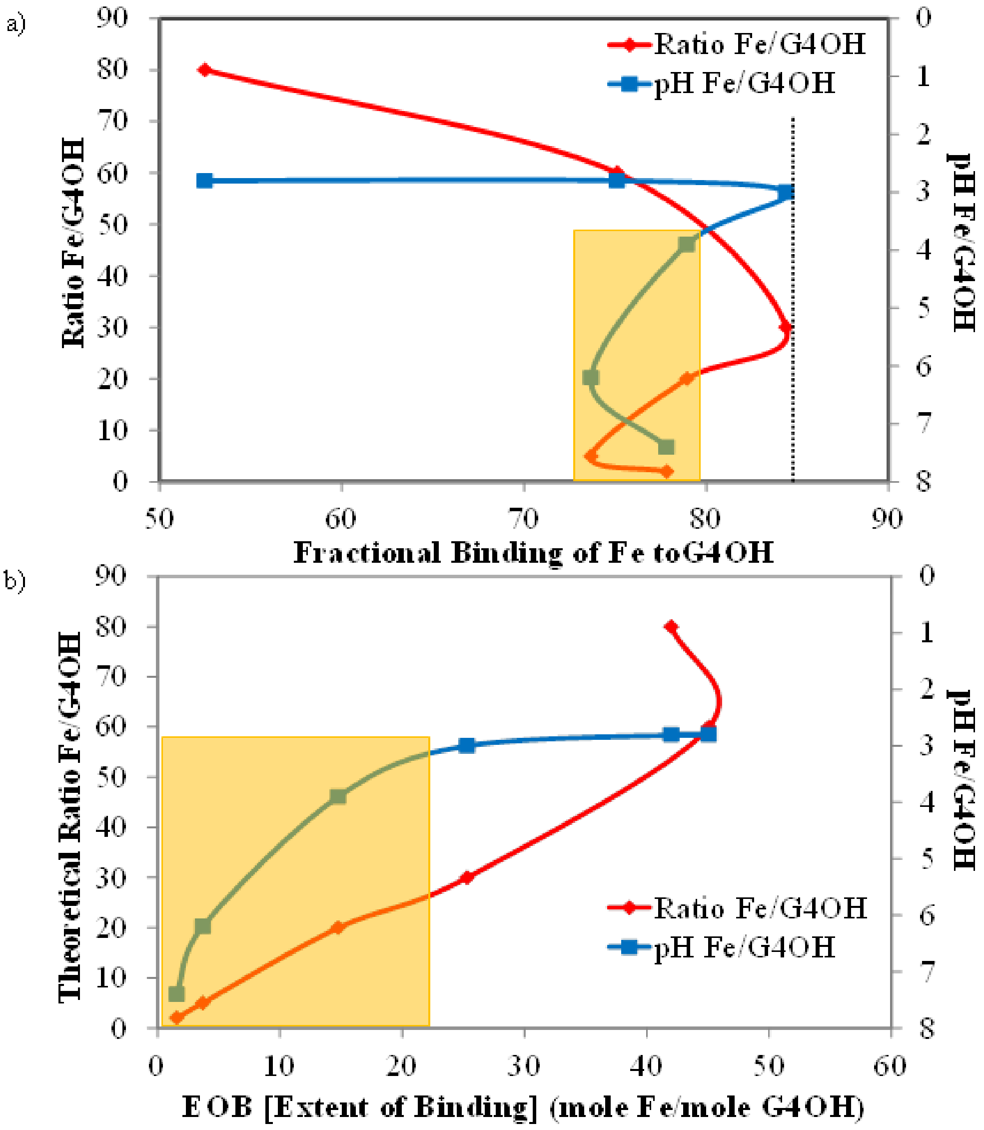

Figure 5.9 Theoretical Fe/G4OH ratio and the solution pH as a function of the Fractional Binding of Fe to G4-OH (a) and Extent of Binding [EOB] of Fe to G4-OH PAMAM dendrimers (b) after 24h dialysis. The red and blue curves correspond to the Fe/G4OH ratio and the solution pH, respectively.

is less than the theoretical Fe/G4OH ratio. Moreover, at high Fe/G4OH ratios (n = 80), the solution contains the significant fraction (47%) of weakly bound or unbound Fe^{3+}.

5.3.2.5 pH adjustment effect on the EOB of G4OH-$(Fe^{3+})_n$

When the solution pH was adjusted to 7.0 during the complexation process, the linear increase in EOB within the range of tested Fe(III)/G4OH molar ratios was observed (Fig. 5.10). In all cases, the FB of Fe(III) cations to the dendrimers was found to be 100%. This behavior can be attributed to the low extent of protonation of tertiary amine groups which can take part in the complexation process. When these groups become fully protonated at pH ~ 3, no binding of Fe(III) is observed with them but only with the O donor groups (i.e., OH and amide groups $RCONH_2$).

Diallo et al. reported that the 100% of FB can be obtained when the pH of aqueous solutions of $Fe(NO_3)_3$ or $FeCl_3$ with G4-NH_2 EDA core PAMAM dendrimers is adjusted to 7.0 (for Fe(III)/G4NH_2 molar ratios up to 250). They suggested that Fe(III) at pH 7.0 can complex with the tertiary/primary amines as well as the amide groups of the G4NH_2 dendrimer.[65] Note that the FB (Fig. 5.10)) of Fe(III) to the G4OH PAMAM dendrimer at pH 3.0 is slightly lower (by ~15%) than that at pH 7.0. This difference can be attributed to a slight decrease in the number of coordination sites available for iron due to the expansion of the fully protonated PAMAM dendrimer in aqueous solutions at pH 3.0.[55]

5.3.3 Quantitative analysis of Au-PAMAM ligand exchange reactions: Time and concentration effects

The relatively strong complexation of Fe(III) to G4OH at pH 3 is not completely unexpected, since U(VI) appears to complex strongly with G4NH_2 even at pH 2. It was

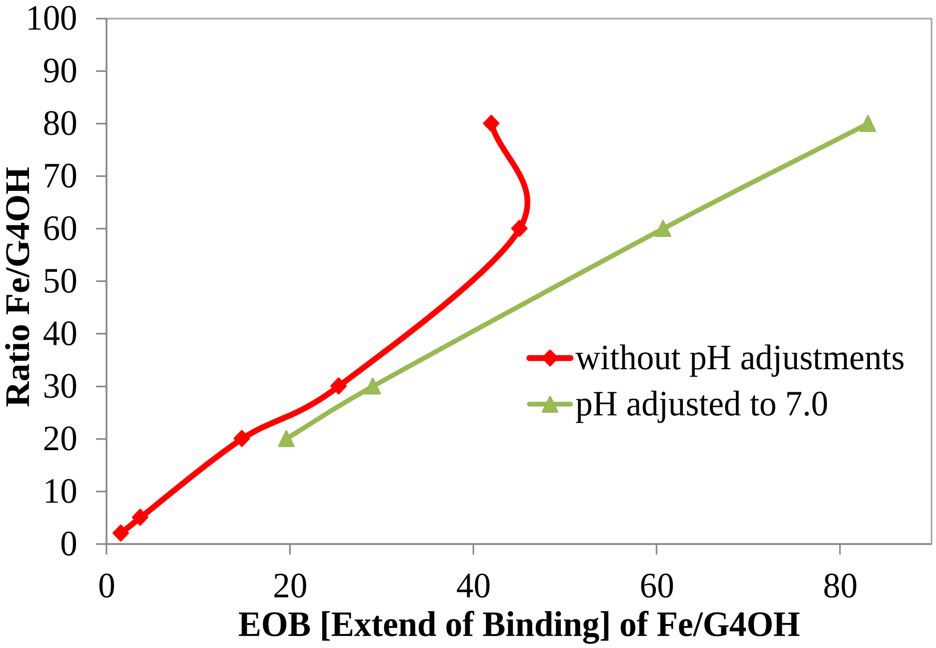

Figure 5.10 EOB of Fe to G4-OH PAMAM dendrimers after 24 h dialysis with and without pH adjustments (pH ~ 7.0). For the pH adjustments 0.1 N NaOH was used.

suggested that this strong complexation involves deprotonation of G4NH$_2$ amine groups followed by coordination with the UO_2^{2+}, which can also be valid for Fe(III).[55] It is also possible that as long as the metal used has high affinity for O donors, it can complex even under acidic conditions with the OH or the amide (RCONH$_2$) groups of the G4OH dendrimer.[98] The binding constants for O donors for U(VI) and Fe(III) are 8.2 and 11.81, respectively, much higher than their binding constants for N donors (2.0, 3.8, respectively), suggesting that even under acidic conditions, considering that the dendrimer tertiary amine groups are protonated, the metals can still complex with O donors.[64] In order to verify the fact that Fe(III) complexes strongly with G4OH due to its high affinity to O donors, experiments with a metal having lower affinity to O donors than Fe(III) but a similar precursor pH ($pH_{[Fe(NO3)3]} = 2.4$) were of a great interest. According to the hard-soft acid-base (HSAB) theory of Pearson, Au is considered to be a soft metal ion that shows an affinity to soft bases with donor atoms such as O < N < S, while Fe^{3+} shows an affinity to hard bases with donor atoms as O > N > S.[63,64,247] Furthermore, 1.4 mM of $HAuCl_4$ precursor solution has pH equal to 3.1, similar to that of $Fe(NO_3)_3$.

Fig. 5.11(a) shows values of FB for G4OH-$(Au^{3+})_n$ after 6 h of dialysis as a function of the theoretical Au/G4OH ratio (n) and the solution pH. The FB values for n = 2, 5, 10, 30, and 60 were found to be 67.6, 61.4, 39.7, and 11.0%, respectively, indicating that the FB of Au decreases as n increases. At n = 30 (pH 3.0), the significant amount of Au(III) is bound to the G4OH PAMAM dendrimer (FB ~ 39.7% and EOB up to 8.7, Fig. 5.11) even though tertiary amines are supposed to be fully protonated. There was no observed binding of Cu(II) to dendrimers at pH 3.0. This strongly suggests that the complexation of gold cations to the G4OH PAMAM dendrimer at pH 3.0 involves

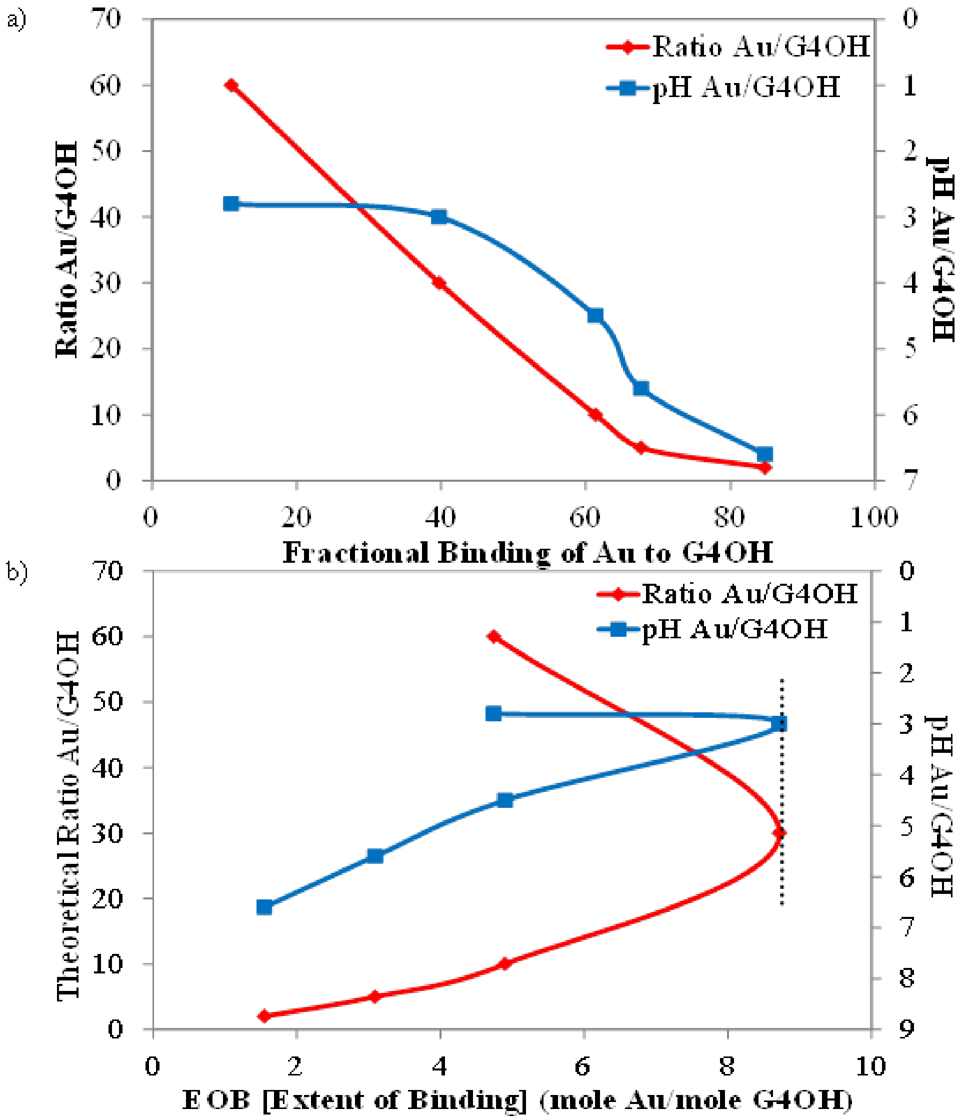

Figure 5.11 Theoretical Au/G4OH ratio and pH as a function of the Fractional Binding of Au to G4-OH (a) and Extent of Binding [EOB] of Au to G4-OH PAMAM dendrimers (b) after 6 h of dialysis. The red and blue curves correspond to the Au/G4OH ratio and the solution pH, respectively.

deprotonation of amine groups followed by their coordination with the Au^{3+} cations. Alternatively, Au^{3+} cations can complex directly with O atoms in the dendrimer interior.

Apparently, Au(III) interacts weaker with G4OH than Fe(III) under acidic conditions, since it has higher affinity for N donors, which are protonated at pH ~ 3.[248] More specifically, gold colloids are negatively charged as $AuCl_4^-$ ions are present in solution, while the dendrimer is positively charged due to the protonation of the amine groups. The interaction is thus electrostatic, involving ion pairing ($RN\text{-}H^+\cdots A^-$).[249] Finally, at higher Au/G4OH ratios (n = 60, pH = 2.8), the solution contains the significant fraction of weakly bound or unbound Au^{3+} (89%). Martinez et al. reported that at pH < 3 in the G4OH-$(Au^0)_8$ solution, the fluorescence intensity dropped significantly, consistent with the unstable nature of these nanoclusters in acidic solutions, which can also explain low FB values at pH 2.8.[250,251]

5.3.4 Comparison between Theoretical Metal/Dendrimer ratio and max EOB of Fe and Au with G4OH dendrimer

Experimental results obtained for Cu(II), Fe(III), and Au(III) indicate that EOB values characterizing the complexation of these cations to the G4OH dendrimer depend on the solution pH. While it was expected that the dendrimer would be protonated at acidic pH and, therefore, unable to complex metal cations, results obtained for G4OH-$(Au^{3+})_{30}$ and G4OH-$(Fe^{3+})_{60}$ demonstrate that at pH ~ 3 EOB values have maxima at 8.7 and 46, respectively, (Table 5.3). This unexpected result can be explained if one would assume that the initially protonated dendrimer becomes deprotonated under acidic conditions and capable of complexing with the metal cations so a certain degree. It is also possible that Au(III) and Fe(III) cations can complex with O donors of the G4OH dendrimer and not with amine groups. Furthermore, the data indicate that Fe(III)

Table 5.3 Theoretical ratio and maximum EOB values of Au(III), Fe(III) to G4-OH and Cu(II) to G4-OH with and without pH adjustments and Cu(II) to G_n-NH_2 (n = 3 -8).[122]

Metal	Theoretical Ratio Metal/Dendrimer	Max Extend Of Binding	pH
Au	30	8.7	3
Fe	60	46	2.8
Cu (WITHOUT pH adjustments)	13	8.2	5.5
Cu (WITH pH adjustments)	60	24	6.1 (adj.)
Cu[G3-NH_2]	11	8 ± 1	
Cu[G4-NH_2]	18	13 ± 1	
Cu[G5-NH_2]	41	29 ± 3	
Cu[G6-NH_2]	91	46 ± 9	
Cu[G7-NH_2]	114	83 ± 9	
Cu[G8-NH_2]	306	153 ± 20	

complexes stronger with the G4OH dendrimer in comparison with Au(III) and Cu(II) because the maximum EOB value for G4OH-$(Fe^{3+})_{60}$ after 1 day of dialysis is only 23% lower than the initial theoretical molar ratio used, while for Au(III) and Cu(II) the difference is 71 and 37%, respectively.

The data obtained in the case of Cu(II) show that when the pH of the G4OH-$(Cu^{2+})_x$ solution was adjusted to 6.1, the EOB values were increased. More specifically, the maximum EOB value of 12 was observed for G4OH-$(Cu^{2+})_{60}$ without pH adjustments, while this value was increased to 24 when pH adjustments were used. Furthermore, the data obtained for G4OH-$(Cu^{2+})_{13}$ and G4NH_2-$(Cu^{2+})_{18}$ show that maximum EOB values for G4OH-$(Cu^{2+})_{13}$ end G4NH_2-$(Cu^{2+})_{18}$ are 37 and 28 % lower than the theoretical molar ratio used, respectively (Table 5.3). The higher maximum EOB value in the latter case can be attributed to the complexation of Cu cations with primary amines of the dendrimer.

5.3.5 Quantitative analysis of Ni-PAMAM ligand exchange reactions: Time and concentration effects

5.3.5.1 Evidence of G4OH-$(Ni^{2+})_n$ complexation

The complexation features of G4OH with Ni(II) (d^8) are rather different from those observed for Cu(II), despite the fact that the molar ratios of Ni^{2+}/G4OH used were almost the same as those for Cu(II). Bianchi et al. reported that the Ni(II) spectrum is independent of pH, which is a main difference between Cu(II) and Ni(II) absorption spectra.[252] The main difference was revealed by the absorption spectrum of the Ni(II) complex. The UV-vis spectrum of $[Ni(H_2O)_6]^{2+}$ displays two absorption bands at 390 and ~ 700 nm which can be assigned as shown in Table 5.4.[242,253,254] Furthermore, a split of the band at 700 nm appears in the $[Ni(H_2O)_6]^{2+}$ spectrum due to spin-orbit coupling

Table 5.4 Spectra of Octahedral Nickel(II) Complexes (band positions in nm).[242,253]

Transition	$[Ni(H_2O)_6]^{2+}$	$[Ni\ en_3]^{2+}$ (en: ethylenediamine)
$^3A_{2g} \rightarrow {}^3T_{1g}$ (F)	700	550
$^3A_{2g} \rightarrow {}^3T_{1g}$ (P)	400	350

which mixes the $^3T_{1g}$ (F) and ^1E_g states which are very close in energy (Fig. 5.12(a)).[242,253] A considerable number of neutral ligands, especially amines, can displace some or all of the water molecules in octahedral $[Ni(H_2O)_6]^{2+}$ species and form complexes such as trans-$[Ni(H_2O)_2(NH_3)_4](NO_3)_2$.[283] When ammines are complexed with Ni(II) in solution, the initial absorption spectra are blue shifted as it is shown in Table 5.4.[255]

UV-vis spectra characterizing 0.34 mM G4OH-$(Ni^{2+})_2$ and 0.05 mM G4OH-$(Ni^{2+})_{60}$ solutions after 5 days of complexation and spectra characterizing corresponding solutions of the precursor (Fig. 5.12(b)-dashed lines) with the same concentration of Ni^{2+} are compared in Fig. 5.12(b). Two bands at 390 and 700 nm are evident in the spectrum of the Ni precursor solution. In the case of the G4OH-$(Ni^{2+})_2$ solution, these peaks are blue shifted to ~ 370 and 605 nm, while in the case of the G4OH-$(Ni^{2+})_{60}$ solution the peaks blue shifted only slightly (Fig. 5.12(b)). Based on these observation we can conclude that the complexation of Ni(II) with G4OH depends on the concentration of Ni(II) in the solution. Moreover, it seems that for low Ni(II)/G4OH molar ratios, such as G4OH-$(Ni^{2+})_2$, there is a weak interaction between Ni(II) and the dendrimer, while interactions between Ni(II) and the dendrimer are much weaker in the case of higher molar ratios (i.e., G4OH-$(Ni^{2+})_{60}$).

5.3.5.2 Complexation kinetics-Determination of complexation time (UV-vis)

Fig. 5.13 illustrates the effect of the Ni(II) concentration on the position and the absorbance of the band at ~ 390 nm, which is attributed to the Ni^{2+}-amine interaction, as a function of the Ni^{2+}/G4OH molar ratio and complexation time. Fig. 5.13(a) shows that the band at 390 nm is blue shifted to 368.9, 372.5, 374.7, 379, 381.7, and 389.6 nm for

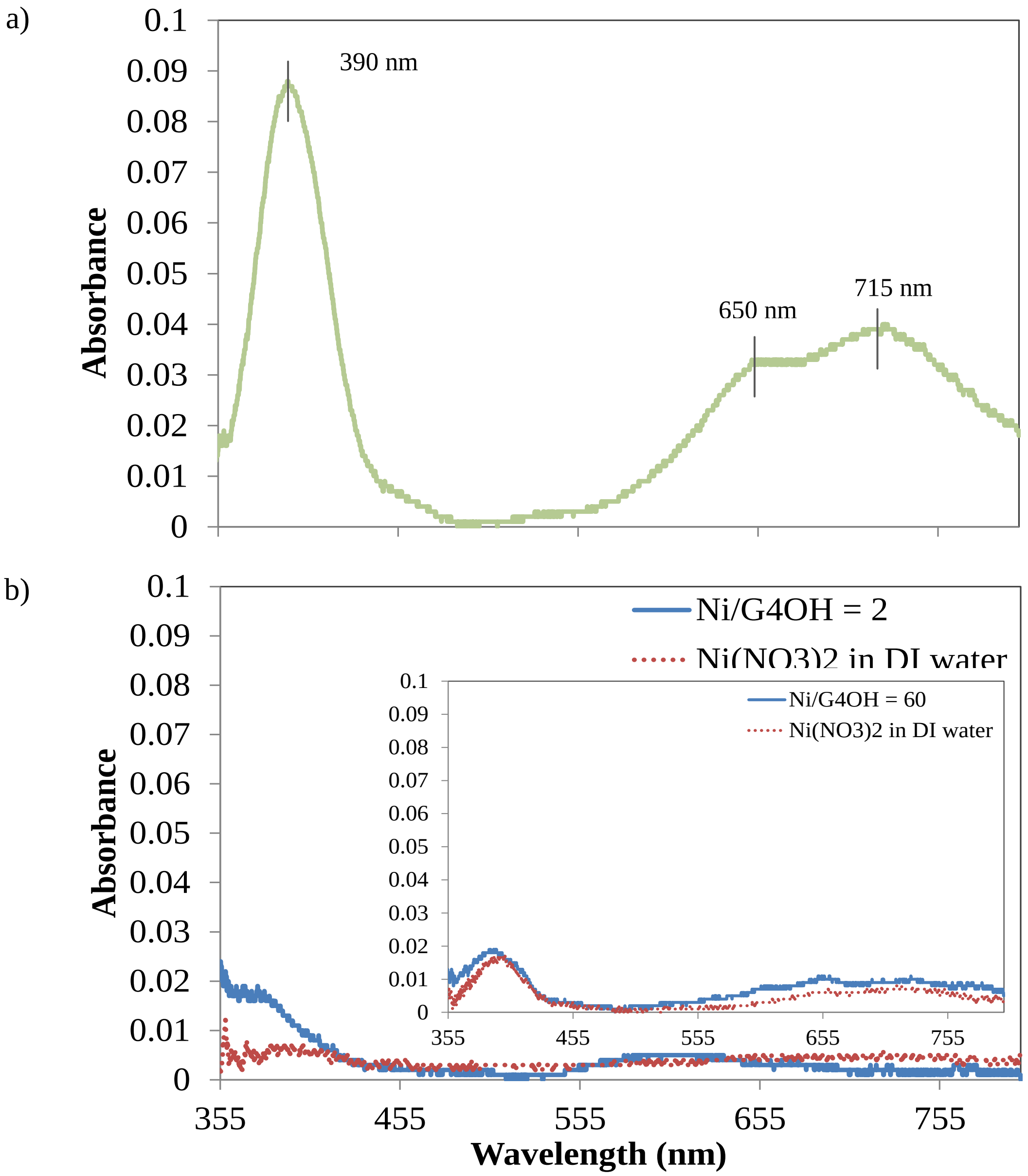

Figure 5.12 UV-vis spectra characterizing (a) the solution of Ni(NO$_3$)$_2$ (3.5 mM) diluted by a factor of 2 immediately prior to the UV-vis measurement and (b) 0.34 mM G4OH-(Ni^{2+})$_2$ and 0.05 mM G4OH-(Ni^{2+})$_{60}$ (inset) compared with spectra of the Ni precursor in DI water prepared with the same Ni concentration. Aliquots of all the solutions prepared were not diluted prior to UV-vis measurement

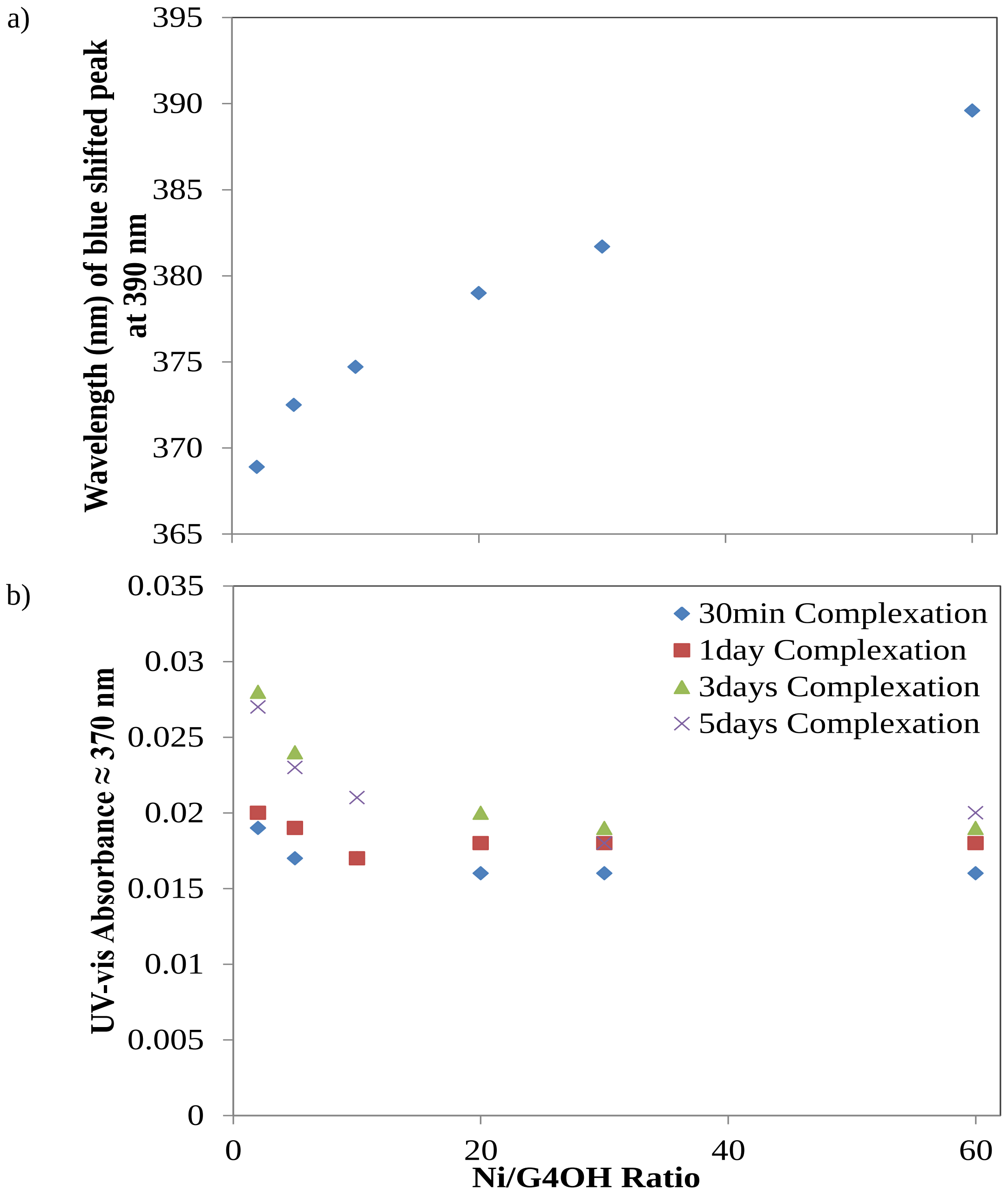

Figure 5.13 The position (nm) (a) and absorbance (b) of UV-vis bands as a function of theoretical Ni(II)/G4OH ratios and the complexation time, respectively. Data in (a) were taken after 30 min of complexation. Aliquots of solutions were not diluted prior to UV-vis measurement. All solutions contained the fixed amount of Ni^{2+} (0.015 mmol of $Ni(NO_3)_2$ from the $Ni(NO_3)_2$ stock solution). The concentration of G4-OH dendrimer in each case varied depending on the desired Ni^{2+}/G4-OH ratio. Specifically, the concentration of G4-OH used was 0.34, 0.26, 0.19, 0.12, 0.09, 0.07, 0.05 mM for Ni^{2+}/G4-OH molar ratios 2, 5, 10, 20, 30, 40, and 60, respectively.

Ni^{2+}/G4OH molar ratios 2, 5, 10, 20, 30 and 60, respectively. It is obvious that the peak at 390 nm gradually returns to its initial position (i.e., 390 nm) with an increase in the Ni^{2+}/G4OH molar ratio, which is consistent with a decrease in the interaction of Ni^{2+} with the dendrimer. In order to determine the complexation time, the absorbance of the blue shifted peak was plotted vs time in Fig. 5.13(b). For G4OH-$(Ni^{2+})_2$, G4OH-$(Ni^{2+})_5$, and G4OH-$(Ni^{2+})_{10}$ solutions, the absorbance of the peak ~ 370 nm increased with increasing the complexation time but no changes were observed after 3 days of complexation. On the other hand, the absorbance of solutions with higher Ni^{2+}/G4OH molar ratios (such as G4OH-$(Ni^{2+})_{20,30,60}$) remained nearly constant with time. These observations can lead us to the conclusion that the complexation time depends on the Ni^{2+}/G4OH ratio. More specifically, the Ni^{2+}-amine complexation is stronger in the case of small Ni^{2+}/G4OH ratios but approximately 3 days are required to complete the complexation process, while Ni^{2+}-amine interactions are weaker in the case of higher molar ratios and the complexation process can be completed in less than 30 min.

Bianchi et al. mentioned that the complexation of Ni(II) can be affected by the kinetic inertness of ligands, in particular those which are sterically hindered. Therefore, the process of Ni(II) encapsulation by the dendrimer may be extremely slow at room temperature and the coordination of Ni(II) occurs primarily at the less hindered binding site such as the external nitrogen atoms of the amine terminated G_xNH_2 PAMAM dendrimer.[252] It is noteworthy that Ni(II) has a marked tendency to impose its own geometry to ligands. At the same time, the presence of PAMAM dendrimers leads to a reduced ability of the “intra-cavity” amine donors to adapt themselves to the rather strict stereochemical requirements of Ni(II). This could thermodynamically favor Ni(II) complexation to nitrogens at the periphery of PAMAM dendrimers.[254]

5.3.5.3 Effect of dialysis on FB

The content of Ni was measured in all G4OH-(Ni^{2+})$_x$ solutions (where x = 2, 5, 30, and 60) before and after dialysis. The data obtained indicate that G4OH-(Ni^{2+})$_2$ and G4OH-(Ni^{2+})$_5$ solutions lost approximately 50% Ni after 6 h of dialysis, while the loss of Ni was approximately 90% in the case of G4OH-(Ni^{2+})$_{30}$ and G4OH-(Ni^{2+})$_{60}$ solutions with higher molar ratios (Fig. 5.14).

After 1 day of dialysis the loss of Ni was increased to 80-90% in the former case, while all Ni was removed from G4OH-(Ni^{2+})$_{30}$ and G4OH-(Ni^{2+})$_{60}$ solutions. These data clearly show that Ni(II) weakly binds to the G4OH dendrimer in G4OH-(Ni^{2+})$_{30}$ and G4OH-(Ni^{2+})$_{60}$ solutions, which is consistent with UV-vis data. For G4OH-(Ni^{2+})$_2$ and G4OH-(Ni^{2+})$_5$ solutions with smaller Ni^{2+}/G4OH molar ratios, approximately ~ 10-20% Ni remains in the solution after 1 day of dialysis, indicating the stronger Ni^{2+}-amine interactions in this case. It is feasible that the remaining Ni can also be dialyzed during more exhaustive dialysis experiments. In general, the interaction between Ni(II) and G4OH is considered to be much weaker that interactions of Cu(II), Fe(III), and Au(III) with G4OH.

5.3.6 Quantitative analysis of Co-PAMAM ligand exchange reactions: Time and concentration effects

Co(II) cations (d^7) are known to form both octahedral $[Co(H_2O)_6]^{2+}$ and tetrahedral complexes $[Co(H_2O)_4]^{2+}$. Because the difference in the stability of these complexes is small, there are several cases in which both types of complexes are present simultaneously. For instance, the inset shown in Fig. 5.15(a) illustrates the UV-vis

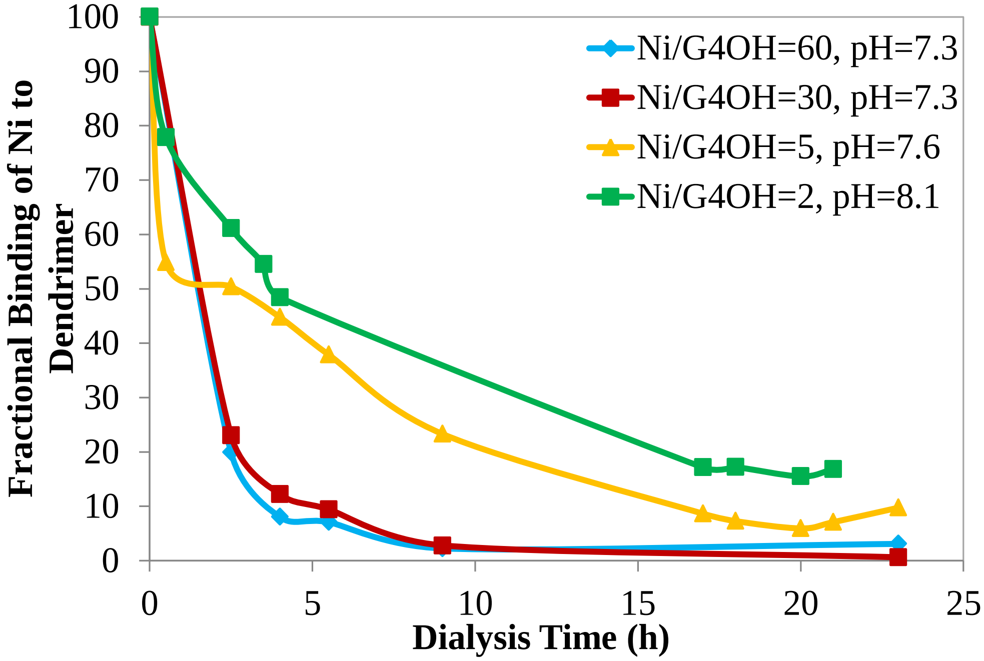

Figure 5.14 Fractional Binding of Ni^{2+} to G4-OH after 3 days of complexation as a function of the dialysis time.

spectrum of the $Co(NO_3)_2$ aqueous solution. Two weak bands observed in this spectrum at ~510 and 621 nm can be attributed to the presence of the octahedral $[Co(H_2O)_6]^{2+}$ ($^4T_{1g}$ (P) $\leftarrow$ $^4T_{1g}$ (F)) and the tetrahedral $[Co(H_2O)_4]^{2+}$ ($^4A_{2g}$ $\leftarrow$ $^4T_{1g}$ (F)) complexes, respectively. The shoulder $^4T_{1g}$ (P) $\leftarrow$ $^4T_{1g}$ (F) appears as a result of the spin-orbit coupling split of the $^4T_{1g}$ (P) excited state.[256-258] While Co(III) shows a particular affinity for nitrogen and various complexes of Co(III) incorporating ammonia, amines, nitro, and nitrogen-bonded SCN groups are well known, no such information can be found for Co(II).[242,256,257]

When the G4OH dendrimer was added to the Co^{2+} precursor solution to form G4OH-$(Co^{2+})_2$, the initial absorption band at ~510 nm shifted to 450 nm, suggesting the interaction of the octahedral $[Co(H_2O)_6]^{2+}$ complex with amine groups of the dendrimer (Fig. 5.15(a)). In this case, the band at 621 nm remains in the same position, indicating that the tetrahedral $[Co(H_2O)_4]^{2+}$ complex does not interact with the amine groups of the dendrimer.[258] In the case of higher Co^{2+}/G4OH molar ratios (i.e., G4OH-$(Co^{2+})_{60}$) the peak at 510 nm remains in the same position, indicating that there is no interaction between $[Co(H_2O)_6]^{2+}$ and amine groups of the dendrimer, while the absorption band at 621 nm disappears, indicating that an increase in the Co(II) concentration in solution moves the equilibrium between octahedral and tetrahedral Co(II) complexes to the octahedral side. The complexation of Co(II) with the G4OH dendrimer is somewhat similar to the complexation of Ni(II) with G4OH because in both cases there is a weak interaction of metal cations with the G4OH dendrimer only for the metal/dendrimer molar ratio of 2.

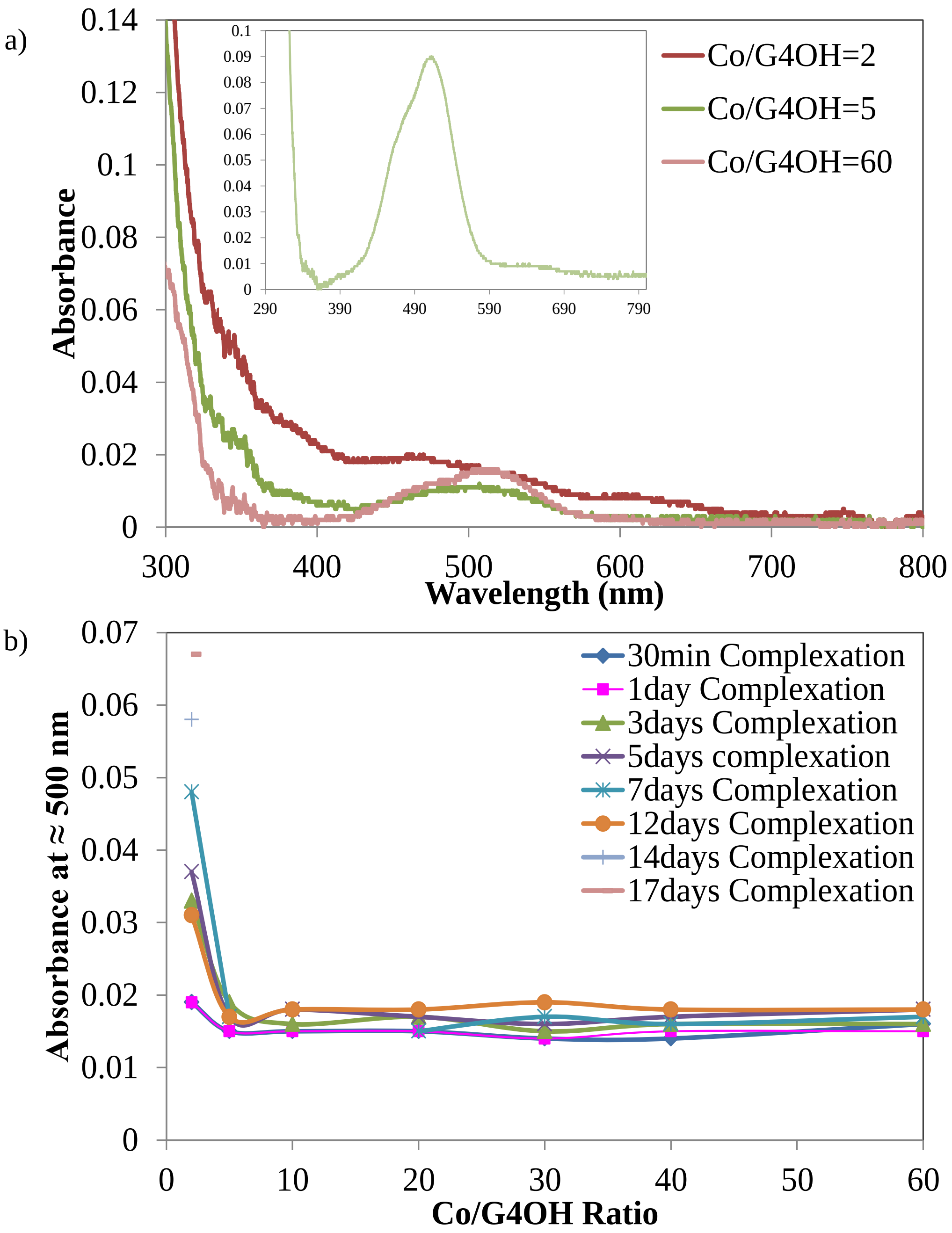

Figure 5.15 UV-vis spectra characterizing (a) G4OH-(Co^{2+})$_x$ (with x = 2, 5, 40, and 60) after 3 days of complexation. The inset plot shows the UV-vis spectrum of the precursor solution (3.4 mM) diluted by a factor of 2 immediately prior to the UV-vis measurement, (b) G4OH-(Co^{2+})$_x$ complex at ~500 nm (x = 2, 5, 10, 20, 30, 40 and 60) as a function of complexation time and Co^{2+}/G4-OH theoretical ratio. Aliquots of the solutions were not diluted prior to UV-vis measurements.

Fig. 5.15(b) illustrates UV-vis spectra as a function of time for G4OH-$(Co^{2+})_x$ with x = 2, 5, 10, 20, 30, 40 and 60. It is evident that the absorbance for all Co^{2+}/G4OH molar ratios remains unchanged with time, except for the G4OH-$(Co^{2+})_2$ case in which the absorbance at 450 nm increases even after 17 days of complexation. Based on these UV-vis data, we can conclude that similar to the case of Ni, the complexation of Co with G4OH is weak and slow, but is somewhat stronger in the case of smaller Co^{2+}/G4OH molar ratios. Finally, nearly 100% of Co(II) cations can be removed from G4OH-$(Co^{2+})_x$ (x = 2, 5, 30, and 60) solutions after 7 h of dialysis (Fig. 5.16). This result indicates the presence of weak Co^{2+}-G4OH interactions, which is consistent with UV-vis data.

5.3.7 Quantitative analysis of Mn, Zn-PAMAM ligand exchange reactions: Time and concentration effects

Complexes of Mn(II) have five d electrons and approximately seven d-d transitions are possible which are characterized by very weak bands in UV-vis spectra even for a simple complex such as $[Mn(H_2O)_6]^{2+}$.[242,259] Mn(II) can form a variety of different complexes but the equilibrium constants for their formation in aqueous solutions are relatively low when compared to those of Fe(III) and Cu(II). The interaction of ammonia with $[Mn(H_2O)_6]^{2+}$ may lead to the formation of $[Mn(NH_3)_6]^{2+}$. Mn complexes with chelating ligands such as ethylenediamine etc. are also known. Zn cations are also capable of forming complexes with amine ligands.[242]

Fig. 5.17(a) shows UV-vis spectra of G4OH-$(Mn^{2+})_2$, G4OH-$(Mn^{2+})_5$, and G4OH-$(Mn^{2+})_{60}$ solutions. The aqueous solution of $Mn(NO_3)_2$ is characterized by a weak absorption band at 400 nm which is slightly shifted to lower wavelengths after G4OH was added to the solution. Similar to what was observed during complexation of Ni(II) and Co(II) with G4OH, the initial peak at 400 nm is shifted to ~355 nm for G4OH-

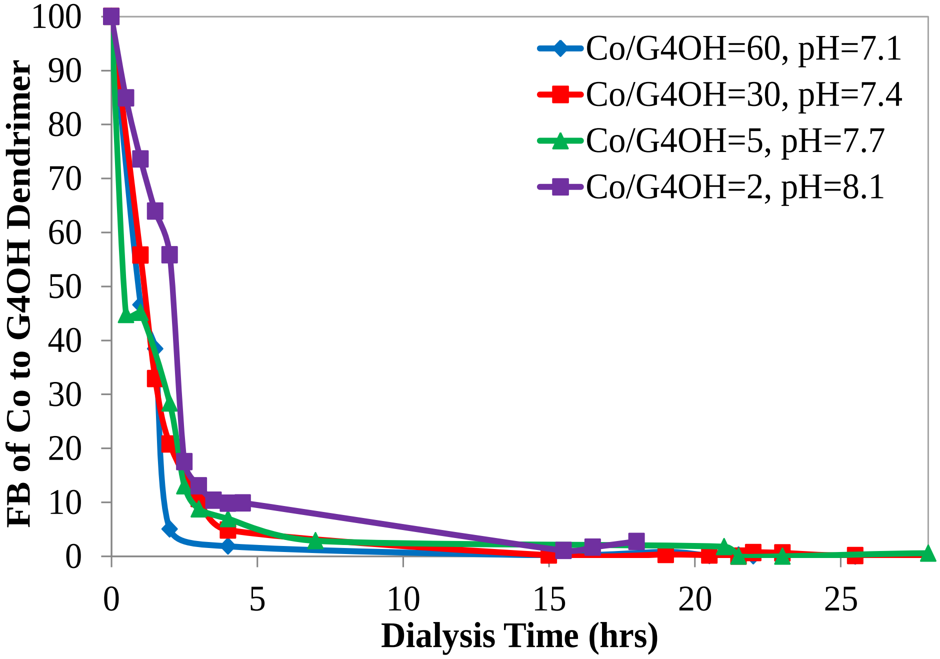

Figure 5.16 Fractional Binding of Co^{2+} to G4-OH measured after 3 days of complexation as a function of the dialysis time.

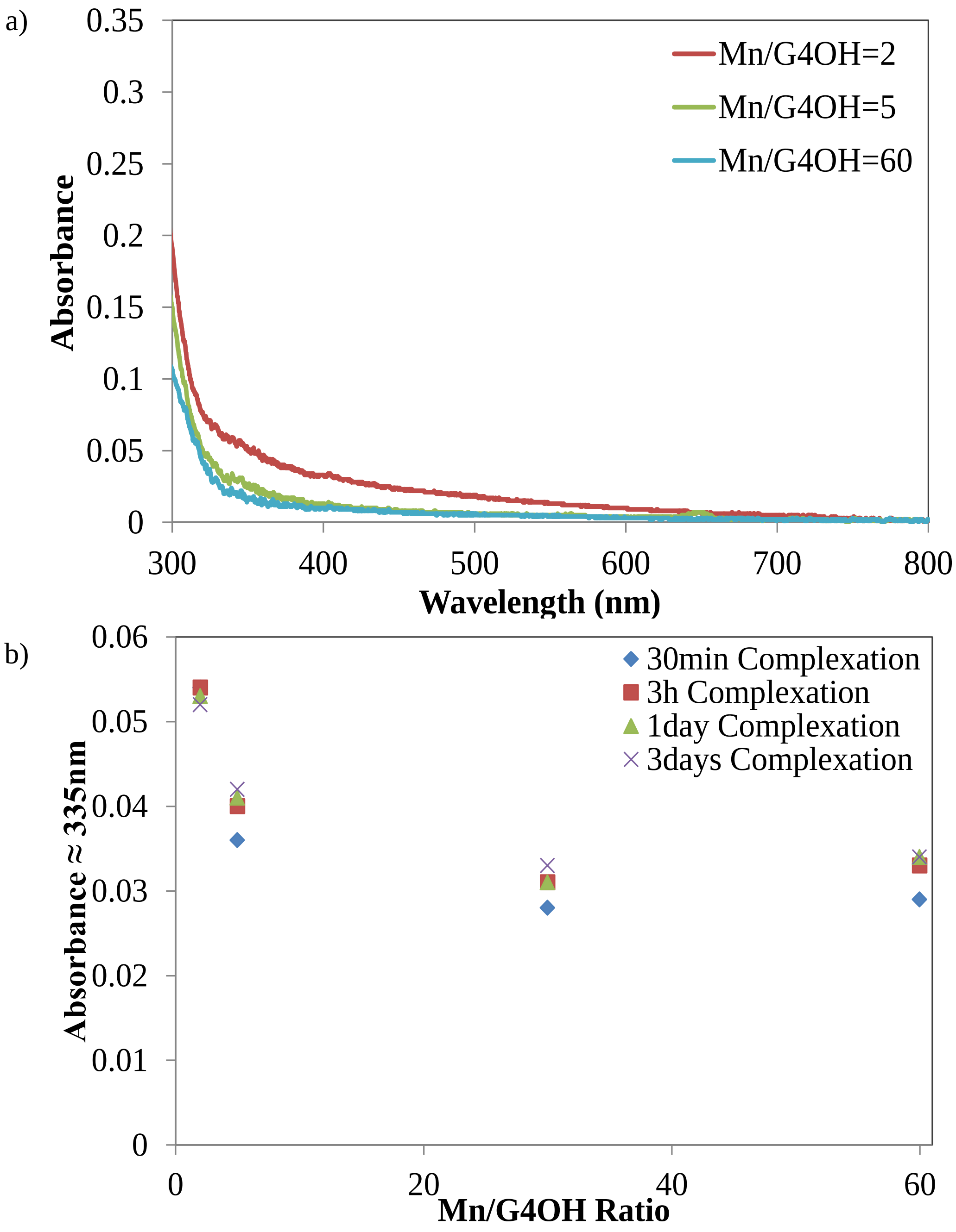

Figure 5.17 UV-vis spectra of G4OH-$(Mn^{2+})_x$ (x = 2, 5, and 60) collected after 30 min of complexation (a) and the absorbance of the G4OH-$(Mn^{2+})_x$ complex at 335 nm (x = 2, 5, 30 and 60) as a function of the complexation time and Mn^{2+}/G4-OH theoretical ratio (b). Aliquots of all solutions were not diluted prior to UV-vis measurements. All solutions contained the same amount of Mn^{2+} (0.03 mmol of $Mn(NO_3)_2$ from the $Mn(NO_3)_2$ stock solution). The concentration of G4-OH used was 0.38, 0.33, 0.16, and 0.10 mM for Mn^{2+}/G4-OH molar ratios 2, 5, 30 and 60, respectively.

$(Mn^{2+})_2$, while for higher Mn(II)/G4OH molar ratios the peak at 400 nm remains almost in the same position, indicating the presence of weak Mn(II)/G4OH interactions. In order to determine the complexation time of Mn(II) to G4OH dendrimer, the absorbance at ~355 nm was monitored as a function of time and the data obtained suggest that the complexation process is completed after approximately 3 h (Fig. 5.17(b)). Experiments with Zn(II)/G4OH solutions show similar results.

In order to determine the strength of the Mn(II) and Zn(II) complexation to the G4OH dendrimer, solutions with different Mn(II)/G4OH and Zn(II)/G4OH molar ratios were prepared and dialyzed. Fig. 5.18 illustrates the FB of Mn(II) and Zn(II) to the G4OH dendrimer as a function of the dialysis time. It is evident that nearly all Mn can be removed from the solution after 6 h of dialysis, consistent with weak Mn-G4OH interactions. Similar data collected for Zn/G4OH solutions also suggest the presence of weak Zn-G4OH interactions. However, in the absence of experimental points between 4 and 20 h of dialysis, the time required for complete removal of Zn from the solution cannot be determined precisely in this case.

5.3.8 Quantitative analysis of Ag-PAMAM ligand exchange reactions: Time and concentration effects

5.3.8.1 Evidence of G4OH-$(Ag^+)_n$ complexation

In a typical preparation procedure for G4OH-$(Ag^+)_{60}$, 150 μL of the silver nitrate stock solution (58.9 mM) was added drop wise under stirring to a desired amount of the G4OH stock solution. The volumetric flask was filled up to 40 mL with DI water resulting in a $[Ag^+] = 0.22$ mM. This procedure was carried out in darkness. UV-vis spectra ($\lambda = 190 – 250$ nm) collected for the aqueous solution of the G4OH dendrimer ($5.31 \cdot 10^{-3}$ mM) are characterized by a band located at approximately 210 nm. When Ag^+

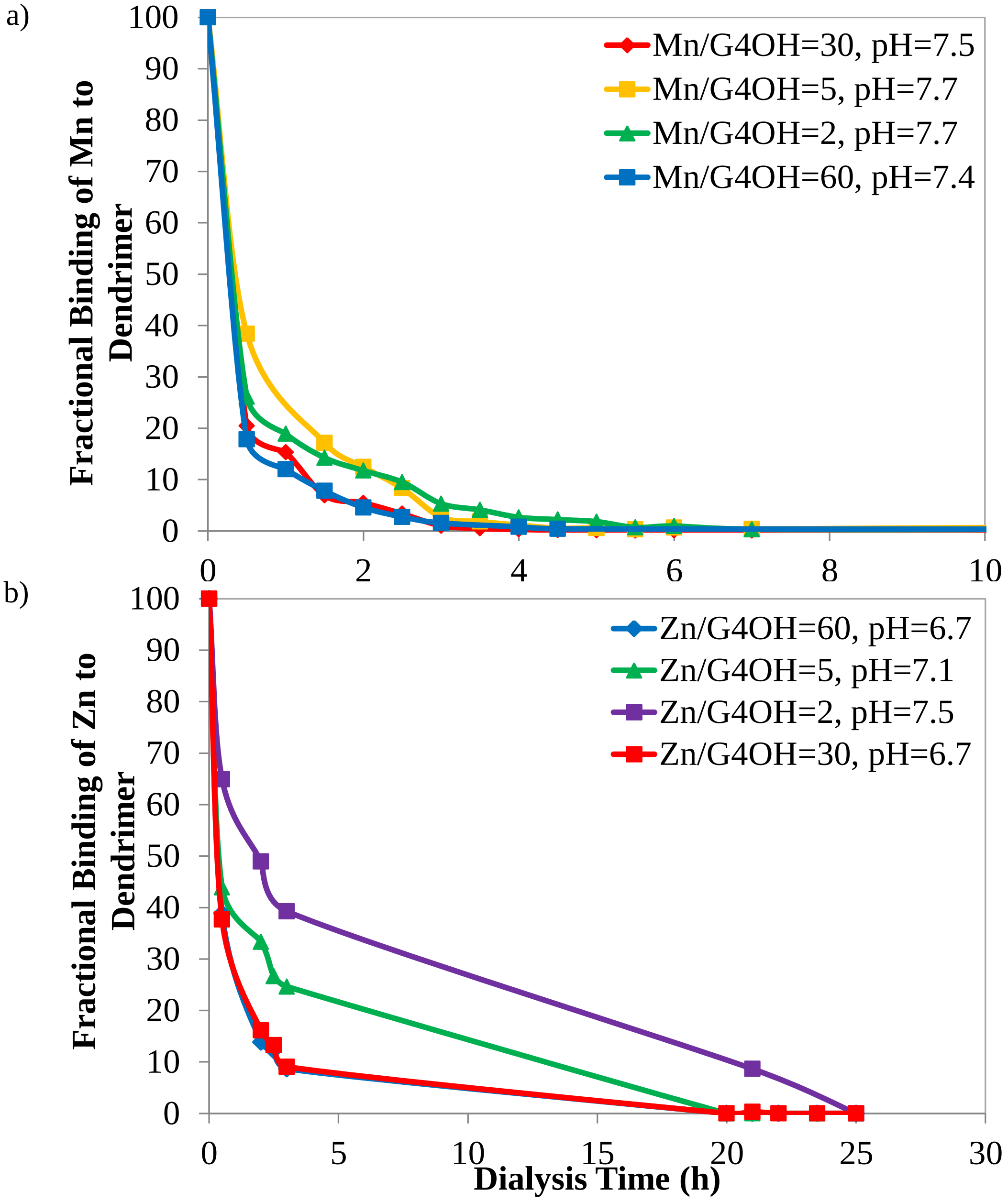

Figure 5.18 Fractional Binging of Mn^{2+} (a) and Zn^{2+} (b) to G4-OH after 3 days of complexation as a function of dialysis time

was added to this solution, a new band appeared at λ_{max} = 420 nm after 4 days of complexation in a dark environment (Fig. 5.19). Upon ageing of this solution for another 12 days, the intensity of the peak at 420 nm was enhanced.[260] It is know that metallic silver has an intense plasmon absorption band in the visible region at approximately 320 nm.[261] The presence of the characteristic red shift of the plasmon absorption band suggests the formation of dendrimer-protected silver nanoparticles with sizes larger than 4 nm.[152,155,262] It is possible that the G4OH dendrimer transfers some electron density to Ag and this process further leads to the formation of Ag particles.[130,261,263] Furthermore, the yellow color of the colloidal silver solution is believed to be a clear evidence for the formation of silver nanoparticles.[147]

5.3.8.2 Complexation kinetics for G4OH-$(Ag^+)_n$ solutions

When the G4OH-$(Ag^+)_{60}$ solution was prepared, it was kept under stirring while the complexation process was monitored by the UV-vis spectroscopy. The initial colorless solution became yellow after 4 days of complexation and finally the solution color became dark brown after 22 days of complexation. After this period of time (22 days), a precipitate was formed and UV-vis spectra were no longer recorded. The formation of large Ag particles with dimensions exceeding those of G4OH molecules could be a reason for the precipitation of Ag.[71] The intensity of the 420 nm band increased substantially with complexation time and a shoulder appeared at approximately 570 nm after 18 days of complexation (Fig. 5.20(a)).

From the shape of the absorption peak one can also acquire at least some information about the size distribution of metal particles which are formed in solution. For example, when metal particles are monodisperse and have the narrow distribution of sizes, the shape of the peak is expected to be symmetric and the value of the full width at

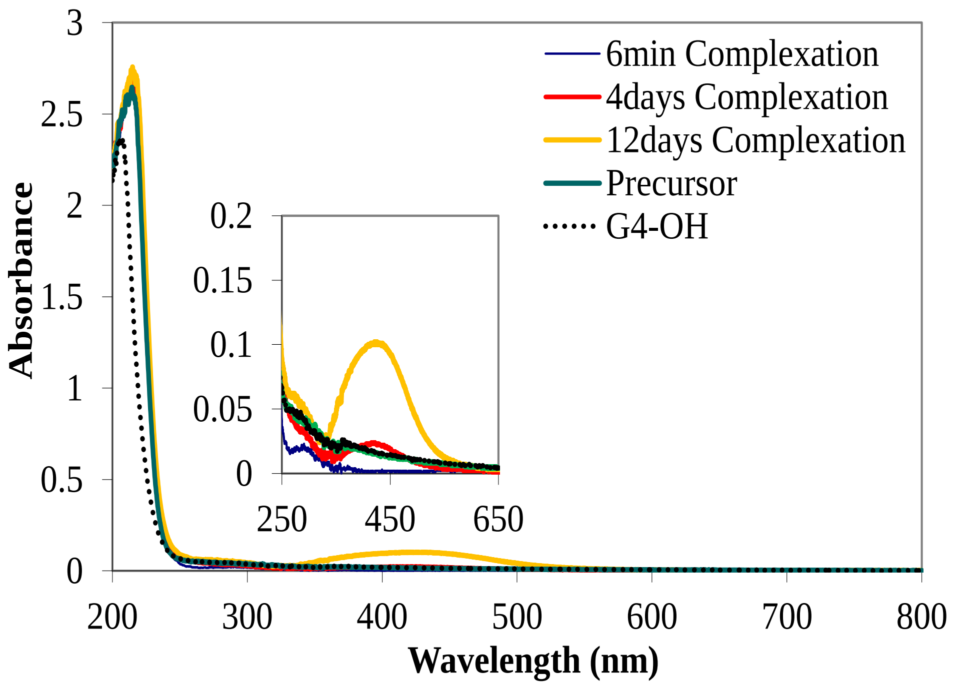

Figure 5.19 UV-vis spectra of $5.31 \cdot 10^{-3}$ mM G4OH and G4OH-$(Ag^{+})_{60}$ solutions as a function of time.

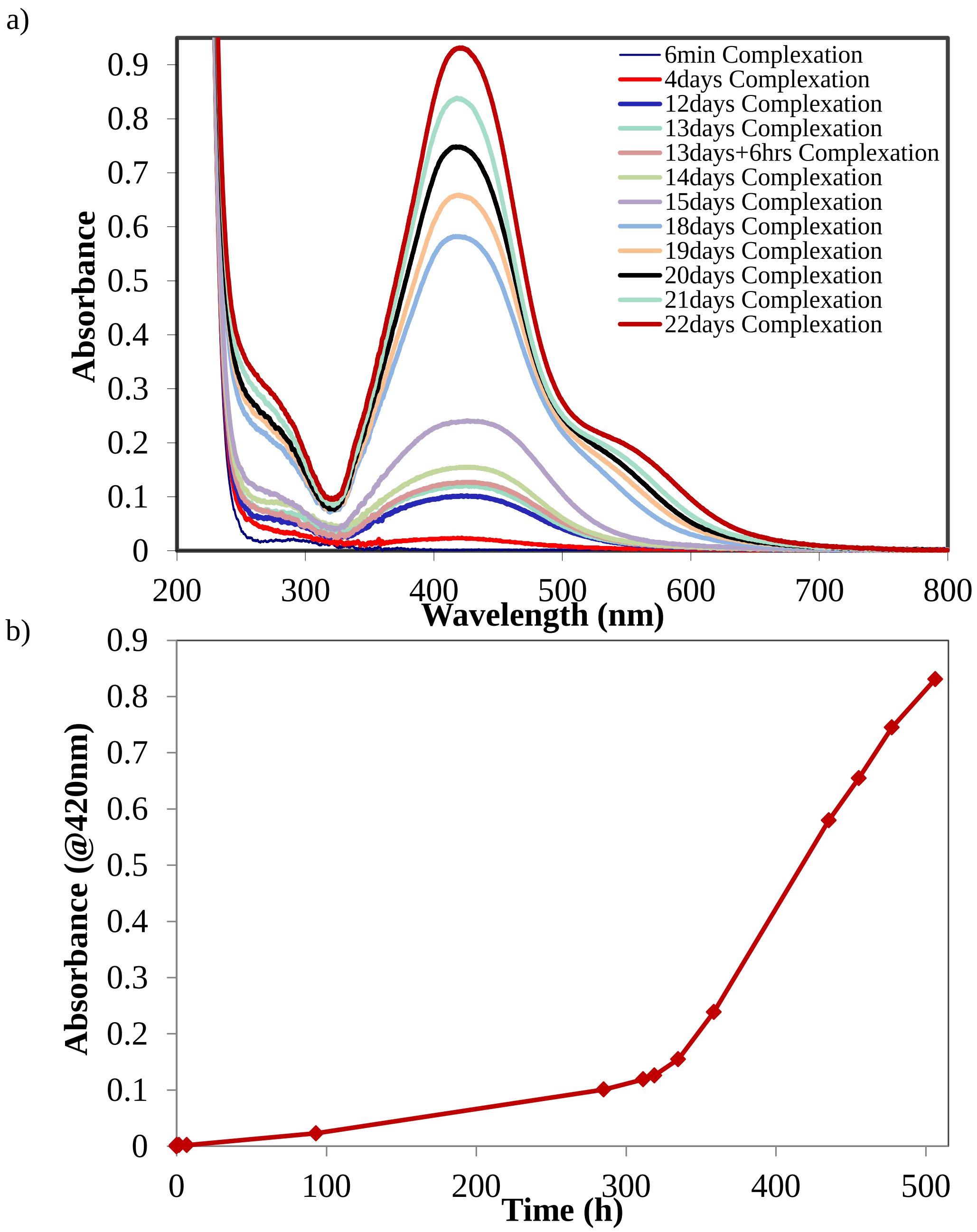

Figure 5.20 UV-vis absorption spectra of $5.31 \cdot 10^{-3}$ mM G4OH and G4OH-$(Ag^{+})_{60}$ solution (a) and maximum absorbance at 420 nm (b) as a function of time. This procedure was carried out in darkness.

half-maximum (FWHM) is expected to be small.[149,263,264] In contrast, when the system is polydisperse, the peak shape is expected to be asymmetric due to the overlap of two or more absorption peaks.[265,266] From the data shown in Fig. 5.20(a) for Ag, one can suggest that the shape of the peak was changed from symmetric to asymmetric after approximately 14 days of complexation, consistent with a suggestion that the size distribution became broader due to the transformation of the Ag colloid system from monodispersed to polydispersed.[263]

Fig. 5.20(b) shows that the band at 420 nm increases slow in intensity during first 300 h but the increase is substantially stronger thereafter. This band is growing continuously for almost a month with no indications of the steady state over the duration of the experiment. The intensity of the silver plasmon resonance in the G4OH-$(Ag^+)_{60}$ solutions was found to be a function of the nanoparticle size and architecture. The increase in intensity suggests the increase in the size of Ag nanoparticles.[261,262,267]

Fig. 5.21 shows UV-vis spectra of the G4OH-$(Ag^+)_{60}$ solution, which was complexed for 1 h, before and after it was treated with the 15-fold weight excess of $NaBH_4$. The spectrum of the G4OH-$(Ag^+)_{60}$ solution has no bands in the 250-720 nm region. When this solution was treated with $NaBH_4$, the solution color immediately turned to dark brown and a precipitate appeared after approximately 30 min of vigorous stirring. The UV-vis spectrum of the solution taken approximately 10 min after $NaBH_4$ was added shows the presence of relatively strong bands at 270, 380, 435 nm. Based on literature reports, the band at 270 nm signifies the formation of small Ag clusters, while the strong and sharp band at 380 nm originates from Ag nanoparticles that have relatively small dimensions. Finally, the broad band located at approximately 435 nm is consistent with the formation of relatively large Ag aggregates.[268-270] Therefore, the treatment of the

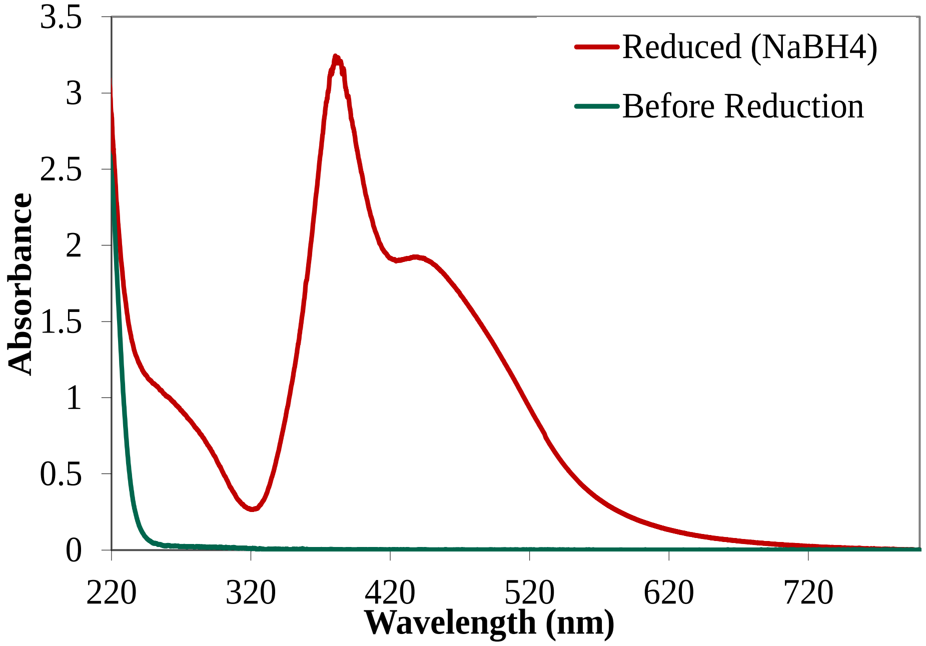

Figure 5.21 UV-vis spectra characterizing the G4OH-$(Ag^{+})_{60}$ solution after 1 h of complexation and the same solution treated with the 15-fold excess of $NaBH_4$.

$G4OH\text{-}(Ag^{+})_{60}$ solution with $NaBH_4$ leads to the formation of Ag clusters and polydispersed Ag nanoparticles which continue to aggregate with time and finally precipitate from the solution.

5.3.8.3 Effect of dialysis on FB

Finally, the data shown in Fig. 5.22 indicate that interactions between Ag^{+} and G4OH are weak because the dialysis of $G4OH\text{-}(Ag^{+})_x$ samples (x = 0.5, 5, and 30) leads to removal of 100% Ag and approximately 4 h is sufficient to complete this process.

5.3.9 EOB of $G4NH2\text{-}(M^{n+})_x$ solutions

Fig. 5.23 provides a direct comparison of EOB values for different metal cations complexed with $G4NH_2$ and G4OH dendrimers. The EOB for the $G4OH\text{-}(Au^{3+})_{30}$ system is 8.7 but this value increases to 30 when the $G4NH_2$ dendrimer is used. This result clearly shows that the complexation of Au(III) with the primary amines of the $G4NH_2$ dendrimer is much stronger than with bindings sites of the G4OH dendrimer. Furthermore, EOB values for $G4OH\text{-}(Fe^{3+})_{30}$ and $G4NH_2\text{-}(Fe^{3+})_{30}$ systems were found to be ~ 25 in both cases. Since the EOB value is the same for both $G4NH_2$ and G4OH dendrimers, this result suggests that Fe^{3+} can complex to the same extent with OH and NH_2 terminal groups of G4OH and $G4NH_2$ dendrimers, respectively. Results obtained for $G4OH\text{-}(Co^{2+})_{30}$ suggest that Co^{2+} does not interact strongly with the G4OH dendrimer since the EOB value is zero in this case. However, Co^{2+} can interact somewhat stronger with primary amines of the $G4NH_2$ dendrimer because the EOB value in this case is 2.5. Finally, Ag, Mn, Ni, Zn, and Cu cations cannot complex strongly with neither of the dendrimers because the EOB values were found to be zero in both $G4OH\text{-}(M^{n+})_{30}$ and $G4NH_2\text{-}(M^{n+})_{30}$ cases.

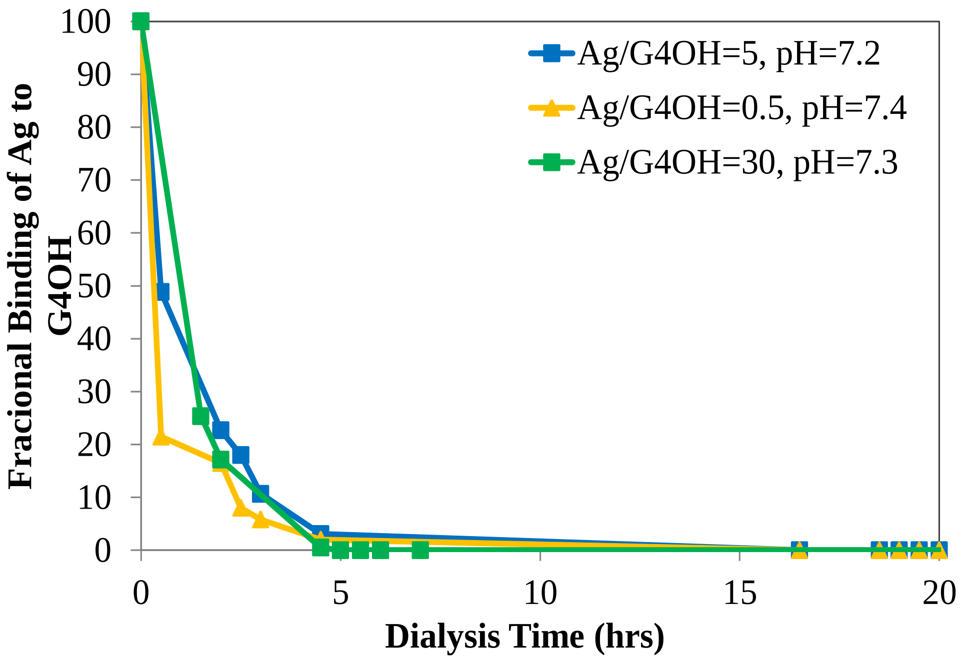

Figure 5.22 FB Ag^+ to G4-OH as a function of dialysis time. All solutions contained the same amount of Ag^+ (3.14 mmol $AgNO_3$ from the 58.9 mM $AgNO_3$ stock solution). The concentration of the G4-OH dendrimer in the final solution was $4.2 \cdot 10^{-1}$, $4.2 \cdot 10^{-2}$, and $7 \cdot 10^{-3}$ mM for Ag^+/G4-OH molar ratios 0.5, 5 and 30, respectively.

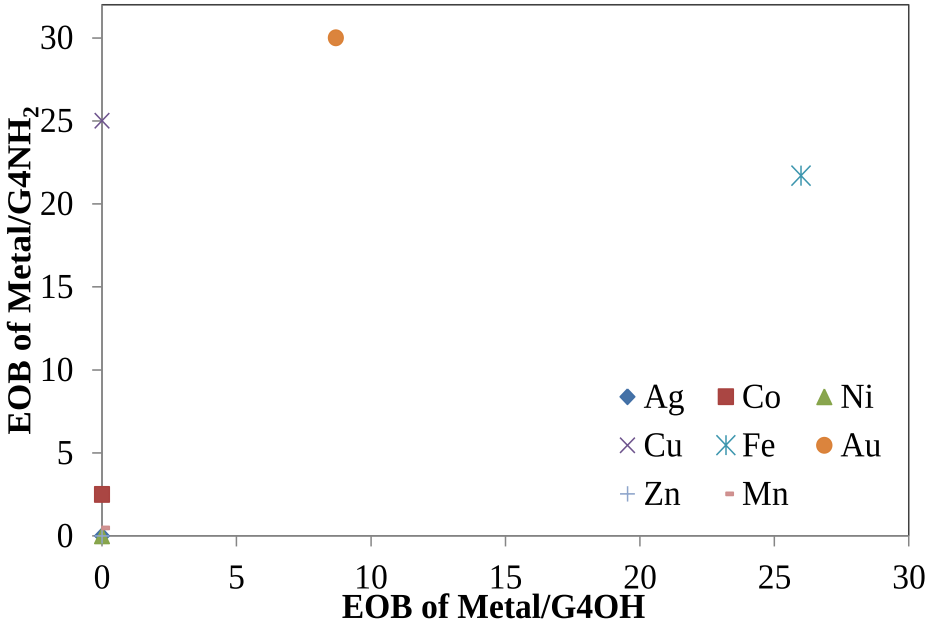

Figure 5.23 EOB values characterizing G4OH-$(M^{n+})_{30}$ and G4NH$_2$-$(M^{n+})_{30}$ solutions dialyzed for 24 h.

5.3.10 FB of Reduced G4OH-(M^{n+})$_{30}$ solutions

In order to determine when it is most appropriate to perform the dialysis step, G4OH-(M^{n+})$_{30}$ solutions were prepared for Ag^+, Co^{2+}, Ni^{2+}, Cu^{2+}, and Mn^{2+} and dialyzed before and after the reduction step was performed. In the latter case, G4OH-(M^{n+})$_{30}$ solutions were treated with the 3-fold excess of $NaBH_4$, with the exception of the G4OH-(Ag^+)$_{30}$ solution which was treated with the 4-fold excess of $NaBH_4$ in NaOH. Fig. 5.24(a) shows FB values obtained for untreated and treated with $NaBH_4$ G4OH-(Ag^+)$_{30}$ solutions as a function of dialysis time. The data clearly show that 100% of Ag is dialyzed from the G4OH-(Ag^+)$_{30}$ solution after 5 h of dialysis. In contrast, similar data obtained for the G4OH-(Ag^+)$_{30}$ solution treated with $NaBH_4$ show that approximately 40 and 30 % Ag remains in solution after 5 and 24 h of dialysis, respectively.

This result may indicate that after the treatment with $NaBH_4$ Ag stronger interacts with the dendrimer or, alternatively, relatively large Ag particles are formed. In the latter case, it is expected that the size of Ag particles governs the loss of Ag during dialysis. For example, when the size of Ag particles exceeds the size of dialysis tubing pores, Ag would not be dialyzed from the solution. Somewhat similar data were obtained for G4OH-(M^{n+})$_{30}$ solutions of Co and Mn (Fig. 5.24(b)). However, the data collected for G4OH-(M^{n+})$_{30}$ solutions of Cu and Ni show that the placement of the dialysis step does not affect substantially the FB values (Fig. 5.24(b)).

5.3.11 Intradendrimer Metal-Displacement Reactions

Since Ag^+ interacts with the G4OH dendrimer only weakly, Ag cannot be loaded into the dendrimer interior and stable Ag/G4OH nanocomposites cannot be prepared via the direct complexation process. However, it was suggested by Crooks et al. that such nanocomposites can be prepared via displacement reactions.[44] In this approach, DENs

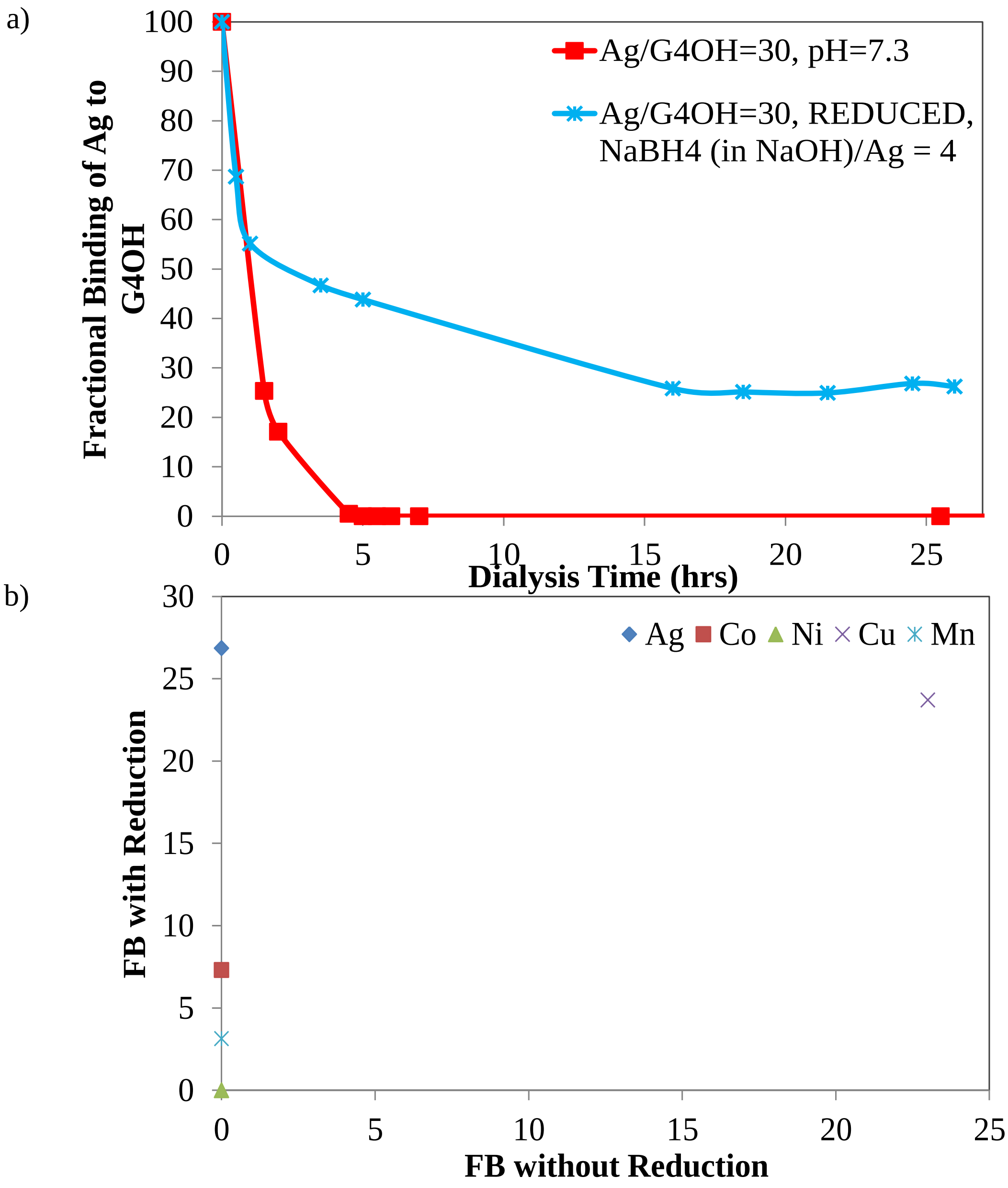

Figure 5.24 Dependence of FB on the dialysis time of G4OH-$(Ag^{+})_{30}$ solutions (a) and comparison of FB values of G4OH-$(M^{n+})_{30}$ solutions of different metals (b) for untreated and treated with $NaBH_4$ solutions.

prepared from a particular metal such as Cu for example, can be exchanged with Ag as long as the latter metal is more noble than the former (Eq. 4). Depending on the solution pH, Cu^{2+} cations formed in solution during the displacement reaction may or may not interact with the dendrimer. This fact opens up some interesting possibilities for intradendrimer reactions.[57,60]

$$Cu^{o} + 2\,Ag^{+} \rightarrow Cu^{2+} + Ag^{o} \qquad \text{(Eq. 4)}$$

5.3.11.1 Preparation of Metal-Dendrimer Nanocomposites by Displacement Reactions

Five G4OH-$(Cu^{2+})_x$ solutions with x = 5, 10, 16, 30 and 60 were prepared. All these solutions had the same amount of $Cu(NO_3)_2$ (1.07 mM) but the amount of G4OH was 3.15, 1.57, $7\cdot10^{-2}$, $3\cdot10^{-2}$, and $2\cdot10^{-2}$ mmol for Cu^{2+}/G4OH molar ratios 5, 10, 16, 30 and 60, respectively. The final volume of each solution was adjusted to 15 mL with DI water. Prior to the reduction treatment, the pH of these solutions was adjusted to 7.0 using 0.1 N NaOH and solutions were purged with N_2 for 30 min. A 3-fold weight excess of $NaBH_4$ was introduced to each solution with a goal to reduce the dendrimer-encapsulated Cu^{2+} to the zerovalent (Cu^0) state. Each solution was sealed and stirred continuously for ~2 h until the production of H_2 was no longer evident. The pH of each resulting solution was further adjusted to 3 using 2% HNO_3 to ensure that hydrolysis of unreacted $NaBH_4$ is not taking place any longer.[78] In addition, after the solution pH is adjusted to 3, the protonation of tertiary amines in the G4OH dendrimer interior occurs (pKa ~ 6.3) and this process enables Ag to interact directly with reduced Cu^0 and not with functional groups of the dendrimer.[108,109] To ensure that the formation of Ag^0 metal nanoparticles is the result of the metal displacement reaction rather than the result of the direct reduction with $NaBH_4$, the solution pH was adjusted to 3.0 and the stoichiometric amount of silver (i.e., 0.34 mL of a 58.9 mM $AgNO_3$) was added to the solution 1 h later.

This preparation routine is further denoted as the 7-3 method (Figure 5.25). In some experiments, the solution pH was further adjusted to 7 with 0.1 N NaOH before Ag was added to the solution. This adjustment was used to ensure that reduced Cu^0 species remain to be encapsulated by the G4OH dendrimer and this preparation routine is further denoted as the 7-3-7 method (Figure 5.25).

5.3.11.2 Effect of dialysis on FB and EOB of Ag and Cu in G4OH-(Cu^o)-2Ag^+ solutions prepared via intradendrimer displacement reactions

Fig. 5.26(a) shows the FB values characterizing G4OH-(Cu^0)-2Ag^+ solutions prepared using the 7-3 method as a function of dialysis time. The data suggest that approximately 80 % of Ag is dialyzed from the solution after 2 h but 10-20% of Ag remains in the solution even after 20 h of dialysis, depending on the Cu/G4OH ratio used. In all these cases, no Cu can be found in the solution after 20 h of dialysis (Fig. 5.26(b)). This result indicates that the displacement reaction between Cu^0 and Ag^+ does not proceed to a completion likely because not all Cu species are reduced in the solution. Moreover, since the solution pH was adjusted to 3.0 after the reduction treatment, such an adjustment could lead to the reoxidation of Cu as well as to the protonation of the dendrimer. It is expected that all these factors would limit the probability of the intradendrimer displacement reaction to occur, consistent with our observations.

Fig. 5.27 illustrates FB values for Ag and Cu in G4OH-(Cu^0)-2Ag^+ solutions prepared by the 7-3-7 method. After G4OH-$(Cu^0)_x$ solutions with x = 5, 10, 16, 30, and 60 were reduced with $NaBH_4$ and the solution pH was adjusted to 3.0 and then readjusted to 7.0 as described previously, 0.34 mL of the 58.9 mM $AgNO_3$ stock solution was added to the mixture and solutions thus formed were dialyzed against DI water. The maximum FB value for Ag observed after 1 day of dialysis was found to be ~60% in the case of the

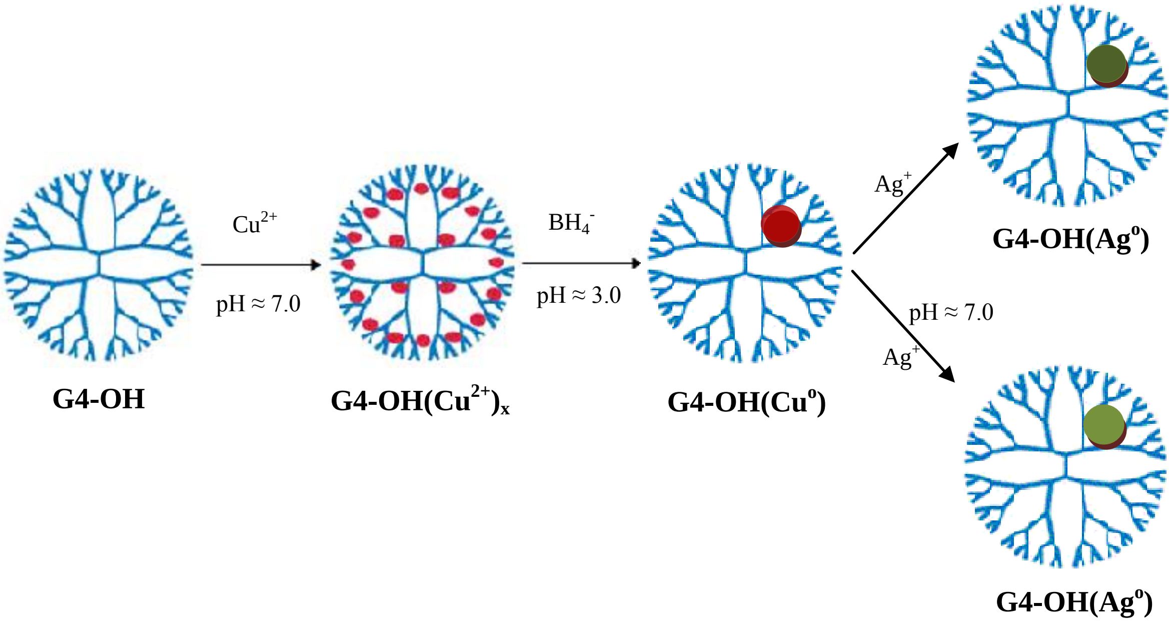

Figure 5.25 Intradendrimer metal-displacement reactions

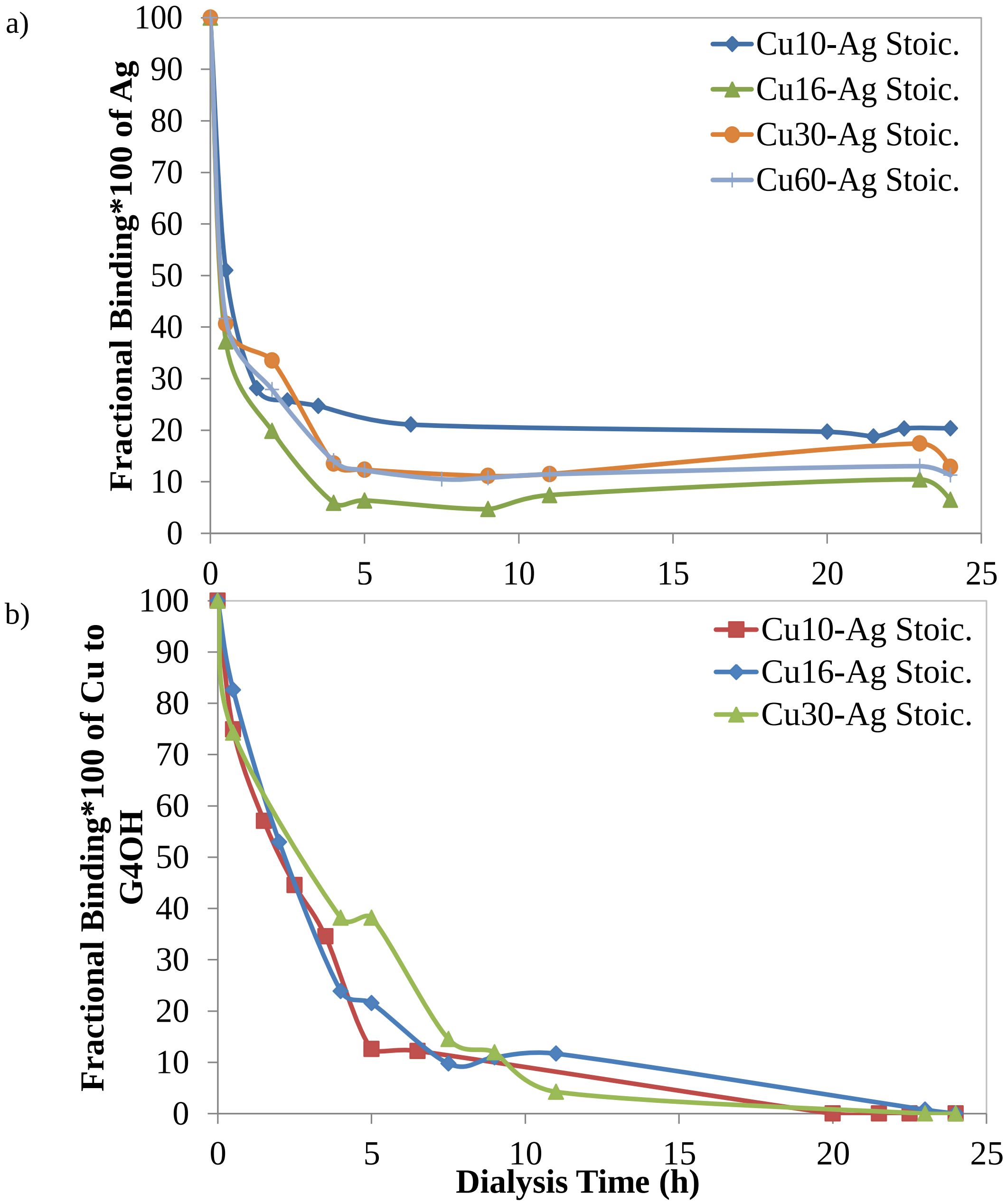

Figure 5.26 FB of (a) G4OH-(Ag^0) and (b) G4OH-(Cu^{2+}) resulting from intradendrimer displacement reactions (method 7-3). Approximately 15 mL of each sample were used for dialysis. All Cu^{2+}/G4-OH solutions initially contained $1.57\cdot10^{-2}$ mmol Cu^{2+} and the content of G4OH in the final solution was 1.57, $7\cdot10^{-2}$, $3\cdot10^{-2}$, and $2\cdot10^{-2}$ mM for G4OH-$(Cu^{2+})_{10}$, G4OH-$(Cu^{2+})_{16}$, G4OH-$(Cu^{2+})_{30}$ and G4OH-$(Cu^{2+})_{60}$, respectively. After 0.34 ml of the $AgNO_3$ stock solution (58.9 mM $AgNO_3$) was added to these solutions, the volume of each solution was adjusted to 15 mL using DI water.

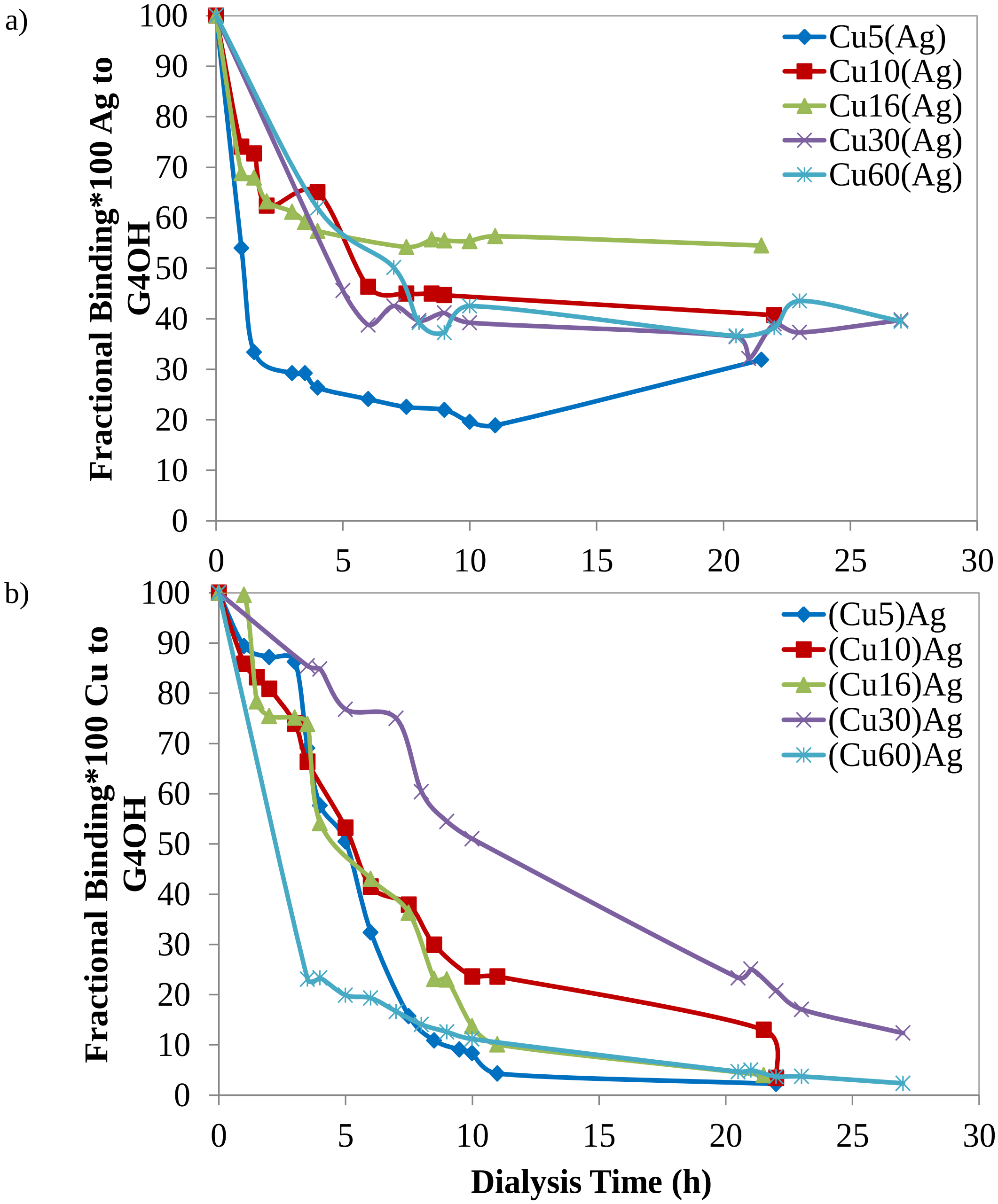

Figure 5.27 FB of (a) G4OH-(Ag^0) and (b) G4OH-(Cu^{2+}) resulting from intradendrimer displacement reactions (method 7-3-7).

G4OH-$(Cu^0)_{16}$ solution (Fig. 5.27(a)). A small amount of Cu^{2+} (< 10%) was retained inside the solution after 1 day of dialysis (Fig. 5.27(b)) but all Cu is expected to be removed if the dialysis procedure is performed for a longer period of time. Two absorption bands were identified in UV-vis spectra of such solutions at ~400 and 300 nm which correspond to the plasmon resonance of Ag particles and to the LMCT of intradendrimer Cu^{2+} species, respectively.[44,78] Based on these observations it was concluded that both Ag^0 and Cu^{2+} were trapped in the dendrimer interior.

Fig. 5.28 illustrates the EOB characterizing Ag/G4OH prepared with 7-3 and 7–3–7 methods after 1 day of dialysis. The EOB values characterizing Ag/G4OH prepared with the 7-3-7 method are much larger as compared to those characterizing the sample prepared with the 7-3 method. In both cases, however, EOB values increase linearly with increasing the theoretical Cu/G4OH molar ratio. If Cu in solution is totally reduced and the displacement reaction proceeds to a completion, the maximum EOB value of Ag/G4OH is expected to be around 120 (G4OH-$(Ag^0)_{120}$) in the case of the G4OH-$(Cu^0)_{60}$ molar ratio because 2 moles of Ag replace 1 mole of Cu. However, the maximum experimental value determined for the Ag/G4OH EOB was found to be 48, which is 60% lower than expected. This result can be explained by incomplete reduction of Cu in solution.

The reduction potential E_o^r is another parameter that should be taken into consideration when displacement reactions are performed (Table 2.2). Since Ag is characterized by a larger reduction potential than Cu, it will be reduced in solution where Cu^0 species are present. Moreover, since the reduction potential for the Cu^{2+}/Cu system is larger than that for the H^+/H_2 system, copper typically does not form hydrogen in solution. However, it is possible that the value of the reduction potential for the Cu^{2+}/Cu

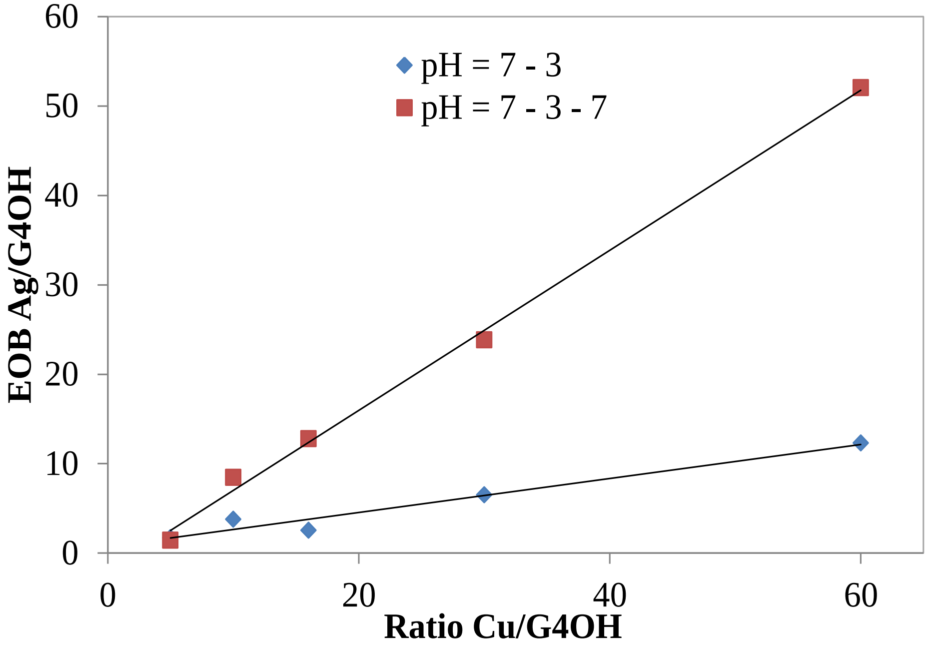

Figure 5.28 EOB of Ag/G4OH as a function of the theoretically used Cu/G4OH molar ratio for both 7-3 and 7-3-7 methods.

system can drop below that characterizing the H^+/H_2 system under certain circumstances and the displacement of hydrogen from solution by metallic copper becomes possible.[271] In this case, the $2H^+_{(aq)} + 2e^- \rightarrow H_{2(g)}$ reaction will interfere with the redox reaction between metals and impede the displacement process.

The data shown in Fig. 5.29 indicate that nearly 100% Ag is dialyzed after approximately 7 h when Cu is not used in the preparation routine. This result suggests that Cu plays a vital role in displacement reactions and the presence of Cu is necessary for retaining Ag inside the solution.

5.3.11.3 Effect of dialysis on FB of Ag, Cu in G4OH-(Cu^o)-4Ag^+ solution

Several attempts were made to enhance the amount of Ag that is retained by the G4OH dendrimer in solution. When 7-3-7 method was used to prepare the G4OH-$(Cu^0)_{16}$ solution and the solution pH was finally adjusted to 7.0, two times the stoichiometric quantity of Ag^+ (0.68 mL from the 85.9 mM $AgNO_3$ stock solution) was added to the mixture. The solution was sealed and held under stirring for 1 h before it was dialyzed. The FB values for Ag as a function of dialysis time are shown in Fig. 5.30(a). The addition of two times the stoichiometric quantity of Ag led to 100% dialysis of Ag and Cu after 5 and 24 h, respectively. This experiment was repeated twice but results obtained were found to be the same. Fig. 5.30 shows that the concentration of Ag in solution drops much quicker than that of Cu likely due to the presence of Ag^+ in a large excess. However, it is remaining unclear at this point why more Ag remains in the solution when the stoichiometric quantity of Ag is used for preparations.

5.4 Conclusions

- Complexation of Cu^{2+} with G4OH is completed after approximately 30 min but the extent of this process does not depend on the metal-to-dendrimer molar ratio

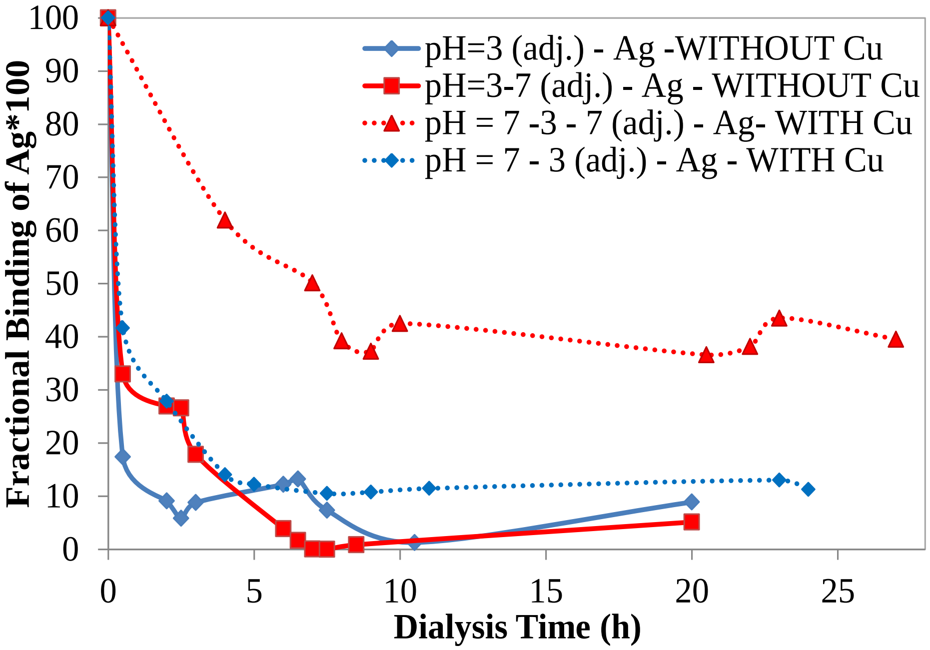

Figure 5.29 FB of G4OH-(Ag^0) as a function of dialysis time for 7-3-7 (red lines) and 7-3 (blue lines) methods. Dashed and solid lines demonstrate data for preparations with and without Cu, respectively.

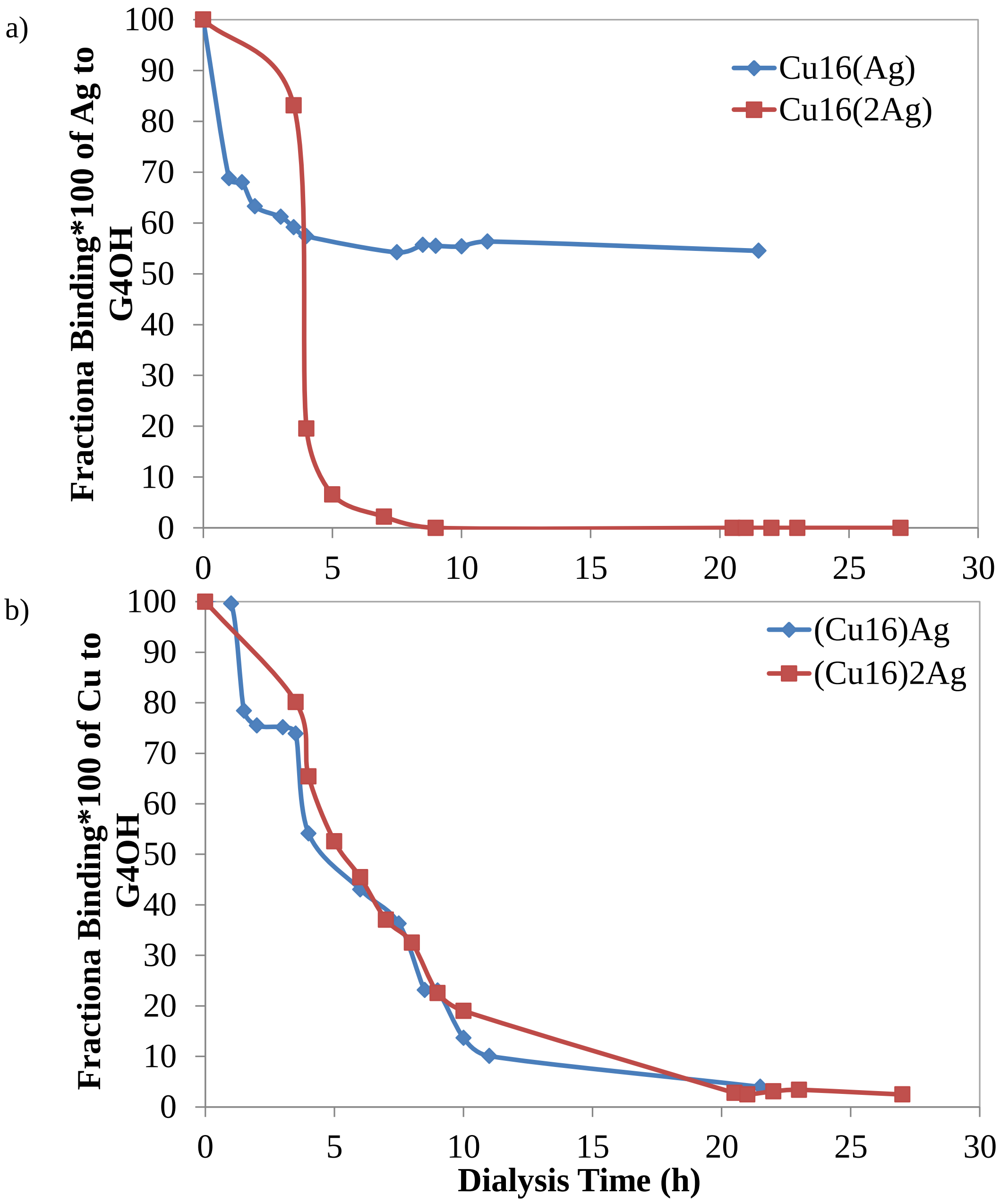

Figure 5.30 FB of Ag (a) and Cu (b) to the G4OH dendrimer as a function of dialysis time. The G4OH-(Cu^{2+})$_{16}$ solution was prepared using the 7-3-7 method. After the last pH adjustment to 7.0, 2 times the stoichiometric quantity of Ag^+ was added to the solution (0.68 mL from the 58.9 mM $AgNO_3$ stock solution).

used when the solution pH is not controlled. The maximum value for the number of Cu ions complexed per dendrimer molecule was found to be 8 at pH ~ 5.8. When the solution pH was adjusted to 6.1, more Cu(II) was complexed with the dendrimer. However, the difference between calculated and experimentally-observed Cu^{2+}/G4OH values after complexation remains substantially different.

- UV-vis data indicate that the complexation process for G4OH-$(Fe^{3+})_{30}$ was completed after approximately 2 days. When the Fe/G4OH ratio in the solution was 60 or higher, the absorption at 300 nm was found to be unchanged after 30 min, indicating that the complexation process is actually completed within the first 30 min. At high Fe/G4OH ratios (n = 80), the solution contained a significant fraction (47%) of weakly bound or unbound Fe^{3+}. When the solution pH was adjusted to 7.0 during the complexation process, the EOB increased linearly within the range of tested Fe(III)/G4OH molar ratios, while the FB of Fe(III) cations to the dendrimers was found to be 100% in all such experiments.
- In the case of G4OH-$(Au^{3+})_{30}$ (pH of 3.0), a significant amount of Au(III) is bound to the G4OH PAMAM dendrimer (FB ~ 39.7% and EOB_{G4OH} and EOB_{G4NH2} values of up to 8.7 and 30, respectively) even though the dendrimer tertiary amines are expected to be fully protonated under such conditions.
- The Ni^{2+}-amine complexation was stronger for low Ni^{2+}/G4OH ratios and approximately 3 days were required to complete the complexation process in this case. The Ni^{2+}-amine interactions appear to be weaker at higher molar ratios nickel-to-dendrimer and the complexation process was completed in less than 30 min. In general, the interaction between Ni(II) and G4OH is much weaker than the interactions of Cu(II), Fe(III), and Au(III) with G4OH.

- The complexation of Co(II) with the G4OH dendrimer was similar to the complexation of Ni(II) with G4OH. However, Co^{2+} can interact somewhat more strongly with the primary amines of the $G4NH_2$ dendrimer (EOB = 2.5).
- Mn and Zn interact very weakly with G4OH, as both metals can be completely removed from the solution after 6 h of dialysis.
- In the case of G4OH-$(Ag^+)_{60}$, interactions between Ag^+ and G4OH are also very weak, since nearly 100% of the Ag can be removed from the solution after 4 h of dialysis. However, in the case of un-dialyzed solutions, Ag nanoparticles can be formed and the size of these nanoparticles increases with the complexation time; in fact, Ag precipitates from solution after approximately 22 days of complexation. The treatment of the G4OH-$(Ag^+)_{60}$ solution with $NaBH_4$/NaOH speeds up the formation of Ag nanoparticles substantially.
- Approximately 15% and 60% of Ag remained in solution even after 1 day of dialysis when G4OH-(C^{u0})-2Ag^+ nanocomposites were prepared using the 7-3 and 7-3-7 methods, respectively. The EOB values characterizing Ag/G4OH composites prepared with the 7-3-7 method are much larger than those characterizing the sample prepared with the 7-3 method. In both cases, however, EOB values increase linearly with increasing the theoretical Cu/G4OH molar ratio. Finally, nearly 100% Ag was dialyzed after approximately 7 h when Cu was not used in the preparation routine, suggesting that the presence of Cu is necessary for retaining Ag in the dendrimer solution.

CHAPTER 6

SILICA-SUPPORTED GOLD/DENDRIMER NANOCOMPOSITES WITH CONTROLLED SIZES OF GOLD PARTICLES

6.1 Introduction

Since gold has a completely filled d band and typically exhibits a very low reactivity, the interest in this metal was low for decades. In early 80^s, however, it was shown that TiO_2-supported Au nanoparticles with sizes in the 2-5 nm range are active for CO oxidation at temperatures as low as -70°C.[272] Ever since, the list of chemical reactions catalyzed by Au nanoparticles was extended to epoxidation, amination, hydrogenation of hydrocarbons, oxidation of alcohols, and C–C coupling reactions.[273,274,275] Some of these reactions require relatively large Au particles but some (i.e., oxidation and hydrogenation) proceed with much higher rates over supported Au nanoparticles with sizes below 2 nm, suggesting that sizes of supported Au particles must be strictly controlled for each individual chemical process. The same is true for other research fields where Au nanoparticles are currently used including electronics, optics, and medicine.[276-279] Therefore, extensive efforts were recently applied to the synthesis of supported gold nanoparticles with desired dimensions and shapes. Unfortunately, conventional preparations techniques based on the impregnation of Au salts and high temperature treatments provide a limited control over Au particle sizes in solid materials because Au easily aggregates at elevated temperatures. The use of organometallic Au complexes as precursors gives better results,[280-282] but such preparations are limited because organometallic gold complexes are not commercially available.

The synthesis of colloidal gold nanoparticles with desired sizes and shapes in solution and their subsequent delivery onto surfaces of solid supports could provide a relatively simple path for the controlled fabrication of solid materials incorporating Au. In this preparation route, the metal precursor is typically reduced in the aqueous solution in the presence of surfactants to preserve the colloidal state of metal nanoparticles formed.[239,283,284] Among different available surfactants, poly(amidoamine) (PAMAM) dendrimers have attracted a lot of recent attention as nanoparticle stabilizers because these macromolecules offer a variety of functional groups for complexation of metal cations and have interior voids which can trap and protect metal nanoparticles from aggregation until they are delivered onto surfaces of solids. These dendrimer features offer an opportunity to control the architecture and the size of metal nanoparticles in solution and to maximize the uniformity of active metal sites in supported materials.

Several literature examples illustrate the successful application of this preparation route for the synthesis of Au-dendrimer nanocomposites. For example, Esumi et al.[68,285,286] examined the formation of Au nanoparticles in the presence of PAMAM dendrimers with amine, sugar, methyl ester, and alkyl groups at the periphery. In all these cases, however, nonuniform Au particles with dimensions in the 2.1 – 12.8 nm range were formed both in the interior and on the exterior of dendrimers. Amis et al.[248,287] reported the synthesis of Au nanoparticles in the 2.0-4.0 nm range from $HAuCl_4$ using amine-terminated PAMAM dendrimers. Crooks et al.[288] described the formation of nearly uniform Au nanoparticles with sizes in the 1.3-1.6 nm range using PAMAM dendrimers with both quaternary ammonium and primary amine groups on their periphery and concluded that the Au/dendrimer ratio effects stronger the size of metal particles formed than the dendrimer generation. Finally, Lu et al.[144] managed to prepare stable and uniform 2.7 ± 0.5 nm Au nanoparticles by reduction of $HAuCl_4$ with $NaBH_4$ in the presence of hydroxyl-terminated PAMAM dendrimers.

In the majority of these examples, aqueous solutions of $HAuCl_4$ and a dendrimer were mixed for a short period of time (i.e., 2-5 min) before the mixture was further treated with a reducing agent, assuming that Au-dendrimer interactions are quick. Therefore, any detailed information related to the extent of Au complexation and type of Au/dendrimer interactions can hardly be found in these reports. Only few reports include at least some data revealing the possible nature of Au/dendrimer interactions. For example, since the $AuCl_4^-$ aqueous solution loses its yellow color immediately upon mixing with the PAMAM-NH_2 solution, it has been suggested that protonated terminal groups of PAMAM-NH_2 dendrimers (pK_a ~ 9.7) interact with $AuCl_4^-$ species electrostatically.[289-291] In other reports, changes in FTIR spectra were used as an indicator of Au-dendrimer interactions. More specifically, Imae et al.[61] have suggested that shifts in the position of amide II and amide III bands indicate conformational changes of the G4NH_2 dendrimer due to interactions with Au particles. Furthermore, since UV-vis spectra of $HAuCl_4$ aqueous solutions have LMCT (ligand-to-metal charge transfer) bands at approximately 290 nm and the absorbance in this region increases in the case of Au/G5NH_2 solutions, the formation of ion pairs between G5NH_2 and $AuCl_4^-$ has been suggested.[251,289,291] Finally, there are several reports suggesting that hydroxyl-terminated PAMAM dendrimers are capable of reducing Au cations in solution.[162,286,292]

While these examples provide at least some indications of Au/dendrimer interactions, there is no a strong consensus on the type of Au/dendrimer interactions involved. It also remains unclear if the desirable complexation of gold with the dendrimer interior indeed takes place and leads to the formation of small and stable Au nanoparticles within the dendritic moieties. Moreover, only few attempts were made to prepare solid catalytic materials on the basis of gold-dendrimer nanocomposites. For example, when $(Au_{55})/G4\text{-}NH_2$ nanocomposites were deposited onto the surface of TiO_2, the average size of supported Au particles was on the order of 2.0 nm.[288] In the material thus formed, Au nanoparticles remain to be capped by the dendrimer and further treatments at elevated temperatures (approximately 400°C) in oxygen/hydrogen atmospheres are required to remove the dendrimer component.[197] However, such harsh thermal treatments are known to lead to a significant sintering of Au.[293]

To avoid such complications, Chandler et al.[237] have demonstrated a different approach which is based on the extraction of Au nanoparticles from Au/dendrimer nanocomposites into the organic phase with thiols, which can be further removed from the surface of supported Au particles under relatively mild conditions. This preparation route allows for a better control over the size of Au particles during thermal treatments while maintaining relatively narrow particle size distributions. For example, average sizes of Au particles extracted from Au/G5OH nanocomposites and supported on TiO_2 were found to be on the order of 3 nm and remained nearly unchanged when thiols were removed under the flow of H_2/N_2 at 290°C for 16 h.[237] As a result, Au/TiO_2 samples prepared via this route were found to be active for CO oxidation.[237]

Alternatively, Somorjai et al.[294] have demonstrated that Au/G4OH nanocomposites with average sizes of Au particles on the order of 2 nm can be loaded intact onto the surface of the SiO_2 support, yielding the solid material with leaching-resistant properties that can be further used as a catalyst for liquid-phase reactions. In this particular case, it was even possible to transfer liquid phase reactions from the batch to flow mode without jeopardizing the catalytic performance of this material. While this literature example persuasively demonstrates potential advantages of supported Au/dendrimer nanocomposites as heterogeneous catalysts for liquid phase reactions, it also provides a strong motivation for better understanding the Au-dendrimer solution chemistry, because Au-dendrimer interactions can be advantageous in tuning the size and chemical properties of Au nanoparticles in the resulting nanocomposites.

In this paper, we examine the use of Au-G4OH nanocomposites for the preparation of Au-G4OH/SiO_2 solid materials. We have shown previously the effect of preparation conditions (i.e., solution pH, dialysis, and Rh/dendrimer ratio) on the extent of Rh-G4OH complexation and sizes of Rh particles formed in supported materials. Therefore, our intension is to determine if the knowledge gained from the Rh-G4OH case can be extended to the inherently more complex Au^{3+}-G4OH system. While the synthesis of supported Au nanoparticles via the dendrimer route has already been reported in the literature,[237,295] there is no literature reports targeting specifically auto reduction of Au cations by dendrimers and, therefore, the growth of Au particles. More specifically, the goal of this work is to explore the solution chemistry in the presence of both Au^{3+} and G4OH PAMAM dendrimers, determine how the extent of the Au^{3+} complexation and reduction by the dendrimer depends on the solution conditions, and examine how these conditions affect sizes of the Au particles formed in solution and in final supported materials. New results reported in this paper highlight the influence of the solution pH on the strength of the Au-dendrimer interactions and sizes of Au nanoparticles finally formed, explore in detail the kinetics of Au^{3+} reduction by the dendrimer in absence of any reducing agents, and ultimately help to optimize the preparation conditions for the synthesis of Au nanoparticles with specific dimensions on the SiO_2 support.

6.2 Experimental

6.2.1 Reagents and materials

Fourth generation hydroxyl- and amine-terminated poly(amidoamine) (PAMAM) dendrimers (further denoted as G4OH and $G4NH_2$, respectively) were purchased as a 10 wt.% solution in methanol (Dendritech). Prior to further use, methanol was removed under N_2 flow at room temperature and 0.42 mM G4OH and 0.18 mM $G4NH_2$ aqueous solutions of dendrimers were prepared and stocked. Water purified to 18.2 MΩ·cm was used to prepare all aqueous solutions. Hydrogen tetrachloroaurate(III) trihydrate ($HAuCl_4 \cdot 3H_2O$) (99.99% purity, Alfa Aesar), n-methylacetamide (≥99% purity, Sigma-Aldrich), propanol (≥99% purity, Alfa Aesar), 2-propanol (99.7% purity, Alfa Aesar), and triethylamine (99% purity, Alfa Aesar) were used as received. 0.1 N NaOH and 0.45 N HCl solutions were prepared from 5 N NaOH (Reagents, Inc.) and 37% HCl (BDH Aristar) and further used for pH adjustments. A commercial powdered SiO_2 support (Evonik) with a BET surface area of 148 m^2/g was used as supplied.

6.2.2 Preparation of Au-dendrimer nanocomposites

The strategy used for the preparation of Au-dendrimer nanocomposites with variable Au/dendrimer molar ratios was similar to that reported elsewhere.[296] In each case, G4OH (0.42 mM, 290 μl) and $G4NH_2$ (0.18 mM, 3 ml) PAMAM dendrimer stock solutions were mixed with an appropriate amount of a $HAuCl_4$ ($2.4\cdot10^{-2}$ M) stock solution and diluted to the volume of 6 ml to yield Au-dendrimer nanocomposites with a fixed concentration G4OH (0.12 mM) and $G4NH_2$ (0.09 mM) dendrimers but variable Au/dendrimer molar ratios. Each mixture was then stirred in opaque flask for an extended period of time (as specified in the text) to allow the complexation of Au^{3+} cations with the functional groups of the dendrimer. For simplicity, the nanocomposites formed during this step are denoted as Au_x/G4OH, where x is the nominal Au/dendrimer molar ratio. The pH of these solutions was measured and the extent of Au-dendrimer interactions was monitored by UV–vis at specific time intervals. When a pH adjustment strategy was employed, the solution pH was adjusted to a desired value at the beginning of the Au-dendrimer interaction process by adding 0.1 N NaOH or 0.45 N HCl solutions in appropriate amounts to the mixture.

6.2.3 Preparation of supported samples

Supported samples were prepared by slurrying a Au_5/G4OH solution that was pH adjusted to 7 with the SiO_2 support. After approximately 1 h of stirring, the solid was removed by filtration and dried over night at room temperature. Based on the elemental analysis, the loading of Au in the final material was approximately 1.5 wt.%.

6.2.4 Atomic absorption spectroscopy

A Perklin Elmer (AAnalyst 400) atomic absorption spectrometer was used to quantify the concentration of Au in solutions. Calibration standards were prepared from a stock solution of 1.0 g/L Au in 5% HCl (Aldrich) and the calibration curve obtained was verified with an independent second standard solution of 1.0 g/L Au in 2% HNO_3 (EMD Chemicals). All solutions were stored in amber glass volumetric flasks for light protection. Before measurements, all solutions were diluted 100 times with 5% HCl to reach the 0-5 mg/L range of Au concentrations.

6.2.5 UV-vis spectroscopy

UV-vis spectra were collected at room temperature using a Shimadzu UV-2010PC spectrophotometer and quartz cells with a path length of 10 mm. All samples were scanned in the 190–800 nm range at 0.5 nm steps. Water purified to 18.2 MΩ·cm was used as the reference for all measurements.

6.2.6 STEM measurements

STEM images were recorded using a JEOL-2100F instrument equipped with a CEOS aberration corrector on the illuminating optics and operating at 200 keV. Typically, a small quantity of each powder sample was placed on a carbon-coated 200 mesh copper grid and the sample was imaged without any further preparation. In the case of liquid samples, a drop of the solution was placed on the copper grid and dried under vacuum for approximately 10 min before imaging.

6.3 Results and discussion

6.3.1. General properties of Au/dendrimer solutions

Consistent with previous literature reports describing the solution chemistry of chemical compounds incorporating amine groups,[297] the main pH-determining equilibrium for the aqueous solution of the G4OH PAMAM dendrimer is the interaction of the tertiary amine groups (pK_a=6.1) with water molecules, leading to their protonation and release of hydroxyls. As a result, a 0.42 mM G4OH PAMAM dendrimer stock solution (colorless) is basic with a pH value of approximately 9.3. In contrast, a $HAuCl_4$ precursor is a relatively strong acid that fully dissociates in aqueous solutions.

Consequently, a $2.4 \cdot 10^{-2}$ M $HAuCl_4$ stock solution (bright yellow) is strongly acidic with a pH value of approximately 1.6.

When appropriate amounts of these solutions were mixed together to create desirable Au/dendrimer ratios, changes in a color of the resulting mixtures from bright yellow to colorless were immediately noticeable for all ratios examined. These initially observed color changes can be associated with Au/dendrimer interactions, which include the acid-base and complexation components. It is well known that $[AuCl_4]^-$ species undergo hydrolysis in aqueous solutions to form $[AuCl_x(OH)_{4-x}]^-$ species, the composition of which depends on the solution pH. The $[AuCl_3(OH)]^-$ species dominate in solution at pH=3, while $[AuCl(OH)_3]^-$ are mainly formed when the solution pH is approximately 7.[298] It has also been shown that various $[AuCl_x(OH)_{4-x}]^-$ species have different LMCT (ligand-to-metal charge transfer) bands in UV-vis spectra,[298] indicating that their optical properties are quite different. Since the enhanced hydrolysis of $[AuCl_4]^-$ species in the presence of basic G4OH is inevitable, it can explain color changes initially observed.

To better understand the nature of Au-dendrimer interactions, the solution pH was monitored as a function of time. Results of these measurements are summarized in Table 6.1 along with projected initial pH values which were calculated for each mixture assuming that no other interactions occur in solution between the $HAuCl_4$ and G4OH PAMAM dendrimer species except the acid-base interactions between protons from the $HAuCl_4$ solution and tertiary amines in the dendrimer structure.[296] The results obtained clearly show that the calculated initial pH values of all examined solutions are significantly larger than the initial pH values measured experimentally, indicating that the chemistry of these solutions is not limited to the acid-base interactions. The enhanced hydrolysis of $[AuCl_3(OH)]^-$ species in the presence of G4OH is an additional process that takes place in solution upon mixing of reactants and affects the solution acidity. Since the degree of hydrolysis increases with the solution pH and is expected to lead to $[AuCl(OH)_3]^-$ species at pH of approximately 7, one can calculate that this process yields maximum two protons per one molecule of the gold precursor. When protons released as a result of such hydrolysis are also accounted for acid-base interactions, the projected initial pH values are expected to be 6.8 and 6.3 for solutions with Au/G4OH ratios 5 and 10, respectively. Therefore, it becomes evident that even when changes in pH induced by hydrolysis are accounted for, calculated initial pH values are still more than one pH unit higher than the initial pH values measured experimentally, suggesting that hydrolysis alone cannot explain the observed differences in pH values.

We have shown previously that the solution pH can be used to monitor the complexation of Rh^{3+} aqua complexes with G4OH PAMAM dendrimer molecules.[296] Moreover, EXAFS data reported for Rh^{3+}/G4OH nanocomposites strongly suggest that the concerted chelation of Rh^{3+} aqua complexes with the protonated tertiary amines leads to their deprotonation and release of protons.[70] As a result, the theoretical pH values calculated for different Rh/dendrimer ratios were found to be significantly larger than the initial pH values measured experimentally, strongly suggesting that the chelation is a primary process affecting the acidity of metal/dendrimer solutions.

In the case of Au^{3+} aqueous solutions, however, the anionic $[AuCl_x(OH)_{4-x}]^-$ complexes are expected to interact with protonated tertiary amines of the G4OH dendrimer electrostatically and this process should not affect the solution acidity, since no covalent bonds (the formation of which would be the driving force for deprotonation of tertiary amines in the dendrimer structure) are formed in such a case.[299] In contrast to this expectation, significant differences between projected and experimental initial pH values were observed, suggesting that Au-G4OH interactions are not only electrostatic in nature. Furthermore, since Au/G4OH and Rh/G4OH solutions exhibit the same type of pH changes, one can suggest that the nature of metal/dendrimer interactions in these two cases is somewhat similar. Therefore, we can infer that G4OH PAMAM dendrimer molecules are capable of complexing at least some Au species and this process leads to deprotonation of tertiary amines and substantially influences the pH of resulting solutions.

Some differences in properties of Au/G4OH and Rh/G4OH solutions were also noticeable. For example, the pH data reported elsewhere[296] for solutions with different Rh/G4OH ratios show that the complexation process is relatively slow and lasts for approximately 23 h. In contrast, the pH of all Au/dendrimer solutions equilibrates within the first several minutes and remains nearly unchanged thereafter (Table 6.1). This result indicates that all events associated with initial Au-G4OH interactions and leading to a release of protons are relatively fast. Moreover, the color of solutions with Au/G4OH ratios 5, 10, 20, and 30 turned wine-red, while the solution with an Au/dendrimer ratio 60 acquired a deep blue color after approximately 15 min. The formation of precipitates was also noticeable in solutions with Au/G4OH ratios 30 and 60. Similar color changes were observed previously when Au/dendrimer solutions were treated with reducing agents, such as hydrazine for example, and attributed to the formation of zero valent Au species.[239] By analogy, it is evident that reduction of Au species takes place in all Au/G4OH solutions examined herein, but this process occurs without any additional reducing agents being present. This could be possible only if the initial Au-G4OH

Table 6.1 pH values characterizing aqueous solutions with different nominal Au/dendrimer ratios.

Nominal Au/dendrimer ratio	$HAuCl_4$ concentration (mM)	G4OH dendrimer concentration (mM)	Initial pH of solution		Final pH
			Experimental	Calculated	
5	0.10	0.02	5.6	7.3	5.6
10	0.20	0.02	4.2	6.9	4.2
20	0.41	0.02	3.8	6.5	3.8
30	0.61	0.02	3.4	6.2	3.4
60	1.22	0.02	3.1	4.8	3.1

interactions are followed by redox reactions, yielding reduced Au species and dendrimer fragments/structures incorporating oxidized functional groups that are responsible for these reactions.

6.3.2 UV-vis spectra

UV-vis spectroscopy is a useful tool that allows monitoring in situ whereabouts of Au^{3+} species. The UV-vis spectrum of the G4OH aqueous solution is characterized by a weak absorption band at 285 nm originating from non-protonated tertiary amines in the dendrimer structure (Fig. 6.1).[300] The $HAuCl_4$ aqueous solution also exhibits the absorption band at approximately 280 nm assigned previously to LMCT transitions in $[AuCl_x(OH)_{4-x}]^-$ complexes (Fig. 6.2).[298] When these solutions are mixed together, the absorbance increases in the 280-285 nm region and the surface plasmon resonance (SPR) peak appears in the 530-540 nm region for all Au/G4OH molar ratios examined (Fig. 6.3). The appearance of the SPR band is consistent with the formation of Au nanoparticles with dimensions exceeding 2 nm on average.[301] Since reducing agents were not used to treat this mixture, it becomes evident that the reduction of Au^{3+} ions to Au^0 takes place via a mechanism in which the G4OH dendrimer operates as a reductant. From data shown in Fig. 6.4, it is further evident that properties of absorption bands at 285 and 535 nm are somewhat similar. The intensity of both bands rapidly increases during the first hour but this process slows down significantly thereafter. As far as the behavior of the SPR band is concerned, the observed pattern is fully consistent with the initial rapid aggregation of Au^0 that slows down significantly when the concentration of non-aggregated Au^0 species depletes in solution.

In contrast, the assignment for the absorption band at 285 nm is not straightforward even though its appearance in UV-vis spectra of Au/dendrimer solutions

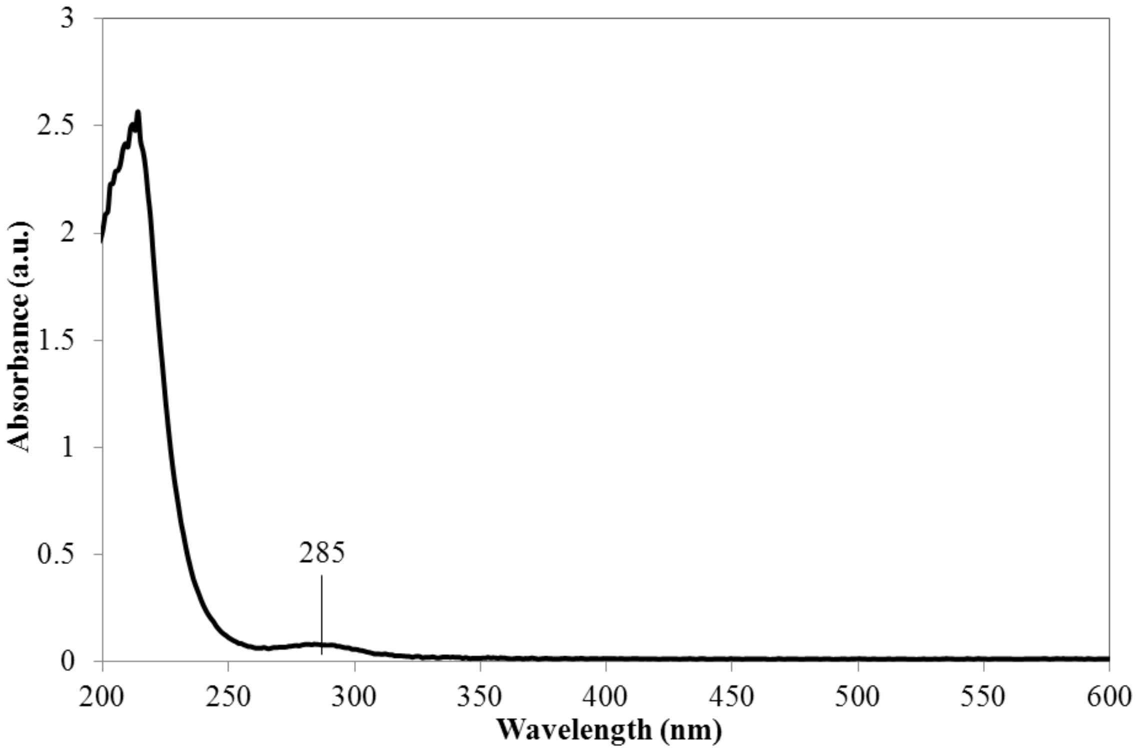

Figure 6.1 UV-vis spectrum of 0.02 mM G4OH aqueous solution.

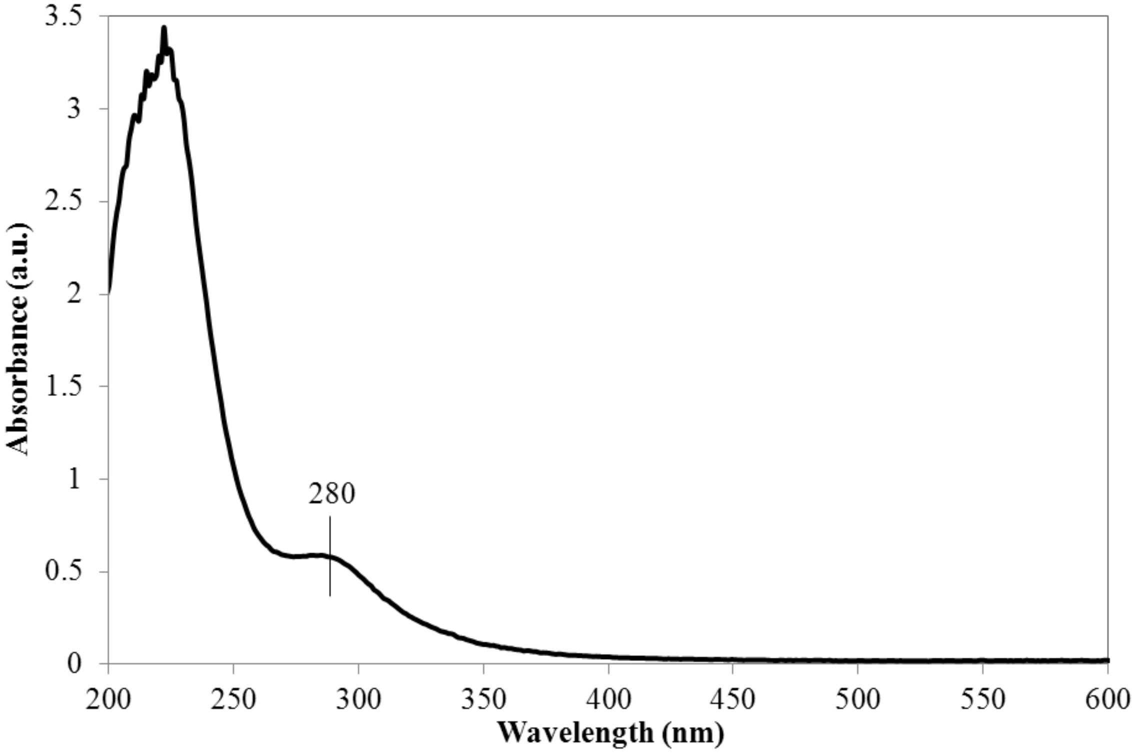

Figure 6.2 UV-vis spectrum of 0.20 mM $HAuCl_4$ aqueous solution.

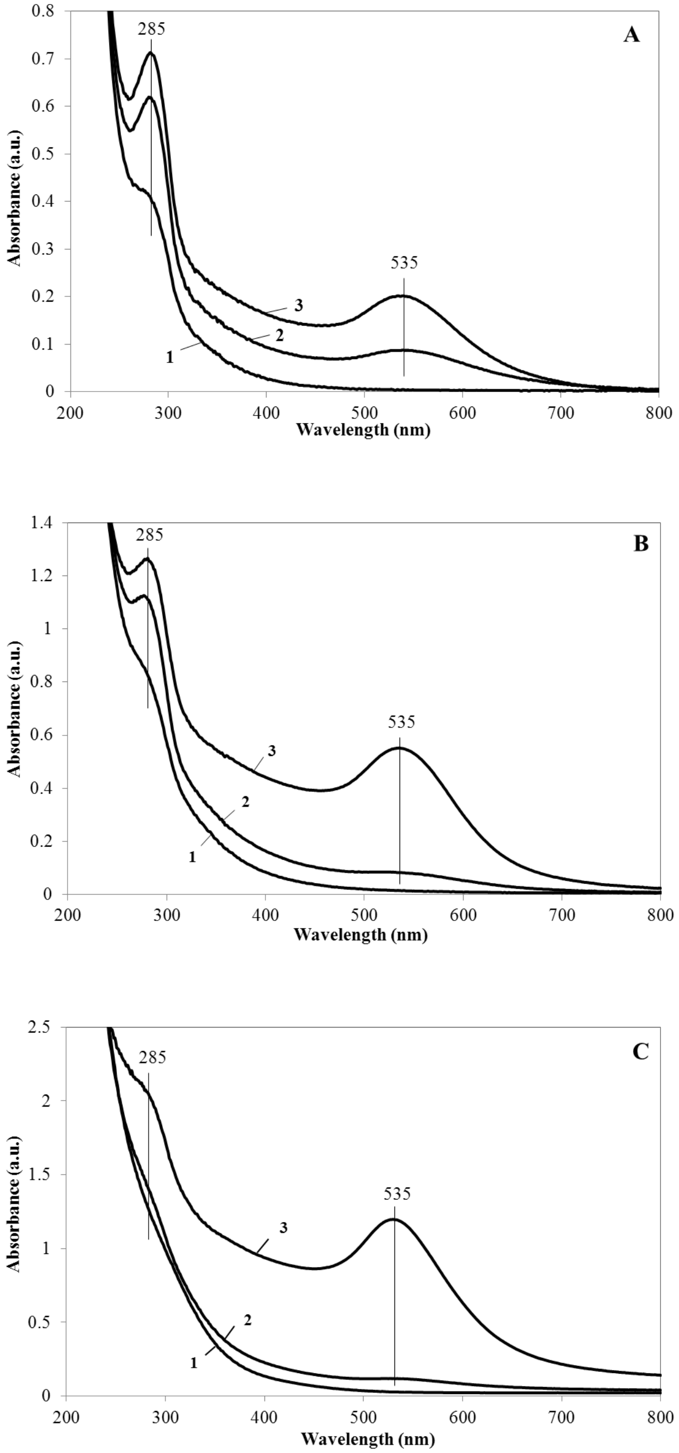

Figure 6.3 UV-vis spectra of (A) Au_5/G4OH (B) Au_{10}/G4OH and (C) Au_{20}/G4OH aqueous solutions collected after (1) 5 min, (2) 15 min, and (3) 1 h.

is well documented in the literature.[239,289,302] Since UV-vis spectra of G4OH and $HAuCl_4$ aqueous solutions exhibit absorption bands in the 280-285 nm region, these bands can potentially overlap when both solutions are mixed together, yielding a spectrum with a stronger absorbance in this region. However, the probability for such an event is extremely low because the acidity of the resulting mixture is significantly different from that of G4OH and $HAuCl_4$ aqueous solutions and the current assignments of the UV-vis bands in each individual case strongly suggests that the changes observed in the solution acidity would rather lead to a decrease in absorbance in the 280-285 nm region.[300,303]

It has been reported that oxidation of PAMAM dendrimers by $(NH_4)_2S_2O_8$ leads to a strong UV-vis absorbance at approximately 290 nm.[304] Consequently, UV-vis bands observed in the 280-290 nm region of Au/dendrimer solutions have been frequently associated with the presence of carbonyl compounds (i.e., aldehydes) which are formed when dendrimer molecules are oxidized by Au salts.[239,285] In the case of the G4OH dendrimer, such compounds can be formed if OH groups at the dendrimer periphery are oxidized by Au^{3+} to form dendrimers with aldehyde functional groups at the periphery (reaction 1) or the oxidative cleavage of the R_2N-C bonds in the dendrimer backbone takes place and leads to a release of aldehydes and secondary amines (reaction 2).

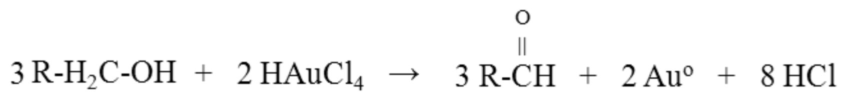

$$3\,R\text{-}H_2C\text{-}OH \;+\; 2\,HAuCl_4 \;\rightarrow\; 3\,R\text{-}\overset{\overset{O}{\|}}{C}H \;+\; 2\,Au^{o} \;+\; 8\,HCl$$

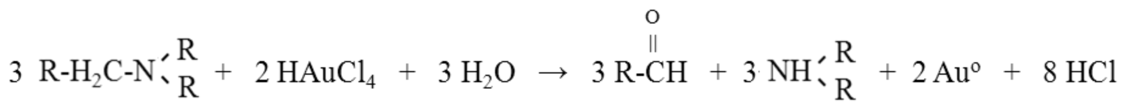

$$3\;R\text{-}H_2C\text{-}N\left\langle\begin{matrix}R\\R\end{matrix}\right. \;+\; 2\,HAuCl_4 \;+\; 3\,H_2O \;\rightarrow\; 3\,R\text{-}\overset{\overset{O}{\|}}{C}H \;+\; 3\,NH\left\langle\begin{matrix}R\\R\end{matrix}\right. \;+\; 2\,Au^{o} \;+\; 8\,HCl$$

From the flat portion of curves shown in Fig. 6.4, it is further evident that the absorbance values for the UV-vis band at 285 nm are approximately 0.6, 1.2, and 2.0 for Au/G4OH solutions with molar ratios 5, 10, and 20, respectively. These data clearly show that the

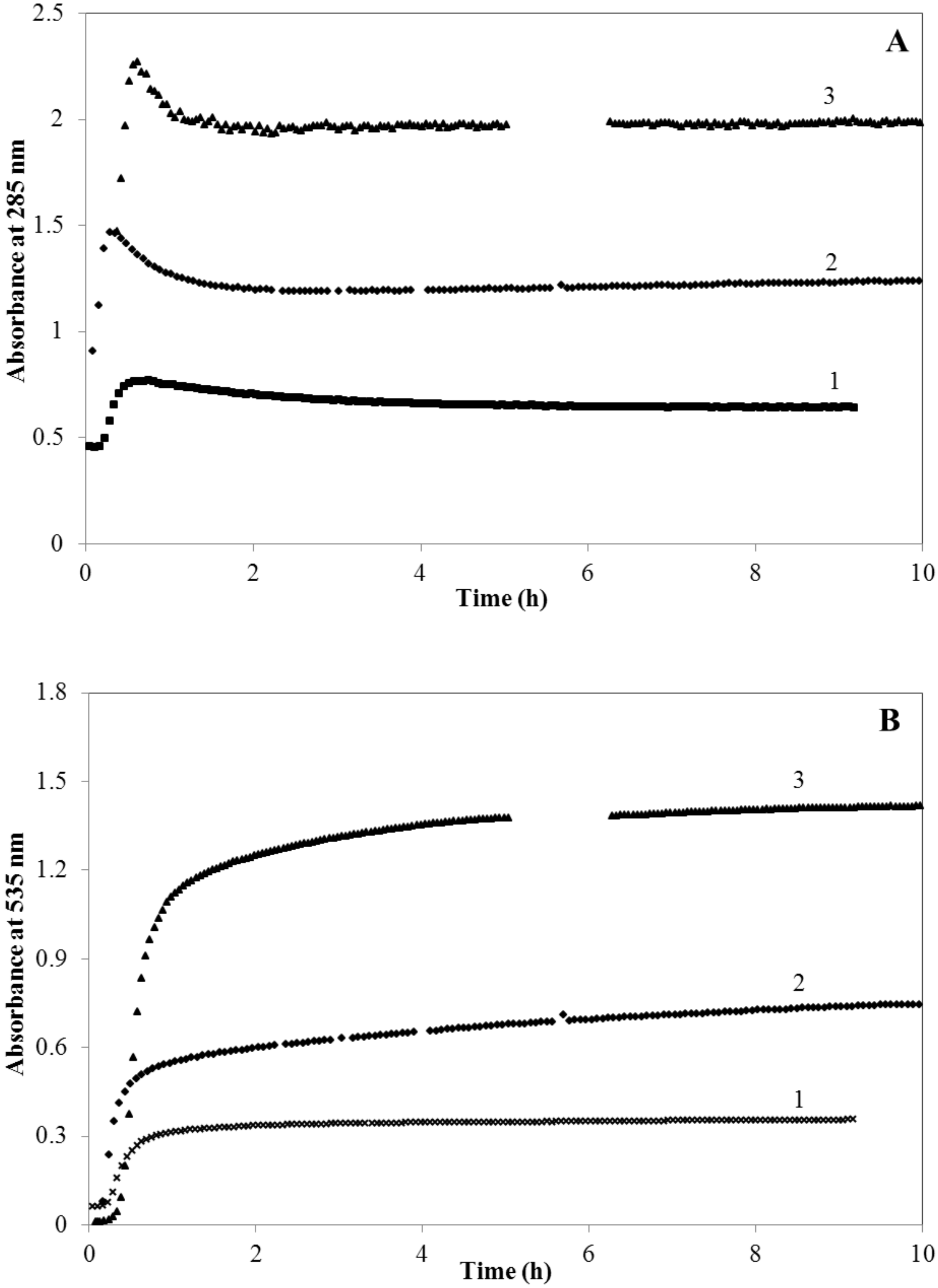

Figure 6.4 Development of bands at 285 (A) and 535 nm (B) as a function of time in UV-vis spectra of Au/G4OH aqueous solutions with molar ratios (1) 5, (2) 10, and (3) 20.

absorbance at 285 nm doubles with a twofold increase in Au concentration. In all these Au/G4OH solutions, the dendrimer has a large excess of functional groups capable of participating in redox reactions with Au^{3+}. Therefore, for any types of stoichiometric redox reactions occurring between G4OH and Au^{3+} and leading to the reduction of Au and formation of carbonyl compounds, the concentration of the latter should be proportional to the amount of gold used as an oxidizer. Since our absorbance data show such correlations and literature reports also indicate that aliphatic aldehydes such as propionaldehyde, isobutyraldehyde, and pivalaldehyde exhibit UV-vis bands in the 283-285 nm region,[305] one could suggest that the band at 285 nm indeed originates from the carbonyl compounds formed in redox reactions.

To verify this suggestion, the concentration of carbonyls presumably formed in solutions with different Au/G4OH ratios was estimated from UV-vis data, assuming that the band at 285 nm originates entirely from such species and their extinction coefficients are not much different from those of aliphatic carbonyl compounds (i.e., approximately 20 M^{-1} cm^{-1} on average).[305] While our estimates show that approximately 30, 60, and 100 mM of carbonyls should be formed in solutions with Au/G4OH ratios 5, 10, and 20, respectively, these concentrations are not realistic because they are more than 200 times larger than the theoretical maximum allowed by the stoichiometry of reactions 1 and 2. Therefore, we can safely conclude that the contribution of aldehydes, which could be formed in described above redox reactions, to the overall absorbance at 285 nm is very small.

Since our data show similar growth patterns for the 285 nm and SPR bands, it is more likely that the former band also represents Au particles that are formed in solution and stabilized by dendrimer molecules. Therefore, the band at 285 nm could be the

LMCT type band that reflects interactions of dendrimer molecules with either the surface of large metal particles or individual Au clusters that are not aggregated in large particles yet.[306]

6.3.3 Nature of functional groups responsible for reduction of Au

Together with observed color changes, our UV-vis data clearly show that initial $[AuCl_x(OH)_{4-x}]^-$/G4OH interactions are followed by the reduction of Au ions and aggregation of reduced Au species thus formed into metal particles. This result is consistent with previous literature reports, indicating that OH-terminated PAMAM dendrimers are capable of reducing Au ions.[162,302,307] However, explanations provided in these literature reports are focused on terminal hydroxyls, which are believed to participate in the reduction process.[286,292] It is also notable that all citations supporting such an idea can be traced back to a single paper that demonstrates that fragments of saccharides attached to the periphery of PAMAM dendrimers effectively reduce Au^{3+} ions.[286,292] At the same time, it remains uncertain if the results reported for sugar-modified dendrimers can be applicable to the G4OH dendritic system because chemical properties of polyol groups of saccharides are quite different from that of hydroxyls in alcohols.

To clarify the nature of functional groups responsible for the reduction of Au, interactions of $[AuCl_x(OH)_{4-x}]^-$ species with n-methylacetamide, propanol, 2-propanol, and triethylamine were examined by UV-vis. In these experiments, the $HAuCl_4$ concentration was maintained at 0.1 mM, while the amount of each chemical compound chosen for the treatment was adjusted appropriately to create a concentration of desired functional groups in solution similar to that existing in the Au/G4OH mixture with a molar ratio of 5. The intension was to monitor interactions of Au^{3+} species with only one type of functional groups (i.e., amide, terminal hydroxyls, or tertiary amines) existing in the G4OH PAMAM dendrimer structure and determine precisely which of these functional groups participate in the reduction process.

When n-methylacetamide, propanol, or 2-propanol were used, no detectable changes in UV-vis spectra were observed for an extended period of time (i.e., 6 h), suggesting that neither amides nor hydroxyls are capable of reducing Au^{3+} ions efficiently at room temperature. In contrast, when triethylamine was used, the SPR peak clearly appeared in UV-vis spectra (Fig. 6.5), consistent with reduction and aggregation of Au. This result strongly suggests that tertiary amines in the dendrimer structure are responsible for the reduction of Au species.

To verify this suggestion further, additional experiments with the $G4NH_2$ dendrimer and $Au/G4NH_2$ molar ratios 5, 10, and 20 were performed. UV-vis results summarized in Fig. 6.6 show the absence of the SPR peak in the 530-540 nm region for $Au/G4NH_2$ molar ratios 5 and 10 during the extended period of time (i.e., 24 h). In contrast, the SPR peak at 535 nm quickly appears for the $Au/G4NH_2$ ratio 20, rapidly grows in intensity during first 5 h, and roughly levels thereafter (Fig. 6.7). Similar to the case of Au/G4OH, the observed pattern is consistent with reduction of Au and rapid aggregation of reduced species thus formed into particles with dimensions exceeding 2 nm on average.[308] Since all 64 primary amines in the $G4NH_2$ structure are fully protonated in aqueous solutions at pH < 7.5,[109] it is expected that these functional groups located at the dendrimer periphery will interact electrostatically with anionic $[AuCl_x(OH)_{4-x}]^-$ species in the first place. While it remains unclear if primary amines of $G4NH_2$ are also capable of reducing Au^{3+} ions at room temperature, the absence of the SPR peak in the case of $Au/G4NH_2$ ratios 5 and 10 strongly suggests that the interaction

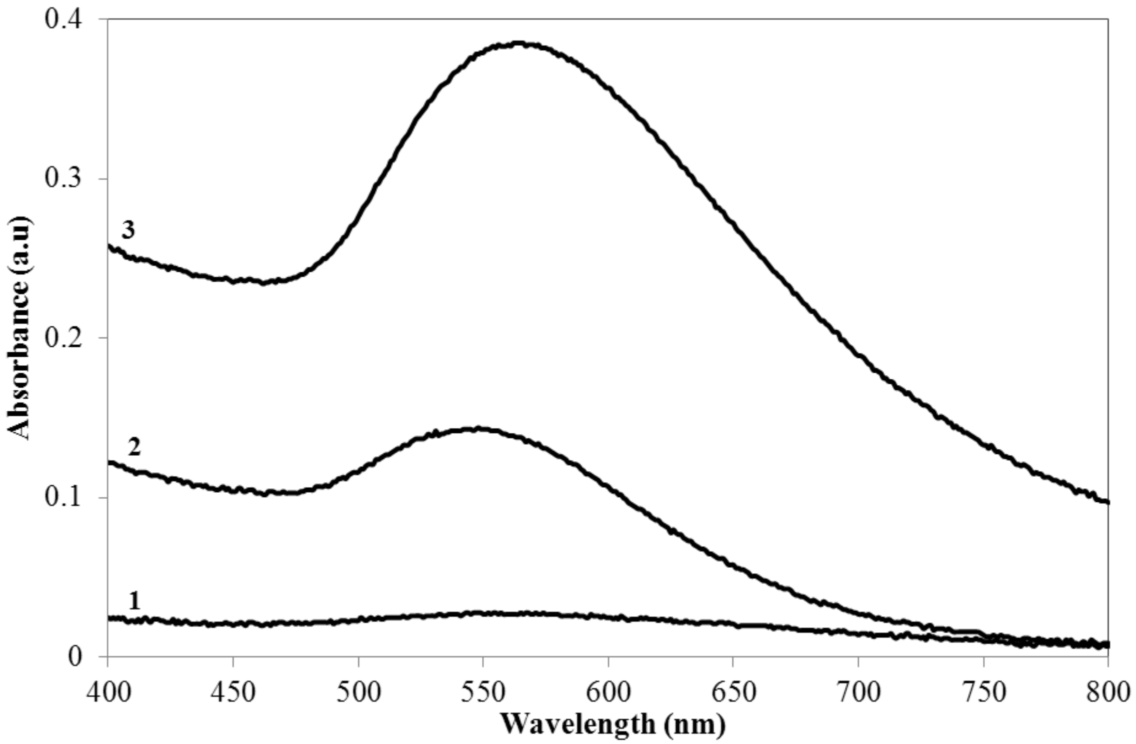

Figure 6.5 UV-vis spectra of 0.1015 mM $HAuCl_4$/1.2586 mM $N(C_2H_5)_3$ aqueous solution after (1) 1.5 h, (2) 2 h, and (3) 6 h.

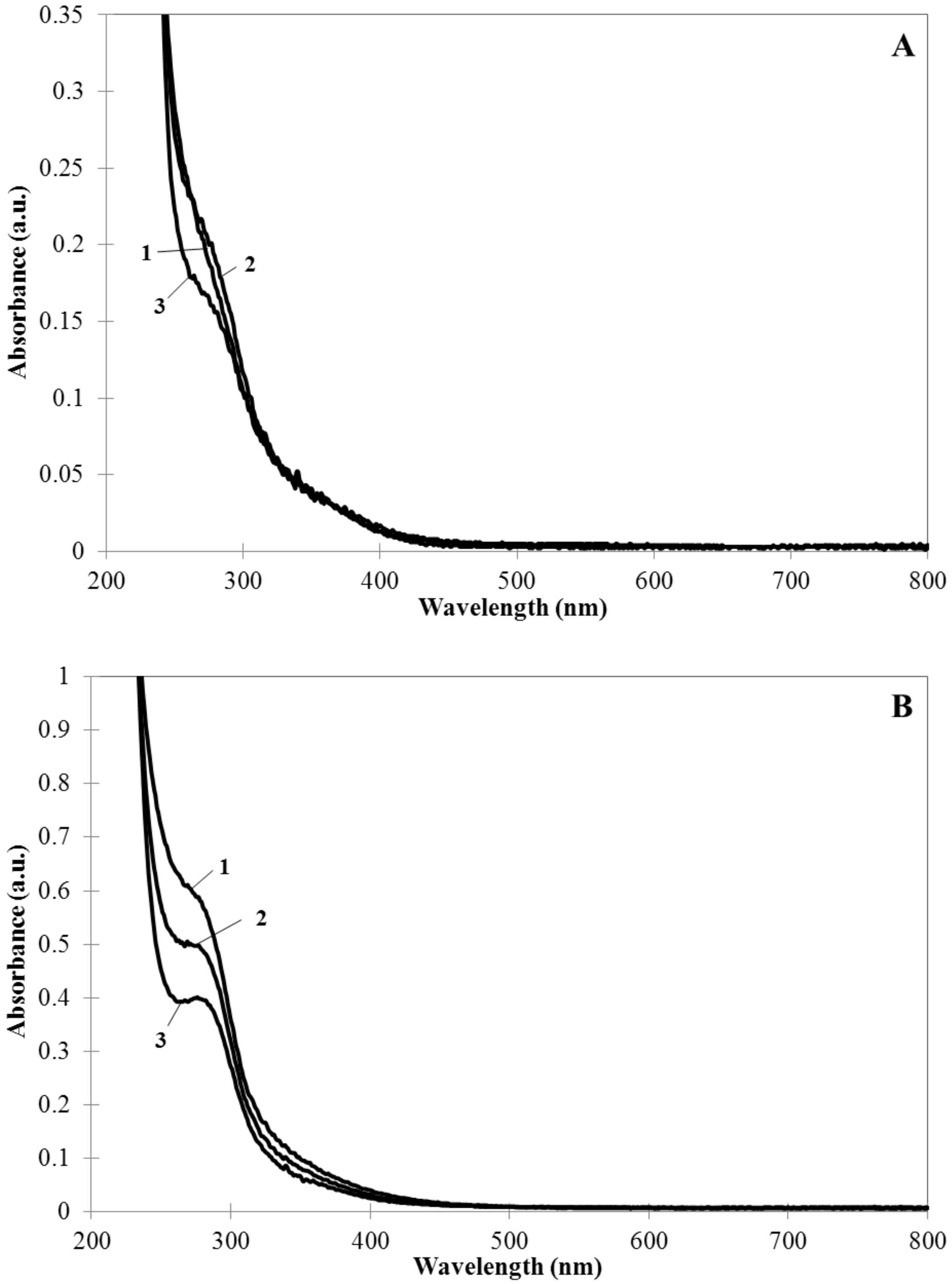

Figure 6.6 UV-vis spectra of Au/G4NH$_2$ aqueous solutions with molar ratios (A) 5 and (B) 10 collected after (1) 5 min, (2) 3 h, and (3) 24 h.

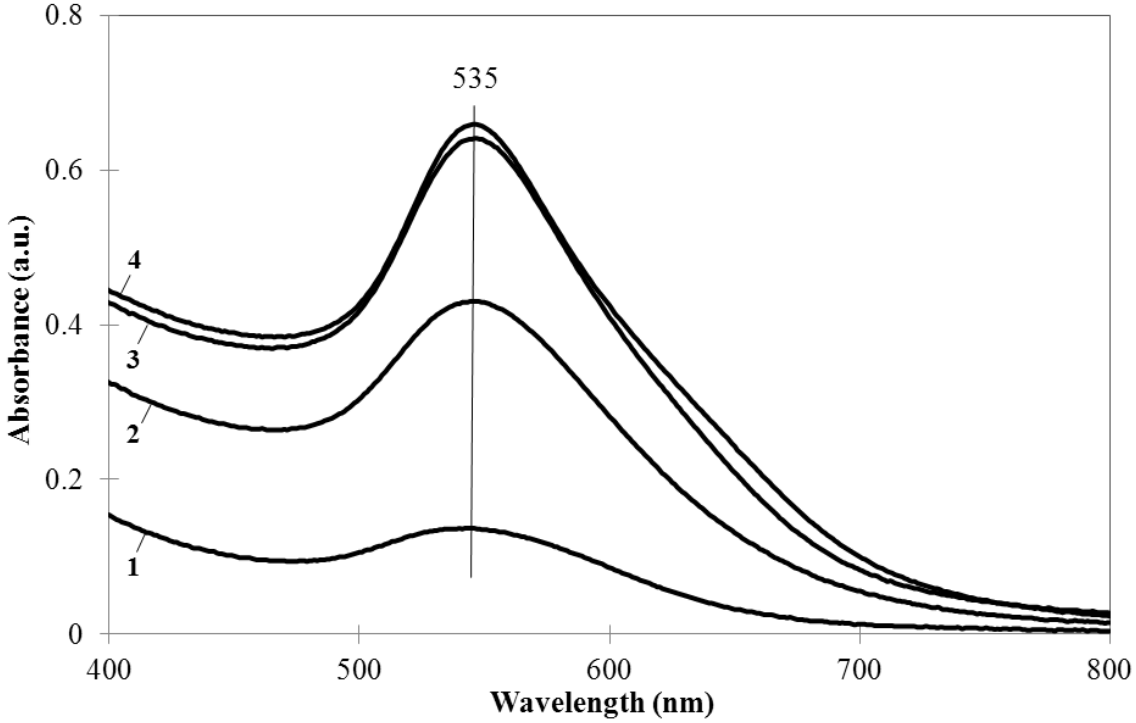

Figure 6.7 UV-vis spectra of Au_{20}/$G4NH_2$ aqueous solution collected after (1) 2 h, (2) 3 h, (3) 5 h, (4) 24 h.

of Au with the G4NH$_2$ dendrimer periphery prevents the aggregation process at relatively low Au/dendrimer ratios if the reduction process were to occur. Most likely, the majority of Au species in this case are located at the dendrimer periphery and their diffusion into the dendrimer interior is limited. At higher Au/G4NH$_2$ ratios, however, a substantial portion of Au^{3+} ions appears in the dendrimer interior and undergoes reduction by tertiary amines with subsequent aggregation into metal particles. Since the periphery of the G4OH dendrimer is not capable of complexing $[AuCl_x(OH)_{4-x}]^-$ ions, most of these species reside in the G4OH interior, where they undergo reduction by tertiary amines and aggregation. This explains as to why the aggregation of Au was observed for all Au/G4OH molar ratios and only for relatively high ratios in the Au/G4NH$_2$ case.

6.3.4 Summary of events occurring in Au/G4OH solution

The experimental results described so far allow assembling the sequence of events occurring in the Au/G4OH solution and yielding reduced Au species. Initially, when the basic solution of the partially protonated G4OH dendrimer is mixed with the acidic solution of the HAuCl$_4$ precursor, acid-base interactions take place. As a result, both the degree of G4OH protonation and hydrolysis of $[AuCl_3(OH)]^-$ species increase. The $[AuCl(OH)_3]^-$ complexes thus formed interact electrostatically with protonated tertiary amines in the dendrimer interior and this process leads to the formation of Au-dendrimer ion pairs. The close proximity of $[AuCl(OH)_3]^-$ species to protonated tertiary amines in the dendrimer structure initiates the complexation process that leads to deprotonation of tertiary amines and formation of Au^{3+}/G4OH complexes. By analogy with what is known for Rh^{3+}/G4OH solutions,[296] $[AuCl(OH)_3]^-$ species most likely lose the remaining chlorine ligands upon complexation. In contrast to Rh^{3+} ions, however, nearly all known Au^{3+} complexes are 4 coordinate and square planar in nature,[309] suggesting that Au^{3+}/G4OH complexes finally formed in the dendrimer interior most likely retain the square planar geometry. The life time of these complexes is evidently short due to the reduction of Au cations by the dendrimer. It has been shown previously that amines of different nature can reduce Au^{3+} ions to Au^0 only when their oxidation potentials fall within the range of reduction Au^{3+}/Au^0 (0.853 V) and oxidation Au^0/Au^+ (1.425 V) potentials characteristic for the Au system.[310] Consistent with these findings, our experiments clearly show that Au^{3+} cations can be effectively reduced to Au^0 by triethylamine because the oxidation potential of these species is approximately 1.08 V.[310] While the oxidation potential of tertiary amines in the G4OH structure is largely unknown, cyclic voltammetry measurements performed with structurally similar polypropylene imine (PPI) dendrimers show voltammetric responses from branching tertiary amines in the 0.7-1.0 V range,[311] indicating that tertiary amines in different chemical structures exhibit quite similar redox properties. Therefore, we can infer that the transfer of electrons from G4OH tertiary amines to Au^{3+} cations yields completely reduced Au species, as no absorption bands expected from isolated Au^+ (190 nm) or aggregated $(Au^+)_n$ intermediates (250 and 340 nm) were observed in UV-vis spectra.[312-314]

When Au^{3+} cations are reduced by tertiary amines in the G4OH dendrimer interior, their nucleation leads to a growth of gold particles, suggesting that the dendrimer itself acts as a reductant for Au ions and as a stabilizer for finally formed Au particles. While solutions with Au/G4OH ratios 5 and 10 were fairly stable for an extended period of time, properties of solutions with higher Au/G4OH ratios were different. For example, UV-vis spectra collected for the Au_{20}/G4OH solution (Fig. 6.8) show the SPR band initially observed at 540 nm acquires a shoulder at 600 nm after

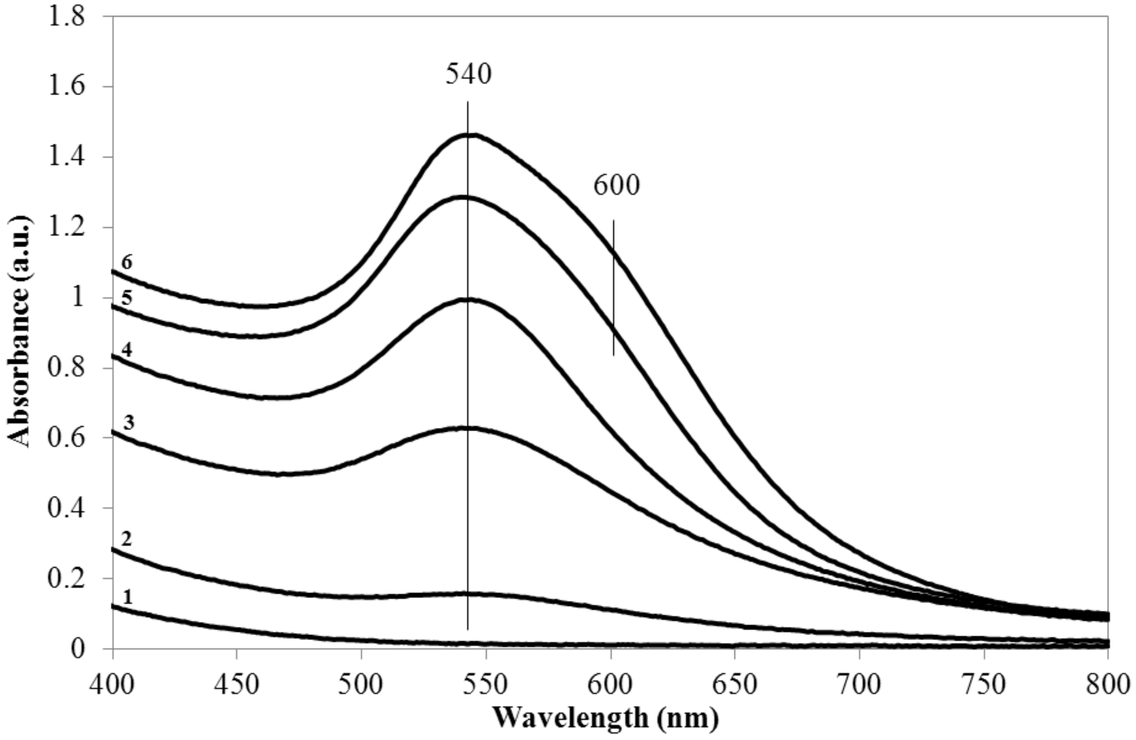

Figure 6.8 UV-vis spectra of Au_{20}/G4OH aqueous solution collected after (1) 10 min, (2) 30 min, (3) 40 min, (4) 1 h, (5) 3.5 h and (6) 24 h.

approximately 3.5 h that continues to develop as a function of contact time. These data strongly suggest that irregular shaped (i.e., elongated) Au particles are formed alongside of spherical ones in this solution.[300,315] Solutions with higher Au/G4OH ratios (i.e., 30 and 60) quickly precipitate, but some Au particles still remain in the supernatant, as evidenced by a single SPR peak at 530 and 540 nm in UV-vis spectra, respectively (Fig. 6.9). Precipitation observed for Au/G4OH ratios 30 and 60 indicates that sizes of some Au particles formed in these solutions are fairly large and neither dendrimer interior nor exterior forms of their stabilization are possible.

Alternatively, we cannot rule out completely a possibility that a certain fraction of G4OH molecules is chemically altered due to participation in redox reactions with Au ions, yielding aldehydes (reactions 1 and 2). Since aldehydes are relatively strong reducing agents,[316] they can also participate in redox reactions with Au^{3+} ions to form carboxylic acids (reaction 3).

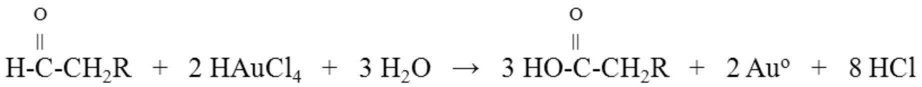

$$\text{H-}\overset{\overset{\text{O}}{\|}}{\text{C}}\text{-CH}_2\text{R} \;+\; 2\,\text{HAuCl}_4 \;+\; 3\,\text{H}_2\text{O} \;\rightarrow\; 3\,\text{HO-}\overset{\overset{\text{O}}{\|}}{\text{C}}\text{-CH}_2\text{R} \;+\; 2\,\text{Au}^{\circ} \;+\; 8\,\text{HCl}$$

It is further expected that carboxylic acids and aldehydes formed in reactions 1-3 can undergo condensation with either tertiary or secondary amines to yield large 3D protein-like domains in solution.[317] When these domains reach a critical size, their sedimentation and precipitation become inevitable and this could also explain the formation of precipitates in solutions.

6.3.5 Sizes of Au particles

It has been reported previously that sizes of Au particles formed in solution can be determined precisely from UV-vis spectra using the intensity of the SPR band and its local minimum at approximately 450 nm.[318] In essence, this method allows monitoring

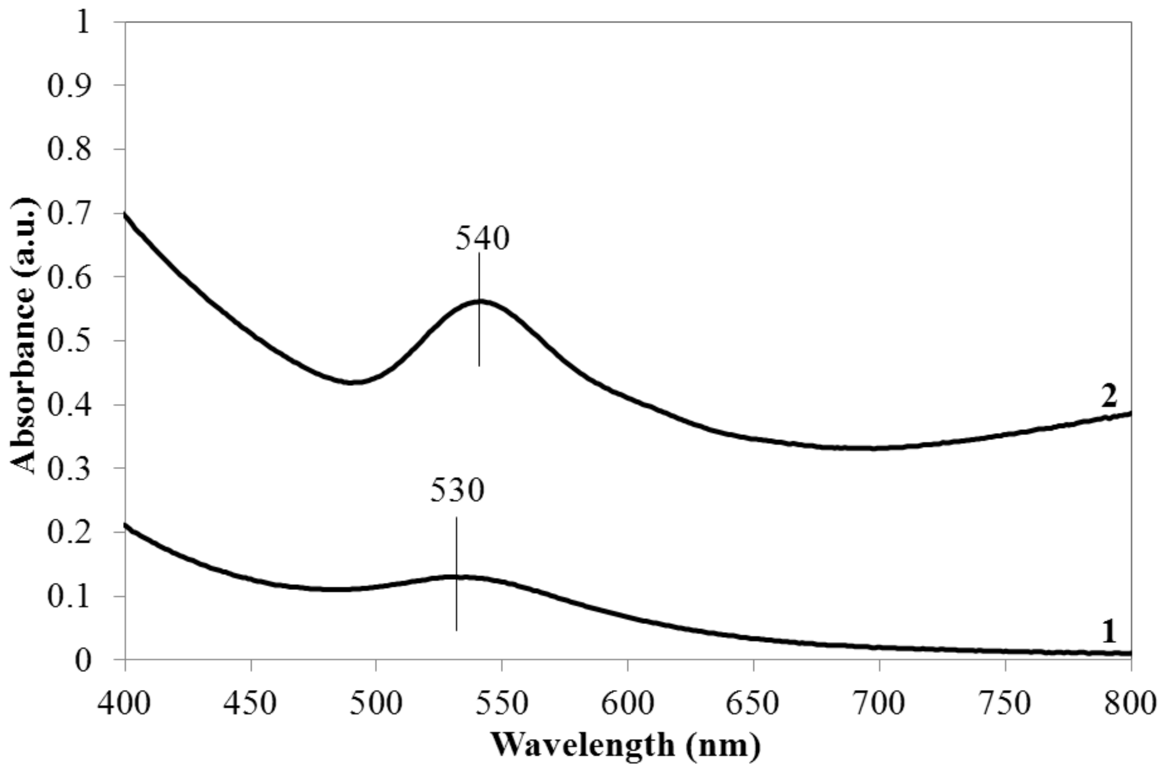

Figure 6.9 UV-vis spectra of the supernatant from precipitated Au/G4OH aqueous solutions with molar ratios (1) 30 and (2) 60.

in situ changes in sizes of metal particles as a function of time when time resolved UV-vis spectra are available. Fig. 6.10 provides an example of such data for most stable Au/G4OH solutions with molar ratios 5 (pH=5.6) and 10 (pH=4.2). In both cases, a rapid growth of Au particles is observed during the first hour after mixing the reactants, but the process slows down significantly thereafter. This pattern clearly shows that tertiary amines in the G4OH interior are relatively strong reducing agents. As a result, only a short period of time is required for reduction of Au ions and nucleation of reduced Au species thus formed. Furthermore, since both of these solutions were found to be stable, it is evident that G4OH molecules effectively stabilize Au particles initially formed in solution and protect them from further aggregation. At least in part, this could explain the change in aggregation rates observed in Fig. 6.10 for both solutions. However, it also possible that the slow growth of Au particles observed after 1 h could be related to the lack of reduced Au species that are remaining free in solution at that point. Average sizes of Au particles formed in Au_5/G4OH and Au_{10}/G4OH solution after 24 h were found to be 6.7 and 9.6 nm, respectively. Consistent with other literature reports,[61,251,296] this result one more time shows that sizes of metal particles can be controlled to some extent by the metal/dendrimer ratio. In the case of Au_5/G4OH and Au_{10}/G4OH solutions, however, dimensions of Au particles formed are substantially larger than the size of G4OH molecules (4.5 nm), indicating that Au particles are not encapsulated by the dendrimer but their interdendrimer stabilization maintains the colloidal state of these solutions.

To determine if the growth of Au particles in Au/G4OH solutions can be controlled, additional experiments with pH adjusted solutions were performed. Results presented in Fig. 6.11 provide a comparison of Au particle sizes as a function of contact

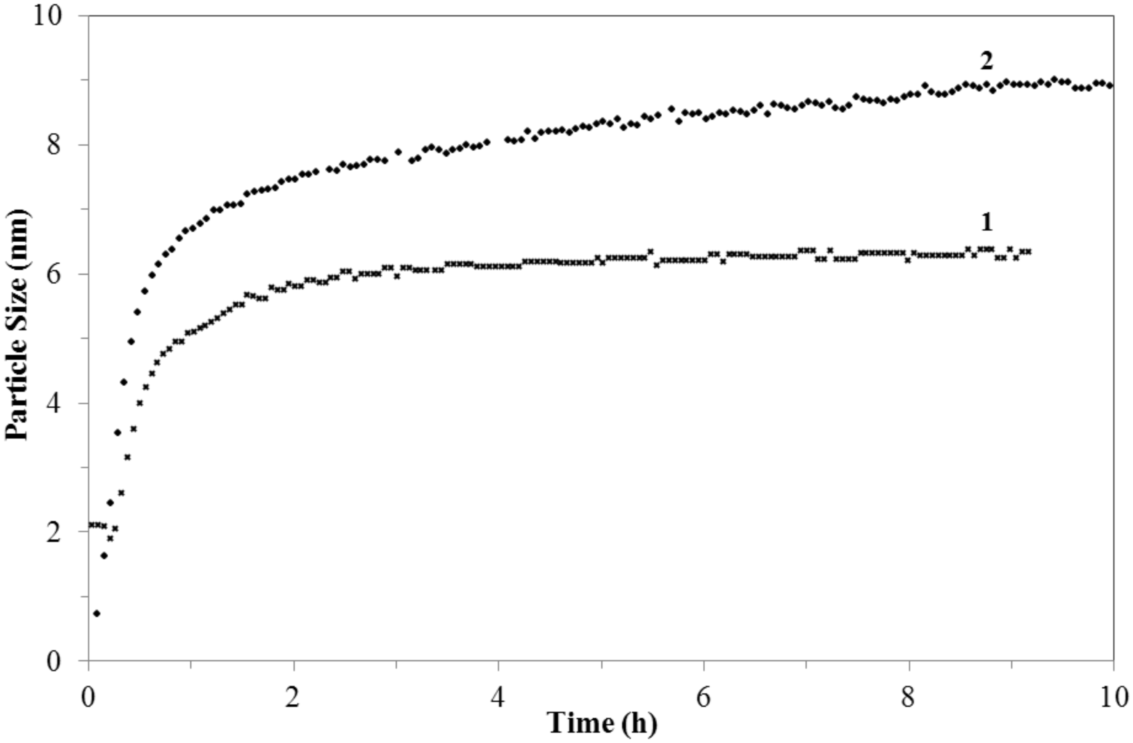

Figure 6.10 Sizes of Au particles formed in Au/G4OH aqueous solutions with molar ratios (1) 5 and (2) 10 as a function of time.

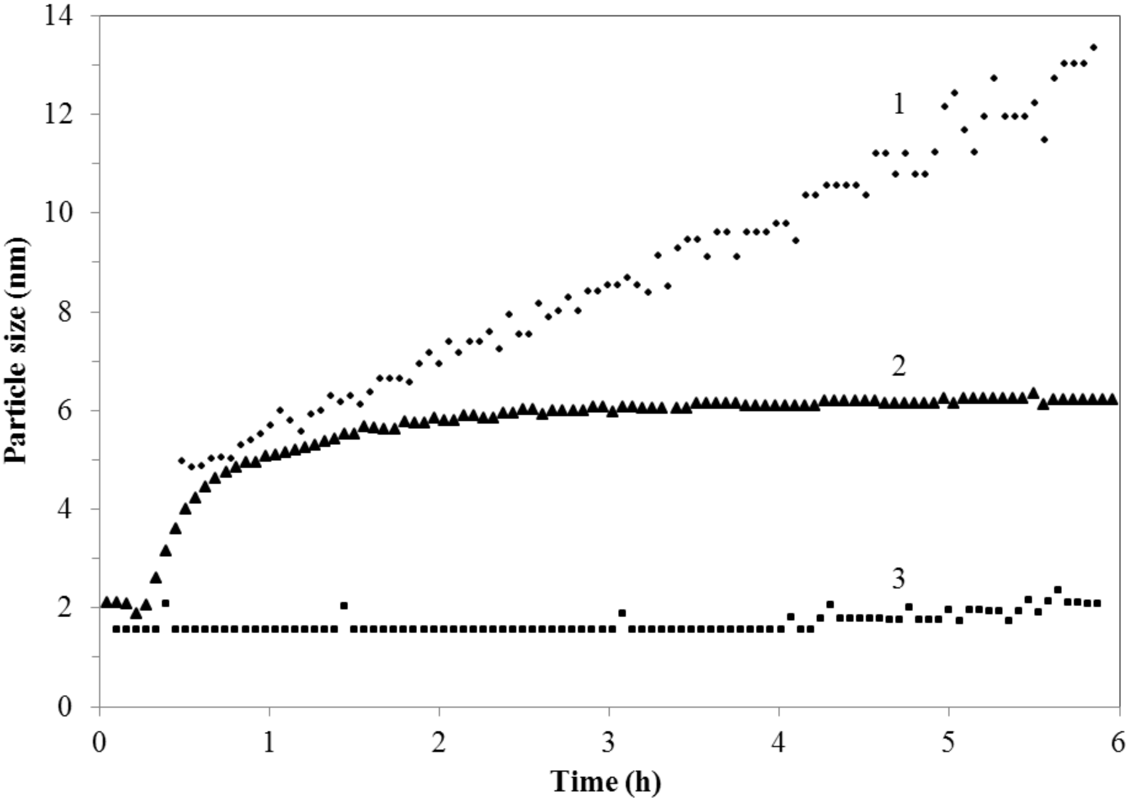

Figure 6.11 Sizes of Au particles formed in pH adjusted Au_5/G4OH aqueous solutions as a function of time: (1) pH=3, (2) pH=5, and (3) pH=7.

time for the Au_5/G4OH solution at different pH values. When the solution pH was immediately adjusted to 3 after mixing the reactants, Au particles with dimensions on the order of 5 nm were formed during first 30 min. Dimensions of these particles continue to increase with time and reach 13 nm at the end of measurements. In contrast, when the Au^{3+}/G4OH solution pH was adjusted to 7, stable Au particles with sizes on the order of 2 nm were formed. When these data are further combined with those acquired for the Au/dendrimer mixture (pH=5.6) for which no pH adjustments were performed, it becomes evident that the size of Au particles decreases significantly with the Au/G4OH solution acidity. In fact, the observed pattern clearly demonstrates that the growth of metal particles in Au/G4OH nanocomposites can be effectively controlled by the solution pH.

It is noteworthy that some other properties of Au/G4OH solutions are also different at various pH values. For example, the speciation of $[AuCl_x(OH)_{4-x}]^-$ complexes gradually changes from $[AuCl_3(OH)]^-$ to $[AuCl(OH)_3]^-$ in the investigated range of pH due to pH-dependent hydrolysis of $HAuCl_4$.[319] The degree of tertiary amine protonation is expected to be 100% at pH=3, but it drops to approximately 10% at pH=7.[109] Moreover, it has been reported that the conformation of PAMAM dendrimers changes significantly with the solution pH.[115] For example, at high pH values, the dendrimer assumes a dense core structure with a maximum density at the dendrimer core and uniform void spacing. However, a dense shell structures are formed at low pH values with maximum density at the dendrimer periphery but nonuniform void spacing. While all these aspects could influence processes occurring in the Au/G4OH solution at different pH values, the extent of their contribution could be different.

It has been shown previously that the reduction of aqueous $HAuCl_4$ by ascorbic acid yields colloids with an average size of Au particles of approximately 18 and 26 nm at pH 3 and 6.2, respectively.[319] The observed difference in particle sizes was attributed to various reduction rates of $[AuCl_3(OH)]^-$ and $[AuCl(OH)_3]^-$ species dominating in solution at these pH values. Since the reduction potential of $[AuCl_3(OH)]^-$ is higher than that of $[AuCl(OH)_3]^-$ by 0.07 V, it has been suggested that faster reduction of the former species facilitates their quick nucleation and smaller metal particles are formed. In contrast to these expectations, the results acquired for Au_5/G4OH solutions clearly show the formation of larger Au particles at pH=3 than at pH values 5.6 and 7, consistent with relatively slow reduction of Au ions and nucleation of reduced species under acidic conditions. Therefore, it is feasible that the Au speciation and any differences existing in reduction potentials of Au species are not quite critical for sizes of Au particles formed in Au/G4OH solutions.

Since all tertiary amines in the G4OH interior are protonated at pH=3 and the dendrimer assumes a dense shell structure, the dendrimer interior is fairly opened and easy accessible for Au ions.[115] Therefore, electrostatic interactions between protonated tertiary amines and $[AuCl_3(OH)]^-$ ions, dominating the speciation of aqueous $HAuCl_4$ at pH=3, are expected to be maximized in this case. As a result, all Au ions could be quickly driven into the dendrimer interior by electrostatic forces where their complexation and subsequent reduction take place. In acidic solutions, however, the Au^{3+}/dendrimer complexation process is expected to be relatively slow because the high concentration of free protons impedes deprotonation of tertiary amines. Since the complexation and reduction processes are directly related to each other, the reduction of Au ions in strongly acidic Au/G4OH solutions is also slow and relatively large Au particles are formed. This conclusion is further reinforced by literature examples demonstrating that slow reduction rates typically favor the formation of fairly large Au aggregates.[320] Furthermore, when the dendrimer interior is fairly opened at low pH values, the dendrimer is not capable of effectively trapping Au particles. As a result, Au particles initially formed in the dendrimer interior are quickly released into solution where they undergo further aggregation, consistent with our experimental observations. As the solution acidity decreases, more non-protonated tertiary amines appear in the dendrimer interior.[109] These naked functional groups have no restrictions for complexation of Au species and exhibit a higher reducing power than protonated tertiary amines, suggesting that the reduction process is accelerated in solutions with higher pH values. Moreover, as the solution acidity declines, the dendrimer interior becomes more crowded due to conformational changes described above, enabling more efficient trapping of Au particles. Therefore, a progressive decrease of Au particle sizes observed for solutions with higher pH values is the consequence of fast Au reduction coupled with better stabilization of Au particles by the dendrimer. Taking into account sizes of Au particles formed in Au_5/G4OH solutions at different pH values, we can further conclude that modes of Au stabilization by the dendrimer are evidently different. Interdendrimer stabilization takes place in solutions with pH values 3 and 5.6, while an intradendrimer mode prevails at pH=7 due to the small size of Au particles (2 nm) formed in this case. Finally, the pattern observed for pH adjusted Au_5/G4OH solutions is strongly reinforced by other literature reports, demonstrating that the fast reduction of Au ions by $NaBH_4$ typically yields relatively small Au particles.[237,248,288]

To verify the size of Au particles formed in the Au_5/G4OH solution at pH=7, a small portion of this solution was deposited onto a Cu grid coated with a carbon film, dried under vacuum, and imaged by STEM. Large spherical aggregates with sizes of approximately 80 nm observed on STEM images (Fig. 6.12A) represent the G4OH PAMAM dendrimer, molecules of which aggregated and formed large globular structures upon solvent removal to maintain the low surface tension. The formation of similar dendrimer structures was observed previously when PAMAM dendrimer solutions were imaged by AFM.[321-323] From STEM images shown in Fig. 6.12A and B, it is also evident that dendrimer aggregates incorporate Au particles with sizes below 2 nm and such Au particles cannot be observed on other parts of the grid where dendrimer aggregates are not present. Therefore, STEM results not only confirm the size of Au particles estimated from UV-vis for the Au_5/G4OH solution, but also show that all Au particles are encapsulated by the dendrimer.

6.3.6 Solid materials prepared from pH adjusted Au_5/G4OH

Since the results described above clearly show that solution pH adjustments help to control sizes of Au particles in Au/G4OH nanocomposites and at pH=7 Au particles on the order of 2 nm can be formed, our final goal was to demonstrate that Au/G4OH nanocomposites with such sizes of metal particles can be used as precursors in preparations of solid materials. For this purpose, Au_5/G4OH and Au_{10}/G4OH nanocomposites were prepared under pH controlled conditions (i.e., pH=7) and further deposited onto the SiO_2 support. Both samples were dried at room temperature and imaged by STEM. STEM images collected for Au_5/G4OH/SiO_2 (Fig. 6.13) show the presence of highly dispersed and uniform Au particles with dimensions on the order of 1.6 nm. Au particles of similar sizes were also present in the Au_{10}/G4OH/SiO_2 material (Fig. 6.14A). In the latter case, however, larger Au aggregates with dimensions on the order of 5 nm were also present (Fig. 6.14B). This result indicates that not all Au species

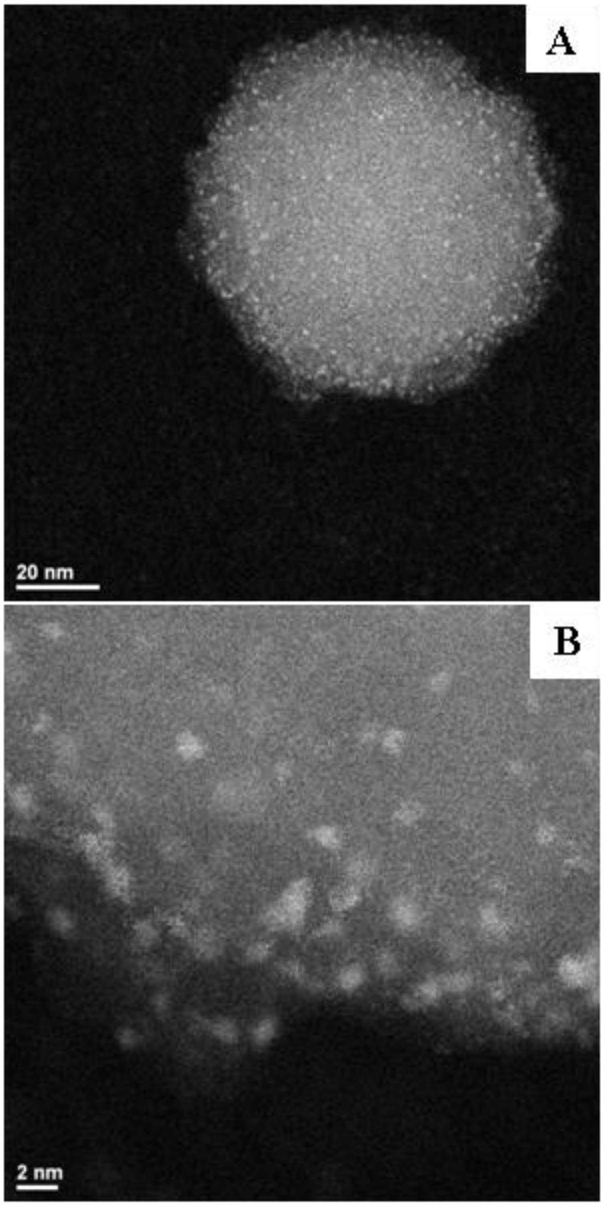

Figure 6.12 STEM images of sample prepared by evaporation of the Au_5/G4OH solution aged for 6 h at pH=7.

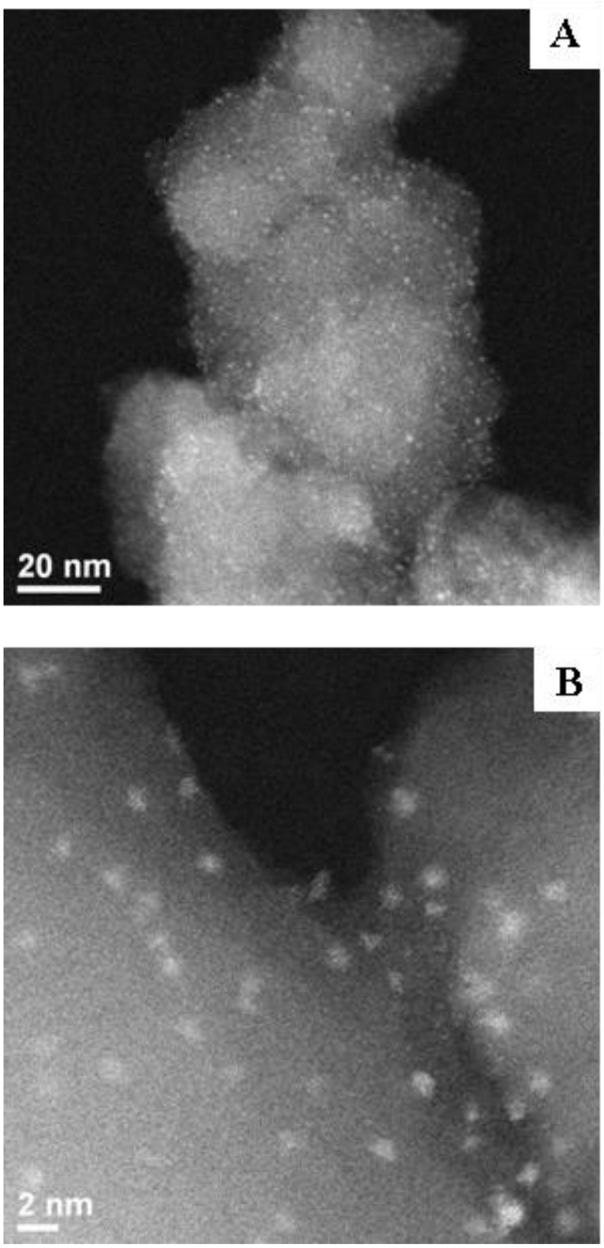

Figure 6.13 STEM images of 1% Au_5/G4OH/SiO_2 prepared from the Au_5/G4OH solution aged for 6 h at pH=7.

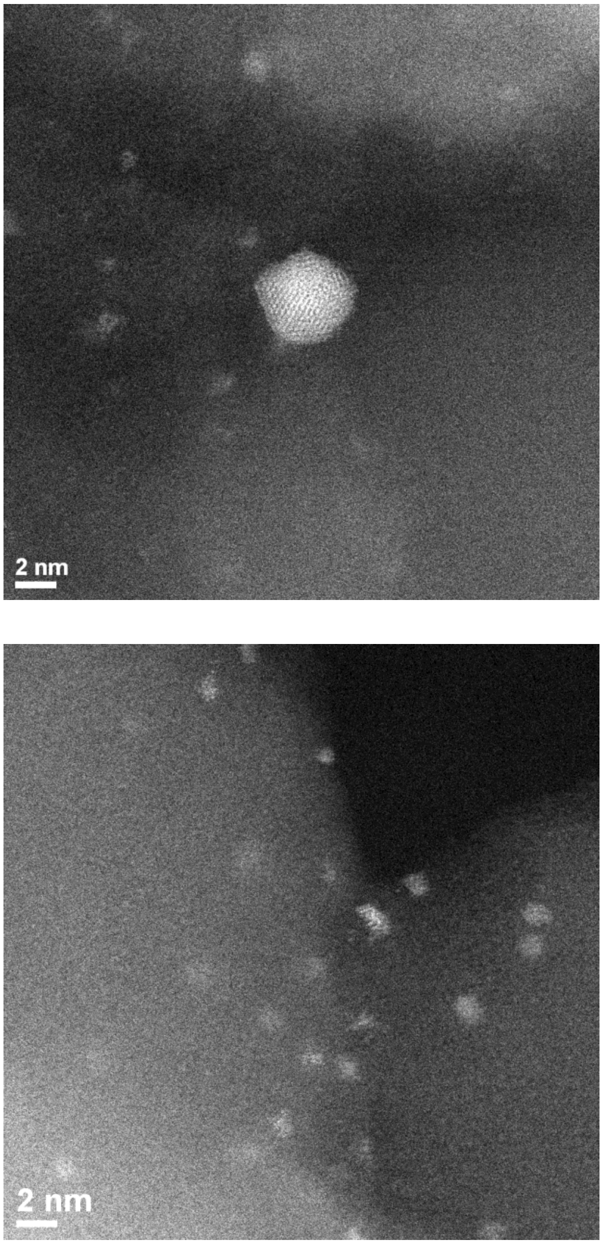

Figure 6.14 STEM images of 1% Au_{10}/G4OH/SiO_2 prepared from the Au_{10}/G4OH solution aged for 6 h at pH=7.

remain encapsulated by the dendrimer when the Au/G4OH ratio is higher than 5 and subsequent aggregation of such species yields relatively large Au particles.

6.4 Conclusions

We have shown the effect of pH adjustments on the growth of Au nanoparticles in Au/G4OH solutions and the eventual sizes of Au particles formed in SiO_2-supported materials prepared via a dendrimer-mediated route. Results show that the pH of all examined Au/G4OH solutions equilibrates within the first several minutes, indicating that all events associated with initial Au-G4OH interactions are relatively fast. The appearance of an SPR band in UV-vis spectra of Au/G4OH solutions is consistent with the formation of Au nanoparticles via a mechanism in which the G4OH dendrimer operates as a reductant. UV-vis results further show that tertiary amines in the dendrimer interior are responsible for the reduction of Au ions. The size of Au particles formed in the Au_5/G4OH solution can be effectively controlled by the solution pH. When the solution pH is adjusted to 7, stable Au particles with sizes on the order of 2 nm are formed. Au_5/G4OH nanocomposites with preformed Au particles can be used as precursors for preparation of supported catalytic materials, as they can be deposited intact on the surface of SiO_2 and yield highly dispersed and nearly uniform Au nanoparticles with dimensions on the order of 1.6 nm. However, when the Au/G4OH ratio is higher than 5, not all reduced Au species remain in the dendrimer interior and the subsequent aggregation of such species yields relatively large Au particles.

6.5 Acknowledgements

The authors gratefully acknowledge Toyota Motor Engineering & Manufacturing North America, Inc., for the partial financial support of this work. The authors further

acknowledge Dr. Douglas Blom at the Electron Microscopy Center of the University of South Carolina for his assistance during collection of the STEM images.

CHAPTER 7

AG DIAMMINE IMPREGNATION ON OXIDES AND OXIDIZED CARBON USING STRONG ELECTROSTATIC ADSORPTION

7.1 Introduction

Silver has drawn great interest because of its high catalytic activity for various chemical reactions, such as the decomposition of ozone,[365] NO_x reduction,[352,364] epoxidation of ethylene and propylene,[343,366] oxi-dehydrogenation of methanol to formaldehyde,[344,346] reduction of nitrophenols,[342,357] and alcohol dehydrogenation to carbonyl compounds.[353,355] Some of these reactions require relatively large Ag particles but some (i.e., alcohol dehydrogenation to carbonyl compounds and H_2–HC–SCR hydrogenation) proceed with much higher rates over supported Ag nanoparticles with sizes below 1 nm, suggesting that sizes of supported Ag particles must be strictly controlled for each individual chemical process. Therefore, extensive efforts were recently applied to the synthesis of supported silver nanoparticles with desired dimensions and shapes. Unfortunately, conventional preparations techniques based on the impregnation of Ag salts and high temperature treatments provide a limited control over Ag particle sizes in solid materials because Ag easily aggregates at elevated temperatures.

Table 7.1 details some of the conventional preparation methods reported in the literature for Ag nanoparticles supported on Al_2O_3 and SiO_2, e.g., incipient wetness (IW), wet impregnation (WI) and sol-gel. In addition, to the different methods of Ag addition, the metal loading and subsequent calcination and reduction temperatures are also given. A number of trends affecting the particle size of the final catalyst can be identified in Table 7.1. First, the majority of the researchers have used $AgNO_3$ as silver precursor and

Table 7.1. Literature survey of preparation methods of Ag/SiO$_2$ and Ag/Al$_2$O$_3$ catalysts.

Precursor / Method	**wt. %**	**Average Particle size (nm)**	**Pretreatment**	**Reaction**
Ag/Al$_2$O$_3$ Catalysts				
AgNO$_3$ / WI	3	5 – 10 nm	Calcination at 500 °C in air (5 h)	CH$_4$-SCR.[353]
AgNO$_3$ / WI	2.5	5.7 nm	Calcination at 500 °C in air (5 h)	SCR of NO$_x$ in the presence of EtOH.[354]
		9.5 nm	Calcination at 500 °C in air (5 h) followed by reduction in 5% H$_2$ at 700 °C	
AgNO$_3$ / Reduction of AgNO$_3$ by ethylene glycol in the presence of PVP).	11	diameter: 150 nm (nanowires)	Reduction in H$_2$ at 350 °C (3 h)	Styrene epoxidation.[355]
AgNO$_3$ / IW	6	10.46	Calcination at 550 °C in air (3 h)	HC-SCR of NO$_x$.[356]
AgNO$_3$ / Sol-gel	5	< 10 nm	Calcination at 600 °C in air (6 h)	HC-SCR (propene and n-octane).[357]
Ag/SiO$_2$ Catalysts				
Ag(NH$_3$)$_2$OH / IW	2	0.8	Calcination at 500 °C in air (2 h) followed by reduction at 200 °C in 3.5% H$_2$ (2 h)	Hydrogenation of acrolein.[358]
AgNO$_3$ / Reduction of AgNO$_3$ with NaBH$_4$ in the presence of CTAB	0.5	224	Drying at 200 °C (6 h) followed by calcination at 600 °C (6 h)	Reduction of 4-nitrobenzo-15-crown.[359]
AgNO$_3$ / IW	10	XRD: 2.9	Calcination at 500 °C (2 h)	Selective liquid-phase oxidation of benzyl alcohol.[360]
		EXAFS: 1.5		
		TEM: 2.5		
AgNO$_3$ / IW	8	4.5	Calcination in O$_2$ at 500 °C (2 h) followed by reduction at 200 °C in H$_2$ (1 h)	Low temperature CO oxidation.[361]
		16.7	Calcination in O$_2$ at 500 °C (2 h) followed by reduction at 500 °C in H$_2$ (1 h)	
Ag(NH$_3$)$_2$NO$_3$ / WI (SBA-15)	1.4	4	Calcination in O$_2$ at 300 °C followed by reduction at 300 °C in H$_2$ (1 h)	No reaction.[362]
	4.6	diameter: 6 nm length: 50 nm (nanowires)		

the common preparation of IW resulting to average silver particle sizes of 10.5 and around 2.5 nm, when Ag was supported onto alumina and silica, respectively.[356,360] The majority of Ag catalysts were activated with calcination in air around 500 °C and leading to higher dispersions compared to catalysts reduced in H_2 after the calcination step.[354] In the latter case, Ag particle size increased with increasing reduction temperature. Specifically, the average size of Ag particles of an 8 % Ag/SiO_2 catalyst prepared with IW and calcined at 500 °C, was 4.5 and 16.7 nm, when reduced at 200 °C and 500 °C, respectively.[361] The synthesis of colloidal silver nanoparticles in most cases is leading to the formation of large Ag particles. For instance, catalysts prepared by chemical reduction of $AgNO_3$ with $NaBH_4$ in aqueous solution using cetyltrimethylammonium bromide (CTAB) as stabilizing agent followed by impregnation of the colloidal solution on hollow mesoporous silica, Table 7.1 shows that the average particle size of a 0.5 % Ag/Silica catalyst was 224 nm.[359]

Up to now, there are only a few reports for the preparation of silver nanostructures using $Ag(NH_3)_2NO_3$ as silver precursor.[347,348362] A modified IW impregnation inspired by strong electrostatic adsorption (SEA) was reported recently in the literature. The difference between IW and SEA was pH adjustments of the initial $AgNO_3$ aqueous solution to 11 using ammonium hydroxide. The final catalyst, 2% Ag/SiO_2, was calcined in air at 500 °C followed by reduction in H_2 at 200 °C for 2 h and had an average silver particle size of 0.8 nm.[358] Pikus et al. synthesized silver nanoparticles embedded on SBA-15 using WI of $Ag(NH_3)_2^+$. Calcination in O_2 at 400 °C followed by reduction at 300 °C in H_2 for 1 h led to relatively small silver nanoparticles (4 nm), for low loadings (1.4 % Ag/SiO_2), whereas long (50 nm) silver nanowires formed when the loading increased to 4.6 % Ag/SiO_2.[362]

Several literature examples illustrate the successful synthesis of silver nanoparticles and nanoclusters. Among these reports of Ag nanocluster catalysts, zeolite-supported Ag_3 clusters for coupling of CH_4 and C_2H_4 by Baba et al.,[351] hydrotalcite-supported Ag for dehydrogenation of alcohols,[350] and size-selected Ag clusters for propylene epoxidation are successful examples.[335] Specifically, it was shown that size-selected clusters of Ag (Ag_3 trimers), and small aggregares of the Ag trimmers (effectively nanoparticles with a diameter of ca. 3.5 nm dispersed on amorphous alumina films exhibit high selectivity in epoxidation of propylene to form PO.[335] DFT calculations showed that the pathway to PO included the activation of the C=C double bond in propylene leading to the formation of the surface oxametallacycle intermediate, which isomerizes in an elementary step to form PO. The critical advantages that make the trimer and aggregate catalysts more selective than larger Ag particles include their unique electronic structure, which allows them to preferentially activate the C=C double bond in propylene (rather than allylic C-H bonds) forming oxametallacycles, and their small size, which sterically limits their ability to activate C-H bonds in the oxametallacycle intermediate.[335] Satsuma et al. showed a detailed investigation of a reaction mechanism of H_2-HC-SCR over subnanometer-sized Ag clusters using both experimental in situ characterizations and theoretical density functional theory (DFT) calculations. A unique size effect and an important role of Ag clusters with hydride species in oxygen activation are clarified.has paid attention to Ag NCs catalysts for green and environmental applications.[330] Finally, Thomas et al. synthesized Ag catalysts supported in Al_2O_3 by the common impregnation technique, calcined at 600 ^oC for 4 h and characterized by the NO_x-TPD method. The maximum NO_x uptake was observed at Ag surface density about 0.7 Ag/nm^2 Al_2O_3, since at this surface density maximum dispersion of Ag_2O clusters was observed.[368,369] Similarly, Kameoka et al. synthesized supported silver catalysts using the slurry method and pretreated the samples with air at 500 ^oC for 2 h. The maximum values of NO_x conversion to N_2 for the NO + O_2 + ethanol system over these supported silver catalysts were as follows: 86% (at 400 ^oC on Ag/Al_2O_3), 68% (at 450 ^oC on Al_2O_3), 18% (at 400 ^oC on Ag/TiO_2), 10% (at 400 ^oC) and 4% (at 350 ^oC on Ag/SiO_2). These results indicate that the NO_x conversion with ethanol strongly depends on the support and the presence of silver.[375]

Although the findings discussed above indicate that small Ag nanoparticles tend to have higher selectivities for specific reaction, such as epoxidation of propylene to PO, there are a number of questions that still need to be addressed. Strategies for the synthesis of size-selected metal particles are inherently complex and do not lend themselves to convenient scale-up.

One of the simplest, least expensive methods of catalyst preparation is the WI, where an oxide support is contacted for a certain time with a liquid solution containing the metal precursor. Afterwards the solid is recovered, dried and then heated in various oxidizing or reducing environments in order to reduce the metal to its catalytically active state.[349] In the majority of cases, if there are no specific interactions between the metal ions and the support, it is possible to end up with big particles. For example, in the case of Ag, limited control over the impregnation conditions leads to the formation of differently shaped (nanowires, spheres) Ag particles with low dispersion (Table 7.1). However in certain circumstances when the impregnation conditions are controlled it is possible to end up with uniform and highly dispersed metal particles. One of these examples is the “Strong Electrostatic Adsorption” (SEA).[326,327]

Every oxide support has a point of zero charge (PZC) and by definition the PZC is the pH at which the surface is neutrally charged. Considering that the support has –OH functional groups, when the pH of the solution is below its PZC, the hydroxyl groups are protonated and become positively charged, and the surface can adsorb anionic metal complexes. The same groups become deprotonated and negatively charged when the pH of the solution is above the PZC of the oxide support, and thus positively charged species can be adsorbed by the support.[328,345] To date, the electrostatic mechanism has been demonstrated mainly for noble metal complexes, including anionic tetrachloroplatinic acid (and related hydrolysis complexes) over alumina, cationic Pt tetraammines over silica.[328,329,331-333,339,345] The size of the Pt nanoparticles can vary by changing in the calcination temperature. For instance, SEA-prepared Pt on silica catalysts, using $Pt(NH_3)_4^{2+}$ as the metal precursor, had the highest dispersions (1.0) at low Pt loading (1% Pt/SiO_2) and drying in air at 100 ◦C followed by reduction in H_2 at 250 ◦C. Calcination at 150 - 400 ^oC led to partial oxidation of $Pt(NH_3)_4^{2+}$ to Pt^{4+} species, which reduce to metallic particles with a dispersion of about 0.4. Finally, calcination above 525 ◦C led to large metallic Pt particles with a dispersion of about 0.07.[333] The SEA method was also applied to cationic and anionic Pt over carbon.[334,336-338] SEA-prepared $[Pt(NH_3)_4]^{2+}$ highly loaded catalysts (20 wt.% Pt or more) over carbon reduced at 200 ^oC showed smaller average sizes (1.1 – 2.0 nm) and tighter standard deviations (about 25% of particle size) than their IW counterparts. Interestingly, the particle size range of $[PtCl_6]^{2-}$ materials over carbon prepared with SEA (reduced at 160 ^oC) and IW was roughly the same (1.5 – 2.5 nm) with similar standard deviations.[336]

The SEA method was also applied to the rational design of a Mn promoted Co catalyst for Fischer–Tropsch synthesis.[340,341] SEA allowed the selective adsorption of a Mn promoter onto the supported Co_3O_4 phase and not onto the TiO_2 support that is not achievable by IW. Thus, even with very small Mn additions, a more active and stable Co catalyst was prepared.[340] Recently, SEA was applied to the synthesis of Pt, Pd and Co ammines supported on mesoporous silica SBA-15.[339] More specifically, reduction at 350 ^oC of a 8 wt.% Pt/SBA-15 catalysts, led to an average particle size of 2.1 nm. Formation of small and homogeneous particles using SEA was observed in the case of Pd on SBA-15 samples as well. Reduction at 200 ^oC, resulted in an average Pd particle size of 1.3 nm for the 8.7 wt.% Pd/SBA-15. Cobalt particles were larger (7.3 – 9.2 nm) for 2.4 – 5.1 wt.% Co/SBA-15, because the much higher temperature required for reduction (800 ^oC) of the adsorbed cobalt ammine complex led to metal sintering. The SEA-prepared Co particles were still much smaller than the IW prepared particles (~ 50 nm) reduced at much lower temperature (450 ^oC).[339]

To the best of our knowledge, the SEA method has not been applied for the synthesis of supported Ag catalysts. The goal of this work was to evaluate the uptake of Ag diammine ($Ag(NH_3)_2^+$) over supports with low and mid-point of zero charge (PZC) (Nb_2O_5, SiO_2, Al_2O_3 and ZrO_2) and to exploit this knowledge to prepare highly dispersed monometallic Ag nanoparticles using the SEA synthesis procedure. The specific objective was to investigate how the amount of $Ag(NH_3)_2^+$ adsorbed by various supports depends on the support nature and the solution pH. STEM and XRD measurements were used to image and determine the size of the resulting supported metal nanoparticles, respectively.

7.2 Experimental

7.2.1. Reagents and materials

Commercial Nb_2O_5·(Companhia Brasileira de Metalurgia e Mineração – CBMM), ZrO_2 (Toyota), γ-Al_2O_3 (Toyota), fumed SiO_2 (Evonik) and oxidized carbon (Asbury) supports with BET surface areas of 186, 96, 167, 148 and 114 m^2/g, respectively, were used as supplied. $AgNO_3$ (99% purity, Aldrich), 1 N NH_4OH (Alfa Aesar), and 5 N NaOH (Alfa Aesar) aqueous solutions were used as received. Water purified to 18.2 MΩ·cm (Milli-Q grade) was used to prepare all aqueous solutions.

7.2.2. Point of zero charge measurements

The PZC of each oxide support was determined by the method described elsewhere.[324] In a typical measurement, appropriate amounts of each oxide support were added to aqueous solutions adjusted to different initial pH values to achieve a surface loading (the total support area per liter of solution) of 10,000 m^2/L. Solutions were allowed to stabilize for approximately 1 h and the pH was measured again. The PZC of the solid corresponds to a plateau in a plot of final pH vs the initial pH.[324] Based on these measurements, Al_2O_3 and ZrO_2 supports were found to have medium PZC values of 7.8 and 6.8, respectively, while SiO_2, Nb_2O_5 and carbon have low PZC values of 4, 3 and 4.7, respectively.

7.2.3. Preparation of $Ag(NH_3)_2NO_3$

Silver diammine nitrate ($Ag(NH_3)_2NO_3$), also known as a Tollen's reagent, was prepared according to a two-step procedure reported elsewhere.[325] More specifically, a $3.15 \cdot 10^3$ ppm $AgNO_3$ aqueous solution was initially prepared by dissolving 0.315 g of $AgNO_3$ in 100 mL of deionized water. The resulting solution was transferred to a 1 L volumetric flask and 450 μL NaOH solution (5 N) was added drop wise to the flask, leading to the formation of a brown precipitate (Ag_2O).

$$2AgNO_{3(aq)} + 2NaOH_{(aq)} \rightarrow Ag_2O_{(s)} + 2NaNO_{3(aq)} + H_2O \qquad (5)$$

The subsequent addition of 12 mL NH_4OH (1 N) to the mixture dissolves the precipitate due to the formation of $Ag(NH_3)_2NO_3$.

$$Ag_2O_{(s)} + 4NH_{3(aq)} + 2NaNO_{3(aq)} + H_2O_{(l)} \rightarrow 2Ag(NH_3)_2NO_{3(aq)} + 2NaOH_{(aq)} \qquad (6)$$

The 1 L volumetric flask was filled with deionized water to yield a 200 ppm Ag concentration in the final solution with a basic pH of 11.3. The solution was vigorously stirred during the whole preparation procedure and an amber flask was used due to the light sensitive nature of silver.

7.2.4. Speciation of Ag at different pH values

Approximately 40 mL aliquots of the stock $Ag(NH_3)_2NO_3$ solution were used to determine the nature of Ag species existing in solution at different pH values. In each case, the pH of the solution was adjusted to a desire value with 1.2 M HNO_3 or 1 M NaOH solutions, as it was appropriate, the acquired solution was stirred until no changes in pH were observed, and examined by UV-vis.

7.2.5. Adsorption measurements

The control and adsorption experiments were performed at a constant surface loading of 1000 m^2/L in the absence and presence of the silver diammine precursor, respectively. In adsorption experiments, appropriate amounts of the oxide supports were added into 40 mL aliquots of the stock $Ag(NH_3)_2NO_3$ solutions the pH of which was adjusted in the 1-13 range ($pH_{Initial}$) with 1.2 M HNO_3 or 1 M NaOH solutions, as it was appropriate. Suspensions thus formed were vigorously stirred and sampled for pH after 1 h (pH_{Final}). Then, 3-4 mL portions of these suspensions were removed, the solid was filtered, and the liquid phase was analyzed by Atomic Absorption (AA) (Perklin-Elmer

AAnalyst 400) for the Ag content. The adsorption density of Ag (Γ_{Ag}), expressed as micromoles Ag adsorbed per square meter of the support surface, was calculated as:

$$\Gamma_{\text{Ag}} = \frac{(C_{Ag,Initial} - C_{Ag,Final})(mmol/L)}{SL\ (m^2/L)} \times 10^3 = \frac{mmol}{m^2}$$

Where $C_{Ag,Initial}$ and $C_{Ag,Final}$ are initial and final concentrations of Ag in solution, respectively, and SL is the surface loading.

7.2.6. Synthesis of Ag/SiO$_2$ and Ag/C

Approximately 1 g of the SiO_2 support was mixed with an appropriate amount of a 200 ppm $Ag(NH_3)_2NO_3$ stock solution the pH of which was adjusted to 8 or 10 to yield the suspension with the surface loading of 10^3 m^2/L. The suspension was allowed to stir for 1 h before the solid was separated by filtration and dried at room temperature for 48 h. The elemental analysis of solutions before and after interaction with the support was used to determine the Ag loadings in solid materials.

0.5 g of the carbon support was mixed with 57.5 mL of 200 ppm $Ag(NH_3)_2NO_3$ solution giving a surface loading of 10^3 m^2/L. The mixture was then pH adjusted to 8, stirred for 1 h and vacuum filtered. The catalyst was dried at room temperature for 48 h. ICP was used to determine Ag weight loadings in the finished catalysts. The same procedure was used for the Ag/C catalyst at pH 13.

7.2.7. Atomic absorption spectroscopy

A Perklin Elmer (AAnalyst 400) atomic absorption spectrometer was used to quantify the concentration of Ag in solutions. Calibration standards were prepared from a 1000 ppm Ag stock solution (J. T. Baker) and the calibration curve obtained was verified with an independent second standard solution of 2 ppm Ag in 5% (v/v) HNO_3 (Ultra Scientific). All solutions were stored in amber glass volumetric flasks for light protection. Before measurements, all solutions were diluted with 5% HNO_3 to reach the 0-5 mg/L range of Ag concentrations.

7.2.8. UV-vis spectroscopy

UV-vis spectra were collected at room temperature using a Shimadzu UV-2010PC spectrophotometer and quartz cells with a path length of 10 mm. All samples were scanned in the 190–800 nm range at 0.5 nm steps. Water purified to 18.2 MΩ·cm was used as the reference for all measurements.

7.2.9. BET measurements

BET surface area measurements were performed using a ChemBET-3000 analyzer (Quantachrome Instruments). Prior to the BET measurements, all oxide supports were outgassed in He at 120 ^{o}C for 3 h. The surface area of each support was then determined using a multipoint BET method for adsorption of N_2 at −196 ^{o}C.

7.2.10. STEM measurements

STEM images were recorded using a JEOL-2100F instrument equipped with a CEOS aberration corrector on the illuminating optics and operating at 200 keV. Typically, a small quantity of each powder sample was placed on a carbon-coated 200 mesh copper grid and the sample was imaged without any further preparation. In the case of liquid samples, a drop of the solution was placed on the copper grid and dried under vacuum for approximately 10 min before imaging.

7.3 Results

7.3.1. $AgNO_3$ speciation in aqueous solution

UV–Vis absorption spectra of silver nitrate and silver diammine aqueous solutions were recorded. These spectra are very sensitive to the coordination of Ag, and the replacement of water by other ligands can be clearly distinguished. The concentration of Ag was 1500 ppm. Silver nitrate spectra showed one main absorption band (Fig. 7.1A) at 300 nm, due to interband transitions in silver (4d→5s, p).[367] Silver diammine has a weaker adsorption band around 400 nm, attributed to d-d transitions (Fig. 7.1B). Since the UV-vis spectrum of these species is very different it can be used to identify them in solution. The Ag^+ and $Ag(NH_3)_2^+$ species are in equilibrium and the formation constant of $Ag(NH_3)_2^+$ species in water at 25 ^{o}C is $K_f = 1.7 \cdot 10^7$.[376] The equilibrium can be shifted to either side by varying the solution pH (Eq.7). In order to prove that, the Ag diammine precursor solution, has pH around 11.3, was acidified and the formation of Ag species was monitored as a function of pH by obtaining UV-vis spectra of the acidified solutions (Fig. 7.1C). By acidifying the Ag diammine precursor solution to pH 9.3 and 8.3 an absorption peak at 300 nm appears, indicating the formation of Ag^+ species. At the same time, the intensity of the peak at 400 nm decreases, indicating the decomposition of the $Ag(NH_3)_2^+$ complex.

$$Ag^+_{(aq)} + 2\,NH_{3(aq)} \leftrightarrow Ag(NH_3)_2{}^+_{(aq)} \qquad \text{(Eq.7)}$$

Fig. 7.2 shows the mole fraction of Ag species as a function of the solution pH. Specifically, for pH lower to 9.3, the majority of species are the Ag^+ ones, whereas the Ag diammine species exist only in a small pH range from pH 9.5 to 12.

7.3.2. Silver diammine adsorption over SiO_2, Al_2O_3, ZrO_2, Carbon and Nb_2O_5

Fig. 7.3A shows the Ag uptake curve by SiO_2: the Ag surface density, defined as the amount of Ag per m^2 of the support, is plotted against the final pH value of the slurries after 1 h of stirring. At pHs below 6.6, there is little adsorption. A broad maximum is observed in the wide final pH range of 9.5 – 10.5 (initial pH range between 11 and 12 for silver diammine solutions). At the adsorption maximum of silver diammine by SiO_2, the uptake is about 1.6 $\mu mol/m^2$, which corresponds to a Ag loading, defined as the

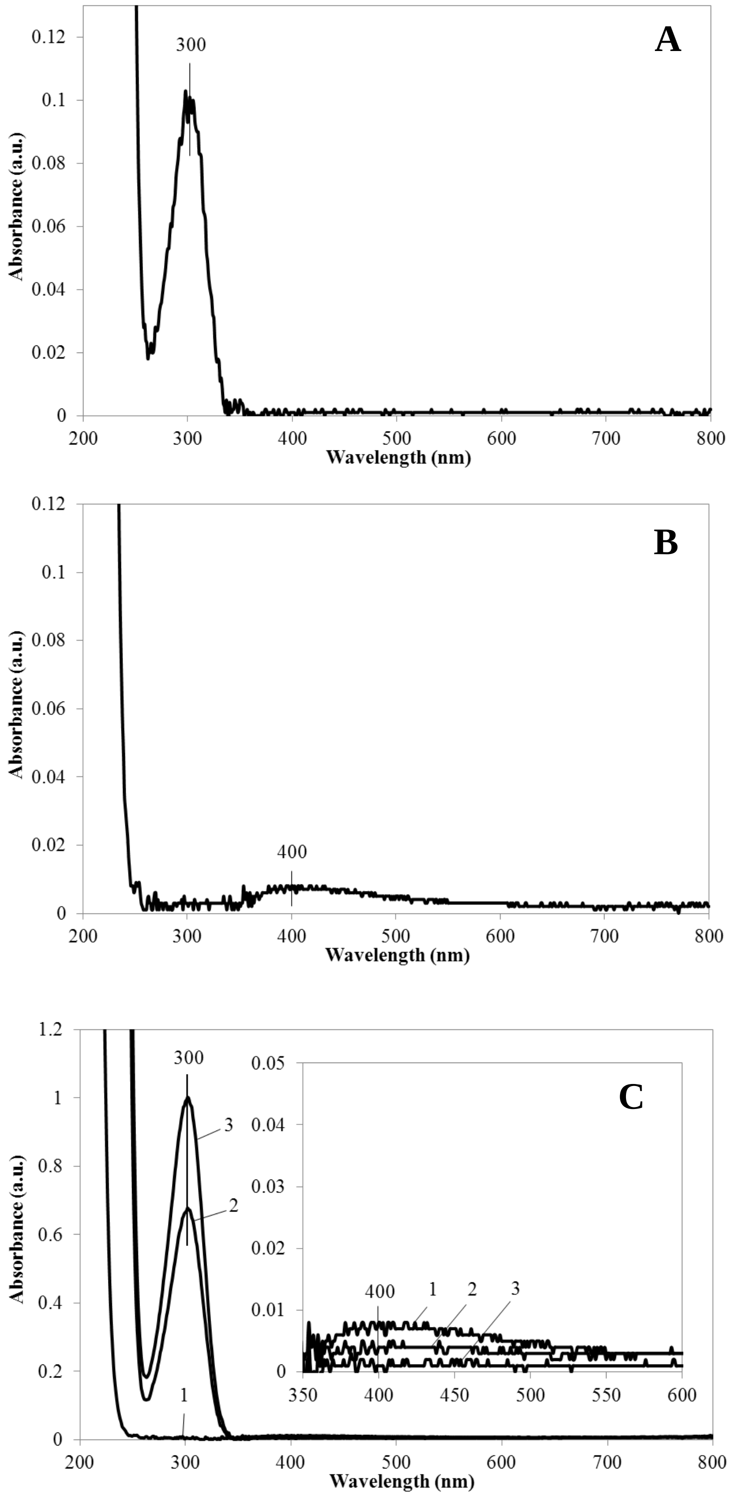

Fig.7.1 UV-vis spectra of (A) 1500 ppm $AgNO_3$ aqueous solution, (B) 1500 ppm $Ag(NH_3)_2^+$ solution and (C) acidified $Ag(NH_3)_2^+$ solution (1500 ppm), at pH (1) 11.3, (2) 9.3 and (3) 8.3.

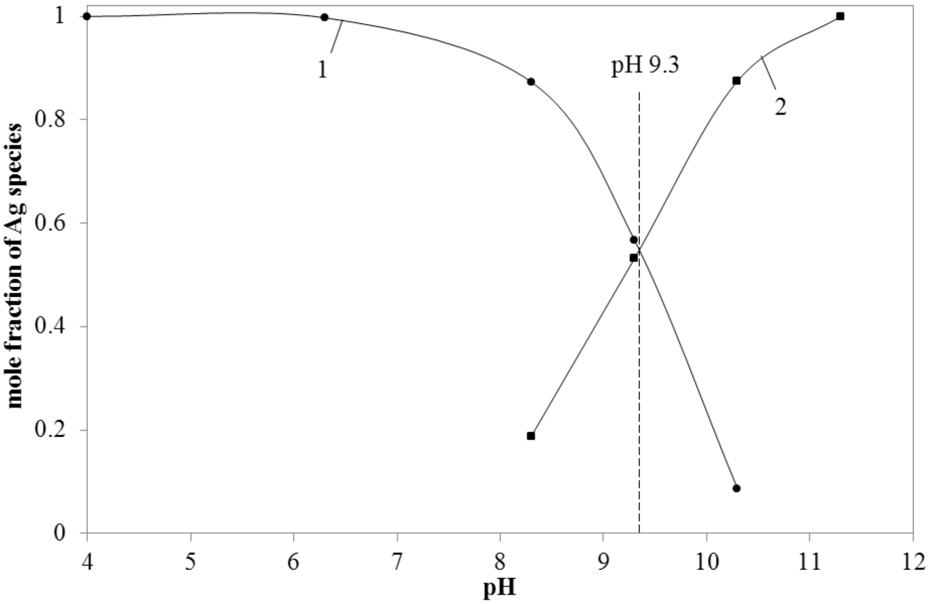

Fig.7.2 Mole fraction of Ag species (1) Ag^+ and (2) $Ag(NH_3)_2^+$ in solution as a function of the solution pH.

percentage of the Ag mass per the total mass of the catalyst, of about 2.5 wt%. This volcano- type curve has been seen previously for ammine complexes over silica.[339,363]

Fig. 7.3B-D display the adsorption curves over Al_2O_3, ZrO_2 and carbon at 1000 m^2/L, respectively. The figures of the adsorption of $Ag(NH_3)_2^+$ over Al_2O_3/ZrO_2/carbon indicate that no/weak adsorption occurs when the final pH is below the PZC of alumina, zirconia, carbon (pH_{PZC} = ~ 7.2, 6.8, 4.7 respectively). In all these cases there are two adsorption peaks, the first one at pH ~ 7.5 and the second one at pH ~ 11.5. Beyond a pH of 11.5, a decrease in adsorption is observed. The maximum uptake of $Ag(NH_3)_2^+$ by Al_2O_3, ZrO_2 and carbon is around 0.4, 0.8 and 1.9 $\mu mol \cdot m^{-2}$, respectively, defined as the percentage of the Ag mass per the total mass of the catalyst, of about 0.6, 0.8 and 0.73 wt%, respectively. One possible explanation for this behavior is the number of hydration layers that Ag diammine retains during its interaction with each one of these supports.

Fig. 7.3E contains the data of contacting 200 ppm (Fig. 7.3E1) and 1500 ppm (Fig. 7.3E2) of $Ag(NH_3)_2^+$ with 1000 m^2/L Nb_2O_5. No adsorption occurs when the final pH is below the PZC of Nb_2O_5 (~3.0). The adsorption surveys were performed at initial pH values in the range of 6-13. At the low Ag concentration, the uptake begins only past the pH_{PZC} of Nb_2O_5, and then reaches a wider plateau from pH 5 to 11.5. The maximum uptake of Ag over niobia, for solutions with initial Ag concentration 200 ppm, is 2 $\mu mol/m^2$, corresponding to full adsorption of Ag in solution. Two maxima, at around final pH 7.5 and 11.5, are observed for the higher Ag concentration. These maxima correspond to Ag uptake 14 and 12 $\mu mol/m^2$, leading to supported Ag/Nb_2O_5 catalysts, with loadings 20 and 12.5%, respectively. Compared with the rest of the oxide supports used, the pH of maximum uptake for Nb_2O_5 is much higher.

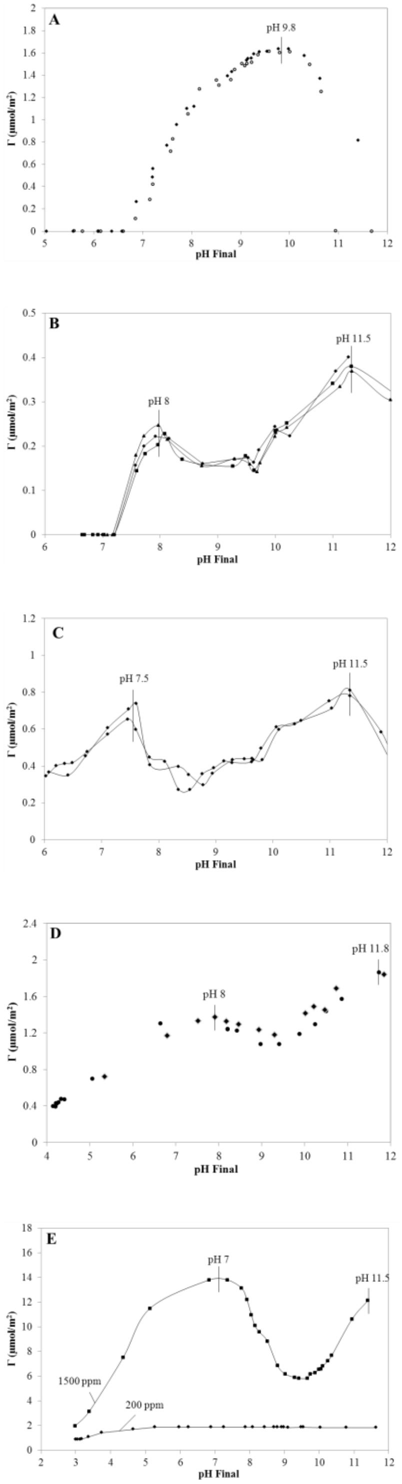

Fig. 7.3 Ag uptake over silica (A), alumina (200 ppm silver diammine) (B), zirconia (200 ppm silver diammine) (C) oxidized cardon (200 ppm silver diammine) (D) and niobia (200 ppm and 1500 ppm silver diammine) (E) versus final pH (1000 m^2/L).

7.3.3. pH shift control experiments

Fig. 7.4A display the pH shifts for silver diammine adsorption experiments at 1000 m^2/L. The pH shift curves after adsorption display similar trends as those in the metal-free control experiment. In the initial pH range of 6–10.5, the final pHs of the adsorption of Ag diammine complex over silica are slightly higher than those in the metal-free control experiment, whereas for $pH_{Initial} < 6$, the final pHs are lower than those in the control experiment. In the highly basic initial pH range of 10.5–12.5, the final pHs in the adsorption experiments of Ag diammine complexes over silica fit the data of control experiment well. Figs. 7.4B,C and E demonstrate that similar results pH shifts for silver diammine were observed over Al_2O_3 (or ZrO_2) and Nb_2O_5. Specifically, the final pHs of the adsorption experiment over Al_2O_3 (or ZrO_2) and Nb_2O_5 are higher than those of the control experiment for the initial pH range of 8.5 – 11 and 7 -11, respectively.

The final pHs of the adsorption of 200 ppm of Ag diammine complex over Nb_2O_5 are lower than the final pHs of the 1500 ppm adsorption. A number of mechanistic details can be inferred from the pH shifts of Fig. 7.4B,C and E.

7.3.4. Silver nitrate adsorption over SiO_2 and Nb_2O_5

Fig. 7.5 display uptake versus pH curves of 200 ppm $AgNO_3$ over silica and niobia, respectively. Similarly with the adsorption of $Ag(NH_3)_2^+$ by silica, at pHs below 6.6, there is little adsorption. The current data overlaps with the adsorption is $Ag(NH_3)_2^+$ by silica. pH adjustments were performed using 0.1 N NaOH and in order to prevent precipitation of Ag_2O the pH was not adjusted to values leading to pH final higher than 9.3. In the case of niobia, no adsorption occurs when the final pH is below the PZC of niobia (~ 3.0). Niobia begins to adsorb $AgNO_3$ at a pH greater than pH_{PZC} and reaches a maximum uptake for pH around 7. Beyond pH 7, the adsorption reached a wide plateau,

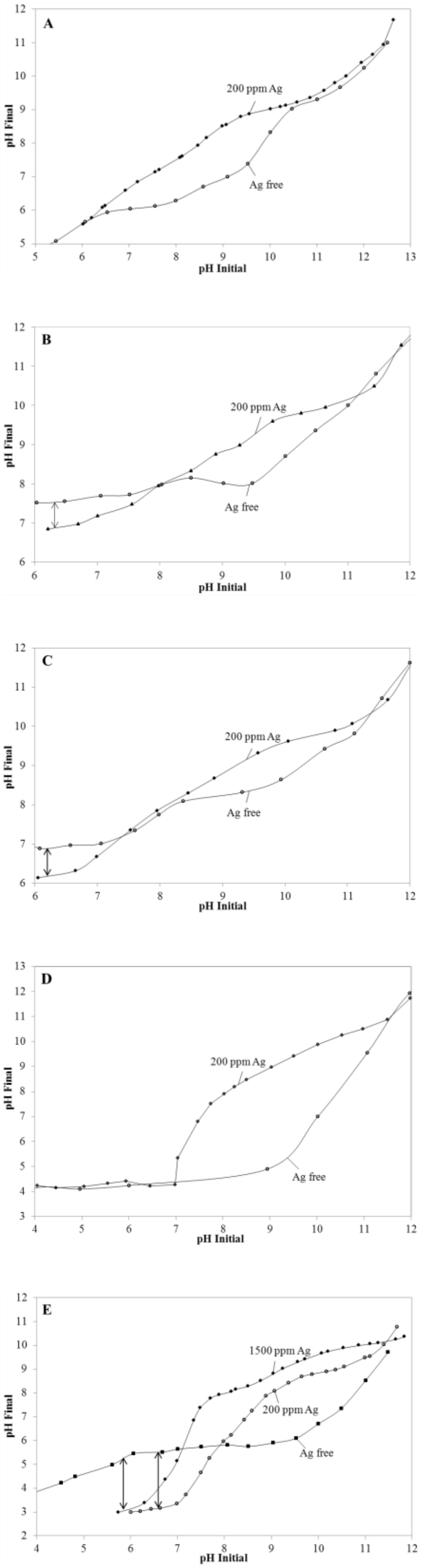

Fig. 7.4 Comparison of pH shift over silica (A), alumina (B), zirconia (C), oxidized carbon (D) with and without $Ag(NH_3)_2^+$.

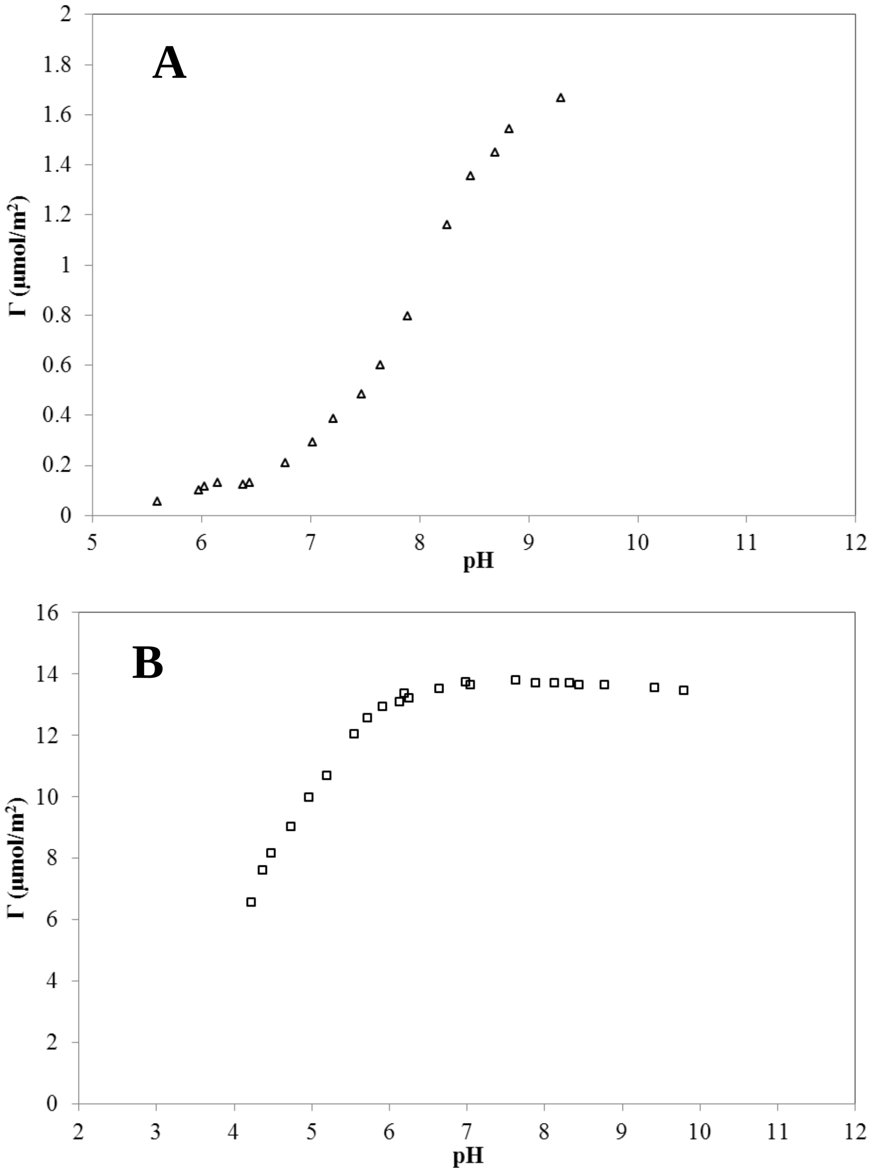

Fig. 7.5 $AgNO_3$ uptake over silica (A) and niobia (B) versus final pH (1000 m^2/L and 200 ppm silver nitrate).

most probably due to the formation of Ag_2O adsorbed on the niobia surface. Comparing the adsorption of $AgNO_3$ versus $Ag(NH_3)_2^+$ by niobia, it is worth noticing that the experimental data overlap for pH < 7.

7.3.5. Characterization of supported Ag/SiO_2 and Ag/C

Since the z contrast is satisfied only for Ag/SiO_2 and Ag/C, TEM images were collected for those materials synthesized at pH 8, 10 and 8, 13 for Ag/SiO_2 and Ag/C, respectively. Representative STEM images of SEA $Ag(NH_3)_2^+/SiO_2$ materials are shown in Fig. 7.6A and B. Interestingly, the average particle size of $Ag(NH_3)_2^+/SiO_2$ materials at pH 8 and 10 was roughly the same (~ 2 nm). Fig. 7.6 C and D show STEM images of SEA $Ag(NH_3)_2^+/C$ at pH 8 and 13, with particle size distribution 3.3 ± 1.3 and 3.5 ± 2.7 nm, respectively. The reduction temperature employed for the $Ag(NH_3)_2^+/SiO_2$ and $Ag(NH_3)_2^+/C$ samples was 60 and 100 ^oC, respectively, with heating rate of 2 $^oC/min$. There was not observed a significant change in the particle size prior and after reduction for the $Ag(NH_3)_2^+/SiO_2$ sample at pH 8 (Fig. 7.6E). On the other hand, reduction of the $Ag(NH_3)_2^+/C$ synthesized at pH 8 and 13 (Fig. 7.6 F and G) lead to the decrease of the particle size from 3.3 ± 1.3 to 2.2 ± 0.8 nm at pH 8 and from 3.5 ± 2.7 to 3.3 ± 3.5 nm at pH 13.

7.4 Discussion

7.4.1. Adsorption at high pH – electrostatic mechanism

The silver diammine complex at high pH (cationic) exhibits the features of electrostatic adsorption. The downturn in uptake at each pH extreme seen in Fig. 7.3A-C can be attributed to the decrease in adsorption equilibrium constants caused by high ionic strength.[328] This effect has been observed previously for a number of base metal anionic and cationic complexes adsorbing onto carbon.[371] The narrowness of the ‘‘volcano’’

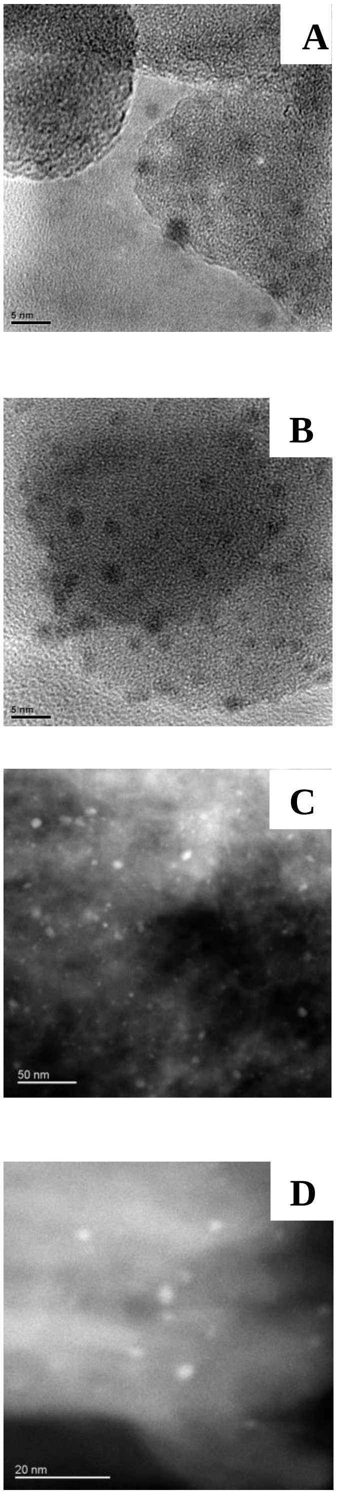

Fig. 7.6 STEM micrographs of samples: (A) 1% Ag/SiO_2 at pH = 8 (dry sample), (B) 2.4% Ag/SiO_2 at pH = 10 (dry sample), (C) 0.73% Ag/C at pH = 8 (dry sample). (D) 0.73% Ag/C at pH = 13 (dry sample).

shape at high pH may stem from the lower density of surface O groups on alumina and zirconia relative to silica (Fig. 7.3A-C). There is an optimal pH at which the electrostatic interaction appears strongest. At 1000 m^2/L for 200 ppm Ag over silica, alumina/ zirconia and carbon, this pH is about 9.8, 11.5 and 11.8, respectively, while for 1500 ppm Ag over low PZC niobia support at 1000 m^2/L, the optimal pH appears to be near 11.5. To our knowledge, this is the first report of an optimal pH at which to perform Ag cation adsorption over support of high and low PZC. Given these features we consider the uptake of silver diammine onto silica, alumina.zirconia, carbon and niobia at high pH to be an "electrostatic adsorption" mechanism, occurring on negatively charged O^- groups. Specifically, in the case of silica at pH 9.8, the negatively charged SiO_2 (PZC ~ 4), can interact electrostatically with the positively charged $Ag(NH_3)_2^+$ precursor.

$$\text{Si-O}^- + \text{Ag(NH}_3)_2^+ \leftrightarrow \text{Si-O}^- - [\text{Ag(NH}_3)_2^+]$$

Adsorption surveys over Nb_2O_5 (Fig. 7.3E), with Nb_2O_5 having a more acidic PZC ($pH_{PZC} < 3.8$) compared to SiO_2 and carbon, revealed that Nb_2O_5 had a stronger potential to attract $Ag(NH_3)_2^+$ in solution. The maximum uptake of Ag over Nb_2O_5 (14 $\mu mol/m^2$) is much greater than the one obtained for the Ag/SiO_2 and Ag/C systems (1.6 and 1.9 $\mu mol/m^2$, respectively). Such variations in the maximum uptake values might be attributed to the number of hydration sheaths retained by adsorption Ag cationic complexes. Our results suggest that over SiO_2 and carbon system, Ag complexes retain one hydration sheath, whereas Ag loses all hydration sheaths over Nb_2O_5. Moreover, Ag complexes retain two hydration sheaths when adsorbed by Al_2O_3 ($pH_{PZC} \approx 7.8$) and ZrO_2 ($pH_{PZC} \approx 6.8$), leading to maximum uptakes of 0.4 and 0.8 $\mu mol/m^2$, respectively, lower than those observed for SiO_2, carbon and Nb_2O_5.

7.4.2. Adsorption at low pH – ion exchange / electrostatic adsorption

In the present set of data, an ion exchange and electrostatic adsorption mechanism are indicated for silver diammine at low pH. The first indication is that the pH shift experiments (Fig.7.4) show a significant H^+ released into solution from the surface for pH lower than ~ 8 for alumina, zirconia and niobia. It is important to note that at low pH the Ag^+ species dominate in the solution. The ion exchange reaction is possible when the following reaction between the surface (S) hydroxyl groups and the Ag^+ species is taking place:

$$\text{S-OH} + Ag^+ \leftrightarrow \text{S-O-Ag} + H^+$$

The chemical interaction is fundamentally different from an electrostatic mechanism in which the silver diammine complexes retain its hydration sheath(s) and are above the surface as ‘‘outer-sphere’’ complexes. The chemical mechanism involves the close approach of the Ag complexes to support surface as they react with the hydroxyl groups. In this interaction, the hydration sheath would be lost, allowing a higher density of complexes to adsorb.[336] This can explain the higher adsorption density observed over niobia (up to about 14 μmol/m^2 in Fig. 7.3E) when compared to the adsorption maximum of 12 μmol/m^2 observed over niobia at pH 11.5. In the case of silica, carbon and niobia (Fig. 7.3A,D and E) the first adsorption maximum appears for pH higher than the PZC of the supports, indicating that the surface is negatively charged and can still interact electrostatically with the Ag^+ species in the solution. Fig. 7.3B and C show that the first adsorption maximum of alumina and zirconia appear at pH close to the PZC of these supports (around 8), indicating that the surface is neutrally charged and the predominate Ag^+-surface mechanism is the ion exchange. We believe that ion exchange and electrostatic adsorption mechanisms act in parallel, with ion exchange predominating when the adsorption maximum exists around the pH_{PZC} of the surface.

The most intriguing claim of an ion exchange mechanism is proffered in the work of Amine et al. [372] who show a correlation of PTA uptake with carboxylic acid groups over a number of oxidized carbons (Denka Black, Vulcan XC72, and BP 2000). They observed a rapid decrease in solution pH, by the release of proton from the surface of carbon black during the exchange with Pt ions, accompanied with a significant uptake of Pt. Similarly to the Amine et al. work, in the present work, there is a release of protons from the support to the solution for pH lower than 6, 8, 7.5 and 8, for silica, alumina, zirconia and niobia, respectively (Fig. 7.4A-C and E). We believe that the release of protons is caused by the ion exchange reaction between the support and the Ag species.

If the adsorption mechanism of silver species over alumina, zirconia and niobia at low pH is ion exchange, then the uptake should be expected to occur at the pH of the PZC of those supports, because the surface is neutral, and the hydroxyl groups dominate alumina, zirconia and niobia surface species. But Fig. 7.3B,C and E show that Ag^+ adsorption adsorption occurs in our experiments when the final pH equals the PZC of alumina and zirconia (around 7.8 and 6.8, respectively), but not with niobia. At high pH ranges, the surface hydroxyl groups become deprotonated, and the number of OH groups decreases accordingly, inhibiting ion exchange. Furthermore, ion exchange predicts that Ag^+ species will deposit over the hydroxyl groups at alumina, zirconia and niobia 1:1 stoichiometry. In our experiment, the maximum Ag uptake over alumina is about 0.24 $\mu mol/m^2$ at a final pH of 8 (initial pH 8). If the entire uptake were caused by ion exchange, then the protons released to the bulk solution should decrease the pH from an initial value of 8 to a final value of 5.2. Similarly with alumina, in the case of zirconia and niobia , if the entire uptake was caused by ion exchange, the H^+ released should decrease the pH from an initial value of 7.5 and 8.5 to 4.7 and 3.6 for zirconia and niobia, respectively. These results are leading us to the same conclusion as previously, that the ion exchange and electrostatic adsorption mechanisms act in parallel at low pH.

7.4.3. Proton transfer to and from the oxide surface

A number of mechanistic details can be inferred from the pH shifts of Fig. 7.4. First, silica in Fig. 7.4A show an ability to give protons in the whole pH range investigated, higher than the PZC of silica (deviation from diagonal in the whole pH range). Alumina, zirconia and niobia, on the other hand, in Fig. 7.4B,C and E show relatively much greater capacity to adsorb protons below the PZC (deviation from the diagonal in the left-hand side of the plot) than the capacity to give protons up above the PZC (deviation from the diagonal on the right side of the plot). In fact, silica has almost full proton-donating capacity. Unlike the amphoteric surface –OH groups on alumina, zirconia and niobia, which can both be protonated at low pH to form $–OH_2^+$, exist as –OH at the PZC, and deprotonate to $–O^-$ above the PZC, the proton transferring functional groups on silica are best characterized as proton-donating, O^-.

Second, the pH plateau for alumina and zirconia is over one and a half pH unit wider than that for niobia at the same surface loading (1,000 m^2/L). This indicates that the surface density of protonizable surface groups on niobia is much less, than that of the alumina and zirconia. These data appear consistent with experimental determinations; the –OH density for alumina, zirconia and niobia are typically cited at around 8,[328] 15,[373] and 12 OH/nm^2,[374] respectively. The smaller density of protonated groups at the alumina can explain the relatively narrow breadth of the pH uptake volcano plots of Fig. 7.3B relative to its width over niobia (Fig. 7.3E).

From pH 6 – 11, 8 - 11.5, 7.5 - 11.5 and 7 - 11.5, for silica, alumina, zirconia and niobia (Fig. 7.4A-C,E) protons are released from the solution to the support. For pH lower than 6, 8, 7.5 and 7, for silica, alumina, zirconia and niobia, respectively, protons are released from the support to the solution and they are being consumed in formation of NH_4^+ from released NH_3 ligands.

7.4.4. Adsorption of $AgNO_3$ over SiO_2 and Nb_2O_5

Fig. 7.5 displays the adsorption curves of $AgNO_3$ over silica (Fig. 7.5A) and niobia (Fig. 7.5B) at 1000 m^2/L. The adsorption of Ag^+ over silica and niobia indicate that no adsorption occurs when the final pH is below the PZC of these supports *(*pH_{PZC} ~4, 3 for silica and niobia, respectively). Silica adsorbs the Ag^+ species at pHs greater than pH_{PZC} and reaches a maximum uptake at a pH of around 9.5. At higher pH, adsorption is retarded by the effect of high ionic strength, which effectively diminishes the value of the adsorption equilibrium constant.[332] The same uptake tendency can be observed in the adsorption experiments of Ag species over alumina and zirconia. Similarly with silica, the maximum adsorption of the Ag^+ species by niobia is observed at pH ~ 7 (Fig. 7.5B). Interestingly, the adsorption reaches a plateau at pH ~ 7 and it remains constant until final pH 10. We believe that the presence of a plateau is attributed to the formation of Ag_2O species in the solution that are absorbed by the niobia surface. It is noteworthy that the adsorption curves of Ag^+ by silica and niobia, follow exactly the same patent as the adsorption curves of $Ag(NH_3)_2^+$ by silica and niobia, respectively. This result is another indication that the first adsorption peak in the case of silica and niobia can be attributed to electrostatic adsorption of Ag^+ species by the deptotonated surface. Although, we haven’t performed similar experiments for the rest of the supports (alumina, zirconia and carbon), we believe that similar adsorption curves would have been observed for these supports as well.

7.4.5. Ag Particle Synthesis

In the present study, Ag/SiO_2 and Ag/carbon catalysts synthesized at a low and high pH with the use of $Ag(NH_3)_2^+$ precursor by the SEA lead to very small Ag particles (2 – 3.5 nm). The Ag particle size at low/high pH gave very similar results leading us to the conclusion that the electrostatic adsorption mechanism (high pH) and the combination of ion exchange and electrostatic adsorption mechanism (low pH) lead to the formation of similarly sized Ag supported particles. Indeed, the Ag particle sizes for 1% Ag/SiO_2 at pH 8 (Fig. 7.6A) and 2.4% Ag/SiO_2 at pH 10 (Fig. 7.6B) is in both cases as small as 2 nm, whereas for the 0.73% Ag/C at pH 8 (Fig. 7.6C) and 0.73% Ag/C at pH 13 (Fig. 7.6D) sample the Ag particle size obtained was 3.3±1.3 and 3.5±2.7 nm, respectively. To the best of our knowledge, the SEA method provides the best solution for obtaining very small Ag particles on both silica and carbon.

7.5 Conclusions

Strong electrostatic adsorption of Ag onto low (silica, carbon and niobia) and high PZC (alumina and zirconia) supports can be used with silver diammine to achieve formation of small and high dispersion Ag particles with a simple reduction in hydrogen. The adsorption of silver diammine is taking place through two different mechanism depending on the pH of the solution. The interaction of silver diammine with low/high PZC surfaces at a high pH ($Ag(NH_3)_2^+$) appears to be wholly electrostatic in nature, whereas at low pH (Ag^+) the interaction appears to be a combination of electrostatic adsorption and ion exchange, depending on whether the adsorption pH is close to the PZC of the surface or not. Indication of the ion exchange mechanism at low pH is the fact that there is a significant H^+ released into solution from the surface for pH lower than 6, 8, 7.5 and 7, for silica, alumina, zirconia and niobia, respectively, and they are being consumed in formation of NH_4^+ from released NH_3 ligands. The Ag diammine species exist only in a small pH range from pH 9.5 to 12, whereas for pH lower to 9.3, the majority of species are the Ag^+ ones. Moreover, the adsorption curved of Ag^+ and $Ag(NH_3)_2^+$ over silica and niobia overlap, indicating that at low pH the is an electrostatic adsorption/ion exchanged taking place between the Ag^+ species and the oxide supports examined.

The adsorption of the Ag species by silica leads to a broad maximum for final pH 9.5 – 10.5. At uptake of Ag at this adsorption maximum is about 1.6 μmol/m^2, corresponding to a Ag loading of about 2.5 wt%. The adsorption of Ag species over Al_2O_3/ZrO_2/carbon goes through two adsorption peaks, at pH ~ 7.5 and 11.5. The maximum uptake of $Ag(NH_3)_2^+$ by Al_2O_3, ZrO_2 and carbon is around 0.4, 0.8 and 1.9 μmol·m^{-2}, respectively. The low adsorption of alumina can be explained by the fact that the first adsorption peak appears to be very close to the PZC of alumina. Similarly to our results, it has been shown that alumina adsorbs CPA (1.6 μmol·m^{-2}) and PTA (0.4 μmol·m^{-2}) at low and high pH, respectively, showing that the adsorption decreases when the final pH approached the PZC of alumina, in this case 8.44.[377] Compared to all the supports used in this study, Nb2O5 had a stronger potential to attract Ag species in solution. The 200 ppm initial concentration of Ag used in the case of niobia was fully adsorbed. Two maxima, at around final pH 7.5 and 11.5, are observed for the higher Ag concentration (1500 ppm). These maxima correspond to Ag uptake 14 and 12 μmol/m^2 much higher compared to the other supports, leading to supported Ag/Nb_2O_5 catalysts, with loadings 20 and 12.5%, respectively. Such variations in the maximum uptake values might be attributed to the number of hydration sheaths retained by adsorption Ag cationic complexes. Over SiO_2 and carbon, Ag complexes retain one hydration sheath, whereas Ag loses all hydration sheaths over Nb_2O_5. Moreover, Ag complexes retain two hydration sheaths when adsorbed by Al_2O_3 and ZrO_2.

Interestingly, the average particle size of $Ag(NH_3)_2^+/SiO_2$ materials at pH 8 and 10 was roughly the same (~ 2 nm). STEM images of SEA $Ag(NH_3)_2^+/C$ at pH 8 and 13, with particle size distribution 3.3 ± 1.3 and 3.5 ± 2.7 nm, respectively.

7.6 Acknowledgements

The authors gratefully acknowledge Toyota Motor Engineering & Manufacturing North America, Inc. for the partial financial support of this work. The authors further acknowledge Dr. Douglas Blom at the Electron Microscopy Center of the University of South Carolina for his assistance during collection of the STEM images.

REFERENCES

1. Astruc, D., Lu, F., Aranzaes, R. *Angew. Chem. Int. Ed.* 44, 7852-7872 (2005)
2. Zhang, H., Han, J., Yang, B. Adv. Funct. Mater. 20, 1533-1550 (2010)
3. Preston, T. C., Nuruzzaman, M., Jones, N. D., Mittler, S. *J. Phys. Chem. C* 113, 14236-14244 (2009)
4. Gröhn, F. Soft Matter 6, 4296-4302 (2010)
5. Anderson, T. H., Donaldson, S. H., Zeng, H., Israelachvilli, J. N. Langmuir 26, 14458-14465 (2010)
6. Shiraishi, Y., Arakawa, D., Toshima, N. Eur. Phys. J. E 8, 377-383 (2002)
7. Deutsch, D. S., Williams, C. T., Amiridis, M. D. *Catalyst Preparation* Chapter 9, 209-305 (2007)
8. Huang, H., Ruckenstein, E. J. Colloid and Interface Science 275, 548-554 (2004)
9. Vidal, F., Guillot, J., Guyot, A. Polym. Adv. Technol. 6, 473-479 (1995)
10. Toshima, N. Macromol. Symp. 270, 27-39 (2008)
11. Ott, L. S., Hornstein, B. J., Finke, R. G. *Langmuir* 22, 9357-9367 (2006)
12. Somorjai, G. A., Park, J. Y. *Top. Catal.* 49, 126-135 (2008)
13. Knapp, R., Wyrzgol, S. A., Reichelt, M., Hammer, T., Morgner, H., Müller, T. E., Lercher, J. A. J. Phys. Chem. C 114, 13722-13729 (2010)
14. Wiley, B., Sun, Y., Xia, Y. *Acc. Chem. Res.* 40, 1067-1076 (2007)
15. Ueji, M., Harada, M., Kimura, Y. J. Colloid Inter. Science 322, 358-363 (2008)
16. Joo, A. H., Park, J. Y., Renzas, J. R., Butcher, D. R., Huang, W., Somorjai, G. A. *Nano Lett.* 10, 2709-2713 (2010)

17. Borodko, Y., Lee, H. S., Joo, S. H., Zhang, Y., Somorjai, G. A. *J. Phys. Chem. C* 114, 1117-1126 (2010)
18. Li, D., He, Q., Cui, Y., Li, J. *Chem. Mater.* 19, 412-417 (2007)
19. Choi, S.-H., Lee, S., Kim, S.-J., Sohn, S.-H., Kang, H.-D., Zhang, Y.-P., Lee, K.-P., Chun, J.-H. Catalysis Letters 105, 59 (2005)
20. Toshima, N., Kanemaru, M., Shiraishi, Y., Koga, Y. *J. Phys. Chem. B* 109, 16326-16331 (2005)
21. Hirakawa, K., Toshima, N. *Chemistry Letters* 32(1), 78-79 (2003)
22. Lo, S. H. Y., Wang, Y-Y., Wan, C-C. *J. Colloid Inter. Science* 310, 190-195 (2007)
23. Park, J. Y., Zhang, Y., Grass, M., Zhang, T., Somorjai, G. A. *Nano Lett.* 8(2), 673-677 (2008)
24. Gao, J., Ren, X., Chen, D., Tang, F., Ren, J. Scripta Materialia 57, 687-690 (2007)
25. Gao, L., Fan, L., Zhang, J., Langmuir 25(19), 11844-11848 (2009)
26. Hirai, H., Yakura, N. Polym. Adv. Technol. 12, 724-733 (2001)
27. Dash, P., Dehm, N. A., Scott, R. W. J. J. Molec. Catal. A: Chem. 286, 114-119 (2008)
28. Metin, O., Ozkar, S. J. Molecular Catal. A: Chemical 295, 39-46 (2008)
29. Krisztian, N.;,Grass, M., Somorjai, G. A. *Nano Lett.* 5(11), 2238-2240 (2005)
30. Nash, M. A., Lai, J. J., Hoffman, A. S., Yager, P., Stayton, P. S. Nano Lett. 10, 85-91 (2010)
31. Adeli, lM., Haag, R. J. Polym. Science: Part A: Polym. Chem. 44, 5740-5749 (2006)
32. Feng, B., Yang, H., Wang, X., Hu, Y., Li, H., Giao, Y., Zhao, X., Huang, Q. Langmuir 26(4), 2505-2513 (2010)
33. Siani, A., Wigal, K. R., Alexeev, O. S., Amiridis, M. D. J. Catal. 257, 5-15 (2008)
34. Wang, D., An, J., Luo, Q., Li, X., Li, M. J. App. Polymer Science 110, 3038-3046 (2008)
35. Wu, J., Zhang, X., Yao, T., Zhang, H., Yang, B. Langmuir 26(11), 8751-8755 (2010)
36. Mukherjee, P., Nandi, A. K. Langmuir 26(4), 2785-2790 (2010)

37. Gladitz, M., Reinemann, S., Radusch, H.-J. Macromol. Mater. Eng. 294, 178-189 (2009)
38. Li, S., Wu, Y., Wang, J., Zhang, Q., Kou, Y., Zahng, S. J. Mater. Chem. 20, 4379-4384 (2010)
39. Murugadoss, A., Chattopadhyay, A. Nanotechnology 19, 1-9 (2008)
40. Zhang, Y., Zhang, H., Zhang, Y., Ma, Y., Zhong, H., Ma, H. Chem. Commun. 6589-6591 (2009)
41. Irfan, M., Seiler, M. Ind. Eng. Chem. Res. 49, 1169-1196 (2010)
42. Peng, X., Pan, Q., Rempel, G. L. Chen. Soc. Rev. 37, 1619-1628 (2008)
43. Crooks, R. M., Zhao, M., Sun, L., Chechik, V., Yeung, L. K. Acc. Chem. Res. 34, 181-190 (2001)
44. Diallo, M. S. Nanotechnology Applications for Clean Water Chapter 11, 143-155 (2009)
45. Chandler, B. D., Lee, J.-K., Kung, H. H., Kung, M. C. Design of Heterogeneous Catalysts Chapter 3, 59-81 (2009)
46. Gitsov, I., Lin, C. Curr. Org. Chem. 9, 1025-1051 (2005)
47. Twyman, L. J., King, A. S. H., Martin, I. K. Chem. Soc. Rev. 31, 69-82 (2002)
48. Tomalia, D. A. Prog. Poly. Sci. 30, 294-324 (2005)
49. Zhang, W.; Li, L.; Wang, X.; Yang, P. Catal. Lett. 127, 429-436 (2009)
50. Murugan, E., Rangasamy, R. J. Polymer Science: Part A: Polymer Chemistry 48, 2525-2532 (2010)
51. Larpent, C., Cannizzo, C., Delgado, A., Gouanve, F., Sanghvi, P., Gaillard, C., Bacquet, G. Small 4(6), 833-840 (2008)
52. Esumi, K., Top Curr. Chem. 227, 31-52 (2003)
53. Ege, S. Organic Chemistry, 3rd Edition, 1994
54. Somorjai, G. A., Park, J. Y. *Chem. Soc. Rev.* 37, 2155-2162 (2008)
55. Crooks, R. M., Lemon, B. I., Sun, L., Yeung, L. K., Zhao, M. Topics *in Current Chemistry* 212, 91-135 (2001)
56. Chandler, B. D., Gilbertson, J. D. *Nanoparticles and Catalysis* Chapter 4, 129-160 (2008)

57. Woodward, P., Rannard, S., Hayes, W. *Handbook of Industrial Water Soluble Polymers* Chapter 8, 239-267 (2007)
58. Boas, U., Heegaard, M. H. Chem. Soc. Rev. 33, 43-63 (2004)
59. 60. Scott, R. W. J., Wilson, O. M., Crooks, R. M. *J. Phys. Chem. B* 109, 692-704 (2005)
60. Manna, A., Imae, T., Aoi, K., Okada, M., Yogo, T. *Chem. Mater.* 13, 1674-1681 (2001)
61. Chandler, B. D., Gilbertson, J. D. *Top. Organomet. Chem.* 20, 97-120 (2006)
62. Pearson, R. G. Chem. in Britain 2, 103-107 (1966)
63. Martell and Hancock, (1996) Metal Complexes in Aqueous Solutions; Plenum Press: New York
64. Diallo, M. S., inventor; 2006 Feb. 2. Water Treatment by dendrimer enhanced filtration. United Stated Patent US 0021938
65. Rothenberg (2008) Catalysis: Concepts and Green Applications; WILEY-VCH Verlag GmbH & Co. KGaA: Weiheim
66. Zhao, M., Sun, L., Crooks, R. M. *J. Am. Chem. Soc.* 120, 4877-4878 (1998)
67. Balogh, L., Tomalia, D. A. *J. Am. Chem. Soc.* 120, 7355-7356 (1998)
68. Pellechai, P. J., Gao, J., Gu, Y., Ploehn, H. J., Murphy, C. J. *Inorg. Chem.* 43, 1421-1428 (2004)
69. Siani, A., Alexeev, O. S., Deutsch, D. S., Monnier, J. R., Fanson, P. T., Hirata, H., Matsumoto, S., Williams, C. T., Amiridis, M. D. *J. Catal.* 266, 331-342 (2009)
70. Štofik, M., Strýhal, Z., Malý, *J. Biosensors and Bioelectronics* 24, 1918-1923 (2009)
71. Herrero, M. A., Guerra, J., Myers, V. S., Gómez, M. V., Crooks, R. M., Prato, M. *ACS Nano* 4(2), 905-912 (2010)
72. Shen, M., Sun, K., Shi, X. *Current Nanoscience* 6, 307-314 (2010)
73. Zhang, Y., Peng, H., Huang, W., Zhou, Y., Yan, D. *J. Colloid and Interface Science* 325, 371-376 (2008)
74. Carino, E. V., Knecht, M. R., Crooks, R. M. *Langmuir* 25, 10279 (2009)
75. Kumar, P. A., Ha, H. P. Catal. Lett. 136, 177-184 (2010)

76. López-De Jesús, Y. M., Vicente, A., Lafaye, G., Marécot, P., Williams, C. T. *J. Phys. Chem. C* 112, 13837-13845 (2008)
77. Zhao, M., Crooks, R. M. *Chem. Mater.* 11, 3379-3385 (1999)
78. Bányai, I., Országh, I., Berka, M., Balogh, L. P. *Polymer Preprints* 46(2), 519-520 (2005)
79. Sharma, V. K., Yngard, R. A., Lin, Y. *Advances in Colloid and Interface Science* 145, 83-96 (2009)
80. Liz-Marzán, M. L. *Mater. Today* 7(2), 26-31 (2004)
81. Eremenko, A. M., Smirnova, N. P., Mukha, I. P., Yashan, H. R. *Theroretical and Experimental Chemistry* 46(2), 65-88 (2010)
82. Creighton, J. A., Eadon, D. G. *J. Chem. Soc. Faraday Trans.* 87, 3881 (1991)
83. Kelly, K. L., Coronado, E., Xhao, L. L., Schatz, G. C. J. Phys. Chem. B 107, 668-677 (2003)
84. Zhao, M., Crooks, R. M. *Angew. Chem. Int. Ed.* 38, 364-366 (1999)
85. Scott, R. W. J., Ye, H., Henriquez, R. R., Crooks, R. M. Chem. Mater. 15, 3873-3878 (2003)
86. Zhao, M., Crooks, R. M. Advanced Materials 11, 217-219 (1999)
87. Huang, W., Kuhn, J. N., Tsung, C.-K., Zhang, Y., Habas, S. E., Yang, P., Somorjai, G. A. Nano Letters 8(7), 2027-2034 (2008)
88. Lafaye, G., Williams, C. T., Amiridis, M. D. Catalysis Letters 96(1-2), 43-47 (2004)
89. Knecht, M. R., Weir, M. G., Myers, V. S., Pyrz, W. D., Ye, H., Petkov, V., Buttrey, D. J., Frenkel, A. I., Crooks, R. M. *Chem. Mater.* 20, 5218-5228 (2008)
90. Gu, Y., Sanders, P., Ploehn, H. J. *Colloid and Surfaces A: Physicochem. Eng. Aspects* 356, 10-15 (2010)
91. Niu, Y., Crooks, R. M. *C. R. Chimie* 6, 1049-1059 (2003)
92. Jin, L., Yang, S.-P., Tian, Q.-W., Wu, H.-X., Cai, Y.-J. *Materials Chemistry and Physics* 112, 977-983 (2008)
93. Wan, H., Li, S., Konovalova, T. A., Shuler, S. F., Dixon, D. A., Street, S. C. *J. Phys. Chem. C* 112, 1335-1344 (2008)
94. Tran, M. L., Gahan, L. R., Gentle, I. R. *J. Phys. Chem. B* 108, 20130-20136 (2004)

95. Tarazona-Vasquez, F., Balbuena, P. B. *J. Phys. Chem. B* 108, 15992-16001 (2004)
96. Tarazona-Vasquez, F., Balbuena, P. B. *J. Phys. Chem. B* 109, 12480-12490 (2005)
97. Diallo, M. S., Christie, S., Swaminathan, P., Johnson, Jr. J. H., Goddard III, W. A. *Environ. Sci. Technol.* 39(5), 1366-1377 (2005)
98. Zhou, L., Russell, D. H., Zhao, M., Crooks, R. M. *Macromolecules* 34, 3567 (2001)
99. Bond, G. C., Thompson, D. T. *Catal. Rev. Sci. Eng.* 41, 319-388 (1999)
100. Gao, J. Ph.D. Thesis, University of South Carolina, Colubia, SC (2005)
101. Gupta, U., Agashe, H. B., Asthana, A., Jain, N. K. Macromolecules 7(3), 649-658 (2006)
102. Koper, G. J. M., Borkovec, M. *Polymer* 51, 5649-5662 (2010)
103. Borkovec, M., Koper, G. J. M., Piguet, C. *Current Opinion in Colloid & Interface Science* 11, 280-289 (2006)
104. Unal, B., Hedden, R. C. *Polymer* 50, 905-912 (2009)
105. Chen, W., Tomalia, D. A., Thomas, J. L. *Macromolecules* 33, 9169-9172 (2000)
106. Kabanov, V. A., Zizin, A. B., Rogacheva, V. B., Gulyaeva, Z. G., Zansochova, M. F., Joosten, J. G. H., Brackman, J. Macromolecules 31, 5142-5144 (1998)
107. Cakara, D., Kleimann, J., Borkovec, M. *Macromolecules* 36, 4201-4207 (2003)
108. Niu, Y., Sun, L., Crooks, R. M. Macromolecules 36, 5725-5731 (2003)
109. Liu, Y., Porcar, L., Hong, K., Shew, C-Y., Li, X., Liu, E., Butler, P. D., Herwig, K. W., Smith, G. S., Chen, W-R. *J. Chem. Phys.* 132, 124901 (2010)
110. Porcar, L., Hong, K., Butler, P. D., Herwig, K. W., Smith, G. S., Liu, Y., Chen, W-R. *J. Phys. Chem. B* 114, 1751-1756 (2010)
111. Maiti, P. K., Bagchi, B. *J. Chem. Phys.* 131, 214901 (2009)
112. Huißmann, S., Wynveen, A., Nikos, C. N., Blaak, B. J. Phys.: Condens. Matter. 22, 232101 (2010)
113. Betley, T. A., Holl, M. M. B., Orr, B. G., Swanson, D. R., Tomalia, D. A., Baker, J. R. *Langmuir* 17, 2768-2773 (2001)
114. Liu, Y., Bryantsev, V. S., Diallo, M. S., Goddard, W. A. *J. Am. Chem. Soc.* 131, 2798-2799 (2009)
115. Ottaviani, M. F., Bossmann, S., Turro, N. J., Tomalia, D. A. *J. Am. Chem. Soc.* 116, 661-671 (1994)

116. Ottaviani, M. F., Montalti, F., Turro, N. J., Tomalia, D. A. J. Phys. Chem. B 101, 158-166 (1997)
117. Wales, C. H., Berger, J., Blass, S., Crooks, R. M., Asherie, N. Langmuir 27, 4104-4109 (2011)
118. Sardar, R., Bjorge, N. S., Shumaker-Parry, J. S. Macromolecules 41, 4347-4352 (2008)
119. Tanis, I., Karatasos, K. Phys. Chem. Chem. Phys. 11, 10017-10028 (2009)
120. Lesniak, W., Bielinska, A. U., Sun, K., Janczak, K. W., Shi, X., Baker Jr., J. R., Balogh, L. P. Nano Letters 5(11), 2123-2130 (2005)
121. Diallo, M. S., Balogh, L., Shafagati, A., Johnson, Jr., J. H., Goddard III, W. A., Tomalia, D. A. Environmental Science & Technology 33(5), 820-824 (1999)
122. Rether, A., Schuster, M. Reactive & Functional Polymers 57, 13 (2003)
123. Alexeev, O. S., Siani, A., Lafaye, G., Williams, C. T., Ploehn, H. J., Amiridis, M. D. *J. Phys. Chem. B* 110, 24903-24914 (2006)
124. Floriano, P. N., Noble IV, C. O., Schoonmaker, J. M., Poliakoff, E. D., McCarley, R. L. *J. Am. Chem. Soc.* 123, 10545-10553 (2001)
125. Li, G., Luo, Y., Tan, H. J. Solid State Chemistry 178, 1038-1043 (2005)
126. Nagy, A., Mestl, G. Applied Catalysis A: General 188, 337-353 (1999)
127. “The Silver Institute” (http://www.silverinstitute.org/supply_demand.php#demand)
128. Martínez-Ctastañón, G. A., Niño- Martínez, N., Loyola-Rodríquez, J. P., Patiño-Marín, N. Materials Letters 63, 1266-1268 (2009)
129. Khan, Z., Al-Thabaiti, S. A., El-Mossalamy, E. H., Obaid, A. Y. *Colloids and Surfaces B: Biointerfaces* 73, 284-288 (2009)
130. Zeng, H., Zhao, C., Qiu, J., Yang, Y., Chen, G. *J. Crystal Growth* 300, 519-522 (2007)
131. He, R., Qian, X., Yin, J., Zhu, Z. *Chemical Physics Letters* 369, 454-458 (2003)
132. Marambio-Jones, C., Hoek, E. M. V. *J. Nanopart. Res.* 12, 1531-1551 (2010)
133. Guingab, J. D., Lauly, B., Smith, B. W., Omenetto, N., Winefordner, J. D. Talanta 74, 271-274 (2007)
134. Berthod, A., Laserna, J. J., Winefordner, J. D. *Applied Spectroscopy* 7, 1137-1141 (1987)

135. Panáček, A., Kvítek, L., Prucek, R., Kolář, M., Večeřová, R., Pizúrová, N., Sharma, V. K., Nevěčná, T., Zbořil, R. *J. Phys. Chem. B* 110, 16248-16253 (2006)
136. Sardar, R., Park, J.-W., Shumaker-Parry, J. S. *Langmuir* 23, 11883-11889 (2007)
137. Popa, M., Pradell, T., Crespo, D., Calderon-Moreno, J. M. *Colloids and Surfaces A: Physicochem. Eng. Aspects* 303, 184-190 (2007)
138. Shin, H. S., Yang, H. J., Kim, S. B., Lee, M. S. *J. Colloid and Interface Science* 274, 89-94 (2004)
139. Chou, K.-S., Ren, C.-Y. *Materials Chemistry and Physics* 64, 241-246 (2000)
140. Patakfalvi, R., Virányi, Z., Dékány, I. *Colloid Polym. Sci.* 283, 299-305 (2004)
141. Jiang, L.-P., Wang, A.-N., Zhao, Y., Zhang, J.-R., Zhu, J.-J. *Inorganic Chemistry Communications* 7, 506-509 (2004)
142. Pastoriza-Santos, I., Liz-Marzán, L. *Langmuir* 18, 2888-2894 (2002)
143. Bao, C., Jin, M., Lu, R., Zhang, T., Zhao, Y. Y. *Materials Chemistry and Physics* 81, 160-165 (2003)
144. Peng, Z., Zhang, J., Sun, X., Yang, J., Diao, *J. Colloid Polym. Sci.* 287, 609-614 (2009)
145. Sutton, A., Franc, G., Kakkar, A. *J. Polymer Science: Part A: Polymer Chemistry* 47, 4482-4493 (2009)
146. Luo, Y., Sun, X. *Materials Letters* 61, 1622-1624 (2007)
147. Sun, X., Dong, S., Wang, E. *Macromolecules* 37, 7105-7108 (2004)
148. Guoping, L., Yunjun, L., Wenting, L., Jie, L., Yujuan, J., Sufang, G. *Chin. J. Chem.* 28, 633-638 (2010)
149. Zhai, C., Wei, C., Xu, J., Yang, P., Du, Y. *Colloid Journal* 71(6), 764-770 (2009)
150. Zheng, J., Stevenson, M. S., Hikida, R. S., Patten, P. G. V. *J. Phys. Chem. B* 106, 1252-1255 (2002)
151. Kavitha, M., Parida, M. R., Prasad, E., Vijayan, C., Deshmukh, P. C. *Macromol. Chem. Phys.* 210, 1310-1318 (2009)
152. Esumi, K., Isono, R., Yoshimura, T. *Langmuir* 20, 237-243 (2004)
153. Xu, D.-M., Zhang, K.-D., Zhu, X.-L. *J. Applied Polymer Science* 104, 422-426 (2007)

154. Jin, L., Yang, S.-P., Wu, H.-X., Huang, W.-W., Tian, Q.-W. *J. Applied Polymer* 108, 4023-4028 (2008)

155. Zhang, Y., Peng, H., Huang, W., Zhou, Y., Xuehong, Z., Yan, D. *J. Phys. Chem. C* 112, 2330-2336 (2008)

156. Reger, D. L., Goode, S. R., Mercer, E. E. (1997) Chemistry: Principles & Practice; Brooks/Cole – Thomson Learning; USA

157. Root, M., (2011) The Tab Battery Book: An in-depth guide to construction, design, and use; McGrawHill; USA

158. Goodson, T. *J. Phys. Chem. B* 107, 3419-3426 (2003)

159. West, R., Wang, Y., Goodson III, T. J. Phys. Chem. B 107, 3419-3426 (2003)

160. Wilson, O. M., Scott, R. W. J., Garcia-Martinez, J. C., Crooks, R. M. Chem. Mater. 16, 4202-4204 (2004)

161. Toshima, N., Yonezawa, T., New J. Chem. 22, 1179-1201 (1998)

162. Lang, H., Maldonado, S., Stevenson, K. J., Chandler, B. D. *J. Am. Chem. Soc.* 126, 12949-12956 (2004)

163. Scott, R. W. J., Datye, A., Crooks, R. M. *J. Am. Chem. Soc.* 125, 3708-3709 (2003)

164. Ye, H., Crooks, R. M. *J. Am. Chem. Soc.* 129, 3627-3633 (2007)

165. Peng, X., Pan, Q., Rempel, G. L., Wu, S. *Catal. Communications* 11, 62-66 (2009)

166. Chung, Y.-M., Rhee, H.-K. *J. Mol. Catal. A: Chem.* 206, 291-298 (2003)

167. Scott, R. W. J., Sivadinarayana, C., Wilson, O. M., Yan, Z., Goodman, W., Crooks, R. M. *J. Am. Chem. Soc.* 127, 1380-1381 (2005)

168. Endo, T., Kuno, T., Yoshimura, T., Esumi, K. *J. Nanosci. Nanotech.* 5(11), 1875-1882 (2005)

169. Knecht, M. R., Weir, M. G., Frenkel, A. I., Crooks, R. M. *Chem. Mater.* 20, 1019-1028 (2008)

170. Endo, T.; Yoshimura, T.; Esumi, K. *J. Colloid Inter. Science* 286, 602-609 (2005)

171. Wilson, O. M., Scott, R. W. J., Garcia-Martinez, J. C., Crooks, R. M. J. Am. Chem. Soc. 127, 1015-1024 (2005)

172. Xie, H., Howe, J. Y., Schwartz, V., Monnier, J. R., Williams, C. T., Ploehn, H. J. *J. Catal.* 259, 111-122 (2008)

173. Myers, S. V., Frenkel, A. I., Crooks, R. M. *Chem. Mater.* 21, 4824-4829 (2009)

174. Bai, L., Wan, H., Street, S. C. *Colloids and Surfaces A: Physisochem. Eng. Aspects* 349, 23-28 (2009)
175. Gates, A. T., Nettleton, E. G., Myers, V. S., Crooks, R. M. *Langmuir* 26(15), 12994-12999 (2010)
176. Chandler, B. D., Long, C. G., Gilbertson, J. D., Pursell, C. J., Vijayaraghavan, G., Stevenson, K. J. *J. Phys. Chem. C* 114, 11498-11508 (2010)
177. Auten, B. J., Hahn, B, P., Vijayaraghavan, G., Stevenson, K. J., Chandler, B. D. *J. Phys. Chem. C* 112, 5365-5372 (2008)
178. Liu, D., López-De Jesus, Y. M., Monnier, J. R., Williams, C. T. *J. Catal.* 269, 376-387 (2010)
179. Somorjai, G. A., Li, Y. *Top Catal* 53, 832-847 (2010)
180. Chung, Y.–M., Rhee, H.- K. *Catalysis Letters* 85, 159-164 (2003)
181. Chung, Y.-M., Rhee, H.-K. *Korean J. Chem. Eng.* 21(1), 81-97 (2004)
182. Torigoe, K., Nakajima, Y., Esumi, K. J. Phys. Chem. 97, 8304-8309 (1993)
183. Hoover, N. N., Auten, B. J., Chandler, B. D. *J. Phys. Chem. B* 110, 8606-8612 (2006)
184. Mahaparta, S. K., Bogle, K. A., Dhole, S. D., Bhoraskar, V. N. Nanotechnology 18, 135602 (5pp) (2007)
185. Scott, R. W. J., Wilson, O. M., Oh, S.-K., Kenik, E. A., Crooks, R. M. *J. Am. Chem. Soc.* 126, 15583-15591 (2004)
186. Kamat, P. V., L. *Phys. Chem. B* 106, 7729-7744 (2002)
187. Gu, Y., Wu, G., Hu, X. F., Chen, D. A., Hansen, T., Loye, H.– G., Ploehn, H. J. *J. Power Sources* 195, 425-434 (2010)
188. Auten, B. J., Lang, H., Chandler, B. D. *Applied Catalysis B: Environmental* 81, 225-235 (2008)
189. Sun, L., Crooks, R. M. *Langmuir* 18, 8231-8236 (2002)
190. Devarajan, S.; Vimalan, B.; Sampath, S. *J. Colloid Interface Science* 278, 126-132 (2004)
191. Beakley, L. W., Yost, S. E., Cheng, R., Chandler, B. D. Applied Catalysis A: General 292, 124-129 (2005)
192. Scott, R. W. J., Wilson, O. M., Crooks, R. M. *Chem. Mater.* 16, 5682-5688 (2004)

193. Singh, A., Chandler, B. D. Langmuir 21, 10776-10782 (2005)
194. Liu, D., Gao, J., Murphy, C. J., Williams, C. T. *J. Phys. Chem. B* 108, 12911-12916 (2004)
195. Zheng, Z., Li, H., Liu, T., Cao, R. J. Catal. 270, 268-274 (2010)
196. Deutsch, D. S., Siani, A., Fanson, P. T., Hirata, H., Matsumoto, S., Williams, C. T., Amiridis, M. D. *J. Phys. Chem. C* 111, 4246-4255 (2007)
197. Deutsch, D. S., Lafaye, G., Liu, D., Chandler, B., Williams, C. T., Amiridis, M. D. *Catalysis Letters* 97(3-4), 139-143 (2004)
198. Lang, H., May, A., Iversen, B. L., Chandler, B. D. J. Am. Chem. Soc. 125, 14832-14836 (2003)
199. Lafaye, G., Siani, A., Marecot, P., Amiridis, M. D., Williams, C. T. *J. Phys. Chem. B* 110, 7725-7731 (2006)
200. Albiter, M. A., Zaera, F. *Langmuir* 26(21), 16204-16210 (2010)
201. Roucoux, A., Schulz, J., Patin, H. *Chem. Rev.* 102, 3757-3778 (2002)
202. Bönnemann, H., Richards, R. M. *Eur. J. Inorg. Chem.* 2455-2480 (2001)
203. Malynych, S., Luzinov, I., Chumanov, G. J. Phys. Chem. B 106, 1280-1285 (2002)
204. Wang, S. C., Chang, K. S., Yuan, C. J. Electrochimica Acta 54, 4937-4943 (2009)
205. Steffen, H., Schwarz, J., Kersten, H., Behnke, J. F., Eggs, C. Thin Sold Films 283, 158-164 (1996)
206. Mozetic, M. Surface & Coatings Technology 201, 4837-4842 (2007)
207. Wu, Z., Xanthopoulos, N., Reymond, F., Rossier, J., Girault, H. Electrophoresis 23, 782-790 (2002)
208. Krüger, P., Knes, R., Friedrich, J. Surface and Coatings Technology 112, 240-244 (1999)
209. Kim, E. J., Haruyama, T., Yanagida, Y., Kobatake, E., Aizawa, M. *Analytica Chimica Acta* 394, 225-231 (1999)
210. Bhattacharya, S., Datta, A., Berg, J. M., Gangopadhyay, S. J. Microelectromechanical Systems 14, 590-597 (2005)
211. Mozetič, M., Zalar, A. Vacuum 71, 233-236 (2003)
212. Zou, J.-J., Liu, C.-J., Zhang, Y.-P. Langmuir 22, 2334-2339 (2006)

213. Li, C., Hsieh, J. H., Cheng, J.-C. Surface & Coatings Technology 200, 3370-3375 (2006)
214. Negri, P., Marotta, N. E., Bottomley, L. A., Dluhy, R. A. Applied Spectroscopy 65, 66-74 (2011)
215. Baker, M. A. Thin Solid Films 69, 359-368 (1980)
216. Raiber, K., Terfort, A., Benndorf, C., Krings, N., Strehblow, H.-H. Surface Science 595, 56-63 (2005)
217. Körner, E., Aguirre, M. H., Fortunato, G., Ritter, A., Rühe, J., Hegemann, D. *Plasma Process. Polym.* 7, 619-625 (2010)
218. Shim, H., Philips, J., Fonseca, I. M., Carabinerio, S. Applied Catalysis A: General 237, 41-51 (2002)
219. Li, W. J. Electronic Materials 39, 295-302 (2010)
220. Janssesns, T. V. W., Clausen, B. S., Hvolbaek, Falsig, H., Christensen, C. H., Bligaard, T., Nørskov, J. K. Topics in Catalysis 44, 15-26 (2007)
221. Hashmi, A. S. K., Hutchings, G. J. Angew. Chem. Int. Ed. 45, 7896-7936 (2006)
222. Diallo, M. S., Christie, S., Swaminathan, P., Balogh, L., Shi, X., Um, W., Papelis, C., Goddard III, W. A., Johnson, Jr. J. H. *Langmuir* 20, 2640-2651 (2004)
223. Vinod, C. P. Catalysis Today 154, 113-117 (2010)
224. Nørskov, J. K., Bligaard, T., Hvolbæk, B., Abild-Pedersen, F., Chorkendorff, I., Christensen, C. H. Chem. Soc. Rev. 37, 2163-2171 (2008)
225. Weststrate, C. J., Resta, A., Westerström, Lundgren, E., Mikkelsen, A., Andersen, J. N. J. Phys. Chem. C 112, 6900-6906 (2008)
226. Yang, J., Tschamber, V., Habermacher, D., Garin, F., Gilot, P. Applied Catalysis B: Environmental 83, 229-239 (2008)
227. Alexeev, O. S., Gates, B. C. *Ind. Eng. Chem. Res.* 42, 1571-1587 (2003)
228. Copéret, C., Chabanas, M., Saint-Arroman, R. P., Basset J.-M. *Angew. Chem. Int. Ed.* 42, 156-181 (2003)
229. Chung, Y.-M., Rhee, H.-K. *Catal. Surv. Asia* 8(3), 211-223 (2004)
230. Pachón, L. D., Rothenberg, G. *Appl. Organometal. Chem.* 22, 288-299 (2008)
231. Andrés, R., Jesús, E., Flore, J. C. *New J. Chem.* 31, 1161-1191 (2007)
232. Li, G., Luo, Y. *Inorganic Chemistry* 47, 360-362 (2008)

233. Diallo, M. S., Arasho, W., Johnson, Jr. J. H., Goddard, W. A. *Environ. Sci. Technol.* 42, 1572-1579 (2008)
234. Jia, C.-J., Schüth, F. *Phys.Chem.Chem.Phys.* 13, 2457-2487 (2011)
235. Tarazona-Vasquez, F., Balbuena, P. B. *J. Phys. Chem. B* 108, 15982-15991 (2004)
236. Korkosz, R. J., Gilbertson, J. D., Prasifka, K. S., Chandler, B. D. Catalysis Today 122, 370-377 (2007)
237. Xie. H., Gu, Y., Ploehn, H. J. *Nanotechnology* 16, S492-S501 (2005)
238. Shi, X., Ganser, T. R., Sun, K., Balogh, L. P., Baker Jr, J. R. Nanotechnology 17, 1072-1078 (2006)
239. Knecht, M. R., Crooks, R. M. *New J. Chem.* 31, 1349-1353 (2007)
240. Shi, X., Sun, K., Balogh, L. P., Baker Jr., J. R. *Nanotechnology* 17, 4554-4560 (2006)
241. Cotton, A. and Wilkinson, G. (eds), Advanced Inorganic Chemistry, 3rd ed. John Wiley & Sons, New York, 1972
242. Pyreu, D. F., Kozlovskii, E. V., Gruzdev, M. S. *Russian J. Coordination Chemistry* 36, 293-297 (2010)
243. Summers, J. S., Baker, J. B., Meyerstein, D., Mizrahi, A., Zilbermann, I., Cohen, H., Wilson, C. M., Jones, J. R. *J. Am. Chem. Soc.* 130, 1727-1734 (2008)
244. Piera, E., Tejedor-Tejedor, M. I., Zorn, M. E., Anderson, M. A. *Applied Catalysis B: Environmental* 46, 671-685 (2003)
245. Bartholomew, C. H. *Applied Catalysis A: General* 212, 17-60 (2001)
246. Hancock, R. D., Martell, A. E. *J. Chemical Education* 73, 654-661 (1996)
247. Gröhn, F., Bauer, B. J., Akpalu, Y. A., Jackson, C. L., Amis, E. J. *Macromolecules* 33, 6042-6050 (2000)
248. Gardea – Torresdey, J. L., Tiemann, K. J., Gamez, G., Dokken, K., Cano-Aquilera, I., Furenlid, L. R., Renner, M. W. *Environ. Sci. Techol.* 34, 4392-4396 (2000)
249. Martinez, J. S., inventor; 2010 Jan. 14. Synthesis of Fluorescent Metal Nanoclusters. United Stated Patent US 0009427 A1
250. Guo, R., Wang, H., Peng, C., Shen, M., Pan, M., Cao, X., Zhang, G., Shi, X. J. Phys. Chem. C 114, 50-56 (2010)

251. Bencini, A., Bianchi, A., Danesi, A., Giorgi, C., Mariani, P., Valtancoli, B. *J. Coordination Chemistry* 62, 82-91 (2009)

252. Négrier, F., Marceau, E., Che, M., Giraudon, J.-M., Gengembre, L., Löfberg, A. *J. Phys. Chem. B* 109, 2836-2845 (2005)

253. Gauli, K., Ram, R. N., Soni, H. P. *J. Molecular Catalysis A: Chemical* 242, 161-167 (2005)

254. Négrier, F., Marceau, E., Che, M., Caro, D. *C. R. Chimie* 6, 231-240 (2003)

255. Verberckmoes, A. A., Weckhuysen, B. M., Schoonheydt, R. A. *Microporous and Mesoporous Materials* 22, 165-178 (1998)

256. Hathaway, B. J., Lewis, C. E. *J. Chem. Soc. A* 7, 1183-8 (1969)

257. Dumond, F., Marceau, E., Che, M. *J. Phys. Chem. C* 111, 4780-4789 (2007)

258. James, R., Moore, E. (2004) Metal-ligand Bonding; Royal Society of Chemistry: Cambridge UK

259. Sun, Y., Liu, Y., Guizhe, Z., Zhang, Q. J. Polym. Res. 15, 269-273 (2008)

260. Henglein, A. *J. Phys. Chem.* 97, 5457-5471 (1993)

261. Ottaviani, M. F., Valluzzi, R., Balogh, L. *Macromolecules* 35, 5105-5115 (2002)

262. He, S., Yao, J., Jiang, P., Shi, D., Zhang, H., Xie, S., Pang, S., Gao, H. *Langmuir* 17, 1571-1575 (2001)

263. Chandra, S., Lang, H. *Materials Chemistry and Physics* 114, 926-932 (2009)

264. Bohren, C. F., Huffman, D. R. (2004) *Absorption and Scattering of Light by Small Particles*; WILEY-VCH Verlag GmbH & Co. KGaA: Weiheim

265. Brown, K. R., Walter, D. G., Natan, M. *J. Chem. Mater.* 12, 306-313 (2000)

266. Cottancin, E., Celep, G., Lermé, J., Pellarin, M., Huntzinger, J. R., Vialle, J. L., Broyer, M. *Theor Chem Acc* 116, 514-523 (2006)

267. Shi, X., Lee, I., Baker Jr, J. R. *J. Mater. Chem.* 18, 586-593 (2008)

268. Ujihara, M., Orbulescu, J., Imae, T., Leblanc, R. M. Langmuir 21, 6846-6854 (2005)

269. Song, K. C., Lee, S. M., Park, T. S., Lee, B. S. *Korean J. Chem. Eng.* 26(1), 153-155 (2009)

270. Cropton, T. R., Battery Reference Book, 3rd ed., Newnes, 2000

271. Takato, M., Kaneda, K. *Green Chem.* 15, 2636 (2013)

272. Green, I. X., Tang, W., Neurock, M., Yates Jr., J. T. *Accounts Research* 47, 805 (2014).
273. Zhang, Y., Cui, X., Shi, F., Deng, Y. *Chem. Rev.* 112, 2467 (2012).
274. Liu, X., He, L., Liu, Y.-M., Cao, Y. *Accounts of Chemical Research* 47, 793 (2014).
275. Kipnis, M. *Applied Catalysis B: Environmental* 152, 38 (2014).
276. Cao, J., Sun, T., Grattan, K. T. V. *Sensors and Actuators B* 195, 332 (2014).
277. Mackey, M. A., Ali, M. R. K., Austin, L. A., Near, R. D., El-Sayed, M. A. *J. Phys. Chem. B* 118, 1319 (2014).
278. Selvam, T. S., Chi, K.-M. *J. Nanopart. Res.* 13, 1769 (2011).
279. Debouttière, P.-J., Coppel, Y., Behra, P., Chaudret, B., Fajerwerg, K. *Gold Bull.* 46, 291 (2013).
280. Orefuwa, S. A., Ravanbakhsh, M., Neal, S. N., King, J. B., Mohamed, A. A. *Organometallics* 33, 439 (2014).
281. Behera, M., Ram, S. *Appl. Nanoscience* 4, 247 (2014).
282. Zhong, R.-Y., Yan, X.-H., Gao, Z.-K., Zhang, R.-J., Xu, B.-Q. *Catal. Sci. Technol.* 3, 3013 (2013).
283. Esumi, K., Suzuki, A., Aihara, N., Usui, K., Torigoe, K. *Langmuir* 14, 3157 (1998).
284. Esumi, K., Hosoya, T., Suzuki, A., Torigoe, K. *Langmuir* 16, 2978 (2000).
285. Gröhn, F., Kim, G., Bauer, B. J., Amis, E. J. *Macromolecules* 34, 2179 (2001).
286. Kim, Y.-G., Oh, S.-K., Crooks, R. M. *Chem. Mater.* 16, 167 (2004).
287. Pérignon, N., Marty, J.-D., Mingtaud, A.-F., Dumont, M., Rico-Lattes, I., Mingotaud, C. *Macromolecules* 40, 3034 (2007).
288. Balogh, L., Valluzzi, R., Laverdure, K. S., Gido, S. P., Hagnauer, G. L., Tomalia, D. A. *J. Nanoparticle Research* 1, 353 (1999).
289. Esumi, K., Suzuki, A., Yamahira, A., Torigoe, K. *Langmuir* 16, 2604 (2000).
290. Esumi, K., Hosoya, T., Suzuki, A., Torigoe, K. *J. Colloid and Interface Science* 226, 346 (2000).
291. Benkó, T., Beck, A., Geszti, O., Katona, R., Tungler, A., Frey, C., Guczi, L., Schay, Z. *Appl. Catal. A* 388, 31 (2010).

292. Gross, E., Liu, J. H.-C., Toste, F. D., Somorjai, G. A. *Nature Chemistry* 4, 947 (2012).
293. Scott, R. W. J., Wilson, O. M., Crooks, R. M. *Chem. Mater.* 16, 5682 (2004)
294. Nazarpoor, Z., Khivantsev, K., Kyriakidou, E., Kubicki, C., Ma, S., Fanson, P. T., Alexeev, O. S., Amiridis, M. D. *J. Colloid and Interface Science* 398, 22 (2013).
295. Nagy, P. *J. Mol. Struct.* 201, 271 (1989).
296. Wang, S., Qian, K., Bi, X.-Z., Huang, W. *J. Phys. Chem. C* 113, 6505 (2009).
297. Karsten, E., Erhard, H., Roland, R., Hartmut, in: A2 (Ed.), Ullmann's Ecyclopedia of Industrial Chemistry, Wiley-VCH, Weinheim, 2000.
298. Pande, S., Crooks, R. M. Langmuir 27, 9609 (2011).
299. Zeng, S., Yong, K.-T., Roy, I., Dinh, X.-Q., Yu, X., Luan, F. *Plasmonics* 6, 491 (2011).
300. Shi, X., Sun, K., Baker, Jr., J. R. *J. Phys. Chem. C* 112, 8251 (2008).
301. Usher, A., McPhail, D. C., Brugger, J. *Geochimica et Cosmochimica Acta* 73, 3359 (2009).
302. Lee, W. I., Bae, Y., Bard, A. J. *J. Am. Chem. Soc.* 126, 8358 (2004).
303. Pocker, Y., Dickerson, D. G. *J. Phys. Chem.* 73, 4005 (1969).
304. Balogh, L. P., Ganser, T. R., Shi, X. *Mater. Res. Soc. Symp. Proc.* 847, 463 (2005).
305. Garcia-Martinez, J. C., Crooks, R. M. *J. Am. Chem. Soc.* 126, 16170 (2004).
306. Daniel, M. C., Astruc, D. *Chem. Rev.* 104, 293 (2004).
307. Kudrev, A. G. *Talanta* 75, 380 (2008).
308. Newman, J. D. S., Blanchard, G. J. *Langmuir* 22, 5882 (2006).
309. Ong, W., McCarley, R. L. *Macromolecules* 39, 7295 (2006).
310. Margitfalvu, J. L., Fási, A., Hegedüs, M., Lónyi, F., Göbölös, S., Bogdanchikova, N. *Catalysis Today* 72, 157 (2002).
311. Pestryakov, A. N., Lunin, V. V., Kharlanov, A. N., Kochubey, D. I., Bogdanchikova, N., Stakheev, A. Y. *J. Molecular Structure* 642, 129 (2002).
312. Tuzovskaya, I., Pestryakov, A., Bogdanchikova, N., Avalos, M., Simakov, A. *Physics, Chemistry and Application of Nanostructures* 346 (2003).
313. Tsai, M.-F., Chang, S.-H. G., Cheng, F.-Y., Shanmugam, V., Cheng, Y.-S., Su, C.-H., Yeh, C.-S. *ACS Nano* 7, 5330 (2013).

314. Wardman, P. *J. Phys. Chem. Ref. Data* 18, 1637 (1989).

315. Helms, B., Guillaudeu, S. J., Xie, Y., McMurdo, M., Hawker, C. J., Fréchet, J. M. J. *Angew. Chem. Int. Ed.* 44, 6384 (2005).

316. Haiss, W., Thanh, N. T. K., Aveyard, J., Fernig, D. G. *Anal Chem.* 79, 4215 (2007).

317. Wang, S., Qian, K., Bi, X. Z., Huang, W. *J. Phys. Chem. C* 113, 6505 (2009).

318. Okitsu, K., Yue, A., Tanabe, S., Matsumoto, H., Yobiko, Y. *Langmuir* 17, 7717 (2001).

319. Li, J., Piehler, L. T., Qin, D., Baker, J. R., Tomalia, D. A. *Langmuir* 16, 5613 (2000).

320. Tsukruk, V. V. *Adv. Mater.* 10, 253 (1998).

321. Betley, T. A., Hessler, J. A., Mecke, A., Banaszak Holl, M. M., Orr, B. G., Uppuluri, S., Tomalia, D. A., Baker, J. R., Jr. *Langmuir* 18, 3127 (2002).

322. Imamura, S., Ikebata, M., Ito, T., Ogita, T. *Ind. Eng. Chem. Res.* 30, 217 (1991)

323. Aoyama, N., Yoshida, K., Abe, A., Miyadera, T. *Catalysis Letters* 43, 249 (1997) Shimizu, K., Sugino, K., Kato, K., Yokota, S., Okumura, K., Satsuma, A. *J. Phys. Chem. C* 111, 6481 (2007)

324. J. Park, J.R. Regalbuto, J. Colloid Interf. Sci. 175, 239 (1995)

325. P.J.H. Scott, Linker Strategies In Solid-Phase Organic Synthesis, John Wiley & Sons, United Kingdom, 2009

326. J.R. Regalbuto, in: J.R. Regalbuto (Ed.), Catalyst Preparation, Science and Engineering, Taylor & Francis, 2007

327. J.R. Regalbuto, in: K.P. de Jong (Ed.), Synthesis of Solid Catalysts, Wiley-VCH Verlag, 2009

328. X. Hao, W. Spieker, J.R. Regalbuto, J. Colloid Interf. Sci. 267, 259 (2003)

329. J.R. Regalbuto, A. Navada, S. Shadid, M.L. Bricker, Q. Chen, J. Catal. 184, 335 (1999)

330. K. Shimizu, K. Sawabe, A. Satsuma, Cat. Sci. Tec. 1, 331 (2011)

331. W.A. Spieker, J.R. Regalbuto, Chem. Eng. Sci. 56, 3491 (2001)

332. M. Schreier, J.R. Regalbuto, J. Catal. 225, 190 (2004)

333. J.T. Miller, M. Schreier, A.J. Kropf, J.R. Regalbuto, J. Catal. 225, 203 (2004).

334. X. Hao, L. Quach, J. Korah, W.A. Spieker, J.R. Regalbuto, J. Mol. Catal. A-Chem.

219, 97 (2004)

335. Y. Lei, F. Mehmood, S. Lee, J. Greeley, B. Lee, S. Seifert, R.E. Winans, J.W. Elam, R.J. Meyer, P.C. Redfern, D. Teschner, R. Schlögl, M.J. Pellin, L.A. Curtiss, S. Vajda, Science 328, 224 (2010)
336. X. Hao, S. Barnes, J.R. Regalbuto, J. Catal. 279, 48 (2011)
337. N. Job, S. Lambert, M. Chatenet, C.J. Gommes, F. Maillard, S. Berthon-Fabry, J.R. Regalbuto, J.P. Pirard, Catal. Today 150, 119 (2010)
338. S. Lambert, N. Job, L. D´Souza, M.F. Ribeiro Pereira, R. Pirard, B. Heinrichs, J.L. Figueiredo, J.P. Pirard, J.R. Regalbuto, J. Catal. 261, 23 (2009)
339. L. Jiao, J.R. Regalbuto, J. Catal. 260, 342 (2008)
340. T.E. Feltes, L. Espinosa-Alonso, E. de Smit, L. D’Souza, R.J. Meyer, B.M. Weckhuysen, J.R. Regalbuto, J. Catal. 270, 95 (2010)
341. Y. Zhao, T.E. Feltes, J.R. Regalbuto, R.J. Meyer, R.F. Klie, Cat. Sci. Tec. 1, 1483 (2011)
342. N. Pradhan, A. Pal, T. Pal, Colloid Surface A 196, 247 (2002)
343. J.G. Serafin, A.C. Liu, S.R. Seyedmonir, J. Mol. Catal. A-Chem. 131, 157 (1998)
344. A.N. Pestryakov, Catal. Today 28, 239 (1996)
345. W. Spieker, J. Regalbuto, D. Rende, M. Bricker, Q. Chen, Stud. Surf. Sci. Catal. 130, 203 (2000)
346. A. Nagy, G. Mestl, Appl. Catal. A-Gen. 188, 337 (1999)
347. D.C. Lim, I. Lopez-Salido, Y.D. Kim, Appl. Surf. Sci. 253, 959 (2006)
348. M. Hanisch, M. Mackovic, N. Taccardi, E. Spiecker, R.N.K. Taylor, Chem. Commun. 48, 4287 (2012)
349. J. Yang, V. Tschamber, D. Habermacher, F. Garin, P. Gilot, Appl. Catal. B-Environ. 83, 229 (2008)
350. T. Mitsudome, S. Arita, H. Mori, T. Mizugaki, K. Jitsukawa, K. Kaneda, Angew. Chem. Int. Ed. 47, 138 (2008)
351. T. Baba, Y. Iwase, K. Inazu, D. Masih, A. Matsumoto, Micropor. Mesopor. Mat. 101, 142 (2007)
352. K. Shimizu, K. Sugino, K. Kato, S. Yokota, K. Okumura, A. Satsuma, J. Phys. Chem. C 111, 6481 (2007)

353. K. Shimizu, R. Sato, A. Satsuma, Angew. Chem. Int. Ed. 48, 3982 (2009)
354. E. Sayah, D. Brouri, Y. Wu, A. Musi, P. Da Costa, P. Massiani, Appl. Catal. A-Gen. 406, 94 (2011)
355. K. Shimizu, K. Sugino, A. Satsuma, Chem. Eur. J. 15, 2341 (2009)
356. K. Arve, K. Svennerberg, F. Klingstedt, K. Era1nen, L.R. Wallenberg, J.O. Bovin, L. Čapek, D.Y. Murzin, J. Phys. Chem. B 110, 420 (2006)
357. K. Esumi, R. Isono, T. Yoshimura, Langmuir 20, 237 (2004)
358. H. Wei, C. Gomez, J. Liu, N. Guo, T. Wu, R. Lobo-Lapidus, C.L. Marshall, J.T. Miller, R.J. Meyer, J. Catal. 298, 18 (2013)
359. R. Vadakkekara, M. Chakraborty, P.A. Parikh, Colloid Surface A 399, 11 (2012)
360. M.J. Beier, T.W. Hansen, J.D. Jan-Dierk Grunwaldt, J. Catal. 266, 320 (2009)
361. X. Zhang, Z. Qu, X. Li, M. Wen, X. Quan, D. Ma, J. Wu, Sep. Purif. Technol. 72, 395 (2010)
362. M. Zienkiewicz-Strazałka, S. Pasieczna-Patkowska, M. Kozak, S. Pikus, Appl. Surf. Sci. 266, 337 (2013)
363. L. Jiao, J.R. Regalbuto, J. Catal. 260, 329 (2008)
364. N. Aoyama, K. Yoshida, A. Abe, T. Miyadera, Catal. Lett. 43, 249 (1997)
365. S. Imamura, M. Ikebata, T. Ito, T. Ogita, Ind. Eng. Chem. Res. 30, 217 (1991)
366. G. Lu, X. Zuo, Catal. Lett. 58, 67 (1999)
367. A. Henglein, D. Meisel, J. Phys. Chem. B 102, 8364 (1998)
368. T. Chaieb, L. Delannoy, C. Louis, C. Thomas, Appl. Catal. B-Environ. 142, 780 (2013)
369. T. Chaieb, L. Delannoy, G. Costentin, C. Louis, S. Casale, R. L. Chantry, Z.Y. Li, C. Thomas, Appl. Catal. B-Environ. 156, 192 (2014)
370. K. Malinger, J. Blanchard, R.P. Doherty, C. Thomas, Catal. Commun. 46, 81 (2014)
371. V. Lopez-Ramon, C. Moreno-Castillo, J. Rivera-Utrilla, L.R. Radovic, Carbon 41, 2020 (2002)
372. K. Amine, K. Yasuda, H. Takenaka, Ann. Chim. Sci. Mater. 23, 331 (1998)
373. F. Shadman, P. Raghu, N. Rana, C. Yim, E. Shero, P. Elec. Soc. S. 2003, 131 (2003)
374. I. Nowak, M. Ziolek, Chem. Rev. 99, 3603 (1999)

375. S. Kameoka, T. Chafik, Y. Ukisu, T. Miyadera, Catal. Lett. 51, 11 (1998)
376. T.L. Brown, H.E. Iemay Jr., B.E. Bursten, C.J. Murphy, P.M. Woodward, Chemistry The Central Science, Pearson Prentice Hall, USA, 2012.
377. M. Schreier, T.E. Feltes, M.T. Schaal, J.R. Regalbuto, J. Colloid Interf. Sci. 348, 571 (2010)